REGULATION OF KINASES BY SYNTHETIC IMIDAZOLES, NUCLEOTIDES AND THEIR DEUTERATED ANALOGUES

by

THOKOZANI CLEMENT NKOSI

submitted in accordance with the requirements for
the degree of

MASTER OF SCIENCE

In the subject

LIFE SCIENCES

at the

University of South Africa

Supervisor: Dr M S Myer

Co-supervisor: Prof C Kenyon

Co-supervisor: Dr C van der Westhuyzen

February 2015

DECLARATION

I, Thokozani Clement Nkosi, hereby declare that Regulation of Kinases by Synthetic Imidazoles, Nucleotides and their Deuterated Analogues is my own unaided work. It is being submitted for the Master of Science degree at the University of South Africa, Pretoria. It has not been submitted before for any degree or examination in any other university.

_____ day of 17 February 2015
(Signature of candidate)

_____ day of 20 Feb 2015
(Signature of supervisor)

_____ day of 17 Feb 2015
(Signature of co-supervisor)

_____ day of 17th Feb 2015
(Signature of co-supervisor)

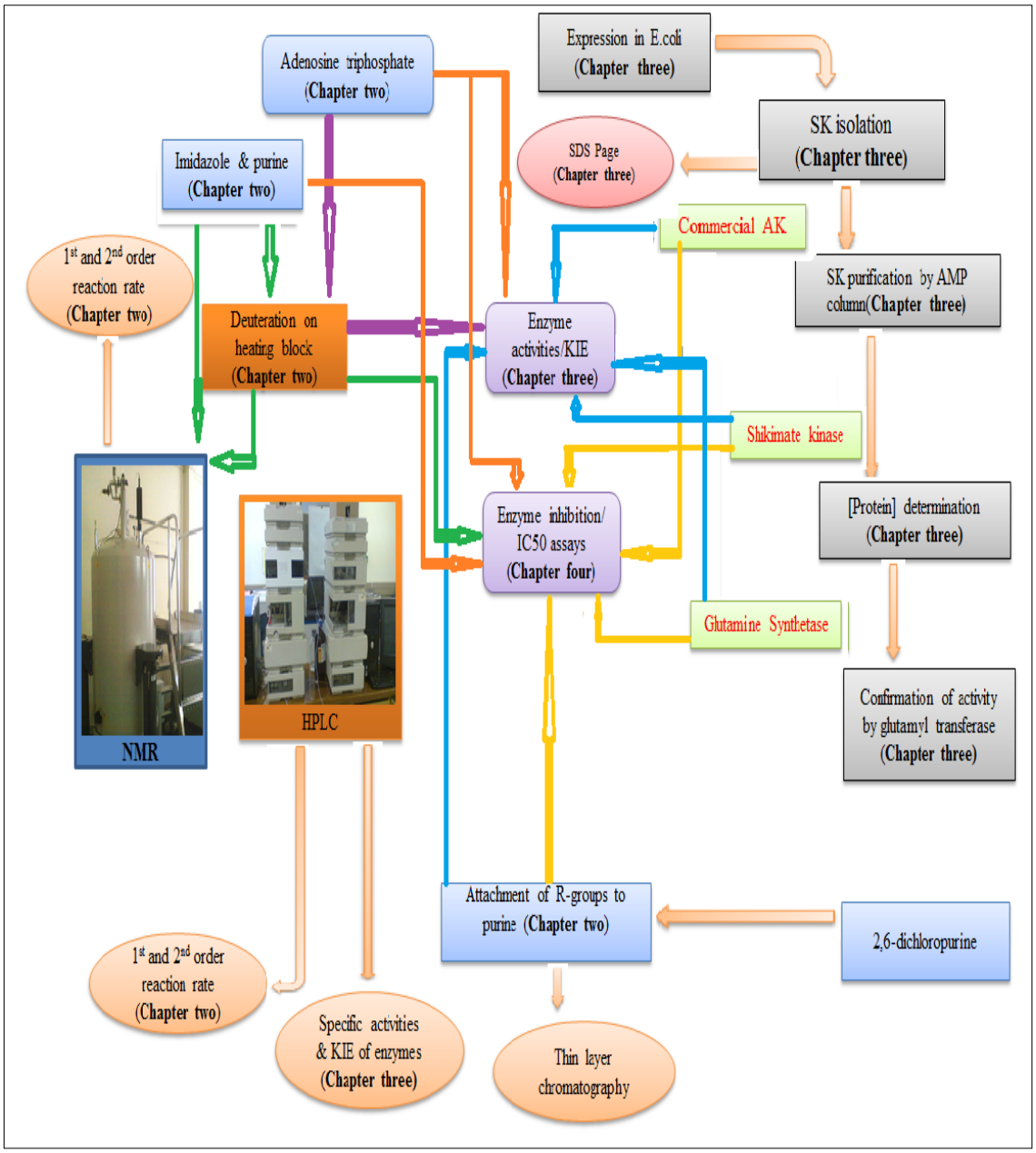

"In the field of observation chance favors only the prepared mind" **Louis Pasteur**

ABSTRACT

Deuteration is the replacement of a hydrogen atom by deuterium atom in a molecule. The replacement begins at the most acidic hydrogen in the molecule. In ATP, the deshielded hydrogen is C8-H which is the first replaced during deuteration. During ATP deuteration some of the ATP is hydrolysed to ADP concurrently. Using kinetic analysis, it was confirmed that the ATP hydrolysis that occurs is 1st order in ATP concentration, while the hydrogen replacement is 2nd order. The ATP and its C8 deuterated analogue were tested against three enzymes shikimate kinase (SK), acetate kinase (AK) and glutamine synthetase (GS) to determine if a kinetic isotope effect (KIE) exists in these systems. With AK and GS, the KIE_D increased as the KIE_H decreased, while with SK the KIE_D decreased as the KIE_H increased as the concentration of the ATP or deuterated analogue increased. Deuteration of imidazole and purine compounds reduced the specific activity of AK or SK at low concentrations in an enzyme-catalysed reaction. From a library of imidazole-containing compounds that inhibited SK, three compounds were selected and their IC_{50} values were determined on the SK-catalysed reaction. These compounds show a differential potency and efficiency between their protonated and deuterated analogues when compared in a 1:1 mixture. Synthesized purines incorporating three different substituents at N-9 were tested against AK or SK for their ability to lower the specific activity of the enzymes used.

KEY TERMS

Acetate kinase, Glutamine synthetase, Shikimate kinase, Adenosine triphosphate rate order, Proton nuclear magnetic resonance, Enzyme activity and Kinetics, Imidazole and Purine deuteration.

ACKNOWLEDGEMENTS

My thanks first and foremost to God Almighty, who has been the source of my energy throughout my studies; without Him none of this would have been possible. I thank my supervisors, Dr Martin Steven Myer (UNISA), Dr Chris van der Westhuyzen (CSIR) and Professor Colin Peter Kenyon (CSIR) for their supervision of my work. Their encouragement, vision, patience and love were invaluable.

Thanks to my entire family who always stood by me faithfully and unconditionally. I would also like to thank the University of South Africa (UNISA) community who have been supporting this study, particular the main library at Muckleneuk and Florida campuses. I would also like to thank the Council for Scientific Industrial Research (CSIR) for allowing me to do this study. I would not have had the knowledge that I have without you. Last but not least, my colleagues at CSIR Biosciences, particular Dr Robyn Roth and Dr Anjo Theron for the time and the support they gave me during the course of the study.

ABBREVIATIONS AND ACRONYMS

Acetyl-CoA	Acetyl-coenzyme A
ADP	Adenosine diphosphate
AK	Acetate kinase
AMU	Atomic mass units
ATP	Adenosine triphosphate
AMP	Adenosine monophosphate
Arg	Arginine
β	Beta
B_0	Main magnetic field
Buffer A	10mM imidazole, pH 7; 10mM $MnCl_2$; 150mM NaCl
Buffer B	10mM Imidazole, pH7; 10mM $MnCl_2$; 450mM NaCl
C	Column
C8-H	Hydrogen attached to the carbon atom at the eight position (IUPAC numbering)
C8-D ATP	Adenosine triphosphate deuterated on the carbon atom at the eight position (IUPAC numbering)
C-D	Deuterium covalently bound to carbon
C-H	Hydrogen covalently bound to carbon
D	UV detector
Da	Dalton
D_2O	Deuterium oxide
ATP-*d*	Deuterated adenosine triphosphate
E	Enzyme
E. coli	*Escherichia coli*
EC_{50}	Half maximal effective concentration
EDTA	Ethylenediaminetetraacetic acid
ES	Enzyme substrate complex
GS	Glutamine synthetase
GTP	guanosine triphosphate
H1	Hydrogen atom at position 1 (IUPAC numbering)
H2	Hydrogen atom at position 2 (IUPAC numbering)
H6	Hydrogen atom at position 6 (IUPAC numbering)
HCl	Hydrochloric acid
HPLC	High performance liquid chromatography
HPP	Pressure pump
IC_{50}	Half maximal inhibitory concentration
IPTG	Isopropyl β-D-1-thiogalactopyranoside
I_{rel}	Relative signal intensities
IUPAC	International Union of Pure and Applied Chemistry
IUB	International Union of Biochemistry

KCl	Potassium chloride
KIE	Kinetic isotope effect
LM + Amp_{100}	Liquid medium containing sugars, alcohol organic acids 100mg/ml ampicillin
Lys	lysine
$MgCl_2$	Magnesium chloride
MtSK	*Mycobacterium tuberculosis* shikimate kinase
$NaHCO_3$	Sodium bicarbonate
NB	nucleotide binding
NMP	Nucleoside monophosphate
NMR	Nuclear magnetic resonance spectroscopy
OD_{600}	Optical Density at 600 nm
P	Product
PDA	Photodiode array
ppm	Parts per million
PTA	Phosphotransacetylase
RS	Solvent reservoir
S	Substrate
SB	Shikimate binding
SDS-PAGE	Sodium dodecyl sulphate polyacrylamide gel electrophoresis
SI	Injection loop
SK	Shikimate kinase
S_N1	Nucleophilic substitution reaction 1
TCA	Trichloroacetic acid
TEA	Triethylamine
Thr	Threonine
TLC	Thin layer chromatography
UV	Ultraviolet light
V_D	Reaction rate of the deutered analogue
V_H	Reaction rate of the protonated analogue
α	Alpha
γ	Gamma
^1H NMR	Proton nuclear magnetic resonance spectroscopy

TABLE OF CONTENTS

CHAPTER 1: DEUTERATION OF ATP, PURINE- AND IMIDAZOLE-CONTAINING COMPOUNDS 19

1.1 Methodology 19

1.1.1 General introduction to methodology 19

1.1.2 ATP structure and function 19

1.1.3 Phosphorylation reactions involving the ATP molecule 20

1.1.4 Deuterium as Molecular Probe 21

1.1.5 Deuteration of ATP 22

1.1.6 Nuclear magnetic resonance spectroscopy (NMR) 23

1.1.7 Determination of ATP deuteration reaction rate order 25

1.1.8 Chemical structures proposing the effect of deuteration 25

1.1.9 High performance liquid chromatography (HPLC) 28

1.1.10 Deuteration of purine- and imidazole-based compounds 30

1.1.11 Substitution of 2,6-dichloropurine 32

1.2 Materials and methods 34

1.2.1 ATP, its deuterated analogue and their reaction rate determination 34

1.2.2 Analysis of ATP and its deuterated analogue by NMR 34

1.2.3 Analysis of AMP, ADP and ATP by HPLC 34

1.2.4 Imidazole and purine deuteration analogues 35

1.2.5 Analysis of imidazole and purine by ^{1}H NMR 35

1.2.6 Synthesis of substituted purine molecules from 2, 6-Dichloropurine 35

1.2.7 Separation of purine by-products by thin layer chromatography (TLC) 36

1.2.8 Recrystallization of purine by-products by dichloromethane: methanol 36

1.3 Results 36

1.3.1 Reaction rate order 36

1.3.2 Rate orders 37

1.3.3 Deuteration of various imidazoles and purines 42

1.3.4 Synthetic substituted purines 45

1.3.5 Discussion 46

CHAPTER 2: THE KINETIC ISOTOPE EFFECT (KIE) IN ACETATE KINASE, SHIKIMATE KINASE AND GLUTAMINE SYNTHETASE IN THE PRESENCE OF ATP OR ATP-d 48

Introduction 48

2.1 Acetate kinase (AK) 48

2.1.1 ATP complexes with acetate kinase 50

2.2 Shikimate kinase (SK) 51

2.2.1 Reactions taking place in the active site of MtSK 53
2.3 Glutamine synthetase (GS) 54
2.4 Kinetic isotope effect resulting from selective deuteration of substrate of an enzyme 56
2.5 Commonalities between shikimate kinase, glutamate kinase and acetate kinase 56
2.6 Materials and methods 56
2.6.1 Acetate kinase assays 56
2.6.1.1 Acetate kinase time assays 56
2.6.1.2 Acetate kinase ATP or ATP-d concentration assay 57
2.6.2.1 Insertion of the SK-encoding gene into an *E. coli* system 57
2.6.2.2 *MtSK* Expression and Purification 58
2.6.2.3 Time assay analysis by shikimate kinase (*MtSK*) 59
2.6.2.4 Shikimate kinase stability assay 60
2.6.2.5 The shikimate kinase ATP or ATP-d concentration assays 60
2.7 Glutamine synthetase assays 61
2.7.1 Deadenylylated GS concentration assays 61
2.8.1 Acetate kinase 61
2.8.2 Shikimate kinase 66
2.8.3 Glutamine synthetase 72
2.9 Comparison of the KIE for AK, SK and GS using ATP and ATP-d 75

CHAPTER 3: THE KINETIC ISOTOPE EFFECT (KIE) IN ACETATE KINASE AND SHIKIMATE KINASE IN THE PRESENCE OF IMIDAZOLE- OR PURINE-BASED INHIBITORS IN EITHER THEIR PROTONATED OR DEUTERATED FORMS 77

Introduction 77
3.1 Enzyme modulation or inhibition 77
3.1.1 IC_{50} determination. 78
3.2 Materials and methods 79
3.2.1 Activity of AK in the presence of protonated imidazole-containing materials and their deuterated analogues 79
3.2.2 Activity of AK in the presence of synthetic purines 79
3.2.3 SK activity in the presence of 10µM protonated imidazole-containing compounds and their deuterated analogues 79
3.2.4 Activity of SK in the presence of 10µM and 100µM protonated imidazole-containing compounds 80
3.2.5 Activity of SK in the presence of 10µM and 100µM deuterated imidazole-containing compounds 80
3.2.6 Activity of SK in the presence of 100µM protonated imidazole-containing compounds or their deuterated analogues 80
3.2.7 Inhibition of SK by synthetic purines 80
3.2.8 Shikimate kinase IC_{50} assays 81

3.3 Results and individual discussion of AK and SK activity in the presence of protonated substrates and their deuterated analogues. 81

3.3.1 Acetate kinase 81

3.3.2 Shikimate kinase 84

3.3.3 Shikimate kinase IC_{50} determination 94

3.4 Comparative discussion of AK and SK activity in the presence of protonated substrates and their deuterated analogues. 100

CHAPTER 4: DISCUSION, SPECULATION AND CONCLUSION 102

4.1 General discussion 102

4.2 Speculation 103

4.3 Summary 103

4.4 Recommendations 104

4.5 Conclusion 104

References 105

Appendix part one 111

Appendix part two 132

LIST OF FIGURES

Figure 1.1: ATP structure showing the hydrophobic and hydrophilic domains (**A**). Also indicated is the atom numbering of the adenylyl moiety(**B**) (Salisu *et al*., 2011; Kenyon *et al*., 2011). 20

Figure 1.2: Schematic diagram showing ATP-mediated phosphorylation by the attack of hydroxyl nucleophile on the γ-phosphate. A phosphorylated molecule is formed, and ATP is converted to ADP. 21

Figure 1.3: A schematic diagram of an NMR spectrometer containing a sample under analysis. 24

Figure 1.4: ATP schematic diagram showing deuteration of ATP. Structure **A** is the protonated ATP molecule; structure **B**, the deuterated form of the ATP molecule. 26

Figure 1.5: Schematic diagrams showing ^{1}H NMR spectra, where **A** is a protonated ATP and **B** spectrum represents the deuterated ATP. Note the difference at 8.48ppm in both spectra (indicated by the arrows): in **B** the signal diminished as deuterium-proton exchange progressed. 27

Figure 1.6: Schematic diagram of an HPLC, showing all of its components used to separate AMP, ADP and ATP from each other. 28

Figure 1.7: HPLC analysis of ATP. **A** is of pure ATP, **B** is of an enzyme-catalysed reaction showing partial hydrolysis to ADP, and **C** is an overlay of **A** and **B.** The arrows indicate the retention time of ADP. 30

Figure 1.8: Chemical structure of imidazole **C** and purine molecule **D** showing the delocalising of π-bonded electrons and the numbering of the molecules. 31

Figure 1.9: Chemical synthetic scheme of 9-methylpurin-6-amine (**A**), 9 ethylpurin-6-amine (**B**)and 9-benzylpurin-6-amine (**C**) from 2,6-dichloro-9H purine. 33

Figure 1.10: A ^{1}H NMR spectrum of ATP showing the proton signals **a**, **b** and **c** used. 37

Figure 1.11: Plot of ln**[**I_{rel}**]** versus incubation time as a function of deuterium oxide concentration. 38

Figure 1.12: Plot of **[**I_{rel}**]**$^{-1}$ versus incubation time as a function of deuterium oxide concentration. 39

Figure 1.13: Plot of ln**[** ADP**]** versus incubation time as a function of deuterium oxide concentration. 40

Figure 1.14: Plot of **[**ADP**]**$^{-1}$versus incubation time as a function of deuterium oxide concentration. 41

Figure 1.15: ^{1}H NMR spectrum of 1-ethylimidazole, before (**A**) and after (**B**) deuteration. The proton replaced by deuterium is shown by a black arrow in **A**, and its position by a red arrow in **B**. 42

Figure 1.16: Hydrogen-deuterium exchange as a percentage of deuteration for various imidazole- or purine-based compounds (see appendix p. 111-130). 45

Figure 1.17: TLC plate showing the different Rf values of three products synthesised from 2,6-dichloropurine 46

Figure 2.1: Acetate kinase catalyses the reaction between acetate and ATP to produce acetyl phosphate and ADP or AMP (Mukhopadhyay *et al*., 2008) 49

Figure 2.2: Crystal structure of (bone marrow kinase) an example of acetate kinase with the N-terminus in blue (upper left arrow), and the C terminus in red (lower left arrow). ATP is shown in the binding cleft as a space-filling model (middle right arrow)(Muckelbauer *et al*., 2011)..... 50

Figure 2.3: Shikimate kinase catalyses the conversion of shikimate to shikimate 3-phosphate while ATP is hydrolysed to ADP or AMP (Daugherty *et al*., 2001). 52

Figure 2.4: **A**: 3D structure of shikimate kinase with ADP and shikimate bound in their respective sites. β-strands are indicated in red, and α-helices in green, with the position of the Mg^{2+} ion in dark blue; **B**: schematic representation of the linkage of α-helices andand β-sheets in the enzyme (**A**: Pereira *et al*., 2004; **B**: Krell *et al*., 1998)..... 53

Figure 2.5: Glutamine synthetase converts glutamate to glutamine by phosphorylation ATP to a γ-glutamyl phosphate intermediate. The γ-glutamyl phosphate intermediate is converted to glutamine via nucleophilic attack by ammonia. 54

Figure 2.6: Hexameric structure of GS with bound ATP/ADP (black stick, indicated by the Arrow). The beta-sheets of various monomers are marked in orange or blue lines. **B**: ATP/ADP binding site with a glutamate mimic (methionine sulfoximine or metsox, indicated as MSO-P), ADP and three Mg^{2+} ions (indicated by the arrow) bound (Krajewski *et al*., 2005)..... 55

Figure 2.7: Diagrammatic representation of a vector containing the aroK gene for use in an *E. coli* expression system…….. 58

Figure 2. 8: An SDS-PAGE gel comparing the migration of the purified sample of shikimate kinase. The molecular weight marker is in the first lane (sizes in kDa on the left) followed by the filtrate loaded onto the Profinia column, the flowthrough, two wash steps, then the eluate in the last lane, containing the *MtSK* protein (indicated by the arrow). 59

Figure 2.9: Specific activity of AK versus increasing time at constant ATP and acetate kinase concentration. The linearity is found between the two arrows. 62

Figure 2.10: Specific activity of acetate kinase against a gradient of 1:1 ATP: ATP-d. The blue series represents specific activity due to ATP-d, and the black series due to ATP..... 64

Figure 2.11: KIE_H and KIE_D versus [1:1 ATP: ATP-d] for acetate kinase enzyme. The blue curve represents KIE_D and the black curve represents KIE_H. 65

Figure 2.12: Stability assay for SK at 4ºC against incubation time at constant enzyme and ATP concentration……..…….67

Figure 2.13: Specific activity SK versus time at constant ATP, temperature and enzyme concentration. 68

Figure 2.14: Specific activity of shikimate kinase against a gradient of 1:1 ATP: ATP-d. The blue series represents specific activity due to ATP-d, and the black series due to ATP..... 70

Figure 2.15: KIE_H and KIE_D versus [1:1 ATP: ATP-d] for shikimate kinase. The blue series represents specific activity due to ATP-d, and the black series due to ATP.. 71

Figure 2.16: Specific activity of glutamine synthetase against a gradient of 1:1 ATP: ATP-d. The blue series represents specific activity due to ATP-d, and the black series due to ATP..... 73

Figure 2.17: KIE_H and KIE_D versus [1:1 ATP: ATP-d] for glutamine synthetase. The blue series represents specific activity due to ATP-d, and the black series due to ATP. 74

Figure 3.3.1: Comparison of the specific activity of AK in the presence of either protonated (black) or deuterated (red) imidazole-containing compounds at 100µM. 82

Figure 3.3.2: Specific activity of the alkylated purines against AK at 10µM (black) and 100µM (blue). Note the enhanced activity in all cases except 1-methylpurine, 2-methylpurine, 2-benzylpurine. 83

Figure 3.3.3: Specific activity of SK in the presence of 10µM protonated (black) or deuterated (red) imidazole-containing compounds. Note the lower specific activity in the presence of the deuterated analogues in all cases……..….85

Figure 3.3.4: Specific activity of SK in the presence of 10µM protonated (black) or deuterated analogues (red) imidazole-containing compounds. Note the equal or slightly higher specific activity in the presence of the deuterated analogues in all cases. 87

Figure 3.3.5: Change in SK specific activity in the presence of protonated inhibiting imidazole-containing compounds at 100µM (black) and 1000µM (red). A dose-response is observed in all instances. 88

Figure 3.3.6: Change in SK specific activity in the presence of deuterated inhibiting imidazole-containing compounds at 100µM (black) and 1000µM (red). A dose-response is observed in most cases. 90

Figure 3.3.7: The effect on the SK specific activity in the presence of protonated (black) and deuterated (red) imidazole-containing compounds at 100µM. The deuterated analogues caused a significant reduction in SK activity relative to their protonated analogues except in the last three compounds. 92

Figure 3.3.8: Reduction and activation of the activity of shikimate kinase when synthetic purines were added at 100µM (black) and 1000µM (blue) compound concentrations. 93

Figure 3.3.9: IC_{50} curve of protonated (black) and deuterated (red) 1-methylbenzimidazole. 96

Figure 3.3.10: IC_{50} curve of protonated (black) and deuterated (red) 4(5) hydroxylmethyl-imidazole. 98

Figure 3.3.11: IC_{50} curve of protonated (black) and deuterated (red) 4-imidazolecarboxylic acid. 100

Figure A.1.1: 2D chemical structure of benzimidazole and its points of deuteration, beginning at N9 hydrogen followed by C8, C1, C4, C2 and C3. 112

Figure A.1.2: ^1H NMR spectrum of benzimidazole is shown in **A**, **B** shows deuteration has proceeded: the black arrow in **A** shows the proton at C2, and the red arrow in **B** shows the proton signal is gone. 112

Figure A.1.3: 2D structure of 1-methylbenzimidazole and its points of deuteration, beginning at C8, followed by C4, C1, C2 and C3 as the arrows show. 113

Figure A.1. 4: ^1H NMR spectra of 1-methylbenzimidazole, before and after deuteration. The hydrogen atom to be replaced is shown in black in **A**, and its position in red in **B**. 113

Figure A.1.5: 2D structure of 6-benzylaminopurine and its points of deuteration, beginning at C9 and followed by C8, C3 and then the aromatic hydrogens in the benzene ring. 114

Figure A.1.6: ^{1}H NMR spectrum of 6-benzylaminopurine, before and after deuteration. The hydrogen atom to be replaced is shown in black in **A**, and its position in red in **B**. 114

Figure A.1.7: 2D chemical structure of 2,6-diaminopurine and its points of deuteration, beginning at C9 hydrogen and followed by C8. 115

Figure A.1.8: ^{1}H NMR spectrum of 2,6-diaminopurine before and after deuteration. The hydrogen atom to be replaced is shown in black in **A**, and its position in red in **B**. 115

Figure A.1.9: 2D chemical structure of 2-iodoadenosine and its point of deuteration at C8. 116

Figure A.1.10: ^{1}H NMR spectrum of 2-iodoadenosine, before and after deuteration. The hydrogen atom to be replaced is shown in black in **A**, and its position in red in **B**. 116

Figure A.1.11: 2D chemical structure of 4-azabenzimidazole and its points of deuteration, beginning at C9 and followed by C8, C1, C2 and C3. 117

Figure A.1.12: ^{1}H NMR spectrum of 4-azabenzimidazole, before and after deuteration. The hydrogen atom to be replaced is shown in black in **A**, and its position in red in **B**. 117

Figure A.1.13: 2D chemical structure of adenine and its points of deuteration, beginning at N9 and N, followed by C8 and C2. 118

Figure A.1.14: ^{1}H NMR spectrum of adenine before and after deuteration. The hydrogen atom to be replaced is shown in black in **A**, and its position in red in **B**. 118

Figure A.1.15: 2D chemical structure of 1-ethylimidazole and its points of deuteration, beginning at C2 followed by C5 and C4. 119

Figure A.1.16: ^{1}H NMR spectrum of 1-ethylimidazole, before and after deuteration. The hydrogen atom to be replaced is shown in black in **A**, and its position in red in **B**. 119

Figure A.1.17: 2D chemical structure of 1(3)-methy imidazole and its points of deuteration, beginning at C2 and followed by C4 and C5. 120

Figure A.1.18: ^{1}H NMR spectrum of 1(3)-methylimidazole, before and after deuteration. The hydrogen atom to be replaced is shown in black in **A**, and its position in red in **B.** 120

Figure A.1.19: 2D chemical structure of 4(5)-(hydroxymethyl imidazole and its points of deuteration, beginning at N3 and followed by C2 and lastly the C4 position. 121

Figure A.1.20: ^{1}HNMR spectrum of 4(5)-(hydroxymethyl)imidazole before and after deuteration. The hydrogen atom to be replaced is shown in black in **A**, and its position in red in **B**. 121

Figure A.1.21: 2D chemical structure of 24(5)-methylimidazole and its points of deuteration, beginning at N3 hydrogen followed by C2 and lastly the C4 position. 122

Figure A.1.22: ^{1}H NMR spectrum of 4(5)-methylimidazole, before and after deuteration. The hydrogen atom to be replaced is shown in black in **A**, and its position in red in **B**. 122

Figure A.1.23: 2D chemical structure of 4-imidazolecarborxylic acid and its points of deuteration, beginning at N3 and followed by C2 and C5. 123

Figure A.1.24: ^{1}H NMR spectrum of 4-imidazolecarborxylic acid, before and after deuteration. The hydrogen atom to be replaced is shown in black in **A**, and its position in red in **B**. 123

Figure A.1.25: 2D chemical structure of 4-imidazolecarboxyaldehyde and its points of deuteration, beginning at N3 and followed by C2 and C5. 124

Figure A.1.26: ^{1}H NMR spectrum of 4-imidazolecarboxyaldehyde, before and after deuteration. The hydrogen atom to be replaced is shown in black in **A**, and its position in red in **B**. 124

Figure A.1.27: 2D chemical structure of 1-butylimidazole and its points of deuteration, beginning at C2 and followed by C4 and C5. 125

Figure A.1.28: ^{1}H NMR spectrum of 1-butylimidazole, before and after deuteration. The hydrogen atom to be replaced is shown in black in **A**, and its position in red in **B**. 125

Figure A.1.29: 2D chemical structure of 1-(3-aminopropyl) imidazole and its points of deuteration, beginning at C2 and followed by C4 and C5. 126

Figure A.1.30: ^{1}H NMR spectrum of 1-(3-aminopropyl) imidazole, before and after deuteration. The hydrogen atom to be replaced is shown in black in **A**, and its position in red in **B**. 126

Figure A.1.31: 2D chemical structure of 1-vinylimidazole and its points of deuteration, beginning at C2 hydrogen and followed by C4 and C5. 127

Figure A.1.32: ^{1}H NMR spectrum of 1-vinylimidazole, before and after deuteration. The hydrogen atom to be replaced is shown in black in **A**, and its position in red in **B**. 127

Figure A.1.33: 2D chemical structure of 4-nitroimidazole and its points of deuteration, beginning at N3 and followed by C4 and C2. 128

Figure A.1.34: ^{1}H NMR spectrum of 4-nitroimidazole, before and after deuteration. The hydrogen atom to be replaced is shown in black in **A**, and its position in red in **B**. 128

Figure A.1.35: 2D chemical structure of 4,5-dicynoimidazole and its points of deuteration, beginning at N3 and followed by C4 and C2. 129

Figure A.1. 36: ^{1}H NMR spectrum of 4,5-dicynoimidazole, before and after deuteration. The hydrogen atom to be replaced is shown in black in **A**, and its position in red in **B**. 129

Figure A.1.37: 2D chemical structure of 5-chloro-1-methylimidazole and its points of deuteration, beginning at N3 and followed by C4 and C2. 130

Figure A.1.38: ^{1}H NMR spectrum of 5-chloro-1-methylimidazole before and after deuteration the hydrogen atom to be replaced is shown in black in **A**, and its position in red in **B**. 130

Figure A.1.39: 2D chemical structure of 5-methyl-4-nitroimidazole and its points of deuteration, beginning at N3 and followed by C2. 131

Figure A.1.40: ^{1}H NMR spectrum of 5-methyl-4-nitroimidazole, before and after deuteration the hydrogen atom to be replaced is shown in black in **A**, and its position in red in **B**. 131

Figure B.1.1: Showing the hydrogen/deuterium replacement at 25% deuterium solution before incubation. ..132

Figure B.1.2: Showing the hydrogen/deuterium replacement at 25% deuterium solution when incubated at 60ºC for 24h. ……..133

Figure B.1.3: Showing the hydrogen/deuterium replacement at 25% deuterium solution when incubated at 60ºC for 48h. ……..133

Figure B.1.4: Showing the hydrogen/deuterium replacement at 50% deuterium solution when incubated at 60 ^{0}C for 72h. 134

Figure B.1.5: Showing the hydrogen/deuterium replacement at 25% deuterium solution when incubated at 60 ^{0}C for 96h. 134

Figure B.1.6: Showing the hydrogen/deuterium replacement at 25% deuterium solution when incubated at 60 ^{0}C for 120h. 135

Figure B.1.7: Showing the hydrogen/deuterium replacement at 25% deuterium solution when incubated at 60 ^{0}C heating block for 144h. 135

Figure B.1. 8: Showing the hydrogen/deuterium replacement at 50% deuterium solution when incubated at 60 ^{0}C for 0h. 136

Figure B.1.9: Showing the hydrogen/deuterium replacement at 50% deuterium solution when incubated at 60 ^{0}C for 24h. 137

Figure B.1.10: Showing the hydrogen/deuterium replacement at 50% deuterium solution when incubated at 60 ^{0}C for 48h. 137

Figure B.1.11: Showing the hydrogen/deuterium replacement at 50% deuterium solution when incubated at 60 ^{0}C for 72h. 138

Figure B.1.12: Showing the hydrogen/deuterium replacement at 50% deuterium solution when incubated at 60 ^{0}C for 96h. 138

Figure B.1.13: Showing the hydrogen/deuterium replacement at 50% deuterium solution when incubated at 60 ^{0}C for 120h. 139

Figure B.1.14: Showing the hydrogen/deuterium replacement at 50% deuterium solution when incubated at 60 ^{0}C for 144h. 139

Figure B.1.15: Showing the hydrogen/deuterium replacement at 75% deuterium solution when incubated at 60 ^{0}C for 0h. 140

Figure B.1.16: Showing the hydrogen/deuterium replacement at 75% deuterium solution when incubated at 60 ^{0}C for 24h. 140

Figure B.1.17: Showing the hydrogen/deuterium replacement at 75% deuterium solution when incubated at 60 ^{0}C for 48h. 141

Figure B.1.18: Showing the hydrogen/deuterium replacement at 75% deuterium solution when incubated at 60 ^{0}C for 72h. 141

Figure B.1.19: Showing the hydrogen/deuterium replacement at 75% deuterium solution when incubated at 60 ^{0}C for 96h. 142

Figure B.1.20: Showing the hydrogen/deuterium replacement at 75% deuterium solution when incubated at 60 ^{0}C for 120 h. 142

Figure B.1.21: Showing the hydrogen/deuterium replacement at 75% deuterium solution when incubated at 60 ^{0}C heating block for 144h. 143

Figure B.1.22: Showing the hydrogen replacement at 100% deuterium solution when incubated at 60 ^{0}C for 0h……144

Figure B.1.23: Showing the hydrogen replacement at 100% deuterium solution when incubated at 60 ^{0}C for 24h…….. 144

Figure B.1.24: Showing the hydrogen replacement at 100% deuterium solution when incubated at 60 ^{0}C for 48h…….. 145

Figure B.1.25: Showing the hydrogen replacement at 100% deuterium solution when incubated at 60 ^{0}C for 72h…….145

Figure B.1.26: Showing the hydrogen replacement at 100% deuterium solution when incubated at 60 ^{0}C for 96h……146

Figure B.1.27: Showing the hydrogen replacement at 100% deuterium solution when incubated at 60 ^{0}C for 120h……146

Figure B.1.28: Showing the hydrogen replacement at 100% deuterium solution when incubated at 60 ^{0}C for 14……147

LIST OF TABLES

Table 1.1: First order rate constants for deuteration of ATP as a function of deuterium oxide concentration. ... 38

Table 1.2: Second order rate constants for deuteration of ATP as a function of deuterium oxide concentration…… ... 39

Table 1.3: First order rate constants of ATP hydrolysis as a function of deuterium oxide concentration ... 40

Table 1.4: Second order rate constants of ATP hydrolysis as a function of deuterium oxide concentration ... 41

Table 1.5: Percentage of proton-deuterium exchange in several purine and imidazole systems. ... 44

Table 2.1: Acetate kinase specific activity as a function of incubation time. Constant enzyme and ATP concentration was used (n =3). ... 62

Table 2.2: Specific activity of acetate kinase as a function of stepwise increases in concentration of a 1:1 ATP: ATP-d mixture under constant incubation time and temperature conditions (n = 3). ... 63

Table 2.3: Kinetic isotope effect on acetate kinase due to ATP (KIE_H) and ATP-d (KIE_D) as a function of [1:1 ATP: ATP-d] (n = 3). ... 65

Table 2.4: SK stability activity as a function of incubation period at 4^oC (n=3) ... 66

Table 2.5: Shikimate kinase specific activity as a function of ADP concentration against incubation time at 37°C. A constant enzyme and ATP concentration was used (n =3) ... 68

Table 2.6: Specific activity of shikimate kinase as a function of stepwise increases in concentration of a 1:1 ATP: ATP-d mixture under constant incubation time and temperature conditions (n = 3). ... 69

Table 2. 7: Kinetic isotope effect on shikimate kinase due to ATP (KIE_H) and ATP-d (KIE_D) as a function of [1:1 ATP: ATP-d]. ... 71

Table 2.8: Specific activity of glutamine synthetase as a function of stepwise increases in concentration of a 1:1 ATP: ATP-d mixture under constant incubation time and temperature conditions (n = 3). ... 72

Table 2.9: Kinetic isotope effect on glutamine synthetase due to ATP (KIE_H) and ATP-d (KIE_D) as a function of [1:1 ATP: ATP-d]. ... 74

Table 3.3.1: Specific activities of assorted imidazole-containing compounds and their deuterated analogues against AK at 100µM. ... 81

Table 3.3.2: Alkylated purine products that enhance or lower the specific activity of AK. ... 83

Table 3.3.3: 10µM SK assays of either protonated imidazole-containing compounds or their deuterated analogues resulting in a drop in specific activity. ... 84

Table 3.3.4: 10µM SK assays of either protonated imidazole-containing compounds or their deuterated analogues resulting in an increase in specific activity. ... 86

Table 3.3.5: Effects of increased inhibitor concentration on SK specific activity in the presence of protonated imidazole-containing compounds. 87

Table 3.3.6: Effects of increased inhibitor concentration on SK specific activity in the presence of deuterated imidazole-containing compounds. 90

Table 3.3.7: Comparison of the SK specific activity in the presence of protonated and deuterated imidazole-containing compounds at 100μM. 91

Table 3.3.8: Comparison of the SK specific activity in the presence of the synthetic purines. 93

Table 3.3. 9: Specific activity of shikimate kinase in the presence of a concentration gradient of either protonated or deuterated 1-methylbenzimidazole. 95

Table 3.3.10: SK specific activity data of shikimate kinase in the presence of a concentration gradient of either protonated or deuterated 4(5)-hydroxymethylimidazole. 97

Table 3.3.11: SK specific activity data of shikimate kinase in the presence of a concentration gradient of either protonated or deuterated 4-imidazolecarboxylic acid. 99

INTRODUCTION

Protein kinases play a central role in cell function as well as in mediating the effects of growth factors. These molecules promote cell proliferation and play a critical role in the field of medicine, as many diseases arise as a result of protein kinases losing their functional integrity (Scapin, 2002). Protein kinases function by modifying other proteins or molecules by transferring a phosphate group from higher energy donor molecules like ATP to a specific substrate (Buss *et al*., 2001; Kenyon *et al*., 2011). This process is called *phosphorylation*. Understanding the mechanism of phosphorylation and its regulation is essential in the design of novel chemotherapeutic agents that target kinase enzymes. The International Union of Pure and Applied Chemistry (IUPAC) and the International Union of Biochemistry (IUB) commission on the classification and nomenclature of enzymes placed the enzymes that transfer high energy phosphate bonds from nucleotides into two divisions: the transferases (kinases) and ligases (synthetases) (Buss *et al*., 2001).

The Enzyme Commission (EC) classification places ligases and transferases in different divisions, with the ligases in division 6 and the transferases in division 2. The ligases are enzymes catalysing the joining of two molecules with the concomitant hydrolysis of the ATP bond, while a kinase is defined as an enzyme which catalyses the transfer of the phosphate group from ATP (or GTP) to a substrate containing an alcohol, amino, carboxylate, or phosphate group as the phosphoryl acceptor (KENYON, Colin, 2007). The ligases and kinases both convert the ATP into either ADP or AMP during phosphorylation. The kinases play a critical role in numerous metabolic and signalling pathways, and their substrates may be a small molecule, lipid, or protein (Kenyon *et al*., 2011).

It has been demonstrated that the C8-H of ATP plays a critical role in the regulation of the phosphorylation reaction carried out by ATP (Kenyon *et al*., 2011). In this study, enzyme kinetics techniques were used to compare the specific enzyme activity of a number of kinase and synthetase enzymes using either ATP or its C8 deuterated analogue as co-substrate. Deuteration involves the substitution of hydrogen (effectively a proton) with deuterium (having both a proton and a neutron) in a molecule (Roger Tung, 2010). Also investigated in this study was the effect of deuteration on the inhibition of kinase enzymes by imidazole- and purine-based compounds and related analogues. Suitable techniques were established for the deuteration of these imidazole and purine compounds. The degree of deuteration of the analogues was determined using ^{1}H NMR. The enzyme assays were carried out by determining the concentration of ATP and ADP in assay mixtures by HPLC as an indirect measure of enzyme rate.

This study was also undertaken to establish a possible mechanistic role of the proton equivalent to that of the C8-H of ATP in imidazole- and purine-based compounds in the binding of these compounds to the active sites of kinase and synthetase enzymes. In addition, the bigger plan was to eventually have these compounds form part of a chemical library of deuterated compounds to subsequently be used for the design of novel selective inhibitors for kinase and synthetase enzymes. As such, this deuterated chemical library can be considered an innovative approach to drug design, having a significant intellectual property potential, particularly when applied as a source of molecular probes to ascertain the extent of inhibition of a number of kinase and synthetase enzymes mechanistically.

For the purposes of this investigation, the following hypotheses were followed:

- The deuteration of ATP at the C8 position alters the *enzyme activity profile* of kinase and synthetase enzymes, which effect is manifest in the reaction.
- Imidazole and purine compounds deuterated at the position equivalent to C8-H of ATP have *altered inhibition profiles* against kinase enzymes when compared with their protonated counterparts.

The list of objectives which will now apply, are as follows:

OBJECTIVES

1. To optimise protocols for the deuteration of imidazole- and purine-based compounds
2. To determine the effect of deuteration of imidazole- and purine-based compounds on subsequent enzyme activity using shikimate kinase, acetate kinase and glutamine synthetase as model systems

CHAPTER 1: DEUTERATION OF ATP, PURINE- AND IMIDAZOLE-CONTAINING COMPOUNDS

1.1 Introduction

1.1.1 General introduction to methodology

ATP, purine- and imidazole-based compounds have a number of similarities in their chemical structures such as aromatic character and at least two nitrogen atoms in their ring systems. This chapter will show how these molecules are deuterated and how their deuterated analogues may be used as molecular probes. During ATP deuteration, ADP is also formed; it is therefore also the aim of this chapter to determine if there is a correlation between the ATP proton/deuterium substitution process and hydrolysis of ATP. Nuclear Magnetic Resonance (NMR) and High Performance Liquid Chromatography (HPLC) were used to explore the qualitative and quantitative analysis of the molecules and their analogues which were produced. One dimensional proton NMR (^{1}H NMR) protocols were used to measure the levels of deuteration in the entire molecule, while HPLC analysis of these samples was used to demonstrate the amount of ATP hydrolysed and possible correlation with inhibition of these enzyme reactions. Various protocols for the synthesis of purine compounds were employed, in order to demonstrate how the different substituents could be incorporated into the purine base molecule. Various molecules were synthesised from 2,6-dichloropurine, which served as a molecular template for subsequent modification reactions. While thin layer chromatography (TLC) shows purity of the sample and/or whether the starting materials were transformed to a new product, it does not confirm modification thereof.

1.1.2 ATP structure and function

As shown in **Figure 1.1**, the ATP molecule consists of both a polar as well as non-polar region. The polar region consists of a ribose sugar and three phosphates, while the adenine moiety makes up the non-polar region (**A** and **B**). Being central to its role as the energy source for living organisms (Novak, 2011), ATP is also involved in a large number of biosynthetic reactions, including transportation of many ions across concentration gradients associated with cellular membranes, as well as in the cellular control and signalling functions necessary to maintain life of biological entities by various molecular phosphorylation mechanisms (Salisu, Kenyon, & Kaye, 2011).

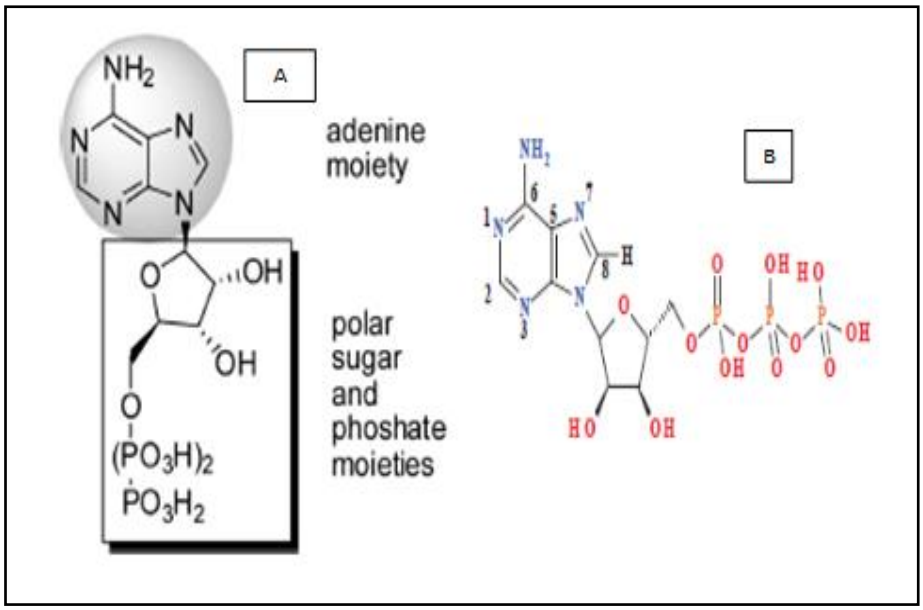

Figure 1.1: *ATP structure showing the hydrophobic and hydrophilic domains (**A**). Also indicated is the atom numbering of the adenylyl moiety(**B**) (Salisu et al., 2011; Kenyon et al., 2011).*

1.1.3 Phosphorylation reactions involving the ATP molecule

In 1894, Emil Fischer introduced the theory that ATP can bind like a substrate to the enzyme based on a shape-fitting mechanism that is complementary to a particular enzyme's binding site. Once this bond is formed, a change in the shape of the enzyme then takes place. As reported by Burnstock *et al*. (2010), Fiske and Subbarow were the first to define the chemistry of ATP in 1929. In 1941, Lipmann elaborated on the function and structure of ATP in the cell (Suwal *et al*., 2012). In general, many reactions in the cell require phosphorylation by ATP as the primary step to make a given compound more reactive. Various moieties, such as adenylyl group, which comprises a purine ring fused to a 5-membered imidazole moiety, are intimately involved in these chemical reactions and were therefore exploited during the course of this investigation.

Kinases and synthase enzymes use the ATP molecule to phosphorylate alcohol or carboxyl groups, or amino acid hydroxyl groups, in the phosphorylation reaction (Kenyon *et al*., 2011). ATP molecules are made up of a nucleoside (adenosine) and three phosphate moieties that are linked by phosphoric acid anhydride bonds. The phosphates are labelled as α, β and γ based on both their position as well as potential energy that is stored in the respective anhydride linkages (Suwal *et al*., 2012). The farthest phosphate from the ribose ring is γ-phosphate group, having the highest chemical potential energy, followed sequentially by

the β- and then the α-phosphate. **Figure 1.2** depicts mechanistically how the hydrolysis of ATP typically takes place to activate an alcoholic ROH group.

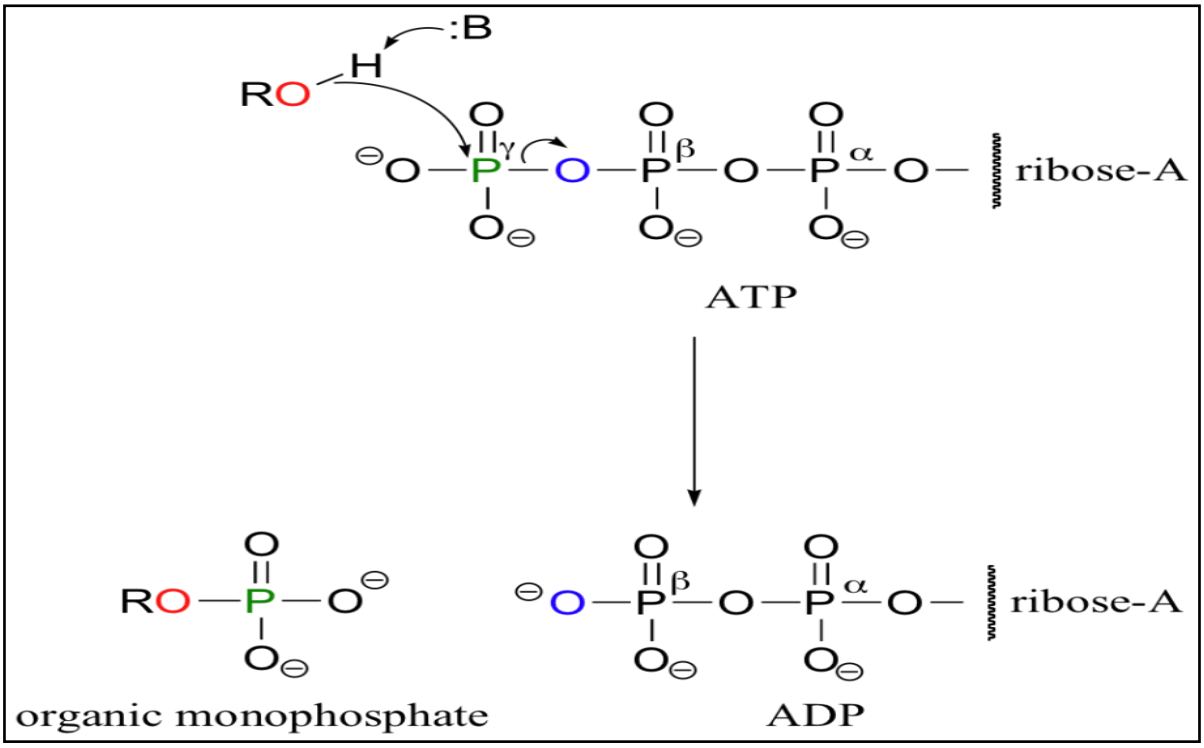

Figure 1.2: *Schematic diagram showing ATP-mediated phosphorylation by the attack of hydroxyl nucleophile on the γ-phosphate. A phosphorylated molecule is formed, and ATP is converted to ADP.*

The oxygen atom of a hydroxyl group (from an alcohol or carboxylate) or the nitrogen atom from an amine can attack the γ-phosphate of ATP molecule via a nucleophilic acyl substitution mechanism. This involves the anhydride bond between the γ- and β-phosphate group being broken and the γ-phosphate binding to the nucleophile, to ultimately form the phosphorylated molecule (Suwal *et al*., 2012). Adenosine diphosphate (ADP), is formed as a result, and is stabilised by environmental water.

1.1.4 Deuterium as Molecular Probe

Molecular deuteration is the substitution of hydrogen (protium or proton), by a deuterium (heavy hydrogen) atom, in a compound (Kenyon *et al*., 2011; Tung, 2010). The deuterium atom is a heavier isotope of hydrogen, differing by a single additional neutron. The resultant change in atomic mass from 1AMU to 2AMU thereby doubles the atomic mass of hydrogen (effectively a naked proton). By the old terminology, the nucleus of deuterium was called a deuteron, in contrast to the nucleus of hydrogen, called a proton or protium (Buteau, 2009;

Limbach, 1991; Tung, 2010). According to Limbach (1991) and Wade (1999), deuterium was first discovered by Urey, Brickwedde and Murphy in 1931 in their study of water electrolysis. Despite the many studies which have since been conducted using deuterated molecules as probes, few have been done on kinase enzymes, specifically with ATP deuterated at the C8 position. The mechanism by which ATP is deuterated involves a change between a carbon to hydrogen (C-H) and carbon to deuterium (C-D) bonds (Wade, 1999). While the compound being deuterated shows slight changes in physical properties, changes in molecular properties such as hydrophobicity, chemical molecular mass and pK_a are more significant (Tung, 2010). Specifically, the C-D bond that is formed is much stronger than the equivalent C-H bond, thereby causing a reduced reaction rate if the C-D (H) bond subsequently plays a role in a chemical reaction mechanism. The ratio of the reaction rate, in the presence of a deuterated molecule, when compared with the reaction rate in the presence of the protonated analogue, is called Kinetic Isotope Effect ($KIE = V_D/V_H$) (Limbach, 1991). KIE_D is defined as the ratio of the reaction rate in the presence of the deuterated material divided by the reaction rate in the presence of the protonated material. The inverse ratio is termed KIE_H (Földesi *et al*., 1996).

1.1.5 Deuteration of ATP

ATP contains an adenine group, which is a bicyclic 5,6-fused heterocyclic aromatic compound containing four nitrogen atoms in the ring structure. The ATP base fulfils the aromatic properties in the adenine molecule by having all carbon atoms in the ring system being sp^2 hybridized to form a resonance stabilised aromatic π-bond system. For the adenine molecule to fulfil the Hückel rule, three of the four bonding orbitals of the nitrogen atom are also sp^2 hybridized. One of the characteristics of lone pairs of nitrogen electrons is to cause molecules containing these atoms to react differently compared to other aromatic compounds. Where ATP molecules are concerned, protons at position 8 and 2 of the adenine ring are the most acidic, being the first to be substituted during the deuteration process.

1.1.6 Nuclear magnetic resonance spectroscopy (NMR)

Nuclear magnetic resonance (NMR) spectroscopy is a physical technique that exploits the magnetic properties of certain nuclei, such as ^{1}H, ^{13}C and ^{15}N. This property is derived from the number of nucleons in an isotope's nucleus, giving rise to spin quantum numbers and a nuclear magnetic moment. A typical NMR instrument has two magnetic poles placed opposite each other so as to create the main magnetic field B_0, at the centre of which a glass tube, containing a sample of interest, is placed (**Figure 1.3**). The shims or sweep coils adjust the main magnetic field B_0 around and through the sample, enabling this region to be as magnetically homogeneous as possible for each sample. Radio waves are then introduced into the sample to allow selective excitation of the spin magnetic moment of each population of nuclei in the sample at a specific resonant frequency. Between the sample and the sweep coils (shims) is an arrangement of transmitter and receiver coils surrounding the sample, termed a sample probe. The probe allows both a radio frequency transmitter as well as a radio frequency receiver/amplifier to operate simultaneously on the sample. Specific radio frequency pulses are introduced into the sample by the transmitter, stimulating the excitation of each distinct type of nucleus in a quantised fashion by absorption of the radio frequency waves. The absorption event is detected as a signal output from the sample by the receiver/amplifier. These electronic signals generated from the interaction of the magnetic field with the magnetic moment of the nuclei in the sample, and subsequently stimulated to resonate at a particular radio frequency, are converted by the software to produce a NMR spectrum at the Control Console and Recorder.

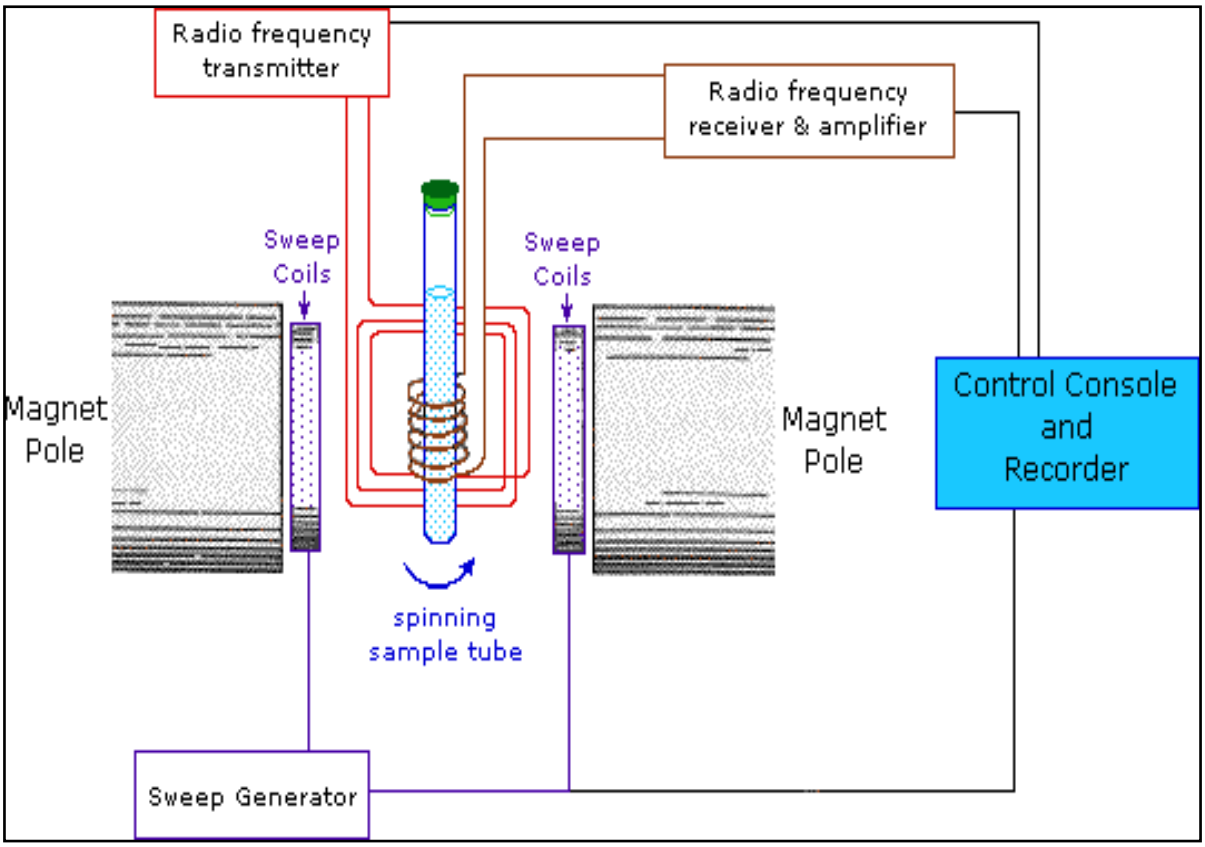

Figure 1.3: *A schematic diagram of an NMR spectrometer containing a sample under analysis.*

Applications of this kind of magnetic resonance technology can provide detailed information about the chemical structure, dynamics, reaction state, and chemical environment of interest within which sample atoms occur. In essence, when a sample is placed in such a magnetic field, the active nuclei of atoms (such as ^{1}H or ^{13}C) absorb electromagnetic radiation at a frequency characteristic of that particular isotope for each atomic nucleus. The resonant frequency, energy of the absorption, and the intensity of the signal are proportional to the strength of the magnetic field, which can be varied to suit a given sample analysis protocol. One dimensional proton NMR (^{1}H NMR) is a protocol that is used to determine the proton location in the molecular structure of a given sample.

An advantage of ^{1}H NMR spectroscopy, is that it can be used for both qualitative and quantitative analysis of molecular structure (Limbach, 1990). Since each nucleus has a different resonance 'range', when hydrogen is substituted with deuterium, the substitution is seen as a loss of signal in a standard ^{1}H-NMR of the deuterated molecule (Limbach, 1991; Heller, 1968). ^{1}H NMR is therefore a convenient technique for quantitatively measuring the deuteration process. This process is monitored by observing intensity changes in a specific

proton signal in the spectrum that corresponds to a hydrogen atom of interest, as it is replaced by deuterium. As seen in **Figure 1.5A** and **B** (p.27), deuteration of ATP can be monitored by the disappearance of the signals indicated. As the signal due to the proton(s) of interest progressively disappears from the spectrum as a function of incubation time, the extent to which deuteration has occurred, at specific positions in the molecule of interest, can be determined by comparing the integrated value of the signal of interest (Lin & Bersohn, 1968).

1.1.7 Determination of ATP deuteration reaction rate order

During ATP deuteration, two processes are observed: (1) some ATP protons are replaced by deuterium to form ATP-*d*, and (2) some of the ATP is hydrolysed to form ADP. In order to determine if a correlation exists between hydrogen-deuterium exchange and hydrolysis of ATP, it is important to know what the rates of ATP hydrolysis and proton-deuterium exchange are, under the same conditions. Since the rate law governing this process can occur as 1^{st} or 2^{nd} order reaction rate kinetics, data from both reactions can be tabulated, for comparison between the two reactions. To quantify this, high pressure liquid chromatographic (HPLC) was used to determine the amount of ATP hydrolysis during deuteration, while ^{1}H NMR protocols were used to determine the rate of deuteration of ATP.

Once both data sets had been collected, the first order reaction rate was determined by plotting a graph of ln[amount of ADP produced] versus incubation time from the HPLC data and subsequently fitted to a straight line . A similar approach can be employed from the ^{1}H NMR data from the integrated area (I) of a signal for a proton of interest at t_a relative to that at t_0, by plotting $\ln[I_a / I_0]$ against reaction time t_a. A second order rate relationship can be tested by plotting either 1/[ADP] or $1/[I_a / I_0]$ versus reaction time, from either the HPLC or ^{1}H NMR data, followed by line-fitting.

1.1.8 Chemical structures proposing the effect of deuteration

When a hydrogen atom in a given molecule has a higher electron density around its nucleus compared to neighbouring hydrogen atoms, it is termed a ‘shielded proton’ due to its possessing a stronger local magnetic field as a result; conversely, electron-density deficient hydrogen nuclei are referred to as ‘deshielded’ protons. As such, when a shielded proton’s apparent magnetic moment interacts with an applied external magnetic field, a reduced chemical shift occurs in the ^{1}H NMR spectrum, compared to that produced by a deshielded proton. Deuterium-hydrogen exchange starts with the most deshielded protons in a molecule, mainly because these acidic protons require less energy for driving the deuteration process due to weaker C-H covalent bonds (Salisu *et al.*, 2011). In **Figure 1.4,** aromatic protons are

depicted (see black arrows), as being the sites where the ATP molecules used in this study were deuterated, beginning at the C8 position, followed by the proton located at C2.

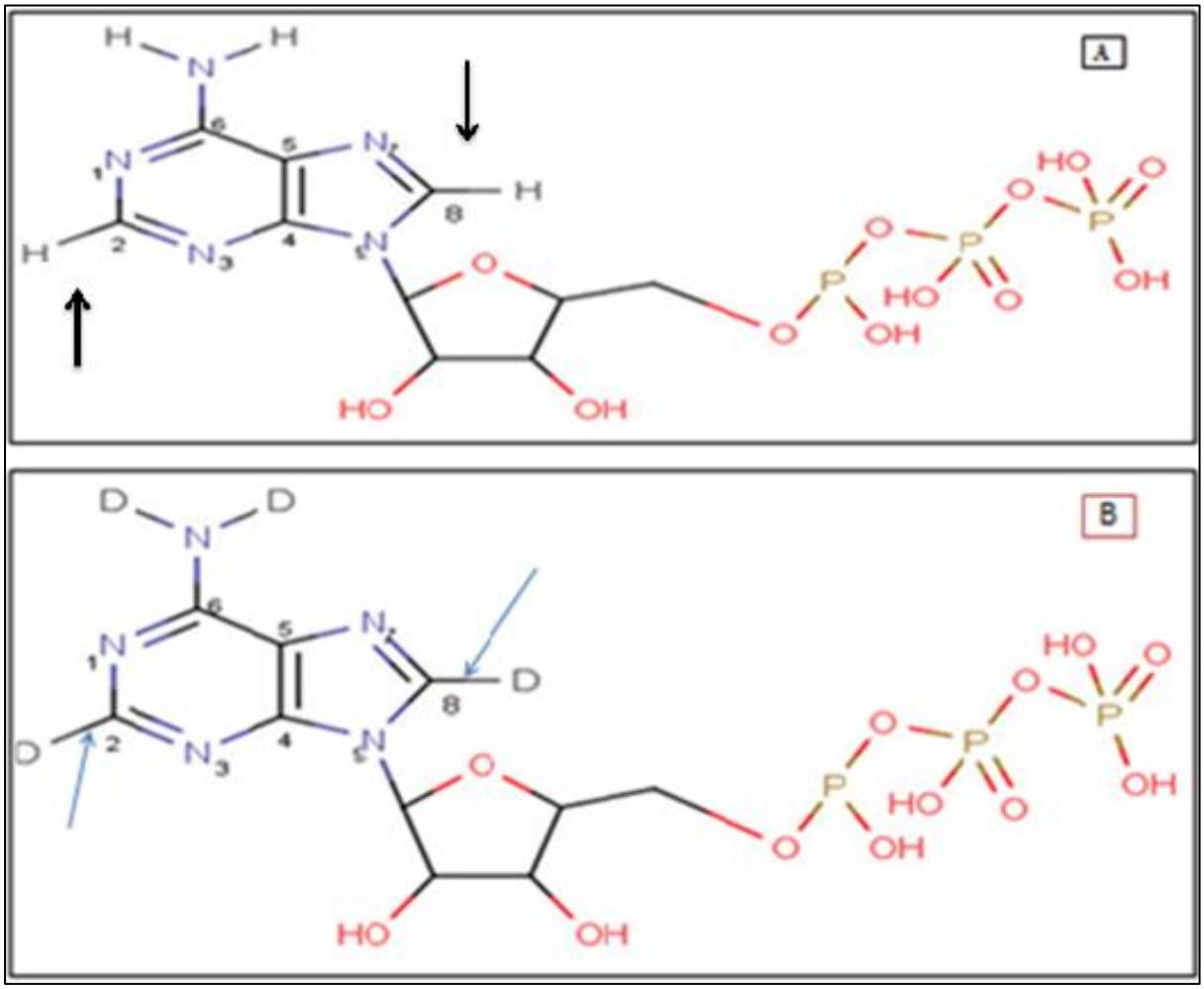

Figure 1.4: *ATP schematic diagram showing deuteration of ATP. Structure **A** is the protonated ATP molecule; structure **B**, the deuterated form of the ATP molecule.*

The protocol for determining that deuteration had taken place involved monitoring the ^{1}H NMR spectrum of the reaction mixture for loss of intensity of the proton signals occurring between 8 and 6ppm. Due to the nature of proton NMR, this intensity is proportional to the number of protons represented by the signal. Thus, deuteration of these aromatic molecules in relation to the location of the relevant hydrogen signal(s) in the ^{1}H NMR spectrum can be used to monitor based on the replacement of hydrogen by the deuterium atom, resulting in disappearance/reduction of the ^{1}H NMR signal. **Figure 1.5A** represents the protonated ATP ^{1}H NMR spectrum, while **Figure 1.5B** shows the effect of the deuteration process on the deshielded protons, as indicated by the black arrow. This ^{1}H NMR spectrum should be viewed in conjunction with the structures in **Figure 1.4A** and **B**.

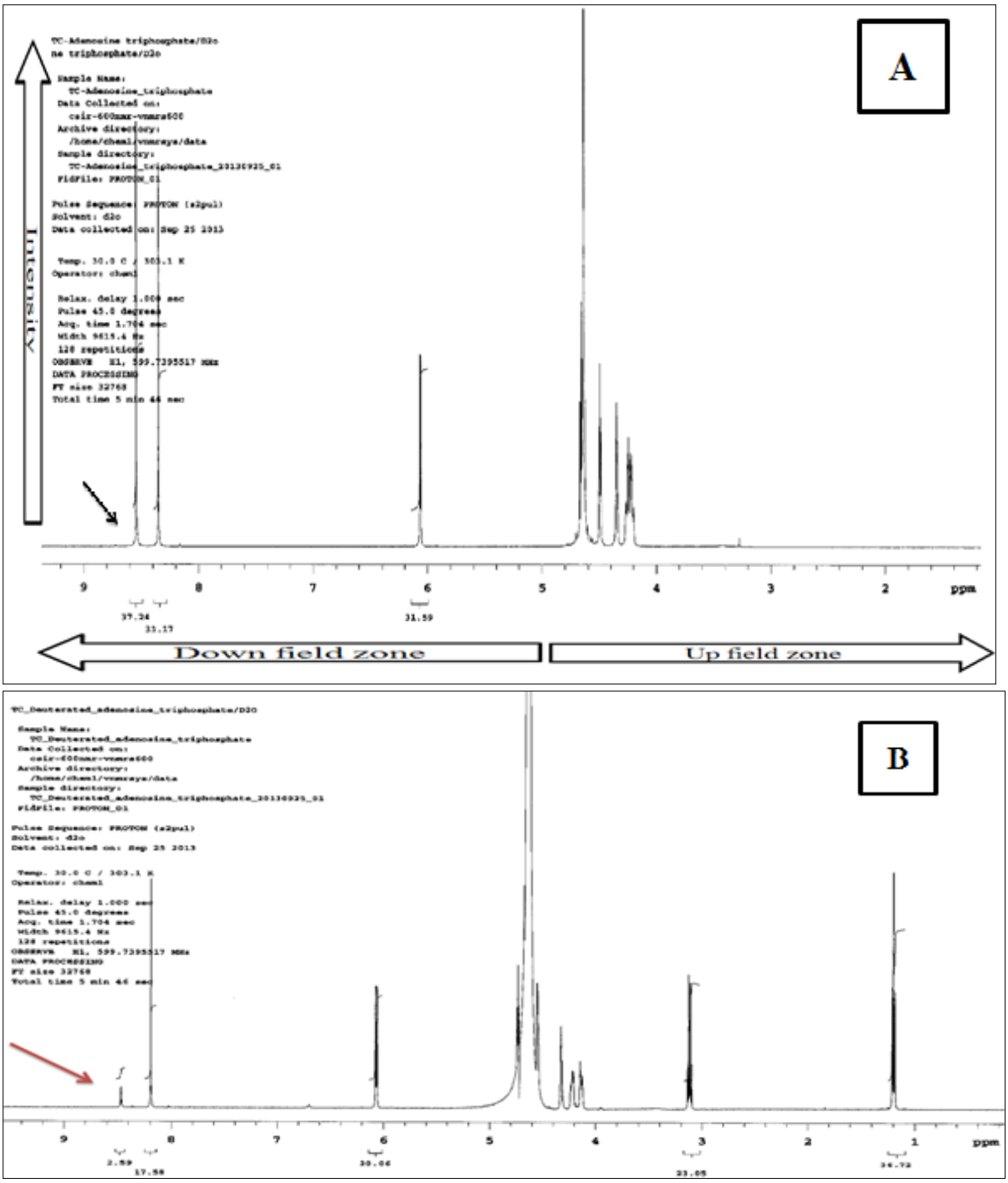

Figure 1.5: *Schematic diagrams showing ^{1}H NMR spectra, where **A** is a protonated ATP and **B** spectrum represents the deuterated ATP. Note the difference at 8.48ppm in both spectra (indicated by the arrows): in **B** the signal diminished as deuterium-proton exchange progressed. The other new proton signals in B resulted from the use of a catalyst in the reaction mixture, namely, trimethylamine.*

1.1.9 High performance liquid chromatography (HPLC)

High-performance liquid chromatography (formerly referred to as high-pressure liquid chromatography) HPLC, is a chromatographic technique used to separate, identify and subsequently to quantify components in a liquid sample mixture. HPLC in this sense can be used to provide both the qualitative and quantitative analysis of a dissolved sample's molecular makeup. In this particular study, an automated Agilent 1100 HPLC instrument was used, employing a Kinetex 5µm C18 250 X4.6mm stationary phase column. The mobile phase (0.0515 M potassium dihydrogen phosphate and PIC reagent and 4.75M acetonitrile) interacting with sample adsorbed onto the solid phase of the column results in an affinity exchange chromatographic system. This allows for the separation of AMP, ADP and ATP in the mixture (Kenyon *et al*., 2011). **Figure 1.6** is a schematic diagram showing how the analyte passes through the HPLC system for separation and characterisation.

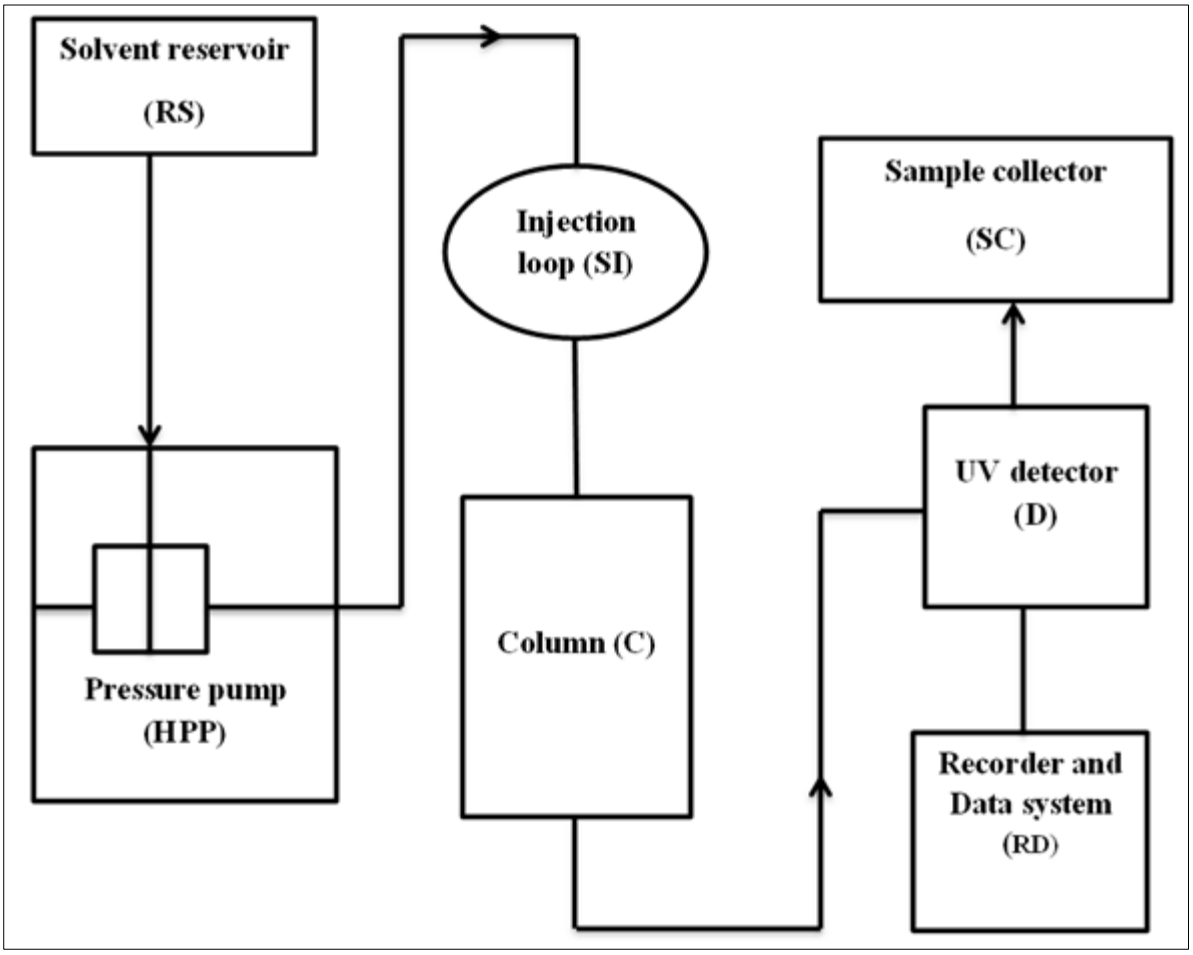

Figure 1.6: *Schematic diagram of an HPLC, showing all of its components used to separate AMP, ADP and ATP from each other.*

The pressure pump (HPP) drives the mobile phase from the solvent reservoir (RS) to the solvent injection port, where the sample solution is then injected into the system via the injection loop (SI). The sample is passed through the column (C), which is packed with stationary phase made up of material which is selected to chemically interact with the sample material. Such a chromatographic system results in differential retention of the various molecules in the sample suspension and their subsequent (differential) elution based on their specific solubility (affinity) for the mobile phase as compared to the stationary phase.

For example, in an AMP, ADP and ATP mixture, the chemical interaction between stationary phase on this reversed phase column and the materials is in the order AMP > ADP> ATP, which is the observed elution order. In this manner, provided that the column packing material is correctly selected for system of interest, separation of the various molecules will be achieved. At the end of the column separation step, detection of molecules in the eluent is achieved by various kinds of detection systems based on UV/visible light, or a photodiode array (PDA), to name a few. In addition, where the desired focus is on separation of molecular ions present in a sample mix, known as mass spectrometry, both an ionising source needs to be in place at the point of sample injection, as well as a UV detector (D) being placed at the end of the system.

During hydrogen-deuterium exchange on ATP molecules, some of the ATP is converted to ADP in the solution. HPLC protocols that were followed identified the ADP produced in the deuteration reaction (KENYON, Colin, 2007). **Figure 1.7** shows a typical HPLC spectrum of the conversion of some ATP to ADP. In the top part of **Figure 1.7**, chromatogram (**A**) shows a pure ATP sample, while the middle chromatogram (**B**), shows both ADP and ATP signals. In chromatogram (**C**), hydrolysis of ATP can be seen on inspection, with lowering of the ATP signal compared to that of the blanked ATP (chromatogram **A** superimposed on **B**).

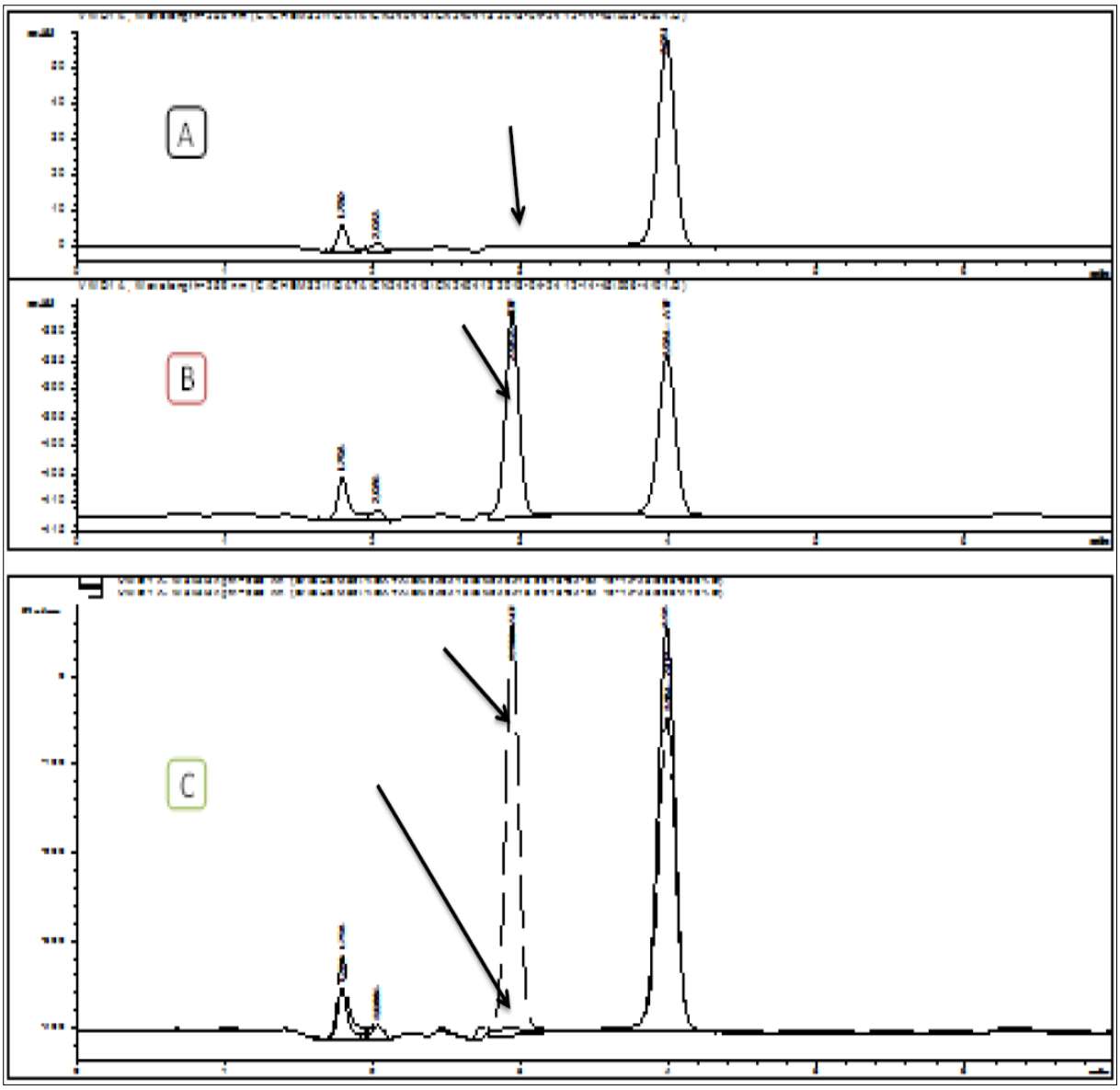

Figure 1.7: *HPLC analysis of ATP. **A** is of pure ATP, **B** is of an enzyme-catalysed reaction showing partial hydrolysis to ADP, and **C** is an overlay of **A** and **B**. The arrows indicate the retention time of ADP. The two other two small peaks in the chromatogram are AMP and PPi, being considered not of particular interest.*

1.1.10 Deuteration of purine- and imidazole-based compounds

Purine- and imidazole-based compounds are five- and six-membered heterocyclic aromatic structures with several nitrogen atoms in their ring structure (Vianello, 2011). Aromatic properties of these kinds of molecules are contributed by electrons on the p-orbitals of the carbon and nitrogen atoms. A lone pair of electrons in the one nitrogen atom in imidazole and three nitrogen atoms in purines play a significant role in forming the π-bond to fulfil aromatic properties in the ring (Watson, Sweet, & Marsh, 1965) as proposed by Hückel's rule. The

purine molecule plays a significant role in biological synthesis of nucleic acids, by acting as an antitumor inhibitor (D'Auria, 2005); Koley *et al*., 2011). These heterocyclic rings are composed of sp^2 hybridized carbon and nitrogen atoms, which allow the p-orbitals to form the conjugate system of π-electrons that delocalize around the ring system of the purine compound, as shown in right hand side of **Figure 1.8.**

When π-electrons delocalize, leaving the nitrogen in a partially positive state, the molecule then becomes less reactive than other aromatic structures. In case of purines, the order of hydrogen-deuterium exchange is C2, C6 and C8, while in the case of imidazole structures, the order is C2 followed by C4 or C5 (Koley *et al*., 2011). **Figure 1.8 C** shows the imidazole numbering. **Figure 1.8 D** shows the lone pairs of electrons in the purine molecule.

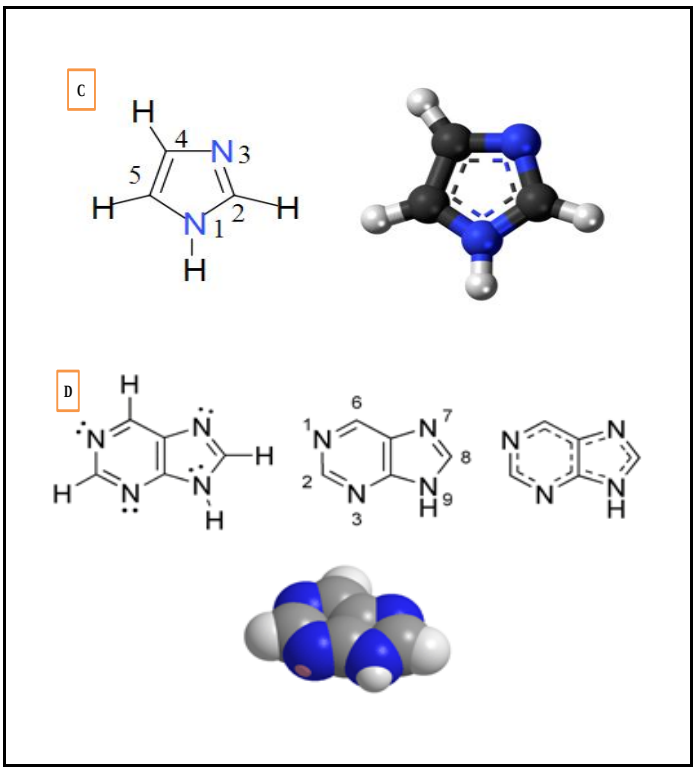

Figure 1.8: *Chemical structure of imidazole **C** and purine molecule **D** showing the delocalising of π-bonded electrons and the numbering of the molecules.*

The hydrogen attached to nitrogen (N-H) in these molecules is highly labile, and is replaced immediately when the molecules are dissolved in deuterium oxide. In general, the proton NMR protocols used in this study were reliably able to confirm that deuteration of these molecules had taken place after comparing the ^{1}H NMR spectrum of the native compound with its deuterated analogue. As was the case with ATP, proton signal intensities from both imidazole and purine were reduced or disappeared completely in the ^{1}H NMR spectrum

following deuteration of these molecules (Giernoth & Bankmann, 2006). The resulting ^{1}H NMR spectra (before and after deuteration) are given in **Appendix Part one** (p. 111-130).

1.1.11 Substitution of 2,6-dichloropurine

2,6-Dichloropurine contains two chloride atoms that are attached at positions 2 and 6 of the aromatic ring structure (Hocek &, Dvor'akov'a, 2003; Koley et al., 2011). Most literature suggests that purine molecules require more time and higher energy in order for the substitution to occur. The purine substitution is always in this order: 6, 2 and 8 (Koley *et al*., 2011). Despite the many studies that have been conducted on purine or 2,6-dichloropurine synthesis, few have compared their inhibitory nature against enzyme activity, particularly when different substituting groups were attached to this purine. Research into purine molecules could reveal their importance as kinase inhibitors (Koley *et al*., 2011). The activities of any of the synthesized molecules in this class could potentially inhibit kinases and synthetases, possibly impacting on the management of diseases that would depend on being able to control the behaviour of these kinds of enzymes. In general, most of these types of molecules are hydrophobic, and so poorly bioavailable (Ogilvie *et al*., 1984). Set against this background, the current investigation was aimed at characterising the possible role 2,6-dichloropurine might play in enzyme kinetic regulation. Modification of 2,6-dichloropurine was considered an ideal starting point, because the molecule has two positions for nucleophilic substitution. Position 6 is the first nucleophilic substitution favoured and it accounts for 67-70% of the reaction products, while position 2 only contributed 40-43% of isolated products (D'Auria, 2005). **Figure 1.9** indicates how the three products can be formed when chlorine atoms in the 2 and 6 positions are respectively replaced with NH_2 and protons. The three substituents that have been introduced are methyl, ethyl and benzyl; once each product was synthesised, it was tested for enzyme inhibition character.

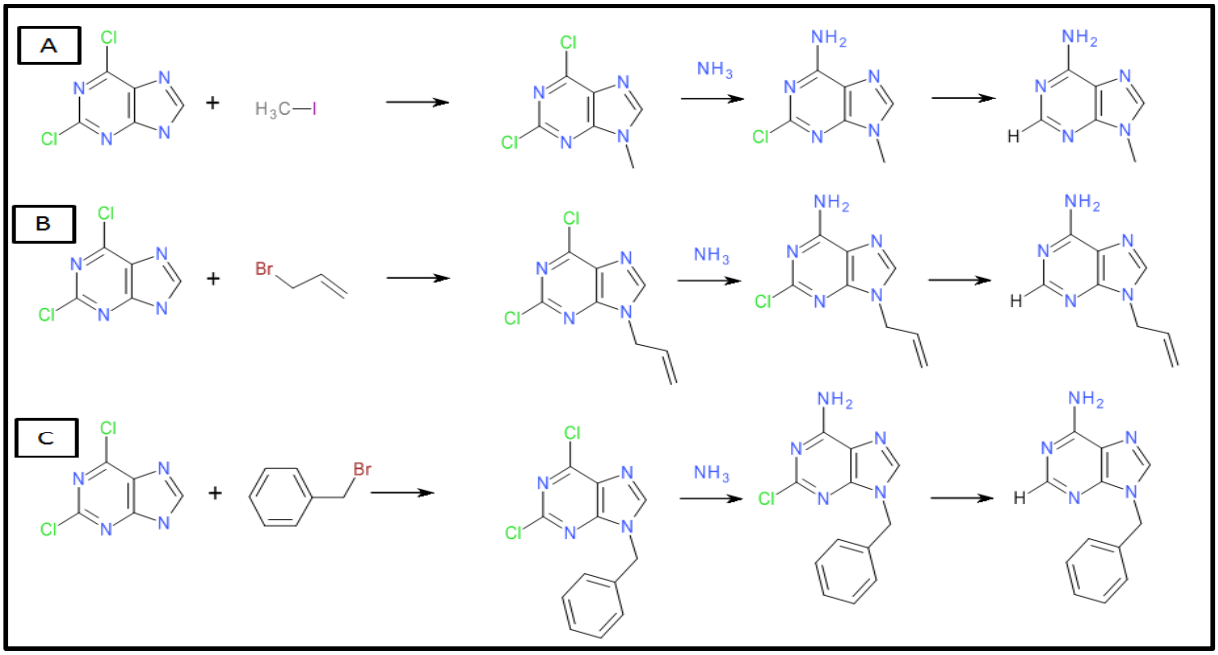

Figure 1. 9: *Chemical synthetic scheme of 9-methylpurin-6-amine (**A**), 9 ethylpurin-6-amine (**B**) and 9-benzylpurin-6-amine (**C**) from 2,6-dichloro-9H purine.*

Using ^{1}H NMR spectroscopy and thin layer chromatography (TLC), the presence of newly synthesized molecules was confirmed. ^{1}H NMR identified the newly attached group by observing additional proton signals in the spectrum.

The TLC confirmed the product's formation based on retention factor (R_f) of starting material and its product. Both molecules (starting material and product) were loaded on aluminium-backed silica TLC plates and eluted with solvent of 400mM ethyl acetate and 76mM hexane. Interactions with the stationary phase and the eluent allow the molecules to have a different R_f based on different adsorption character of each molecule in the solution. The R_f is the ratio of distance travelled by the sample (product or starting material), divided by the distance travelled by the solvent front. If the product has formed, the R_f of the starting material and of its product will differ, but if the reaction has not occurred, the R_f will be identical under the same condition (Adler, Purich, & Stadtman, 1975). The bi-products synthetic purine compounds were named based on the eluted on size exclusion when there were separated. The compound that come out first in the column were named 1- purine compound while those come at the second were named 2- purine compound.

1.2 Materials and methods

1.2.1 ATP, its deuterated analogue and their reaction rate determination

A 20mM ATP (Roche diagnostic) water solution in 5ml sterile snap cap tube was prepared with an increasing percentage of deuterium oxide (D_2O) (Sigma Aldrich) in four test tubes (25, 50, 75 and 100%) and labelled accordingly. A 69.3µl of triethylamine (TEA) (Sigma Aldrich) was added uniformly to all four 5ml sterile snap cap tubes to make 0.1mM TEA. In each test tube, a 0.10ml of reaction mixture was removed and introduced into a 0.5ml Eppendorf tube, closed and labelled as time zero and D_2O%. This preparation was then stored at 4^oC in a fridge for further analysis on both HPLC and NMR instruments. The remaining sample preparations in Eppendorf tubes were closed and incubated at 60^oC on heating block. After every twenty four hour period, six 0.1ml amounts were removed from each reaction solution, placed in separate 0.5ml Eppendorf tubes and kept at 4^0C for further analysis.

For analysis of these samples, each 0.1 ml sample was split into two. Firstly, Eppendorf tubes containing 0.05ml of 20mM ATP and dried in a vacuum concentrator (Savant SC110 Speedy Vac) at 130rpm at 37^0C in order to evaporate the TEA. Each of these preparations were then re-diluted with 0.45ml D_2O and analysed by NMR to characterise both 1^{st} and 2^{nd} order reaction kinetics. From the remaining amount of each sample preparation, a 0.045ml sample was taken and diluted with 0.41ml deionised water or nano water, to make a 2.19mM solution for HPLC analysis and subsequent characterisation with respect to both 1^{st} and 2^{nd} order reaction kinetics.

1.2.2 Analysis of ATP and its deuterated analogue by NMR

For ^1H NMR analysis, 0.05ml of each sample prepared above was diluted with 0.45ml D_2O, to make up a 2mM solution. This was added to an NMR tube and inserted into a Varian 600Hz NMR, using 64 scans and a 2 second relaxation time at 30^0C for data collection. Sample mixtures were analysed together with their time zero or blanked samples. The ^1H NMR spectra thus generated were collected for calculation of rate order reaction kinetics using Graph Pad Prism software.

1.2.3 Analysis of AMP, ADP and ATP by HPLC

The remaining half (0.455ml) of each sample was dissolved in deionised water as described in Section 1.2.1, and then divided into triplicate samples (0.135ml in each vial) for HPLC analysis. The concentration of ADP produced and the amount of ATP left was measured from the resultant traces. Once the HPLC spectra data had been recorded, data was consolidated

using the GraphPad Prism 6 software, after which 1st and 2nd order reaction rate kinetics could be determined.

1.2.4 Imidazole and purine deuteration analogues

Commercial imidazole- or purine-containing samples were prepared at 100 mM concentrations in a 1.5ml Eppendorf tube, diluted with D_2O and added to a 0.99mM triethylamine (TEA) solution. A 0.10ml blank sample was transferred to a 0.5ml Eppendorf tube before incubation and kept at 4^oC in a fridge. The remaining solution was closed with an Eppendorf locker to prevent evaporation of TEA, incubated at 60^oC on a heating block for three to five days. After the incubation period, 0.05ml samples of the 100mM solution were removed, placed in a 0.5ml Eppendorf tube and spun dried in a vacuum concentrator as before. This was diluted with 0.5ml D_2O and inserted to 1.5ml Eppendorf tube and kept at 4^oC fridge for analysis.

1.2.5 Analysis of imidazole and purine by ^1H NMR

The stored purine and imidazole samples were analysed by NMR. A 0.05ml sample of the 100mM deuterated sample was diluted with 0.45ml D_2O and analysed on a Varian 600Hz NMR to determine the ^1H NMR spectra. The NMR was set to 64 scans and 2 seconds relaxation time at the room temperature. All the samples were prepared together with their time zero or blanked solution. The deuteration percentage was calculated from the integrated area of the substituted proton, divided by the sum of this integrated area, together with that of the neighbouring protons and multiplied by 100%.

1.2.6 Synthesis of substituted purine molecules from 2, 6-Dichloropurine

A 5,29mmol solution of 2,6-dichloropurine, 22,5ml acetone, and 10.58mmol sodium carbonate was prepared in a reaction vessel equipped with a reflux condenser. The mixture was boiled under reflux for 20min and then 5.29mmol iodomethane or ethyl bromide or bromobenzene was added in one portion. The reaction mixture was allowed to boil under reflux for 14 hours, after which the mixture was filtered through 0.4µm Whatman filter paper. The yellowish solution was concentrated in a rotary evaporator. The concentrate was purified through a column as follows: the silica columns were prepared and equilibrated with the mobile or elution solution of 4:1 (v/v) ethyl acetate: hexane solution. For the benzylbromide reaction, an elution gradient 3:2 (v/v) to 4:1 (v/v) ethyl acetate: hexane solution was used.

1.2.7 Separation of purine by-products by thin layer chromatography (TLC)

The passage of all eluted samples was monitored by thin layer chromatography(TLC) and visualised using a 6W UV lamp (Hocek et al., 2003). With the same concentration of mobile phase solution, migration of the various components on the TLC plate allowed for subsequent grouping of by-product fractions in a repetitive manner using a rotor evaporator to remove the mobile phase and concentrate the product.

This whole process was done in a repetitive manner, where drops of each sample were spotted on a TLC plate to determine each respective retention factor (R_f), using the original 2,6-dichloropurine material on the left hand side of the plate.

1.2.8 Recrystallization of purine by-products by dichloromethane: methanol

Purine by-products were recrystallized by dissolving them in 7:3 (v/v) dichloromethane: methanol in a small beaker which was then sealed with parafilm. A small portion of each of these crystallised samples was analysed by ^{1}H NMR (Watson, Sweet & Marsh, 1965). The remainder of each of the powdered samples were labelled, dated and kept at room temperature until required for testing for activity in an enzyme assay, to be elaborated on at a later point in this dissertation.

1.3 Results

1.3.1 Reaction rate order

Both the ^{1}H NMR and the HPLC spectral data were used to determine if first or second order reaction rate kinetics were operative. From the HPLC spectral data, the ADP concentration together with reaction time was used to prepare graphs of ln[ADP] or $[ADP]^{-1}$ versus reaction time (in hours) to test for either first or second order reaction rate kinetics, respectively, with respect to ATP hydrolysis. In the case of the ^{1}H NMR spectral data, three signals were considered of interest, all in the 6-9 ppm region of the spectra recorded. The proton signals are shown in the **Figure 1.10** as (**a**), (**b**) and (**c**). The ratio of signal intensities (as I_{rel}) was calculated using:

$$I_{rel} = I_a / (I_a + I_b + I_c)$$

This was to normalise the intensities of the signals used internally. A graph of either $\ln[I_{rel}]$ or $[I_{rel}]^{-1}$versus reaction time (in min) was constructed, in order to test for first or second order reaction rate kinetics, respectively, with respect to ATP C8 deuteration.

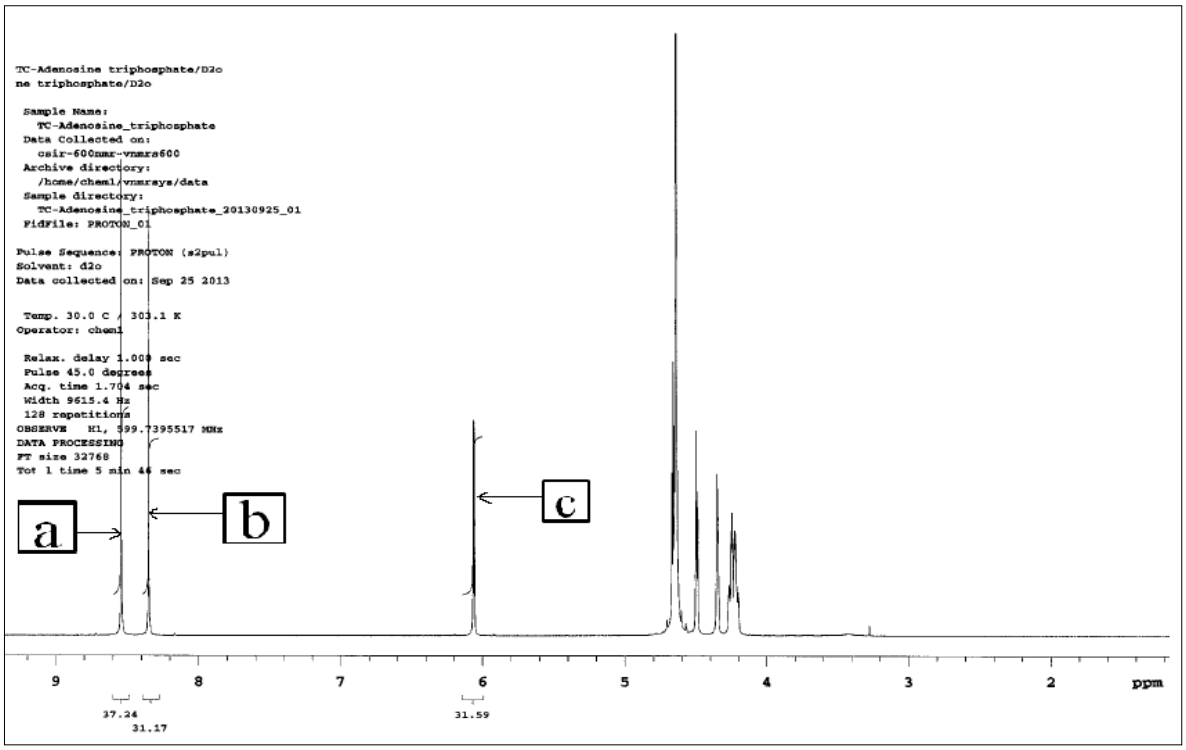

Figure 1.10: *A ^{1}H NMR spectrum of ATP showing the proton signals **a**, **b** and **c** used.*

1.3.2 Rate orders

The following **Tables (1.1-1.4)** and **Figures (1.11-1.14)** reflect a systematic approach to hydrogen-deuterium exchange and subsequent testing for either first or second order kinetics for deuteration. The proton signal of interest is clearly seen in **Figure 1.5** (p. 27), comparing the ^{1}H NMR of ATP at top with that of deuterated ATP at the bottom. The most deshielded proton (indicated with a red arrow in the ^{1}H NMR spectra of the deuterated material) disappears over time when compared to undeuterated ATP.

The **Appendix part two** (p. 131-146) shows how ATP deuteration varies as a function of increasing concentration of deuterated solvent. These spectra show how the proton signals disappear as time and [D_2O] increases at 60^{o}C. From these ^{1}H NMR data in **Appendix part two** (p. 131-146) the following **Tables (1.1-1.4)** and **Figures (1.11-1.14)** reflecting first and second order rate data were generated.

Table 1.1: *First order rate constants for deuteration of ATP as a function of deuterium oxide concentration.*

Time / h	25% D_2O	50% D_2O	75% D_2O	100% D_2O
0.00	-0.96	-0.96	-0.97	-0.95
48.00	-1.00	-1.05	-1.13	-1.37
72.00	-1.01	-1.09	-1.21	-1.76
96.00	-1.05	-1.18	-1.34	-1.97
120.00	-1.07	-1.21	-1.44	-2.23
144.00	-1.18	-1.27	-1.57	-2.47

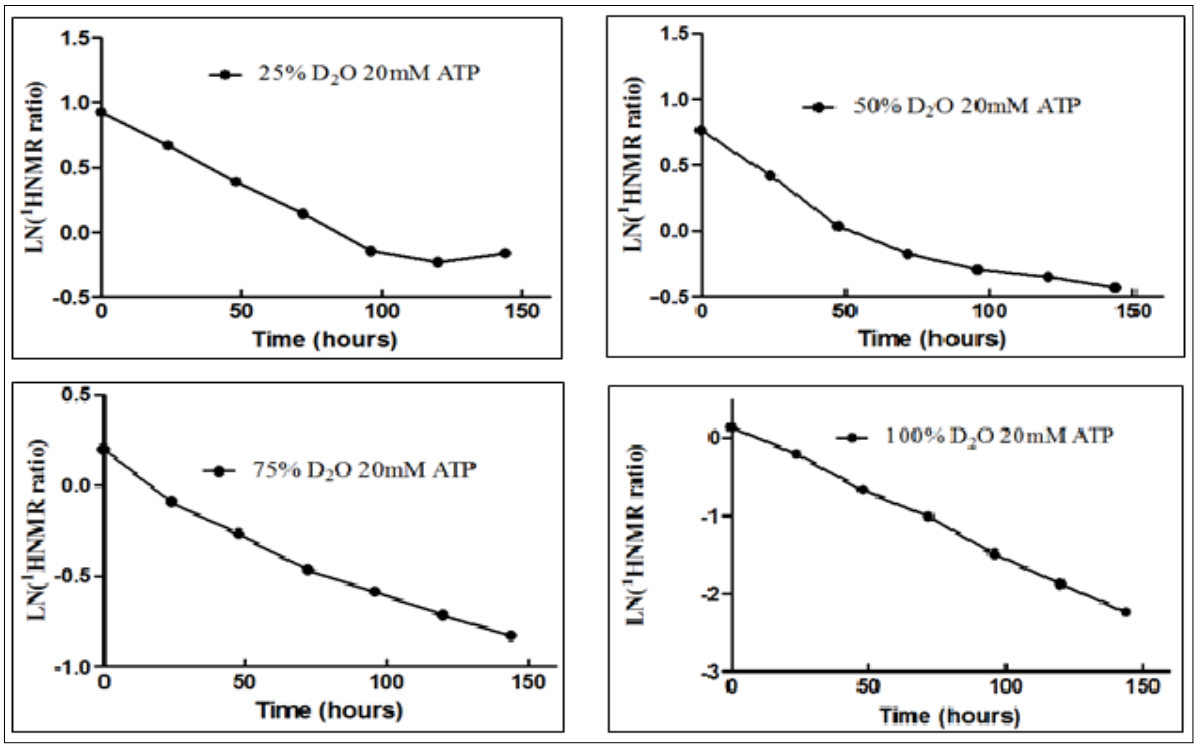

Figure 1.11: *Plot of ln[I_{rel}] versus incubation time as a function of deuterium oxide concentration.*

Table 1.2: *Second order rate constants for deuteration of ATP as a function of deuterium oxide concentration.*

Time / h	25% D_2O	50% D_2O	75% D_2O	100% D_2O
0.00	2.62	2.62	2.63	2.60
48.00	2.71	2.85	3.11	3.92
72.00	2.74	2.98	3.37	5.79
96.00	2.87	3.25	3.80	7.20
120.00	2.91	3.35	4.20	9.33
144.00	3.27	3.54	4.81	11.79

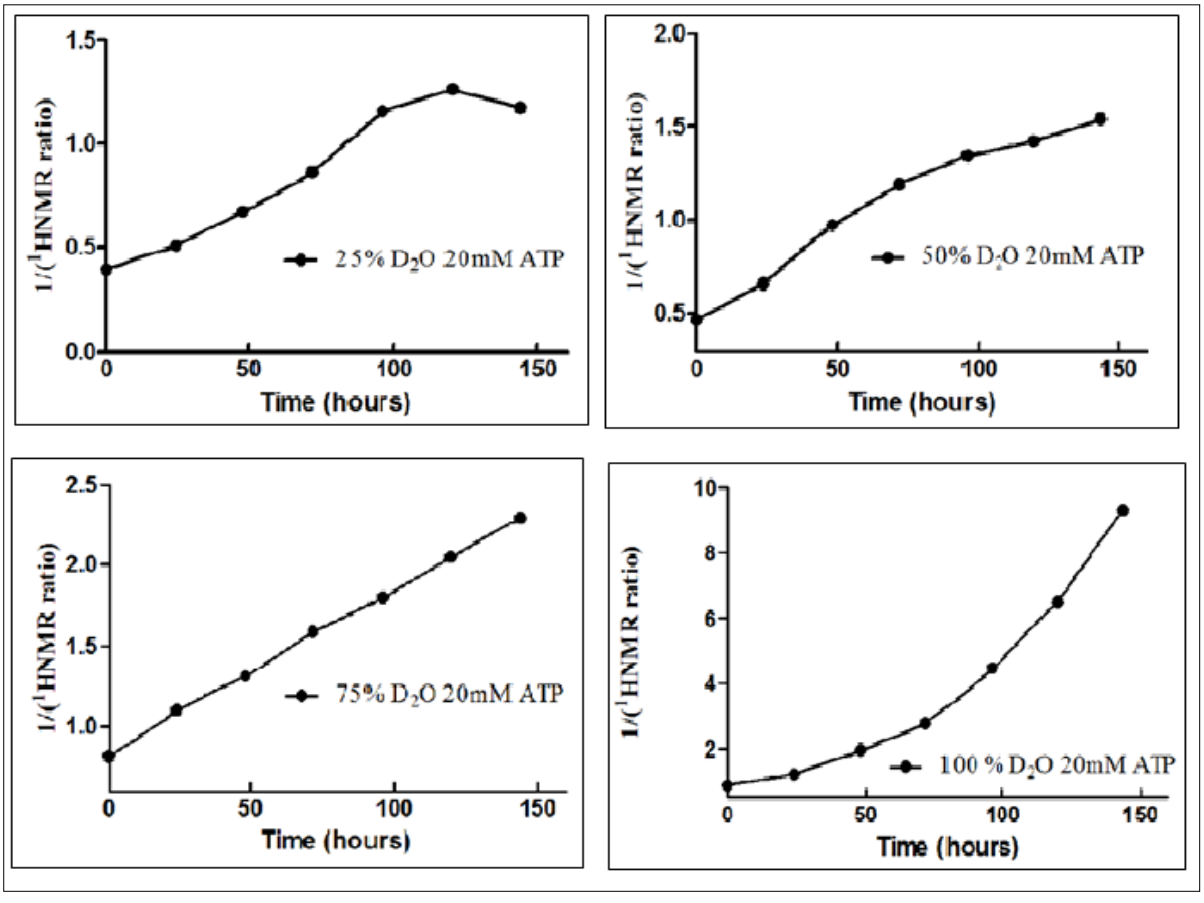

Figure 1.12: *Plot of $[I_{rel}]^1$ versus incubation time as a function of deuterium oxide concentration.*

Table 1.3: *First order rate constants of ATP hydrolysis as a function of deuterium oxide concentration.*

Time / h	25% D_2O	50% D_2O	75% D_2O	100% D_2O
0.00	0.00	0.00	0.00	0.00
48.00	-2.67	-2.26	-1.96	-1.90
72.00	-2.29	-1.86	-1.59	-1.50
96.00	-1.88	-1.66	-1.15	-1.08
120.00	-1.64	-1.39	-0.88	-0.82
0.00	0.00	0.00	0.00	0.00

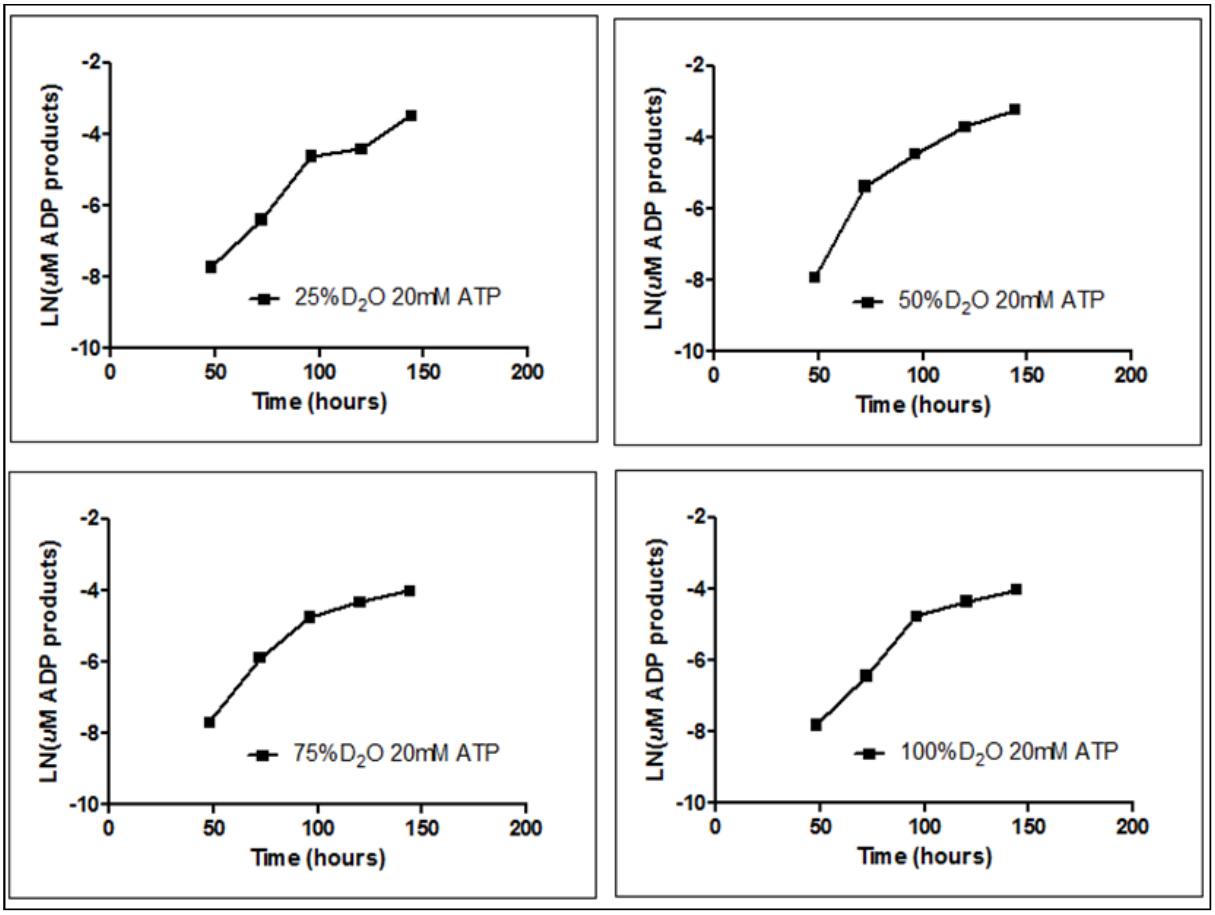

Figure 1.13: *Plot of ln[ADP] versus incubation time as a function of deuterium oxide concentration.*

Table 1.4: *Second order rate constants of ATP hydrolysis as a function of deuterium oxide concentration.*

Time / h	25% D_2O	50% D_2O	75% D_2O	100% D_2O
0.00	0.00	0.00	0.00	0.00
48.00	14.42	9.62	7.10	6.66
72.00	9.89	6.42	4.92	4.50
96.00	6.58	5.27	3.15	2.96
120.00	5.18	4.00	2.41	2.28
144.00	4.62	3.16	1.97	1.87

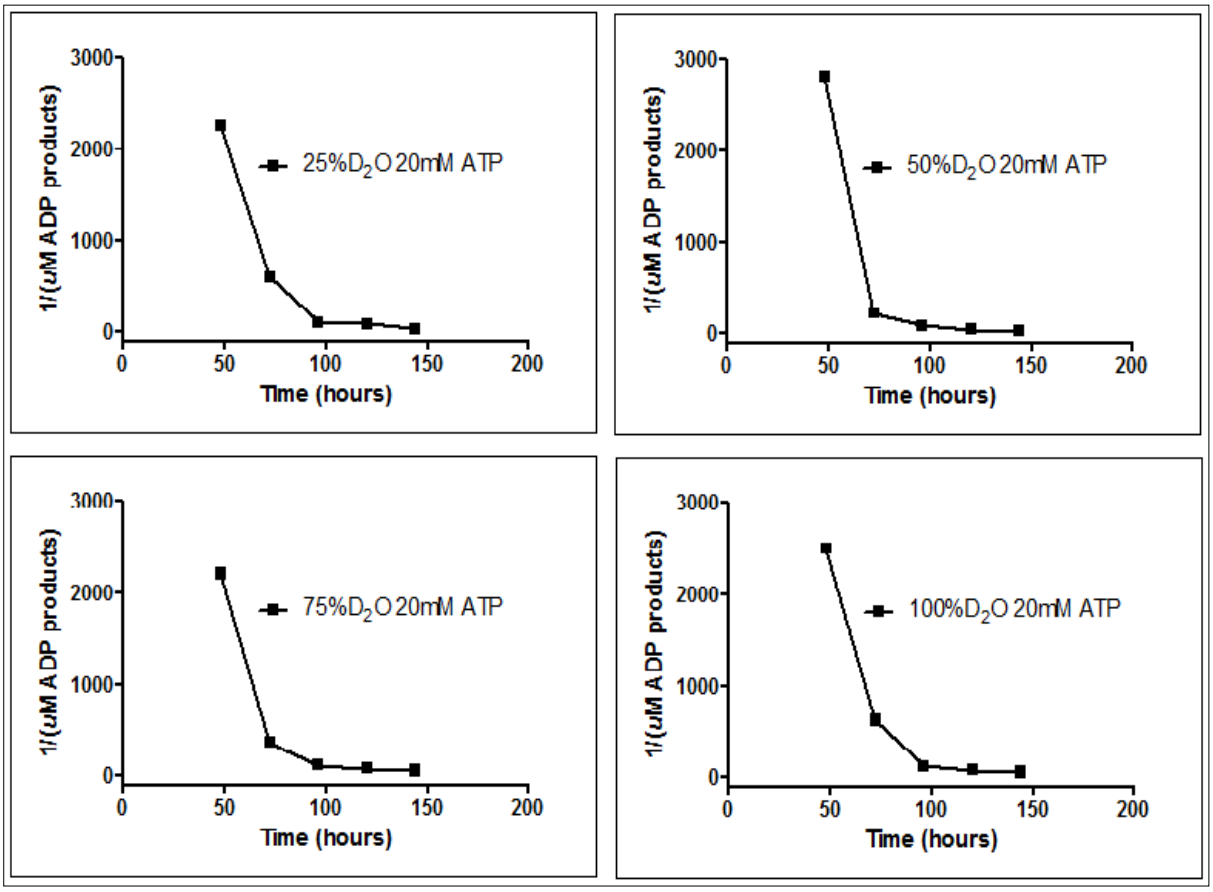

Figure 1.14: *Plot of $[ADP]^{-1}$ versus incubation time as a function of deuterium oxide concentration.*

1.3.3 Deuteration of various imidazoles and purines

The following **Table 1.5** (p.44) and **Figure 1.16** (p.45) show the percentage of deuteration of some imidazole- and purine-contaning compounds. The percentage was calculated as the ratio of I_{rel} calculated as before at time t_n with I_{rel} at t_0. An example showing how the calculation was performed is shown using **Figure A.1.17** in the **Appendix part one** (p.118). That figure is repeated here as **Figure 1.15.**

In **Figure 1.15**, the protonated (**A**) and deuterated (**B**) NMR spectra of 1-ethylimidazole with the proton signals **a, b** and **c** used in the calculation are shown. Here, **a** is the proton signal that was reduced by deuteration, **b** and **c** are reference or neighbouring proton signals in this molecule.

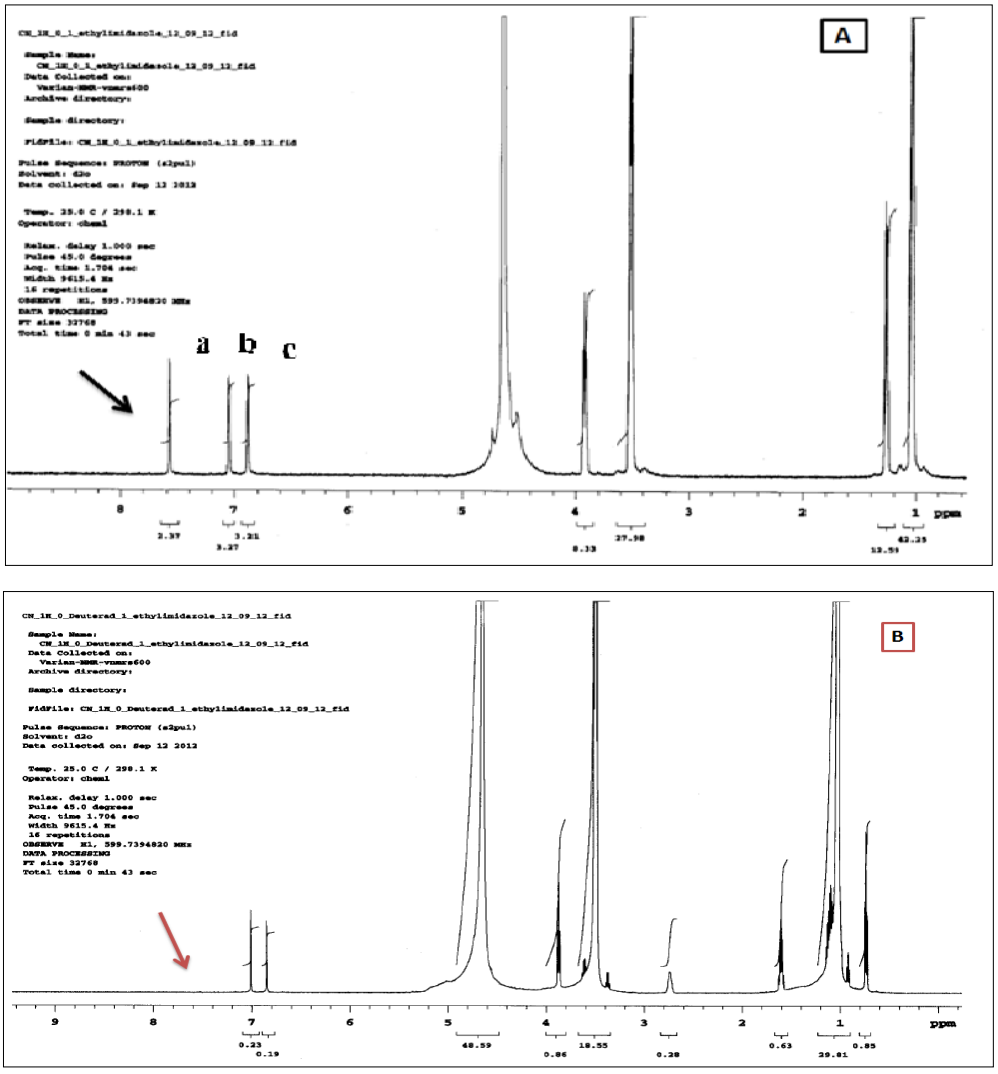

Figure 1.15: *^{1}H NMR spectrum of 1-ethylimidazole, before (**A**) and after (**B**) deuteration. The proton replaced by deuterium is shown by a black arrow in **A**, and its position by a red arrow in **B**.*

In this example, the integrated intensities used for t_0 from spectrum **A** are: I_a = 2.37, I_b = 3.27 and I_c = 3.21

I_{rel} at t_0 for spectrum **A** is given by:

$$I_{rel}(t_0) = I_a(t_0)/ [I_a(t_0)+ I_b(t_0)+ I_c(t_0)]$$
$$= 2.37/ (2.37+3.27+3.21)$$
$$= \underline{0.27}$$

I_{rel} at t_n for spectrum **B** is given by:

$$I_{rel}(t_n) = I_a(t_n)/ [I_a(t_n)+ I_b(t_n)+ I_c(t_n)]$$
$$= 0.00 / (0.00 + 0.23 + 0.19)$$
$$= \underline{0.00}$$

So, the degree of deuteration = $100\{1- [I_{rel}(t_n) / I_{rel}(t_0)]\}= 100\{1 - [0 / 0.268]\} = 100\%$.

Using a similar calculation, the deuteration percentages were calculated for all the purine and imidazole compounds (see **Tables and Figure in Appendix part one** (p. 111-130). Note that the position of deuteration is structure-dependant.

Table 1.5: *Percentage of proton-deuterium exchange in several 100µM purine and imidazole systems. All the compounds were deuterated by incubation at 60 ^{0}C for 5 days before analysis with ^{1}H NMR.*

Name of compound	**Figure number in appendix**	**% Deuterium substituted**
Adenine	Figure A.1.14	43.41
2-Iodoadenosine	Figure A.1.10	79.00
6-Benzylaminopurine	Figure A.1.6	70.00
Benzimidazole	Figure A.1.2	100.00
5-Methyl-4-nitroimidazole	Figure A.1.40	38.79
1-(3-Aminopropyl)imidazole	Figure A.1.30	100.00
4-Imidazolecarboxaldehyde	Figure A.1.26	100.00
1-Butylimidazole	Figure A.1.28	100.00
4(5)-Methylimidazole	Figure A.1.22	100.00
1-Ethylimidazole	Figure A.1.16	100.00
1(3)-Methylimidazole	Figure A.1.18	100.00
4-Imidazolecarboxylic acid	Figure A.1.24	100.00
4(5)-Hydroxymethylimidazole	Figure A.1.20	100.00
5-Chloro-1-methylimidazole	Figure A.1.38	100.00
2,6-Diaminopurine	Figure A.1.8	100.00
4,5-Dicyanoimidazole	Figure A.1.36	19.29
4-Nitroimidazole	Figure A.1.34	100.00
4-Azobenzimidazole	Figure A.1.12	65.12
1-Vinylimidazole	Figure A.1.32	100.00
1-Methylbenzimidazole	Figure A.1.4	100.00

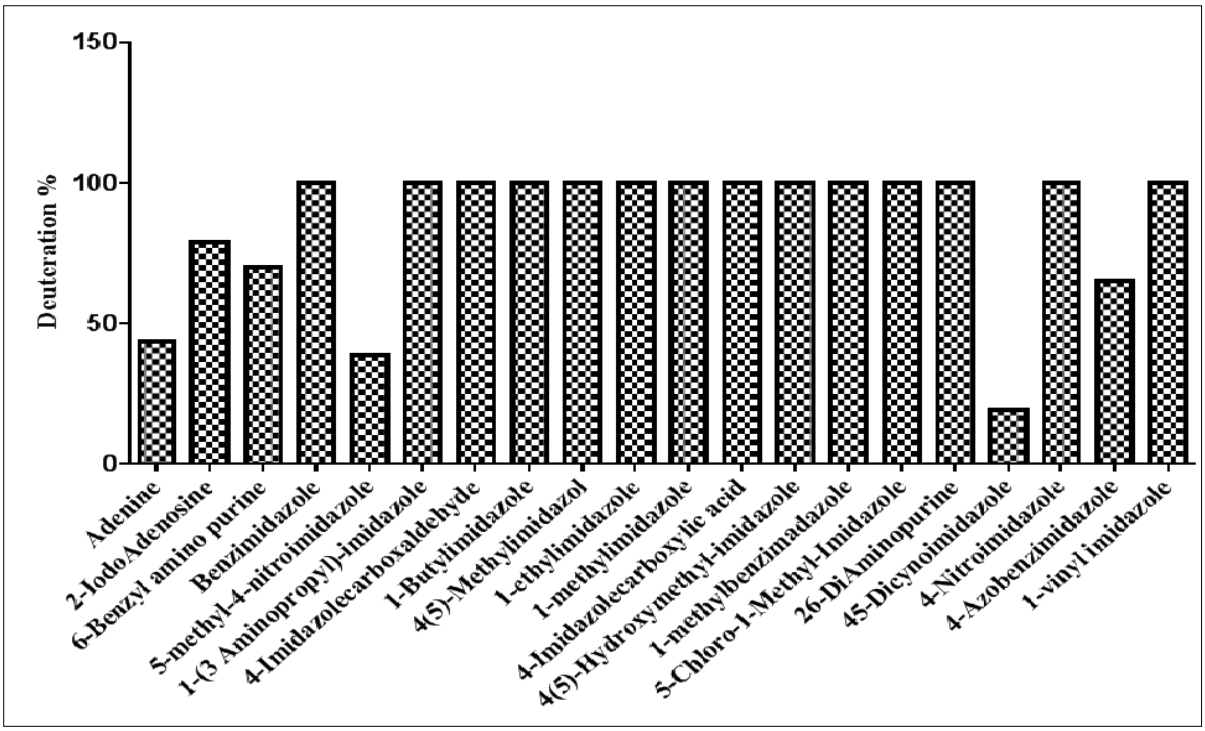

Figure 1.16: *Hydrogen-deuterium exchange as a percentage of deuteration for various imidazole- or purine-based compounds (see* ***appendix part one*** *(p. 111-130)).*

1.3.4 Synthetic substituted purines

Figure 1.17 shows the reaction mixtures using 2,6-dichloropurine as starting material separated on silica thin layer chromatography (TLC). On left-hand side is 2,6-dichloropurine (R_f 0.37), followed by the products 9-methylpurin-6-amine (R_f 0.51 and R_f 0.39), 9-ethylpurin-6-amine (R_f 0.73 and R_f 0.57) and 9-benzylpurin-6-amine (R_f 0.70 and R_f 0.79). The solvent front is indicated with a purple line in the **Figure 1.17**.

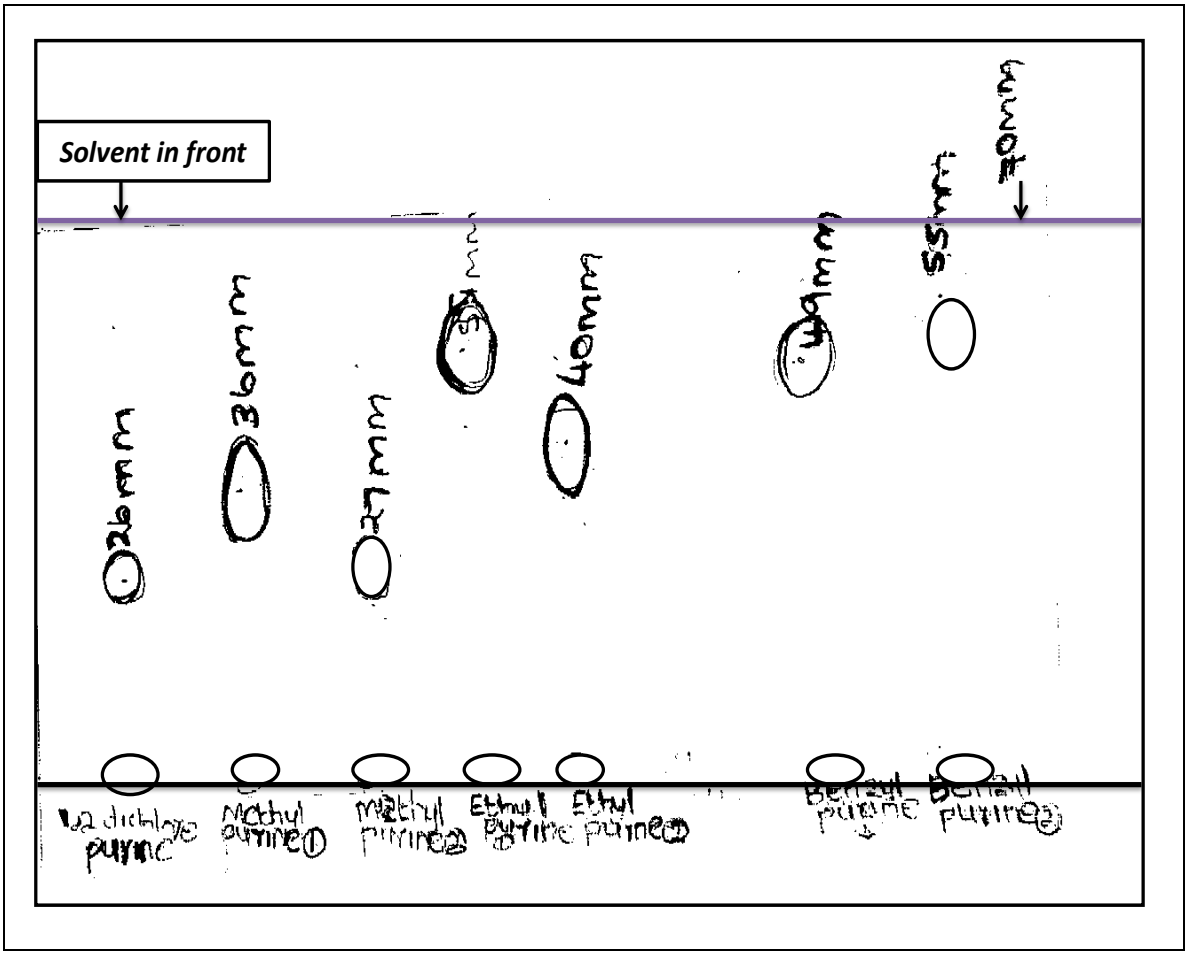

Figure 1.17: *TLC plate showing the different Rf values of three products synthesised from 2,6-dichloropurine.*

1.3.5 Discussion

The study done on ^{1}H NMR confirms that the rate of ATP deuteration at C8 depends on the concentration of deuterium oxide (D_2O) and ATP, as well as the incubation period at 60^{o}C (Heller, 1968). When the temperature was kept constant, the deuterium-proton exchange increases as the [D_2O] increases. As the deuteration increased, the ATP hydrolysis also increased, although not at the same rate. When the reaction was inspected by the reaction rate order method of Faizi *et al*., 2010 in **Figures 1.11-1.14** (p.38-41), it was clear that ATP hydrolysis was a first order reaction in [D_2O] because **Figure 1.14** did not form a straight line. The deuteration could be either 1st or 2nd order, as was shown in **Figures 1.11** and **1.12,** with nearly a straight line being formed in both instances**.**

The study also determined that hydrogen-deuterium exchange is not kinetically identical to ATP hydrolysis under the same conditions. The reaction rate order method supported that ATP C-8 deuteration was second order in both [ATP] and [D_2O]. The ^{1}H NMR spectrum also showed that the C-8 proton of the ADP thus formed is also deuterated in the process.

As indicated in the introduction, protons with successively higher acidity would sequentially be substituted with deuterium under these conditions. The ^{1}H NMR spectra of ATP showed that hydrogen/deuterium replacement began with the hydrogen located on 8ppm on the ^{1}H NMR spectrum, being the most acidic or deshielded of the protons in the ATP molecule. Once the hydrogen located in that position in molecule was fully deuterated, the second which is quarter deuterated, the proton/deuterium replacement took place on the next (second) de-shielded proton, which was located at 7.3ppm of ^{1}H NMR spectra while the third becoming partially deuterated. However, this replacement took a relatively longer time, reflecting its poorer reactivity compared to the first proton. As [D_2O] increased in the solution, the chance of intermolecular encounters increased, with a higher level of deuteration being observed with 100% D_2O using 20mM ATP as seen in **Figures 1.11** and **1.12**. This result is also apparent in the data of the **Appendix Part two Figure B.1.1- B.1.28 (**p.137 to 146). As previously indicated, the higher availability of deuterium in the solution assisted in proton/deuterium substitution, particularly at a higher [D_2O] when compared to the lower [D_2O] in solution.

The deuteration of imidazole- and purine-based molecules was found to occur in high yield, with more than 80% of the compounds being found to be >70% deuterated, as was apparent from **Figure 1.16** (p.45). Where deuteration of ATP was concerned, for the entire compound, the exchange was found to take place at the most deshielded location on the ^{1}H NMR spectrum as before.

CHAPTER 2: THE KINETIC ISOTOPE EFFECT (KIE) IN ACETATE KINASE, SHIKIMATE KINASE AND GLUTAMINE SYNTHETASE IN THE PRESENCE OF ATP OR ATP-*D*

INTRODUCTION

The enzymes acetate kinase, shikimate kinase and glutamine synthetase all catalyse the hydrolysis of ATP to produce ADP or AMP. Energy stored in ATP is released upon hydrolysis of the phosphoric anhydride bonds. The primary phosphate group on the ATP molecule that is hydrolysed when energy is needed to drive anabolic reactions is the γ-phosphate group. Located the farthest from the ribose sugar, it has a higher energy of hydrolysis than either α- or β-phosphates. The bonds formed after the phosphorylation of a substrate residue by ATP are lower in energy than the phosphoric anhydride bonds of ATP.

During enzyme-catalysed hydrolysis of ATP, or phosphorylation by ATP, the available free energy can be harnessed by a living system to do work. This chapter deals with the chemical structure of ATP, the role of the adenyl moiety in the phosphorylation reaction mediated by ATP in all three enzymes, as well as the importance of these enzymes in various aspects of biological chemistry. From a kinetic / mechanistic point of view, the reaction proceeds as follows:

$$E + S \leftrightarrow ES \leftrightarrow ESP \rightarrow E + P$$

where E is the enzyme involved, S is the substrate and P is the product of the reaction. Initially the enzyme (E) combines with the substrate (S) and form an intermediate complex (ES). The enzyme then partially converts some of the substrate to yield another intermediate that now includes some of the product as part of the intermediate complex. This is not a simple process, with the mechanism depending on many factors, including pH, the concentration of the reactants and products, incubation period and also temperature. This part of the study focuses on specific activity of the enzymes together with the kinetic isotope effect (KIE), which is used to compare ATP and its deuterated analogue as co-substrates for some selected enzymes. Graph Pad Prism 6 software was used to analyse for a KIE in enzyme co-substrate reactions, before and after deuteration of the co-substrate, specifically focussing on the behaviour of ATP-dependant enzymes.

2.1 Acetate kinase (AK)

Acetate kinase (AK) was discovered in 1944 by Lipmann and first isolated in 1954 by Ochoa (Buss *et al*., 2001). The enzyme is a prototypic carboxylate kinase and is one of the earliest recognized phosphoryl transfer enzymes (Buss *et al.*, 2001). AK is found in aerobic as well as

anaerobic microorganisms, archaea, fungi and mammals. It plays a major role in global cycling of carbon by anaerobic decomposition of organic matter to methane (Schmidt, Biegel, & Müller, 2009). AK catalyses the transfer of the phosphoryl moiety from ATP, to the carboxylate group of acetate to form acetyl phosphate and ADP. The reaction is shown in **Figure 2.1** (Mukhopadhyay, Hasson, & Sanders, 2008):

$$ATP + Sodium\ acetate + Mg^{2+} \leftrightarrow ADP + acetyl\ phosphate + Mg^{2+}$$

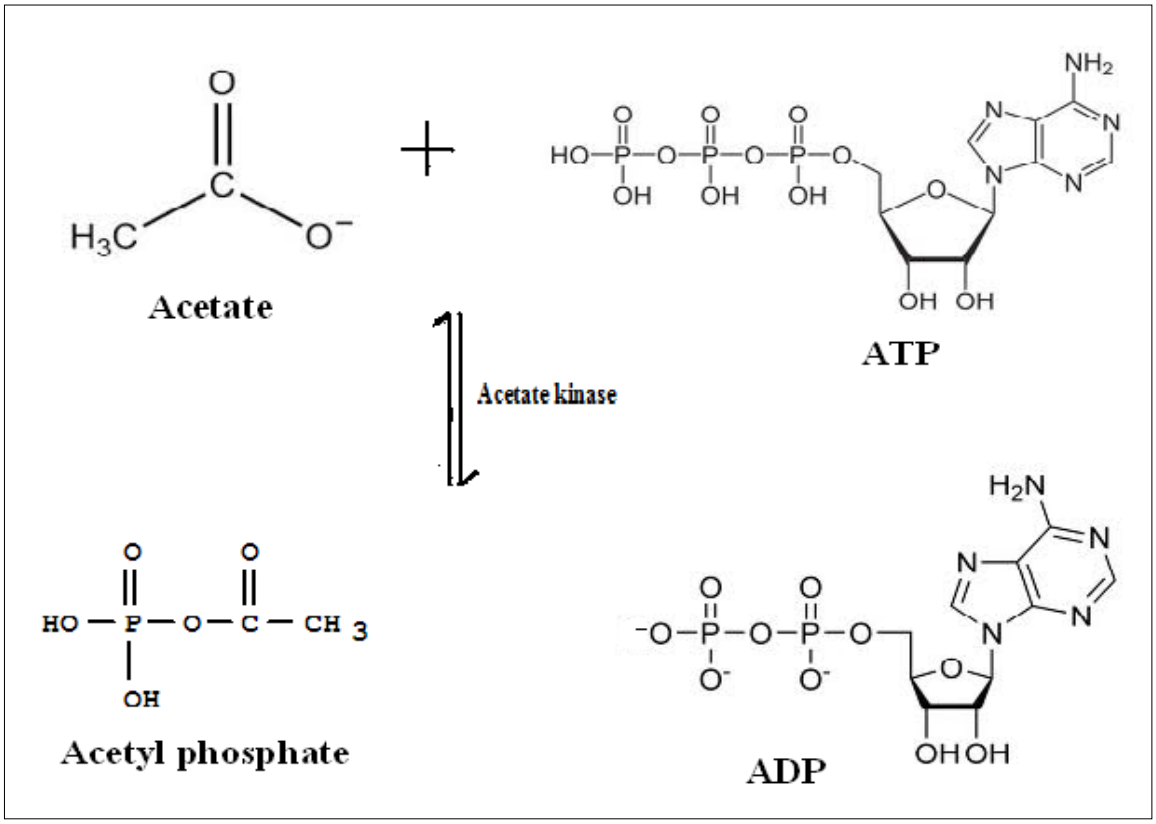

Figure 2.1: *Acetate kinase catalyses the reaction between acetate and ATP to produce acetyl phosphate and ADP or AMP (Mukhopadhyay et al., 2008).*

The enzyme is central to carbon and energy metabolism and has been demonstrated to be a member of ASKHA (Acetate and sugar kinase Hsp70, actin), a phosphotransferase super family (Kenyon *et al*., 2011; Mukhopadhyay *et al*., 2008; Scapin, 2002). Together with acetyl-coenzyme A (Acetyl-CoA), AK is a key bacterial synthetic enzyme. Synthesis of acetyl phosphate is an important biosynthetic product that is converted to Acetyl-CoA by phosphotransacetylase (PTA) according to:

$$Acetyl\text{-}phosphate + CoA + PTA \leftrightarrow Acetyl\text{-}CoA + P_i$$

It is also a potential regulator of bacterial signal-transduction (Buss *et al*., 2001). **Figure 2.2** shows example of the structure of an AK enzyme, whose structure can be likened to that of a hamburger, i.e. two halves of a bun enclosing an ATP 'patty'. The upper 'bun' in blue (left

upper black arrow) represents the N-terminal part of the complex, while the red ribbon (left lower arrow) forms the lower 'bun', or C-terminal part of the structure. The ATP molecule (right middle arrow – space-filling model) is shown 'sandwiched' between the C-terminal and the N-terminal ends, forming the 'hamburger patty' in the **Figure 2.2**. This site between the two 'buns' binds ATP or its deuterated analogues, and is the focus of the present investigation that will be discussed at length in the next section.

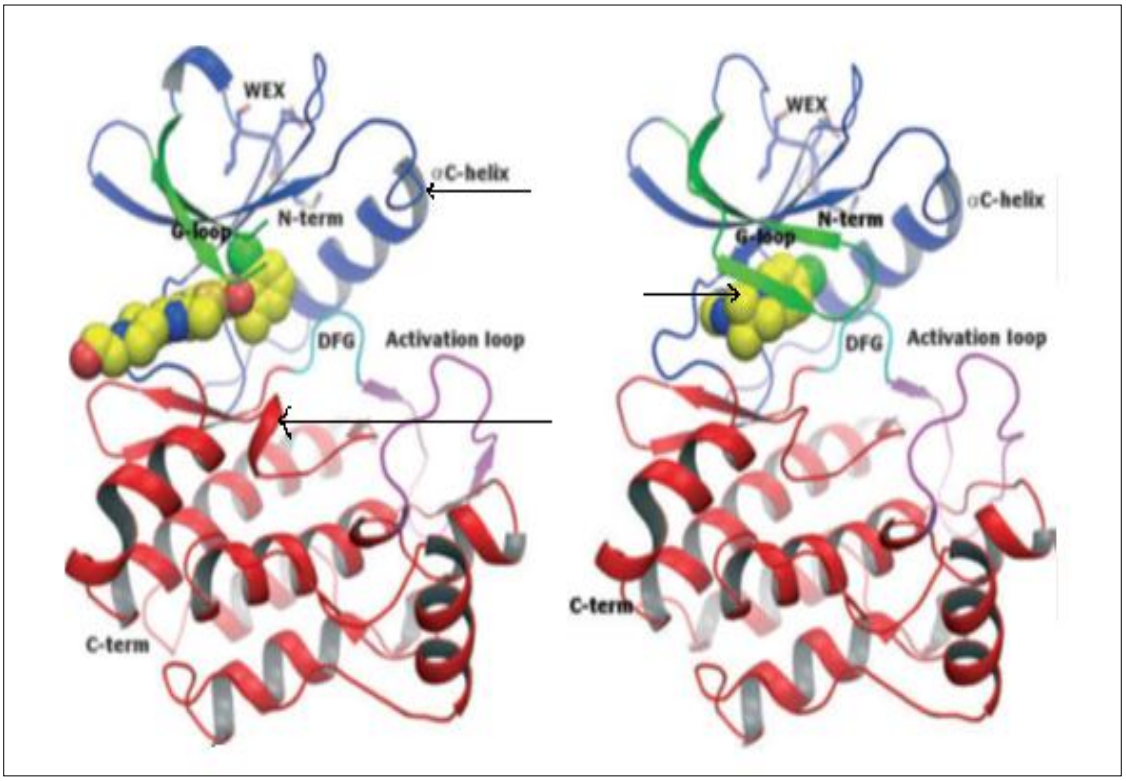

Figure 2.2: *Crystal structure of (bone marrow kinase) an example of acetate kinase with the N-terminus in blue (upper left arrow), and the C terminus in red (lower left arrow). ATP is shown in the binding cleft as a space-filling model (middle right arrow) (Muckelbauer et al., 2011).*

2.1.1 ATP complexes with acetate kinase

Previous studies done on the interaction of ATP with kinases has revealed that this interaction is most likely governed by the structure of both ATP and the enzyme. The resultant complex formation is believed to play an important role in enzyme activity. In particular, the adenine moiety of ATP binds in the hydrophobic pocket of AK formed from residues Val57, Leu49, Ala70, Meth120 and Tyr122 on a β-sheet (Ingram-Smith *et al*., 2005). The adenine moiety is anchored via a hydrogen bond to the select group of amino acids in the ATP binding pocket of AK. The existence of this hydrogen bond is important, because if the hydrogen bonding group is replaced with a hydroxyl group, the level of enzyme activity is diminished (Zheng et

al., 1993); Suwal *et al*., 2012). Additionally, the ribose sugar is hydrogen-bonded through the 2'-OH, while all the ATP phosphates project towards the loop and interact with residues from both domains. The α- and β-phosphates then interact with Lys72 in the β-strand and Glu91 in the α-helix.

The γ-phosphate extends towards the solvent-accessible region of the binding site, and is hydrophilic. In this manner, both enzyme and ATP adenine structure facilitate the transfer of the γ-phosphate to the hydroxyl group of the amino acids of a particular substrate (Gorrell *et al.*, 2005). AK thus forms an interaction pocket, allowing the γ-phosphate group to function as part of a catalytic cycle that includes a hydroxyl group of the target co-substrate (Gorrell *et al*., 2005). The metal ion (Mg^{2+}) coordinates to the α- and β-phosphate groups through their oxygen atoms, helping to position the γ-phosphate correctly with respect to this co-substrate hydroxyl group (Ingram-Smith *et al*., 2005). The enzyme facilitates the transfer of γ-phosphate to carboxylate of acetate to produce acetyl phosphate and ADP (Gorrell *et al., 2005*; Mukhopadhyay *et al*., 2008).

2.2 Shikimate kinase (SK)

Shikimate kinase is the fifth enzyme in the shikimate pathway. SK specifically catalyses the reversible transfer of γ-phosphate from ATP to the 3-hydroxyl group of shikimic acid to yield shikimate 3-phosphate and ADP. The reaction is shown schematically in **Figure 2.3** (Cheng, Chang & Wang, 2005; Pereira *et al*., 2004). The reaction is as follows:

$$\text{ATP} + \text{Shikimate} + Mg^{2+} \leftrightarrow \text{Shikimate 3-phosphate} + \text{ADP}$$

There are two isoforms of shikimate enzyme: SK-I and SK-II: both share 30% homology of their DNA sequences (Krell, Coggins & Lapthorn, 1998). This study uses SK-II, which is involved in the synthesis of chorismate.

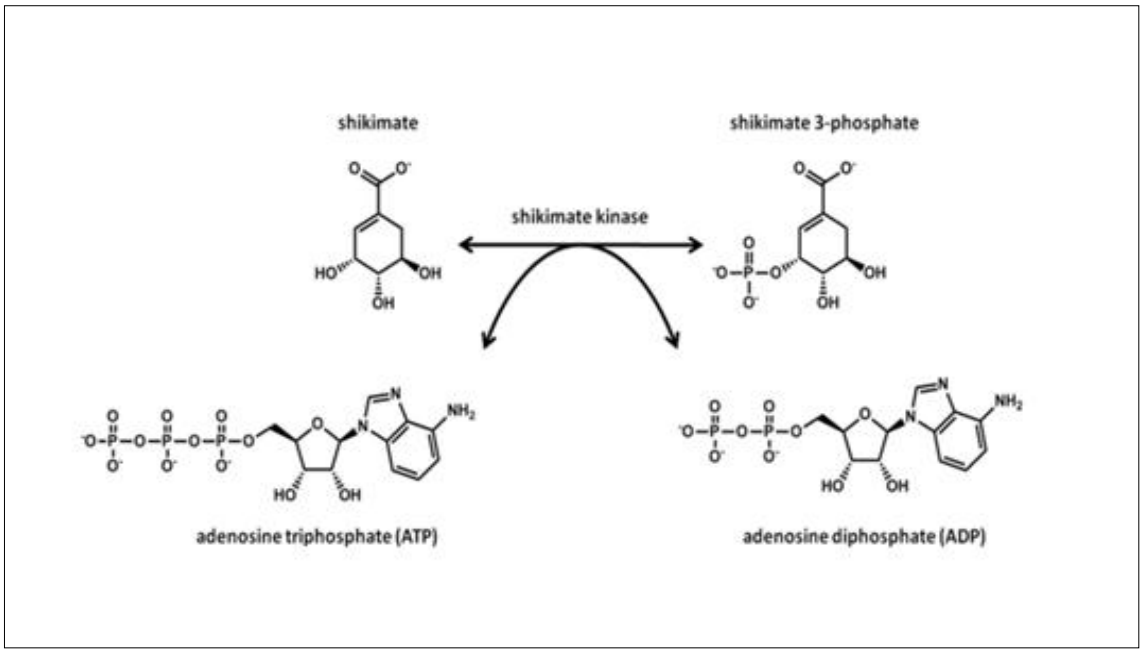

Figure 2.3: *Shikimate kinase catalyses the conversion of shikimate to shikimate 3-phosphate while ATP is hydrolysed to ADP or AMP (Daugherty et al., 2001).*

The role played by SK-II in synthesizing chorismate is particularly relevant to combating infections caused by pathogens such as *Mycobacterium tuberculosis*, which requires SK-II for the maintenance of biochemical pathways, including the synthesis of chorismate (Daugherty *et al*., 2001). In general, SKs have become a target for synthesis of antimicrobial and herbicidal agents (Krell, Coggins & Lapthorn, 1998) mainly because of co-infection with human immunodeficiency virus (HIV) in individuals also infected with tuberculosis (TB) (Reichau *et al*., 2011). The resultant increase in mortality in certain sectors of the South African population, particularly in the Western Cape, makes finding effective ways to combat these ailments a crucial task for improving the future health of this society. While many studies have been conducted for potential inhibitors of enzyme activity of various pathogens (Kumar *et al*., 2010), very few were designed to compare activity of their equivalent deuterated analogues as potential inhibitors (Vonrhein, Schlauderer & Schulz, 1995).

The shikimate kinase enzyme consists of five β-strands in the order of β2, β3, β1, β4 and β5 surrounded by α-helices (**Figure 2.4 A**&**B**). These β-strands are separated from one another on either side by α-helices. When the linkage of the structure is viewed from the N-terminal to the C-terminal end, the series of α-helices are as follows: α1 and α8 on one side α4, α5 and α7 on the other crosswise, as seen on the **Figure 2.4B** (Krell, Coggins & Lapthorn, 1998).

This particular study uses a shikimate kinase enzyme from *Mycobacterium tuberculosis (MtSK*), which is classified under the kinase family of nucleoside monophosphate kinases. All nucleoside monophosphate kinases have five β-strands occurring parallel to each other to form the active site (Filgueira de Azevedo *et al.*, 2002; Kenyon *et al.*, 2011). In general, enzymes of this type have four domains based on changes occurring when ATP binds to the reactive site. These domains are: the shikimate binding (SB) domain, LID domain, nucleotide binding (NB) domain and reduced core domains (**Figure 2.4B**, (Krell, Coggins & Lapthorn, 1998).

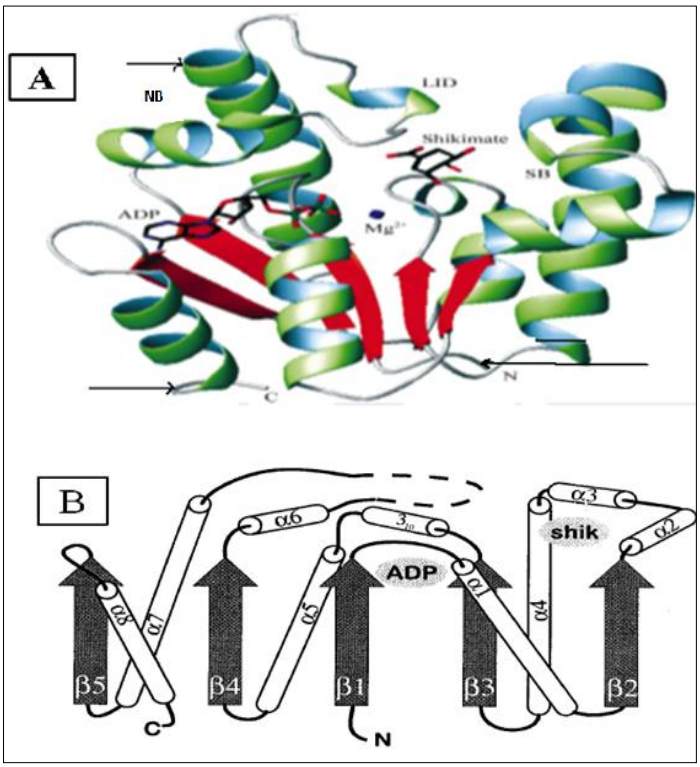

Figure 2.4: ***A****: 3D structure of shikimate kinase with ADP and shikimate bound in their respective sites. β-strands are indicated in red, and α-helices in green, with the position of the* Mg^{2+} *ion in dark blue;* ***B****: schematic representation of the linkage of α-helices and β-sheets in the enzyme (A: Pereira et al., 2004; Krell, Coggins & Lapthorn, 1998).*

2.2.1 Reactions taking place in the active site of *MtSK*

Referring to **Figure 2.4** in **A**, the adenine moiety of ATP is held in between the Arg110 and Pro155, while the LID domain loop interacts with the γ-phosphate during the catalysis step of the reaction. Arg117 binds with the α- and β-phosphates and water to stabilise the transition state created by the negative charge on the oxygen atom from the α-β bridge. The six-coordinate bond of Mg^{2+} ion is disrupted by attachment of the shikimate to form the Mg^{2+}-

MtSK-ADP-shikimate complex. The Mg^{2+} ion in this intermediate forms a complex with the β-phosphate oxygen of ADP, four water molecules and Asp34 (Pereira *et al*., 2004).

2.3 Glutamine synthetase (GS)

Glutamine synthetase (GS) is found in prokaryotes, plants and animals, and plays an essential role in the nitrogen metabolism of all living organisms (Occhipinti *et al*., 2010). In *E. coli,* the enzyme has a molecular weight of 600 kDa and is composed of 12 identical subunits that are arranged in two superimposed hexagonal rings (Bodasing *et al*., 1985; Stadtman., 2001). This enzyme, due to its shape, is referred to as a snowflake molecule, and is principally active when the cell experiences nitrogen-limiting conditions. GS activation is modulated by covalent attachment of one adenosine monophosphate group to each subunit of the structure (known as adenylylation). GS catalyses the reversible conversion of L-glutamic acid to L-glutamine using ATP, as shown in **Figure 2.5** (Stadtman, 2001):

$$\text{Glutamate} + NH_3 + \text{ATP} + Mg^{2+} \leftrightarrows \text{Glutamine} + \text{ADP} + Mg^{2+}$$

The GS catalyses the attachment of γ-phosphate atom from ATP to the glutamate, forming glutamyl-phosphate in the presence of ammonia, is converted into glutamine (Krajewski *et al*.,2008).

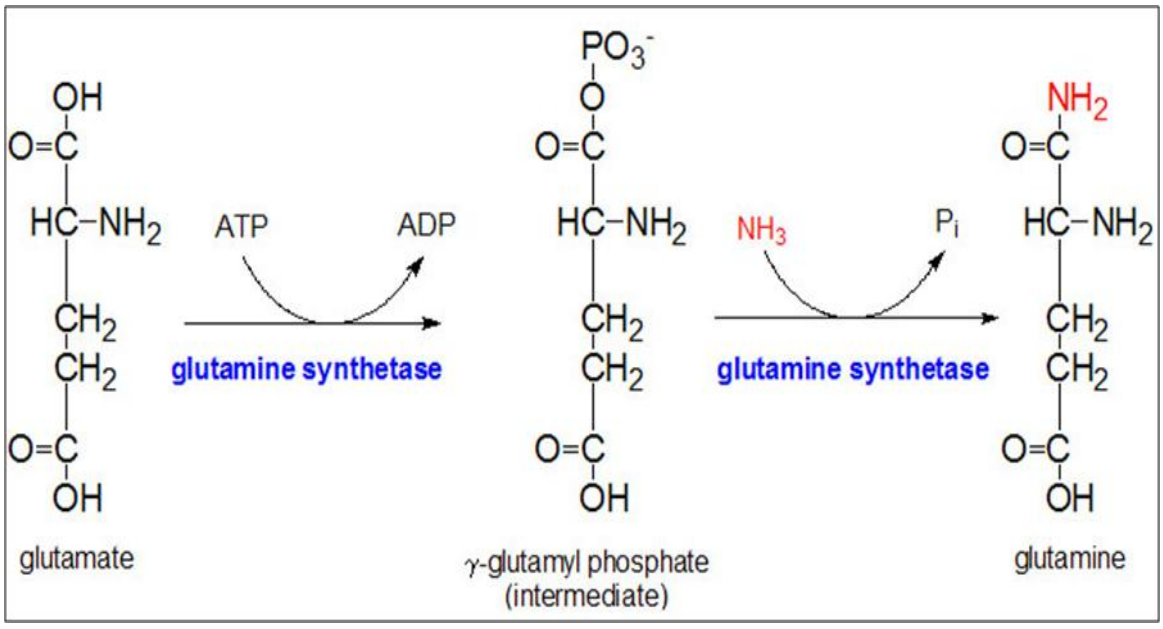

Figure 2.5: *Glutamine synthetase converts glutamate to glutamine by phosphorylation ATP to a γ-glutamyl phosphate intermediate. The γ-glutamyl phosphate intermediate is converted to glutamine via nucleophilic attack by ammonia (http://themedicalbiochemistrypage.org/nitrogen-metabolism.php).*

The active site is found in between the intra-ring subunits. Ammonia and ATP enter via a channel at the interface between the rings (**Figure 2.6 A** and **B)** (Wray & Fisher, 2010). A metal ion in the active site helps to properly orientate ATP, ammonia and glutamate (**Figure 2.6 A**). The GS enzyme exists in either adenylylated or deadenylylated form (Ronzio, Rowe & Meister, 1969; Stadtman, 2001; Ferguson and Sims, 1974).

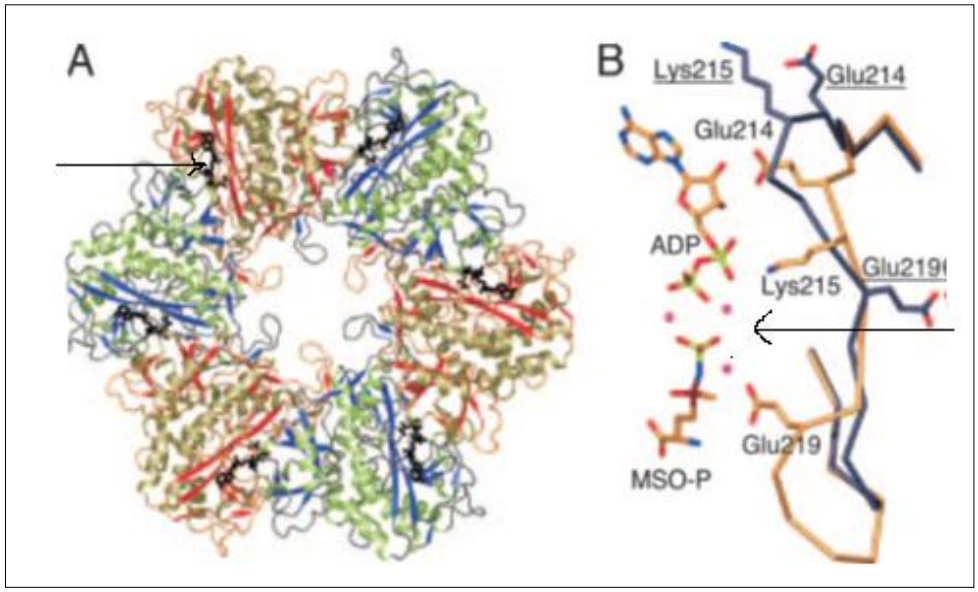

Figure 2.6: ***A****: Hexameric structure of GS with bound ATP/ADP (black stick, indicated by the Arrow). The beta- sheets of various monomers are marked in orange or blue lines.* ***B****: ATP/ADP binding site with a glutamate mimic (methionine sulfoximine or metsox, indicated as MSO-P), ADP and three* Mg^{2+} *ions (indicated by the arrow) bound (Krajewski, Jones & Mowbray, 2005; Krajewski et al., 2008).*

As previously mentioned, GS is found in both plants and animals, where it catalyzes the ATP-dependent formation of glutamine from glutamate (Zozaya-Hinchliffe *et al*., 2005; Eisenberg *et al*., 2000). GS in plants and animals does not undergo the adenylylation/ deadenylylation cascade, which is typical of prokaryotic organisms. However, in the majority of plants, the GS enzyme pairs with glutamate synthase to deaminate the product glutamine and form two molecules of glutamate (Occhipinti *et al*., 2010). Plant GS occurs in two forms, GS1 and GS2, based on subcellular location (Cullimore & Sims, 1981). GS1 is located in the cytoplasmic matrix, while GS2 is found in the plastids of plant cells (Simonović & Anderson, 2008; Occhipinti *et al*., 2010).

2.4 Commonalities between shikimate kinase, glutamate kinase and acetate kinase

Shikimate kinase, acetate kinase and glutamine synthetase all have commonalties with the transferral of the γ-phosphate from ATP to the carboxyl group of the co-substrate, resulting in the formation of ADP or AMP, together with a new phosphorylated co-substrate.

2.5 Kinetic isotope effect resulting from selective deuteration of substrate of an enzyme

The Kinetic Isotope Effect (KIE), in the present context, refers to the ratio of the reaction rates determined from the reaction with a fully protonated molecule, relative to its counterpart, that has been selectively deuterated at a mechanistically active position (Wade, 1999), i.e.:

$$KIE = K_H / K_D$$

As such, the deuterated substrate molecule ends up with higher molar mass, due to a doubling of the mass of the labile (and mechanistically relevant) proton (Hennig, Oswald & Schmatz, 2006). Further, the C-D (deuterium) bond is shorter and stronger than the equivalent C-H bond (Wade, 1999). This causes changes in the enzyme catalysis reaction itself (Vigano *et al*., 2004), giving rise to anomalies resulting from mass defects in the enzymatic reaction, that are identifiable using kinetic analysis. The binding energy of the reaction may also be affected by the deuteration process (Sen & Kohen, 2010).

2.6 Materials and methods

2.6.1 Acetate kinase assays

Acetate kinase was purchased from Sigma-Aldrich. A stock solution of 0.0005U/ml was prepared in deionised water and stored at -20^{o}C until required.

2.6.1.1 Acetate kinase time assays

Each assay contained 26.67mM Trizma-HCl pH 6.8, 3.667mM sodium acetate, 0.034mM $MgCl_2$, and 0.4mM ATP in a 5ml test tube. All the reagents were in the tube prior to addition of the enzyme, which was stored in an Eppendorf tube in an ice cooler box. For each reaction mixture, a time zero sample was taken prior the addition of the enzyme. Following addition of the enzyme, the solution in each of a series of tubes was quickly mixed and placed in a 37^{o}C incubator. Thereafter, a 350µl aliquot of the reaction mixture was removed from each vessel at 15, 30, 60, 120, 180, and 240 min after enzyme addition and transferred to a 1.5ml Eppendorf tube. Each aliquot was treated with 3µl of 63mM trichloroacetic acid (TCA) to

denature the protein, and the resulting solids removed by pelleting with a bench top centrifuge. After carefully labelling of the aliquots according to incubation time, the materials were stored on ice for later analysis. The mixtures were divided into 110µl triplicates, loaded into HPLC vials and analysed by HPLC to determine amount of ADP produced as a function of incubation time.

2.6.1.2 Acetate kinase ATP or ATP-d concentration assay

Each assay contained 26.67mM Trizma-HCl pH 6.8, 3.667mM sodium acetate, 0.034mM $MgCl_2$, 0.0005U/ml acetate kinase in a 1.5ml test tube. The effect of ATP or ATP-*d* concentration was determined over a range of concentrations (200, 400, 600, 800, 1000, 1200 and 1400 µM) (Kenyon *et al*., 2011). The reactions were prepared without enzyme and incubated at 37^{o}C for five min before addition of 924µl in 10ml volume of 0.0005U/ml enzyme stock solution, except for each blank which did not contain enzyme. Reactions were terminated after 30min with an addition of 2µl of 63mM of Trichloroacetic acid (TCA) and immediately centrifuged. The AMP, ADP, ATP concentrations were determined by HPLC. All enzyme activities were expressed as specific activities [(µmole ADP formed).min^{-1}. (mg protein)$^{-1}$]. The kinetics of the enzymes was determined using Graph Pad Prism software.

2.6.2 Shikimate kinase

Shikimate kinase was cultured, purified and isolated from a recombinant *Escherichia coli* production strain which contained an expression vector including the gene coding for SK, obtained from the laboratory of Chris Abell, University of Cambridge. SK was cloned and purified using the following method: *E. coli* was used as a vector because it is a cheap, manageable, well-studied bacterium capable of producing both types of SK; however, the SK-II is the most active isoform in this bacterium.

2.6.2.1 Insertion of the SK-encoding gene into an *E. coli* system

Plasmid pBAN0209 containing the *M. tuberculosis aroK* gene encoding *MtSK*, was supplied by the laboratory of Chris Abell, University of Cambridge. pBAN0209 consists of the *aroK* gene cloned into the pET15b (Novagen) system, resulting in the IPTG-inducible expression of an enzyme containing the N-terminal 6-His purification tag, as indicated in the vector diagram in **Figure 2.7** (Rosado *et al*., 2013)

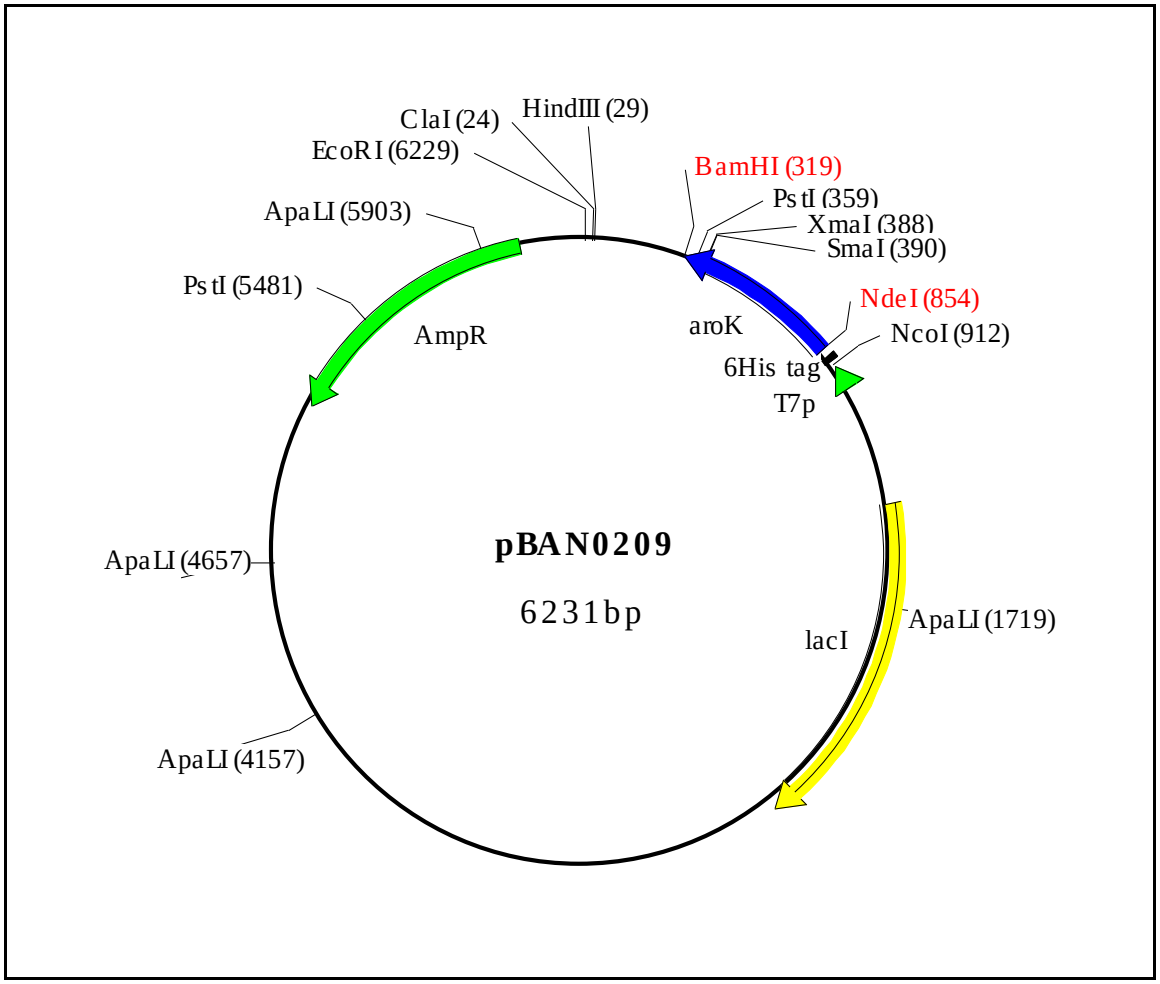

Figure 2.7: *Diagrammatic representation of a vector containing the aroK gene for use in an E. coli expression system.*

2.6.2.2 *MtSK* Expression and Purification

E. coli BL21(DE3) competent cells were transformed with the pBAN0209 vector for subsequent IPTG-induced gene expression. Single colonies were selected for inoculation into 50ml LM + Amp_{100} (liquid medium containing 5g of NaCl, 10g of yeast extract,10 of tryptone +100 µg/ml ampicillin) and cultivated overnight at 37°C, after which 2.5ml of this culture was transferred to 250ml of the same medium. Cultivation continued until $OD_{600} \cong$ 0.5-0.8 was recorded on a PerkinElmer lambda 35 UV/VIS spectrometer. 250µl 1M IPTG (Isopropyl β-D-1-thiogalactopyranoside) was added for induction of gene expression under control of the T7*lac* promoter and the culture was grown at 30°C overnight.

The biomass from a 250ml culture flask was harvested, re-suspended in 20ml Binding Buffer (500mM NaCl, 40mM Tris, 5 mM imidazole pH 7.9) and sonicated for 20min on a 50% on-off cycle. The sonicated mixture was then centrifuged at 10000rpm in an SS34 rotor for

10min at 4°C, after which the supernatant was clarified through a 0.45 µm syringe filter and loaded onto the Bio-Rad Profinia Protein Purification System. Analysis of the different fractions from the purification was carried out using an 11% SDS-PAGE system (Vonrhein, Schlauderer, & Schulz, 1995) that indicated the presence of a major band in the 28kDa range (**Figure 2.8**).

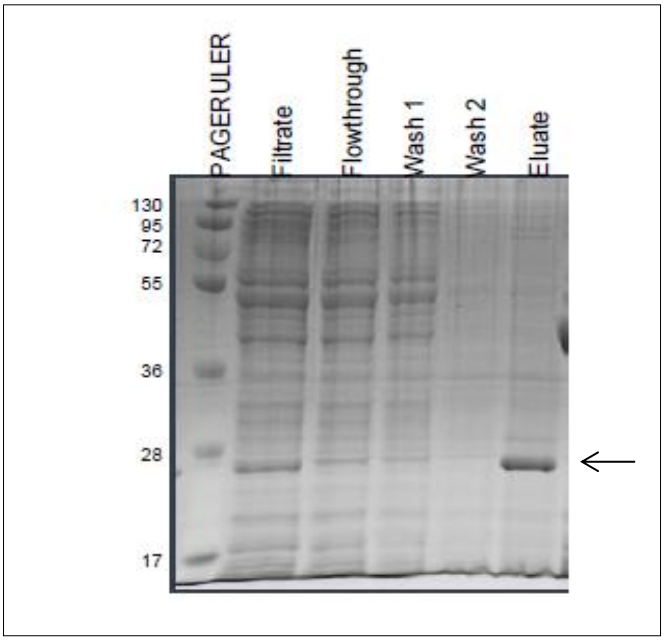

Figure 2. 8: *An SDS-PAGE gel comparing the migration of the purified sample of shikimate kinase. The molecular weight marker is in the first lane (sizes in kDa on the left) followed by the filtrate loaded onto the Profinia column, the flowthrough, two wash steps, then the eluate in the last lane, containing the MtSK protein (indicated by the arrow).*

Dialysis of the eluted protein was carried out overnight at 4°C using Pierce Snakeskin Dialysis tubing with a 10 kDa Molecular Weight Cut-Off (MWCO), in Dialysis Buffer (50mM Tris pH 7.5, 1M NaCl) (Rosado *et al*., 2013; Vonrhein *et al*., 1995). Aliquots of the dialysed enzyme were snap-frozen in liquid nitrogen and stored at -75°C until needed. When required, shikimate kinase concentration was determined by Qubit® 2.0 Fluorometer.

2.6.2.3 Time assay analysis by shikimate kinase (*MtSK*)

The stored *MtSK* was diluted with deionised water to make a 0.0001U/ml stock solution and stored at -72^{o}C until needed. The SK time assay contained a solution made up of 100mM KH_2PO_4/K_2HPO_4 (pH 6.8), 0.02mM $MgCl_2$, 0.2mM ATP, 10mM KCl and 2mM shikimic acid. A 750µl of the diluted 0.0001U/ml *MtSK* was added to 5ml of this stock solution,

initially kept at 4°C, and the mixture was then vortexed and transferred to a 37°C ProBlot™ Jr Oven. A series of 350µl aliquots were taken at 0, 30, 60, 90, 120 and 180min and transferred to 500µl Eppendorf tubes. The reaction in each tube was then terminated by addition and subsequent vortexing with 2µl of a 5.7mM EDTA stopping reagent. 110µl amount of each terminated reaction was then transferred into HPLC vials, in triplicate and analysed. Once HPLC spectra were generated, the data for each reaction was recorded and reworked using Graph Pad Prism software in order to plot time specific activity graphs.

2.6.2.4 Shikimate kinase stability assay

Two different assays were performed, namely *time* assays and *stability* assays. In the time assay described in the previous section, the reaction mixture was incubated at 37°C, and at each time interval a sample was taken for analysis. With the stability assay, the reaction mixture was kept at 4°C for each time interval, after which a 350µl aliquot was removed from the sample mixture, incubated at 37°C for 20min, after which the reaction was stopped and analysed. The stability assay contained 100mM KH_2PO_4/K_2HPO_4 pH 6.8, 0.02mM $MgCl_2$, 0.4mM ATP, 10mM KCl and 2mM shikimic acid. A 750µl of diluted *MtSk* (1.73µg/ml) was added in a 5ml reaction test tube, which contained the reaction mixture kept at 4°C, after which vortexing took place. The reaction mixture was kept at 4°C. Thereafter, a series of 350µl amounts, at time intervals of 15, 30, 60, 90,120 and 180min, were removed and transferred to 500ul Eppendorf tubes, which were incubated at 37°C for 20min. Each reaction was subsequently stopped by adding 2µl of a 200mM EDTA to each reaction tube, followed by centrifugation at 13000rpm for 2min. An amount of 110µl of each terminated reaction was then transferred HPLC vials in triplicate, to determine the AMP, ADP, ATP formation. Once HPLC spectra were generated, the data for each reaction was recorded and reworked using Graph Pad Prism 6 software in order to plot enzyme activity graphs.

2.6.2.5 The shikimate kinase ATP or ATP-d concentration assays

The assay contained 100mM KH_2PO_4/K_2HPO_4 pH 6.8, 0.020mM $MgCl_2$, 10mM KCl and 2mM shikimic acid and a concentration series of 200 - 1200µM ATP or ATP-*d* in 500µl Eppendorf microfuge tubes. *MtSK* was diluted to 1.73µg/ml by diluting 75µl of *MtSK* enzyme to 500µl of stock solution in each tube at 4°C. A blank was removed from each ATP/ATP-*d* reaction mixture prior to the additional of enzyme. The reactions were incubated at 37°C for 20min. After incubation, all reactions were stopped with the addition of 2µl of 200mM EDTA. All samples were analysed in 110µl triplicate amounts aliquotted into HPLC vials to determine the amount of ADP formed. The data obtained from HPLC was used to

plot specific activity as well as KIE of ADP formation against the ATP or ATP-*d* concentration, by using graph on Graph Pad Prism software.

2.7 Glutamine synthetase assays

2.7.1 Deadenylylated GS concentration assays

The deadenylylated GS assays were prepared in 1.5ml Eppendorf tubes kept at 4^{o}C in 0.5ml reaction vessels as follows: 4mM sodium glutamine, 4mM NH_4Cl, 0.022mM $MgCl_2$, ATP/ATP-*d* solutions in a 200µM - 3000µM concentration series, 20mM imidazole (pH 7.3), 0.003U/ml deadenylylated GS. The components were mixed quickly. A 110µl aliquot was taken as a blank sample, to which 0.95µl of a 100% TCA stopping solution was immediately added. The remaining reaction mixture was then placed in a 37^{o}C incubator for 30min. At the end of 30min period, 2.85µl of 100% TCA stopping reagent was added to the mixture and mixed, followed by centrifugation at 3000rpm for 2min. The solutions were loaded in HPLC vials in triplicate, for determining the amount of ADP formed. The collected data on HPLC was the plotted as specific activities versus the ATP concentration, with the aid of Graph Pad Prism 6 software.

2.8 Results and discussion: KIE for AK, SK and GS using ATP and ATP-*d*

2.8.1 Acetate kinase

Time assays were performed on acetate kinase to select the optimal incubation period for subsequent assays in the study. The results obtained are summarised in **Table 2.1** and **Figure 2.9** below.

Table 2.1: *Acetate kinase specific activity as a function of incubation time. Constant enzyme and ATP concentration was used (n =3).*

Time / min	Av. specific activity / µM ADP.(mg protein)$^{-1}$.(min)$^{-1}$	sd / µM ADP.(mg protein)$^{-1}$.(min)$^{-1}$
0.00	0.00	0.00
10.00	34136.95	416.94
20.00	51274.17	223.89
40.00	67487.94	1221.54
80.00	87363.14	2944.72
120.00	99731.91	4500.64

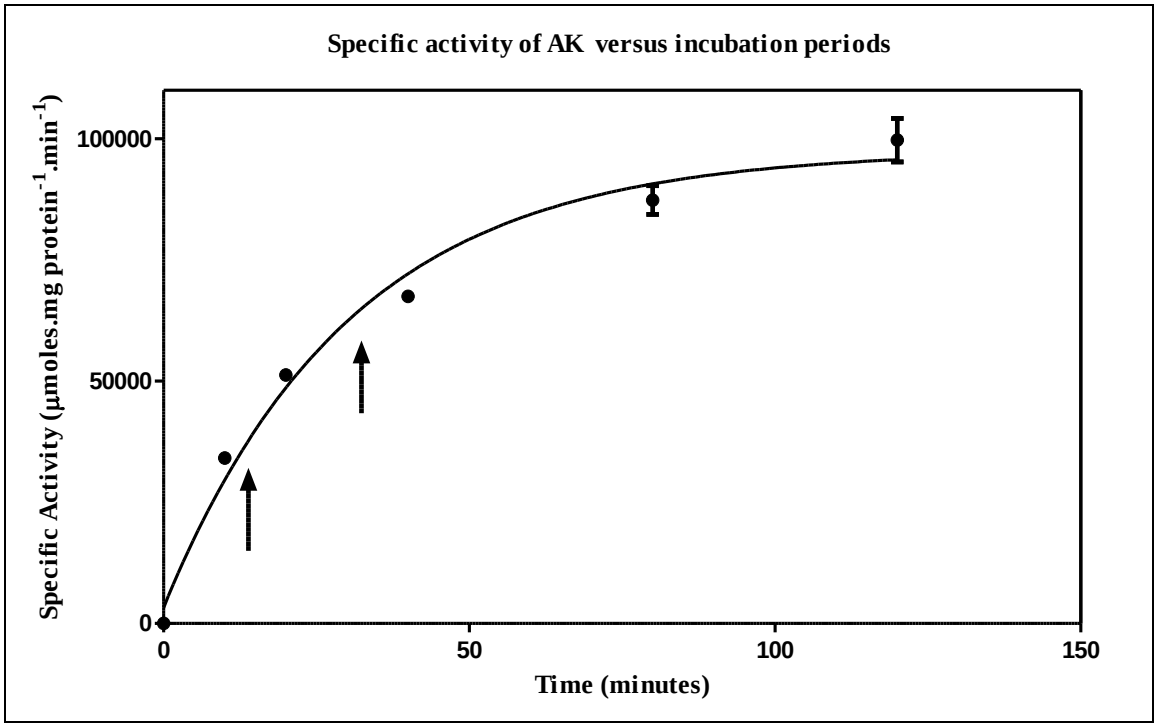

Figure 2.9: *Specific activity of AK versus increasing time at constant ATP and acetate kinase concentration. The linearity is found between the two arrows.*

The incubation period was selected in the initial linear phase before the enzyme reached equilibrium. For acetate kinase, the optimal time was found to be 25 ± 3min, as indicated

with the arrows on **Figure 2.9**. With this information on hand, attention was placed on AK in ATP or ATP-*d* competition assays, with equimolar concentrations of these species present for the purposes of KIE analysis. These data are presented in **Table 2.2** and **Figure 2.10.**

Table 2.2: *Specific activity of acetate kinase as a function of stepwise increases in concentration of a 1:1 (ATP: ATP-d)reaction mixture under constant incubation time and temperature conditions (n = 3).*

Concentration of co-substrate mixture	**ATP specific activity / µM ADP.(mg protein)$^{-1}$.(min)$^{-1}$**		ATP-*d* **specific activity / µM ADP.(mg protein)$^{-1}$.(min)$^{-1}$**	
[1:1 ATP: ATP-*d*] / µM	**Mean**	**Sd**	**Mean**	**sd**
0.00	0.00	0.00	0.00	0.00
200.00	178246.33	44592.66	170742.00	6027.54
400.00	281766.33	13452.41	293916.33	5886.30
600.00	355483.33	9654.68	399271.33	12742.09
800.00	406405.33	13504.47	453103.00	1753.22
1000.00	408763.66	3532.52	478260.00	2827.49
1200.00	411279.00	1184.73	485216.66	11602.03
1400.00	428084.66	654.77	484651.66	5417.05

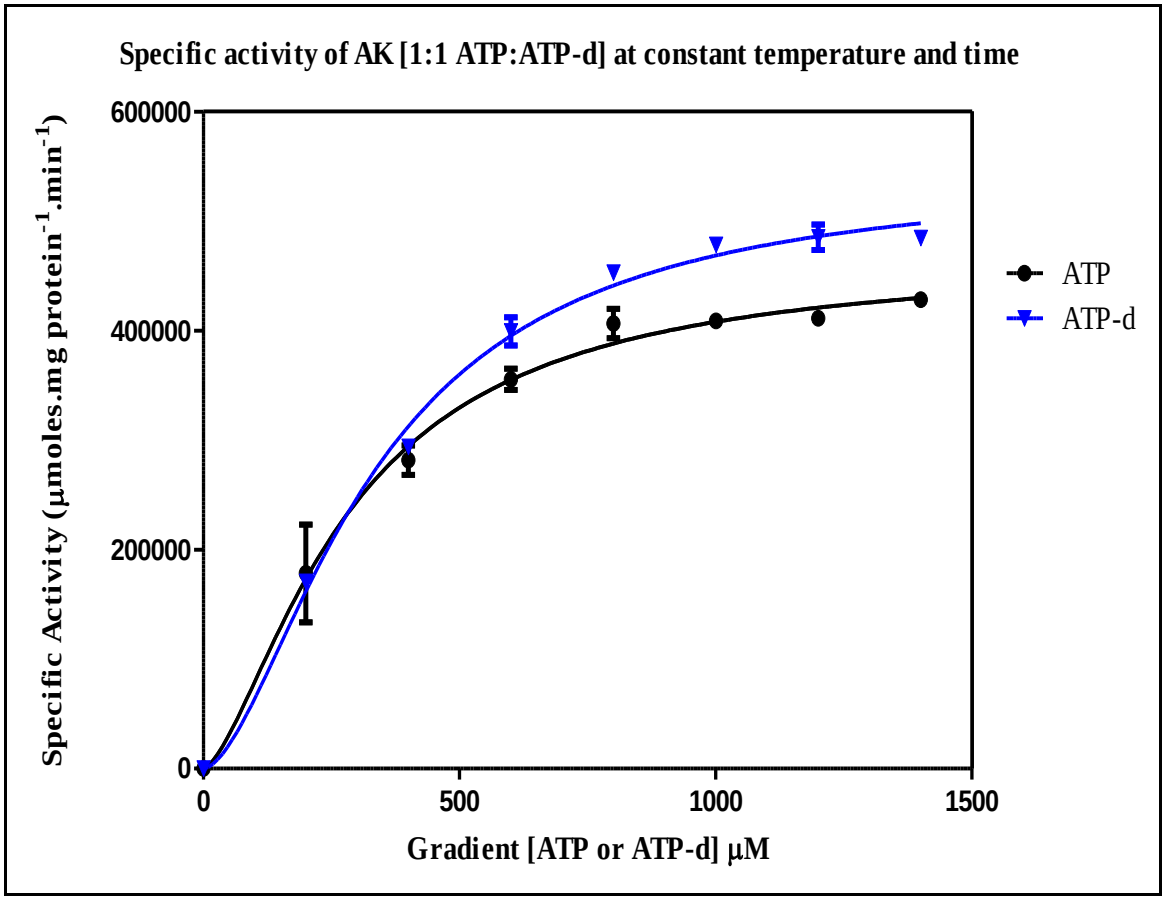

Figure 2.10: *Specific activity of acetate kinase against a gradient of 1:1 (ATP: ATP-d). The blue series represents specific activity due to ATP-d, and the black series due to ATP.*

The data shows that there is a significant increase in AK specific activity in the presence of ATP-*d*, as compared to the activity in the presence of ATP. The concentrations of ATP and ATP-*d* determined from each of the above assays were then used to illustrate the kinetic isotope effect on AK. These data are presented in **Table 2.3** and **Figure 2.11** below.

Table 2.3: *Kinetic isotope effect on acetate kinase due to ATP (KIE_H) and ATP-d (KIE_D) as a function of [1:1 ATP: ATP-d] (n = 3).*

[Sample]	**ATP**		ATP-*d*	
[1:1 ATP: ATP-*d***] / µM**	**Mean (V_H/V_D)**	**sd**	**Mean (V_D/V_H)**	**sd**
200.00	1.05	0.03	1.01	0.03
400.00	0.96	0.03	1.04	0.03
600.00	0.89	0.03	1.12	0.04
800.00	0.90	0.03	1.12	0.04
1000.00	0.86	0.00	1.17	0.01
1200.00	0.85	0.01	1.17	0.01
1400.00	0.88	0.01	1.13	0.01

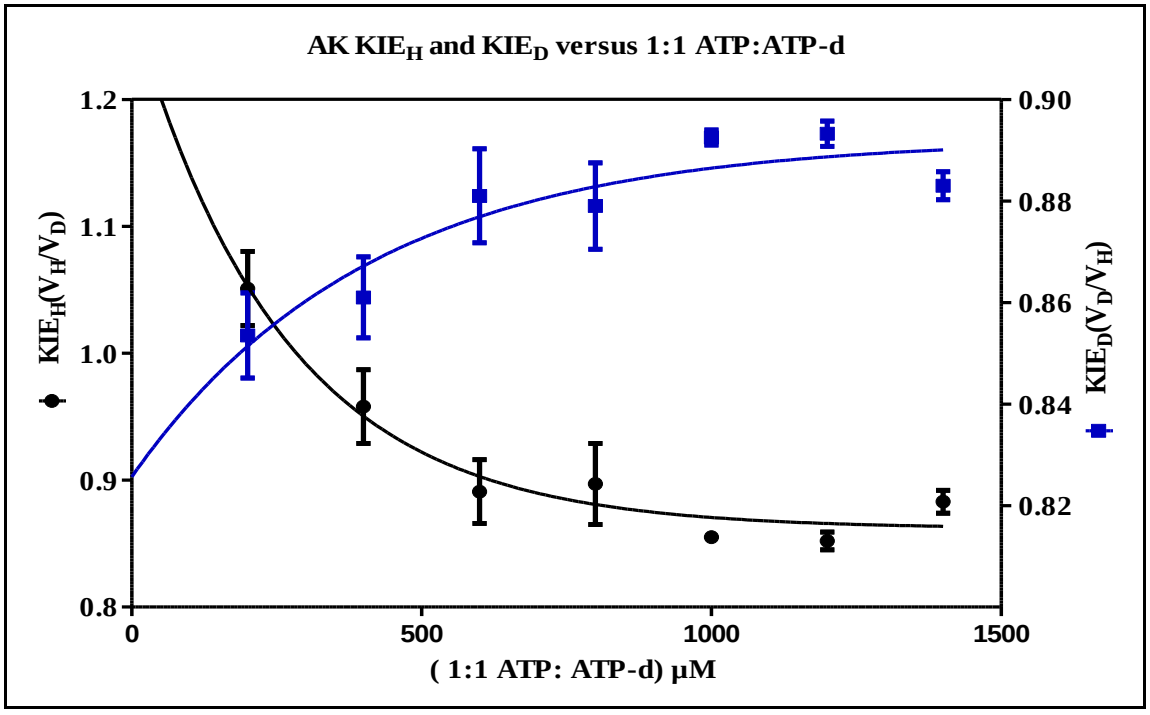

Figure 2.11: *KIE_H and KIE_D versus [1:1 ATP: ATP-d] for acetate kinase enzyme. The blue curve represents KIE_D and the black curve represents KIE_H.*

2.8.2 Shikimate kinase

We had previously observed that the enzyme activity of SK changed significantly when thawed from storage temperature (-72ºC) to liquid temperature 4ºC, or even during subsequent analysis (Kenyon *et al.* 2011), To determine how the enzyme stability changed, by way of its measured activity, when kept at 4^{o}C, a simple time course experiment at that temperature was performed. Data subsequently generated is furnished in **Table 2.4** and **Figure 2.12** below.

Table 2.4: *SK stability activity as a function of incubation period at 4^{o}C (n=3).*

Time / min	Av. Specific activity / µM ADP.(mg protein)$^{-1}$.(min)$^{-1}$	sd
0.00	0.00	0.00
15.00	142.10	0.62
30.00	98.80	1.19
60.00	82.89	0.51
90.00	62.64	0.47
120.00	39.42	0.65
180.00	37.91	0.18

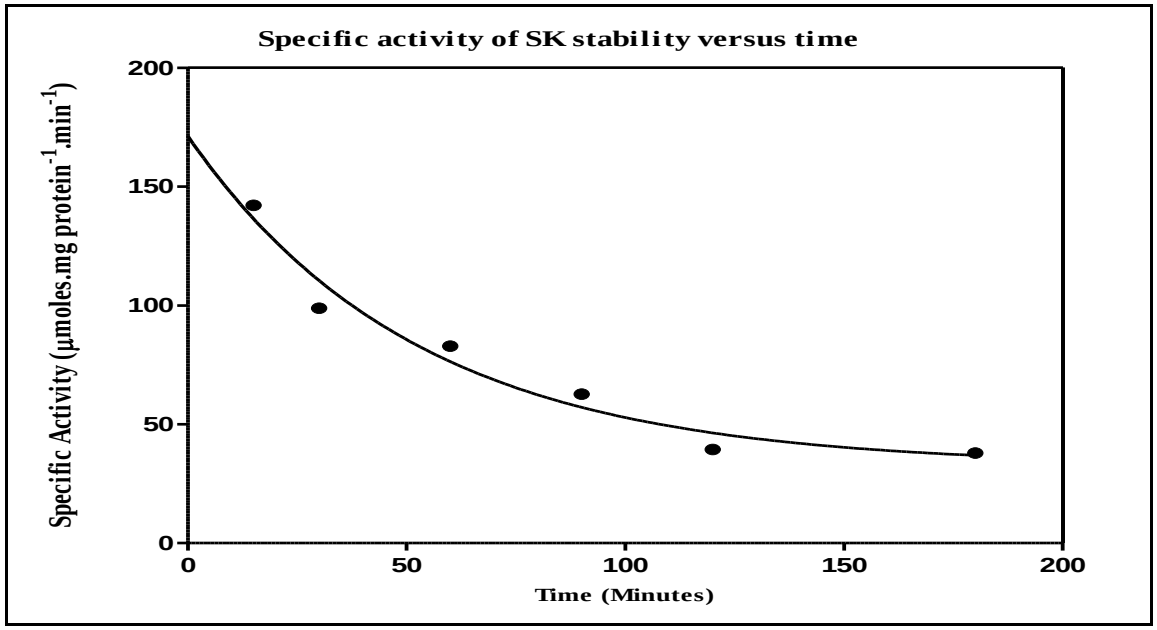

Figure 2.12: *Stability assay for SK at 4ºC against incubation time at constant enzyme and ATP concentration.*

Most enzymes at 4ºC was supposed to be inactive since this temperature was not its optimal temperature or instead of decreasing as the curve does it was supposed to be increasing but since the enzyme was not stable and it would slightly lose its biological activity. Taking this into consideration, the following reactions were carried in highly meticulous procedures, keeping the time the diluted enzyme remained at 4°C to a consistent minimum. In **Table 2.5** and **Figure 2.13** the shikimate assay was inspected for the optimal incubation period, which is in the linear phase before the enzyme reached equilibrium.

Table 2.5: *Shikimate kinase specific activity as a function of ADP concentration against incubation time at 37°C. A constant enzyme and ATP concentration was used (n =3)*

Time / min	Av. Specific activity / µM ADP.(mg protein)$^{-1}$.(min)$^{-1}$	sd / µM ADP.(mg protein)$^{-1}$.(min)$^{-1}$
0.00	0.00	0.00
30.00	201.35	8.98
60.00	281.80	3.32
90.00	357.03	20.47
120.00	415.65	7.44
180.00	457.47	1.97

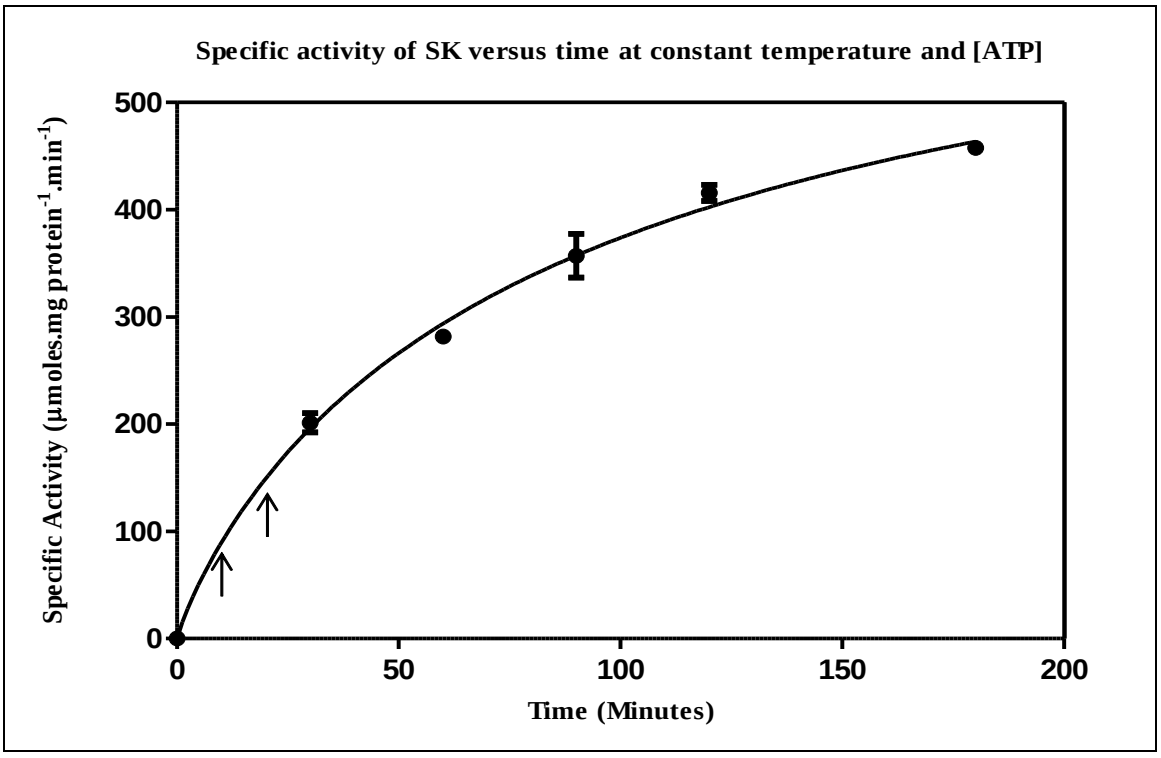

Figure 2.13: *Specific activity SK versus time at constant ATP, temperature and enzyme concentration.*

The incubation period selected for SK was found to be 20 ± 2min as the arrows showing. With this data in hand, a return to the kinetic studies was done for AK, but this time on *MtSK*. The data are summarised in **Table 2.6** and **Figure 2.14** below.

Table 2.6: *Specific activity of shikimate kinase as a function of stepwise increases in concentration of a 1:1(ATP: ATP-d) mixture under constant incubation time and temperature conditions (n = 3).*

Sample name	**ATP specific activity / µM ADP.(mg protein)$^{-1}$.(min)$^{-1}$**		ATP-*d* **specific activity / µM ADP.(mg protein)$^{-1}$.(min)$^{-1}$**	
[1:1 ATP: ATP-*d***] / µM**	**Mean**	**sd**	**Mean**	**sd**
0.00	0.00	0.00	0.00	0.00
200.00	610.98	20.25	262.14	1.26
400.00	819.07	2.45	448.72	17.99
600.00	1167.57	19.89	511.24	33.64
800.00	1326.69	74.71	505.84	3.77
1000.00	1461.14	26.86	496.22	0.14
1200.00	1412.59	42.25	512.89	2.28
1400.00	1280.99	11.85	513.82	0.59

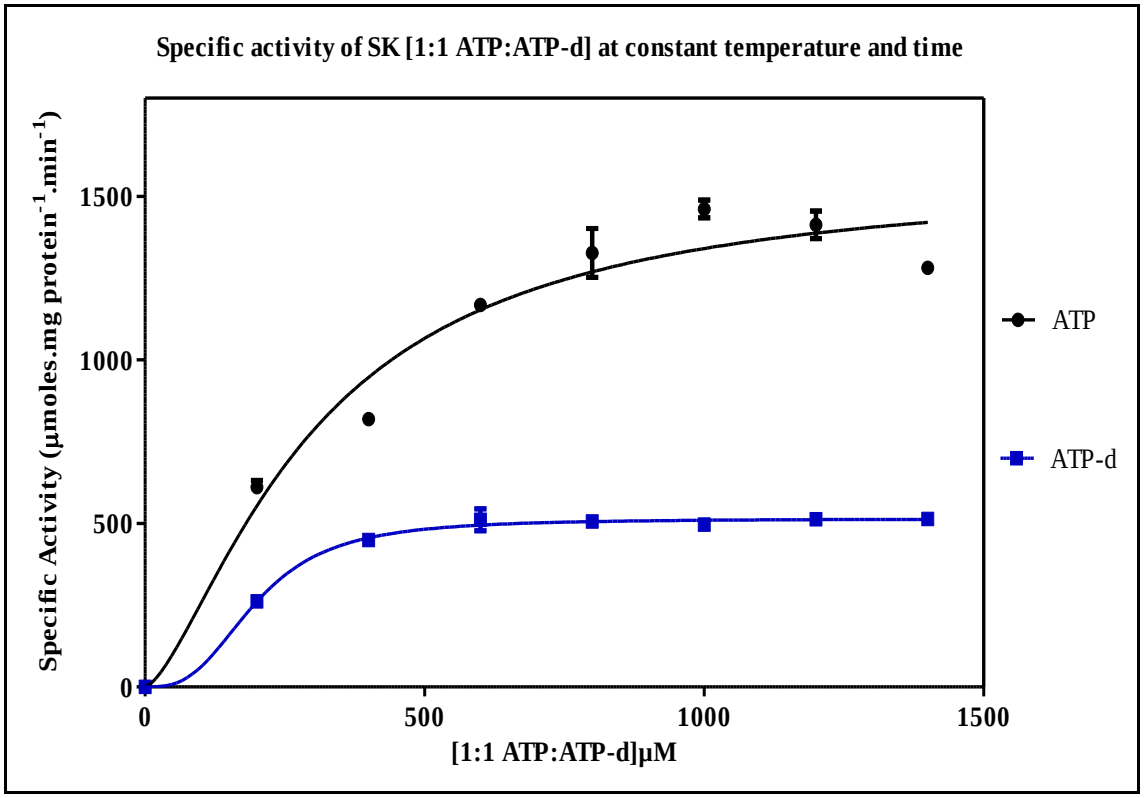

Figure 2.14: *Specific activity of shikimate kinase against a gradient of 1:1(ATP: ATP-d). The blue series represents specific activity due to ATP-d, and the black series due to ATP.*

Unlike what was found for AK, SK showed a significant reduction in specific activity when using ATP-*d* compared to ATP itself. To further substantiate this finding, this data was analysed in terms of the kinetic isotope analysis data presented in **Table 2.7** and **Figure 2.15** below.

Table 2. 7: *Kinetic isotope effect on shikimate kinase due to ATP (KIE_H) and ATP-d (KIE_D) as a function of [1:1 ATP: ATP-d].*

[1:1 ATP: ATP-*d*] / µM	**KIE_H (V_H/V_D)**	**KIE_D (V_D/V_H)**
200.00	2.33	0.43
400.00	2.35	0.43
600.00	2.36	0.42
800.00	2.48	0.40
1000.00	2.63	0.38
1200.00	2.82	0.35
1400.00	2.84	0.35

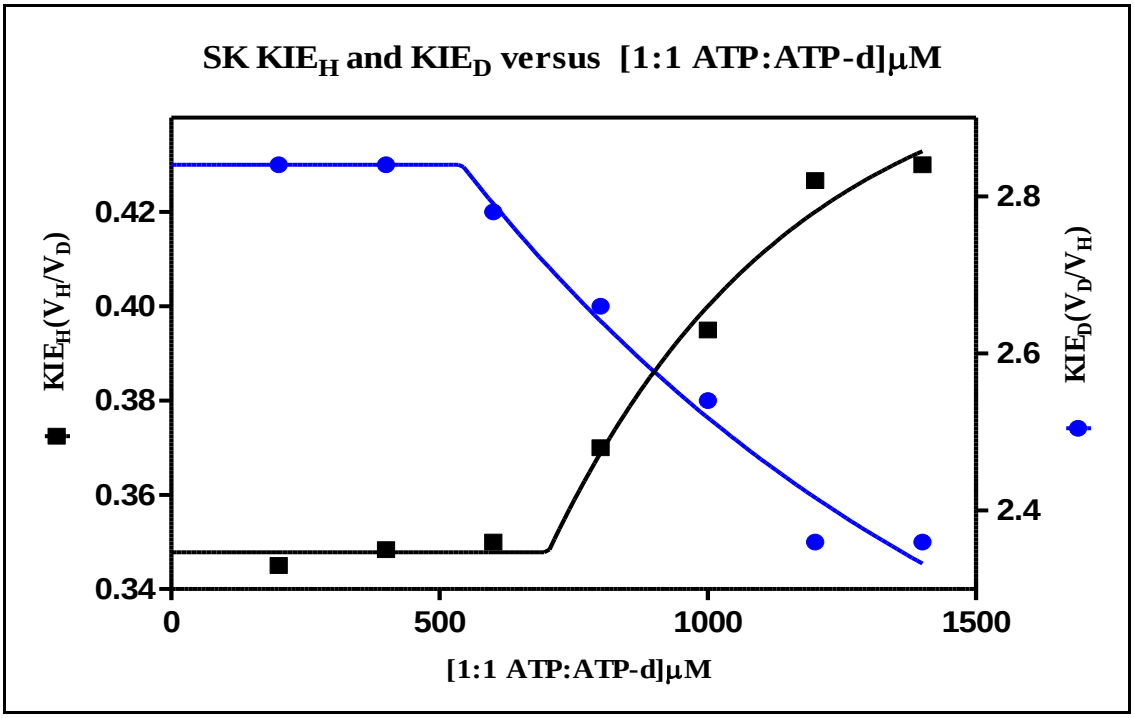

Figure 2.15: *KIE_H and KIE_D versus [1:1 ATP: ATP-d] for shikimate kinase. The blue series represents specific activity due to ATP-d, and the black series due to ATP.*

2.8.3 Glutamine synthetase

From the previous paper of Kenyon *et al.* (2011), the same incubation period and reaction conditions were used when analysing the activity of GS enzyme. This results in saving time and reagents by not inspecting the incubation period. With this data (**Table 2.8**) in hand, a return to the kinetic studies was done as before, but this time on GS. The data are summarised in **Table 2.8** and **Figure 2.16** below.

Table 2.8: *Specific activity of glutamine synthetase as a function of stepwise increases in concentration of a 1:1 (ATP: ATP-d) mixture under constant incubation time and temperature conditions (n = 3).*

Sample name	**ATP specific activity / µM ADP.(mg protein)$^{-1}$.(min)$^{-1}$**		ATP-*d* **specific activity / µM ADP.(mg protein)$^{-1}$.(min)$^{-1}$**	
[1:1 ATP: ATP-*d***] (µM)**	**Mean**	**sd**	**Mean**	**Sd**
235.26	0.00	0.00	0.00	0.00
915.62	189.90	0.21	3354.80	357.70
1630.45	1618.50	0.07	7074.20	0.07
2330.30	3362.00	0.29	10054.30	0.08
2589.92	4599.90	0.09	12205.90	0.06
2945.63	5406.60	0.35	12233.90	1.40
3518.48	7396.40	0.19	12789.70	0.44
3885.85	7763.80	0.04	12518.10	0.09

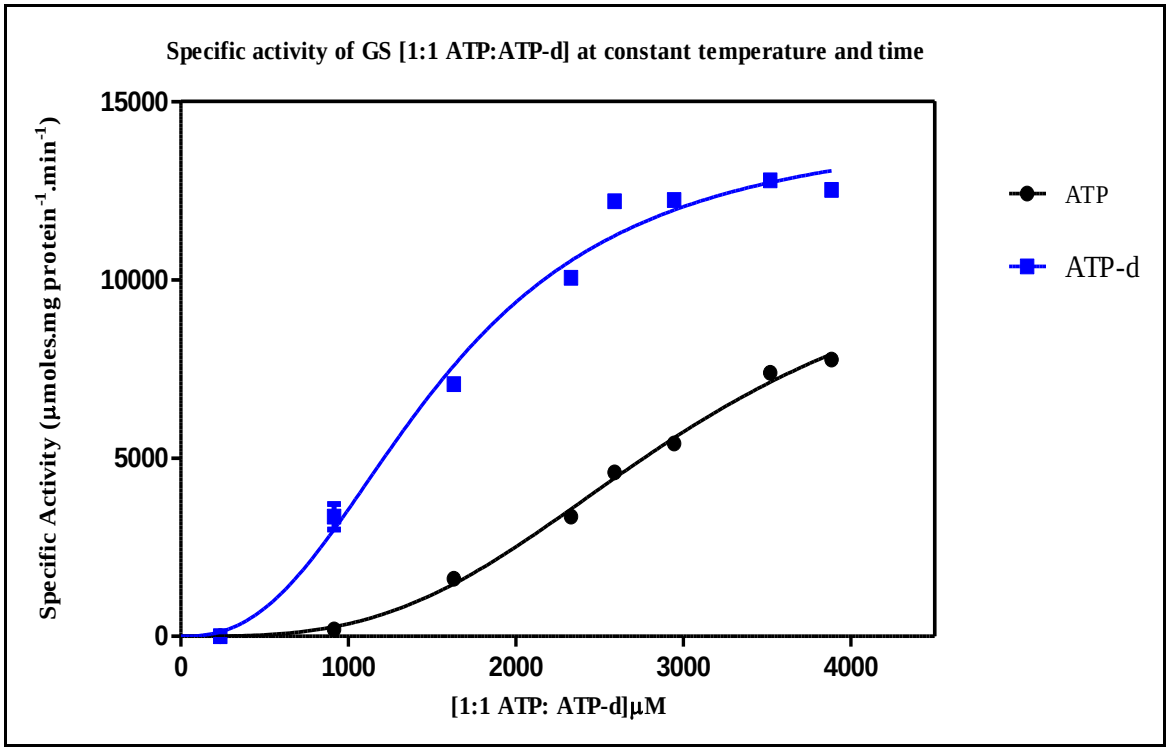

Figure 2.16: *Specific activity of glutamine synthetase against a gradient of 1:1 ATP: ATP-d. The blue series represents specific activity due to ATP-d, and the black series due to ATP.*

The above data shows a significant increase in GS specific activity in the presence of ATP-*d* when compared to ATP as the concentrations 1:1 ATP: ATP-*d* were increased. The above results are similar to those obtained for AK (**Figure 2.10** (p. 64), in that a far higher specific activity is obtained for the reaction of GS with ATP-*d* than for ATP. However this difference is higher in GS when compared to the results obtained for AK. This is further explored in the kinetic isotope effect analysis presented in **Table 2.9** and **Figure 2.17** below.

Table 2.9: *Kinetic isotope effect on glutamine synthetase due to ATP (KIE_H) and ATP-d (KIE_D) as a function of [1:1 ATP: ATP-d].*

[1:1 ATP: ATP-*d*] / µM	KIE_H (V_H/V_D)	KIE_D (V_D/V_H)
1277.90	5.07	0.20
1590.85	4.72	0.21
1903.80	3.99	0.25
2216.76	3.27	0.31
2529.71	2.71	0.37
2842.67	2.31	0.43
3155.62	2.02	0.50
3468.58	1.81	0.55
3781.53	1.67	0.60

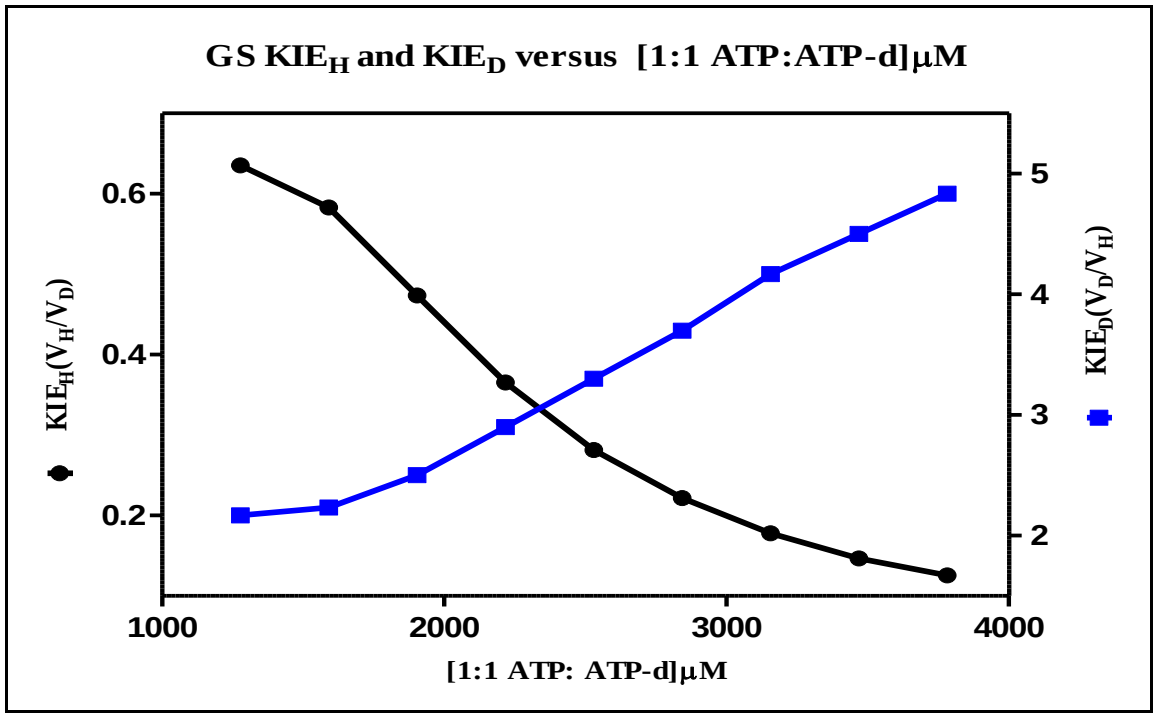

Figure 2.17: *KIE_H and KIE_D versus [1:1 ATP: ATP-d] for glutamine synthetase. The blue series represents specific activity due to ATP-d, and the black series due to ATP.*

2.9 Comparison of the KIE for AK, SK and GS using ATP and ATP-d

The time assays for both AK and SK in **Table 2.1** or **Figure 2.9** (p. 62) and **Table 2.5** or **Figure 2.13** (p. 68) respectively, showed that different enzymes have different optimal incubation periods for the reaction conditions specified here. AK incubation period was found at 25 ± 3min while the SK incubation period was 20 ± 2min. GS had been optimised in terms of incubation period previously (Kenyon *et al*., 2011); the published incubation period was thus employed for GS.

The SK stability assay in **Table 2.4** (p. 66) or **Figure 2.12** (p. 67) was used to verify the instability of diluted SK when kept at 4^{o}C after thawing from the -72^{o}C storage temperature. A steady drop in the specific activity of SK was found when kept at 4^{o}C for an increasing length of time, as shown by the graph sloping down in **Figure 2.12** (p. 67).

When the specific activities of the enzymes were determined with increasing concentration of 1:1 ATP: ATP-*d*, AK in **Table 2.2** (p. 63) or **Figure 2.10** (p. 64) showed higher specific activity with ATP-*d* than ATP. Similar findings were observed against GS, as seen in **Table 2.8** (p. 72) or **Figure 2.16** (p. 73)**.**

However, when SK was used [**Table 2.6** (p. 69) and **Figure 2.14** (p. 70)], higher specific activity was found with ATP than ATP-*d*. KIE graphs of AK [**Table 2.3** (p. 65) or **Figure 2.11** (p. 65)] and GS [**Table 2.9** (p. 74) or **Figure 2.17** (p. 74)] have similar shapes, showing increasing KIE_D with decreasing KIE_H, implying similar behaviour in these two enzymes. However, the opposite trend was observed for SK's KIE [**Table 2.7** (p. 71) or **Figure 2.15** (p. 71)]. By way of reviewing the KIE data generated in this particular study, both primary and secondary KIE's were observed, e.g. if AK and GS in **Figure 2.11** (p. 65) and **Figure 2.17** (p. 74) were secondary KIE then the SK in **Figure 2.14** (p. 70) was the primary KIE. At this point, an attempt was made to clarify the enzyme's behaviour when comparing the KIE in the presence of ATP and ATP-*d*. In general, the KIE thus described can be used as a convenient tool for tracking the mechanistic details of the interactions between the reactants and the enzyme binding site following the deuteration process (Hennig, Oswald, & Schmatz, 2006; Wade, 1999). Primary KIE occurs when the covalent bond of an isotopic (C-D) atom is broken or formed. Secondary KIE occurs when a covalent bond in an isotopic (C-D) atom is not directly involved in bond cleavage or formation, but occurs next to the site where cleavage occurs, resulting in a secondary bond which is both steric and inductive (Wade, 1999).

Comparison of the energy used by both KIE types during bond formation and breaking, results in the primary KIE requiring a higher energy than the secondary KIE (Turowski *et al*.,

2003; Wade, 1999). In enzymatic reactions of this kind, the secondary KIE is essential, because the larger size of the deuterium atom causes a reduction of vibration frequency of C-D bond compared to C-H bond (Hennig *et al*., 2006; Turowski *et al*., 2003). This results in a decrease in the binding affinity of a deuterated molecule compared to its protonated counterpart for the same enzyme (Turowski *et al*., 2003); Wade, 1999).

From the KIE analysis in the present study, particularly which determined for AK and GS, could be of the secondary kind while the SK could be primary kind or vice versa based on their KIE graphs. This secondary KIE most likely indicated that the deuterated ATP substrate caused the KIE_D to increase until the AK or GS reactions reached their equilibrium states. Speculation about the mechanism by which AK or GS uses ATP, probably implicates the C8-H atom directly in the suspected mechanism of action, being based on the shape of the graphs **Figure 2.11** (p. 65) and **Figure 2.17** (74). On the other hand, the SK data generated in this study **Figure 2.15** (p. 71) could be a primary KIE. However, follow up on this speculation requires additional experimentation beyond the scope of the present study.

CHAPTER 3: THE KINETIC ISOTOPE EFFECT (KIE) IN ACETATE KINASE AND SHIKIMATE KINASE IN THE PRESENCE OF IMIDAZOLE- OR PURINE-BASED INHIBITORS IN EITHER THEIR PROTONATED OR DEUTERATED FORMS

INTRODUCTION

This chapter focuses on changes in activity of shikimate kinase (SK) and acetate kinase (AK) caused by protonated and deuterated analogues of their substrates. All assays were designed so that enzymes were able to perform at their optimal rates by using standardised reagents under optimised temperature and pH conditions. The reaction rates were determined in the presence of protonated or deuterated substrates in a 1:1 ratio of enzyme to substrate. Comparison of the effects of these substrates on SK or AK activity was done graphically.

3.1 Enzyme modulation or inhibition

Enzyme inhibition is defined as the reduction of the rate of enzyme activity or enzyme specific activity due to the action of an added compound or substrate in an enzyme-catalysed reaction (Martiny-Baron *et al.*, 1993). The term 'modulator' is used more generally to label the decrease (inhibition) or increase (activation) of specific activity of a given enzyme as a result of the presence of modified substrate (Saboury, 2009). This study deals with modulator molecules from which inhibitors are to be selected based on the % activities of AK and SK assayed with these materials. To simplify things, the % activities for these studies were expressed as:

% specific activity = [specific activity with inhibitor/specific activity without inhibitor] x 100

Both the reaction with and without inhibitor materials were prepared simultaneously under identical conditions.

There are two kinds of inhibition, namely reversible and irreversible inhibition (Perloff *et al*., 2009). In reversible inhibition, the inhibitors can be washed away from the enzyme by a process such as dialysis, or by increasing the concentration of substrate; in this particular method, the enzyme does not lose its biological activity (Martiny-Baron *et al.*, 1993). By contrast, when an irreversible reaction occurs, the inhibitors cannot be removed or washed away; when this method is used, the enzyme loses its biological activity. In general, with reversible reactions, the weak or non-covalent bonds dominate, whereas with irreversible inhibition, covalent bond formation between an enzyme and inhibitor predominate (Saboury, 2009).

There are four types of reversible inhibition, namely competitive, non-competitive, uncompetitive and mixed inhibition (Saboury, 2009). Competitive inhibition occurs when there is a physicochemical resemblance between the substrate and the inhibitor, resulting in competition between the two for the binding site of the enzyme. With non-competitive inhibition, the substrate and inhibitors are generally dissimilar, binding simultaneously at different locations on the enzyme. This generally results in allosteric (conformational) modification of the enzyme, translating into a lower reaction rate. This study does not focus on the type of inhibitor used, but rather with identifying inhibitors and then subsequently trying to determine what the nature of inhibitor interaction is with a particular enzyme.

Initially, the modulators were tested at 100µM and 1000µM concentration against the various enzymes to determine the change in % specific activity. Once substrate preparations causing decreased enzyme activity were identified, IC_{50} inhibition constants were determined for these selected materials only. This was done on both AK and SK enzymes. A similar procedure was performed on the three products synthesised from 2,6-dichloropurine to the point of inhibition of the enzyme's specific activities; however, IC_{50} values were not determined for these compounds as this was considered beyond the scope of the study.

3.1.1 IC_{50} determination.

In enzymology, dose-response refers to the manner in which the changing concentration of a molecule affects the activity of the protein target molecule (Schmidt and Ebel, 1987). Generally, the dose-response curve is sigmoidal, with the value at 50% maximum activity being characteristic of the enzyme against the particular target molecule. This value is referred to as either IC_{50} (in the case of a specific protein) or EC_{50} (when a cell, tissue or organism is used) (Shoichet, 2006). The dose-response curve consists of a plot of log[inhibitor] against enzyme specific activity in response to added inhibitor (Shoichet, 2006)

The standard IC_{50} curve yields four parameters, namely maximum response, minimum or baseline response, the slope and IC_{50} value (Bella and Tabesh, 1985; Perloff *et al*., 2009). The magnitude between the baseline and the maximum of the dose curve along the y-axis defines the efficacy of the compound, particularly if the deuterated compound has a higher efficacy than its protonated counterpart. The potency of a given compound is based on how the curve curls along the x-axis, in other words the manner in which the graph shifts along the x-axis. The IC_{50} values for the protonated and deuterated compounds were determined in a concurrent fashion. In this way a direct comparison between protonated and deuterated analogues was achieved.

3.2 Materials and methods

3.2.1 Activity of AK in the presence of protonated imidazole-containing materials and their deuterated analogues

The AK activity assay involving ten compounds, was prepared as follows: 10ml tubes containing a solution mixture of 26.67mM Tris-HCl, pH 7.5, 3.67mM sodium acetate, 34µM $MgCl_2$ and 0.25pg/ml AK enzyme was diluted with deionised water to reach a total volume of 7.7ml. The solution mixture was incubated at 37^{o}C for 5min to allow the solution to reach the optimal temperature for the enzyme to function. After 5min, 330µl of a 100µM solution of either the protonated or deuterated imidazole-containing compound in deionised water was added. Lastly, 1.2µl of a 60mM ATP solution was added to the enzyme / inhibitor mixture, and the solution was incubated at 37^{o}C for 25min. Each reaction mixture was stopped with 2µl of 100mM aqueous TCA. All the reactions were loaded into HPLC vials in triplicate (110µl) and the concentration ADP determined in each. The specific activity was calculated for each inhibitor from these data and a graph constructed with the aid of Graph Pad Prism software.

3.2.2 Activity of AK in the presence of synthetic purines

Six synthetic purines (1g each) in 1.5ml Eppendorf tubes were dissolved in 1000µl deionised water. These materials were assayed as outlined in 3.2.1, except that the assays were run at two different concentrations, concurrently, in two 1.5ml Eppendorf tubes, namely at 57µg/l and 29µg/l. After quenching, all the reaction solutions were analysed for ADP concentration by HPLC, done in triplicate as previously (p. 60).

3.2.3 SK activity in the presence of 10µM protonated imidazole-containing compounds and their deuterated analogues

A 5ml of a solution made up of 100mM KH_2PO_4/K_2HPO_4 pH 6.8, 20µM $MgCl_2$, 10mM KCl, 2mM shikimic acid and 7.5ng/ml SK enzyme was prepared as the stock reaction solution. The solution was then vortexed to ensure thorough mixing. Into 1.5ml Eppendorf tubes were placed 0.18µl of 20mM solution of the protonated or deuterated modulator, in nano water (10µM modulator in reaction). Thereafter, 330µl of the stock reaction mixture was pipetted into each 1.5ml Eppendorf tube containing the modulator compound, which was then mixed

and incubated at 37^{o}C for 5 min. Following on this, 1.4µl of 60mM ATP was then added to a concentration of 0.24mM ATP in the reaction, with nano water used for the blank reaction. All the mixtures were vortexed to mix and incubated in a 37^{o}C incubator for 20min, then quenched with 2µl of 5.7mM EDTA. Each terminated reaction was then centrifuged at 13000rpm for 2min, followed by triplicate HPLC analysis of 110µl aliquots for ADP concentration. Data generated for measuring conversion of ATP to ADP was graphed using Graph Pad Prism 6 software.

3.2.4 Activity of SK in the presence of 10µM and 100µM protonated imidazole-containing compounds

The activity assay was performed as in **section 3.2.3**, except that 1.78µl and 17.8µl of a 20mM protonated modulator solution were used, to make a concentration of 10µM and 100µM of protonated imidazole compound in solution. The reactions were terminated and analysed as before.

3.2.5 Activity of SK in the presence of 10µM and 100µM deuterated imidazole-containing compounds

The activity assay was performed as in **section 3.2.3**, except that 1.78µl and 17.8µl of a 20mM deuterated modulator solution was used to make a concentration of 10µM and 100µM of deuterated imidazole compound in solution. The reactions were terminated and analysed as before.

3.2.6 Activity of SK in the presence of 100µM protonated imidazole-containing compounds or their deuterated analogues

The activity assay was performed as for **section 3.2.3**, except that 1.78µl of a 20mM protonated and deuterated imidazole modulator solution was used to make a concentration of 100µM of protonated and deuterated imidazole compound in solution. The reactions were terminated and analysed as before.

3.2.7 Inhibition of SK by synthetic purines

Solutions of six synthetic purines were prepared from 1g of material in 1000µl nano water, as a standard solution for each sample. A 20µl amount of each standard solution was diluted with deionised water to a final concentration of 57µg/l, while a 10µl subsample was diluted to 29µg/l, both to a final volume of 350µl. The solutions were added to assay mixes as described in **section 3.2.3** and analysed by HPLC as previously described.

3.2.8 Shikimate kinase IC_{50} assays

A series of 1:5 (v/v) dilutions of protonated or deuterated imidazole-containing compounds (made from 40µl of the stock inhibitor solution, or each successive diluted inhibitor solution in 160µl deionised water) was prepared for the each selected inhibitor. The assay was performed as in **section 3.2.3**, with a blank of deionised water instead of inhibitor. The stopping reagent was added to the blank mixture before the addition of ATP. The 'experimental' tube was also prepared as for the blank, except that the stopping reagent was not added before incubation. Analysis was carried out as in **section 3.2.3**.

3.3 Results and individual discussion of AK and SK activity in the presence of protonated substrates and their deuterated analogues.

3.3.1 Acetate kinase

The following figures and tables show the altered activity of acetate kinase when imidazole-containing protonated compounds and their deuterated analogues were added to the AK-catalysed reaction. The change in % activity was compared to the % activity of 'experimental' reaction as reference, since it was prepared in the absence of inhibitor. These assays tested for the alteration of % activity when the concentration of each compound was standardised at 100 µM, compared to changes in % activity when these compounds were subsequently deuterated. The % AK activity was also tested for the synthetic protonated purine products at 10µM and 10µM.

Table 3.3.1: *Specific activities of assorted imidazole-containing compounds and their deuterated analogues against AK at 100µM.*

Type of Compound	**100µM Protonated imidazole compounds**		**100µM Deuterated imidazole compounds**	
Sample name	**Avg SP%**	**SD**	**Avg SP%**	**SD**
Blank	5.43	6.40	5.43	5.45
Experiment	100.00	0.00	100.00	0.00
6-Benzylaminopurine	80.15	2.80	23.73	5.40
1-Methylimidazole	111.52	3.65	88.12	7.31
4-Nitroimidazole	137.87	8.49	77.50	8.20
1-Butylimidazole	111.52	2.22	118.71	7.34
4-Imidazolecarboxaldehyde	97.28	5.68	105.15	7.97
1-Methylbenzimadazole	130.65	5.60	101.46	9.02
Benzimidazole	125.23	7.36	113.92	8.79

2,6-Diaminopurine	116.16	4.14	108.11	8.88
1-Vinylimidazole	122.35	10.52	99.94	6.74

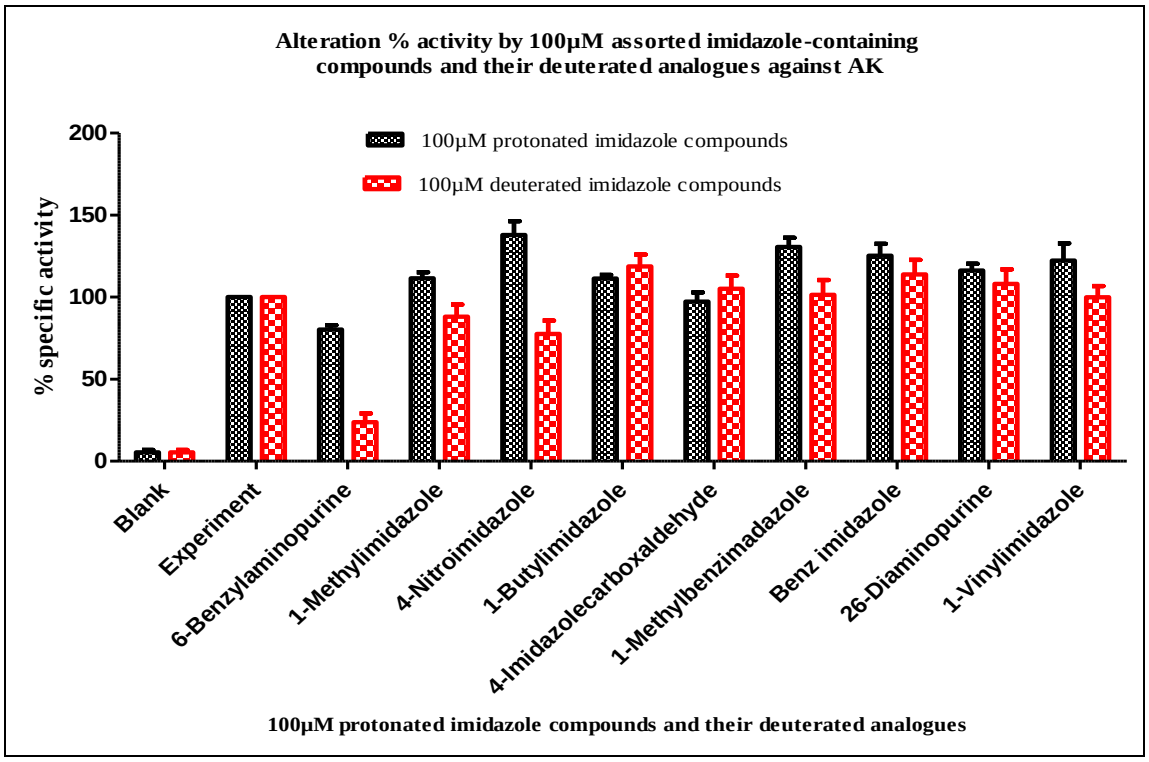

Figure 3.3.1: *Comparison of the specific activity of AK in the presence of either protonated (black) or deuterated (red) imidazole-containing compounds at 100µM.*

In **Figure 3.3.1** few compounds are shown to inhibit AK activity, with most promoting it instead. The exceptions were with the deuterated forms of 6-benzyl-aminopurine, 4-nitroimidazole, 1-methylimidazole and, marginally, 1-vinylimidazole and 2,6-diaminopurine. The protonated form of 6-benzyl-aminopurine may inhibit, but the error recorded prevents concrete assessment of this. The deuterated 6-benzylaminopurine was the strongest inhibitor of AK activity; however, this compound formed a precipitate when added to the reaction. As such, based on these results, it can be speculated that a compound comes out of solution once its' reactive site becomes folded or altered, effectively preventing any further chemical reactivity.

The following **Table 3.3.2** and **Figure 3.3.2** show the effects of synthetic purines on AK activity at 10µM and 100µM.

Table 3.3.2: *Alkylated purine products that enhance or lower the specific activity of AK.*

Concentration	10µM of alkylated purine		100µM of alkylated purine	
Sample	**Avg SP%**	**SD**	**Avg SP%**	**SD**
Blank	0.00	0.00	0.00	0.00
Experiment	100.00	0.00	100.00	0.00
1-Methylpurine	64.43	3.93	152.87	17.48
1-Ethylpurine	87.63	11.41	103.01	8.15
2-Ethylpurine	115.45	28.15	198.08	15.07
1-Benzylpurine	93.29	15.16	134.21	7.11
2-Methylpurine	41.01	7.96	18.85	3.20
2-Benzylpurine	117.17	6.80	55.94	7.73

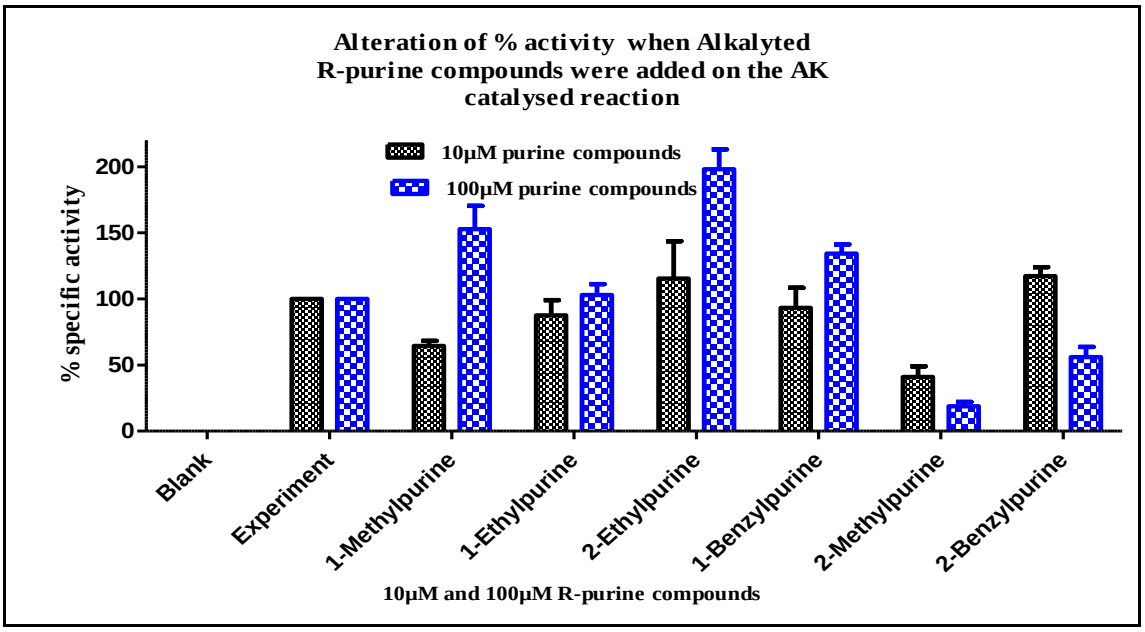

Figure 3.3.2: *Specific activity of the alkylated purines against AK at 10µM (black) and*

100µM (blue). Note the enhanced activity in all cases except 1-methylpurine, 2-methylpurine, 2-benzylpurine.

Different alkylated purine compounds were tested for modulation against AK, using methyl, ethyl and aromatic benzyl groups attached to purine molecules, and the effect on AK when these alkylated groups were added was compared. Only two compounds inhibit AK at the higher concentration, namely 2-methylpurine, and 2-benzylpurine. With the other compounds, activation of AK was observed at the higher concentration. In 1-methylpurine at activation was observed, but 2-methylpurine showed inhibition. The inhibition sequence was in the order methyl- > benzyl- > ethyl-.

3.3.2 Shikimate kinase

In the following **Table 3.3.3** and **Figure 3.3.3**, the activity of shikimate kinase in the presence of imidazole-containing compounds and their deuterated analogues, as well as synthetic purines, are explored at 10µM concentrations of protonated or deuterated compound.

Table 3.3.3: *10µM SK assays of either protonated imidazole-containing compounds or their deuterated analogues resulting in a drop in specific activity.*

Type of Compound	**10µM Protonated imidazole compounds**		**10µM Deuterated imidazole compounds**	
Sample	**Avg SP%**	**SD**	**Avg SP%**	**SD**
Blank	0.00	0.00	0.00	0.00
Experiment	100.00	0.00	100.00	0.00
4-Imidazolecarboxaldehyde	85.49	2.66	39.72	2.98
4(5)-Methylimidazole	116.96	0.89	66.44	4.79
1-Ethylimidazole	33.14	3.15	62.35	1.44
1-Methylimidazole	68.80	2.85	30.99	5.15
4-Imidazolecarboxylic acid	87.98	2.01	66.28	9.42
1-Methylbenzimidazole	94.47	3.82	58.15	3.04
5-Chloro-1-methylimidazole	55.49	0.52	4.12	4.69
2,6-Diaminopurine	54.99	0.84	32.90	2.72
4-Azabenzimidazole	88.92	2.27	52.82	10.81
6-Benzylaminopurine	32.97	5.76	20.46	3.37

4,5-Dicyanoimidazole	88.63	2.12	55.64	5.46
Adenine	102.01	2.95	77.08	0.65
3-(3-Aminopropyl)-imidazole	47.87	1.26	53.51	1.03

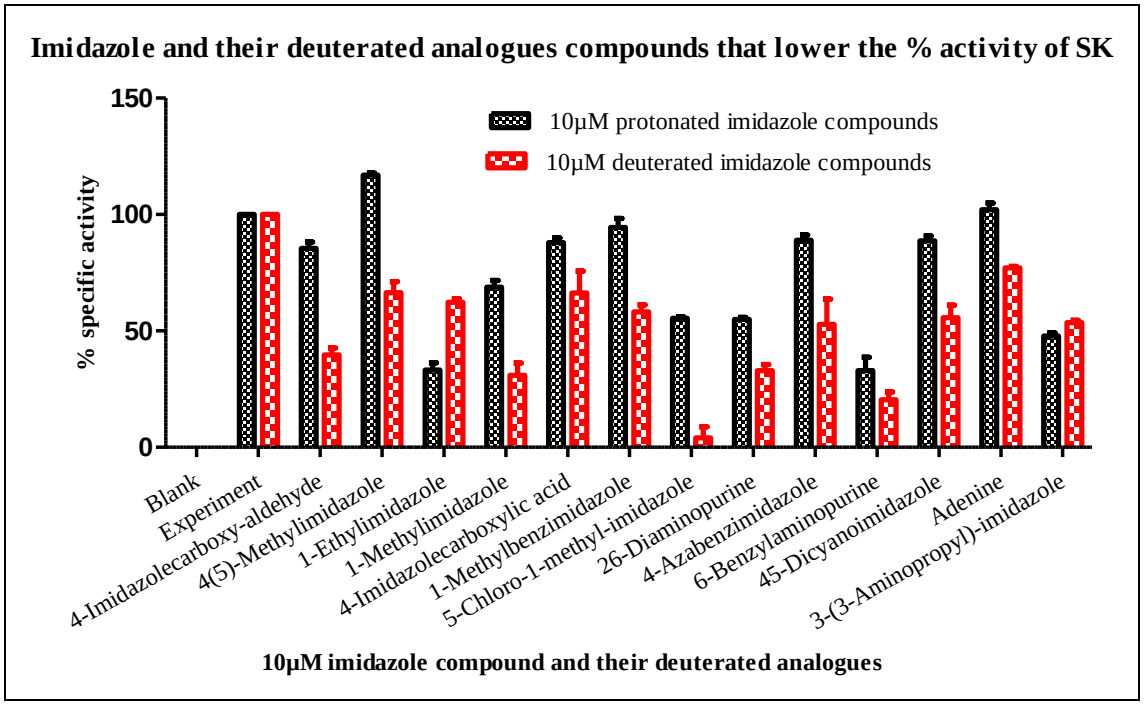

Figure 3.3.3: *Specific activity of SK in the presence of 10µM protonated (black) or deuterated (red) imidazole-containing compounds. Note the lower specific activity in the presence of the deuterated analogues in all cases.*

The protonated and deuterated imidazole-based compounds were added in the SK in equal concentrations to give a direct comparison. In **Figure 3.3.3** most of the deuterated imidazole compounds showed significant inhibition as compared to their protonated equivalents, except for 3-(3-aminopropyl)-imidazole and 1-ethylimidazole. The deuterated and protonated 3-(3-aminopropyl)-imidazole showed similar inhibition, while protonated 1-ethylimidazole showed better inhibition than its deuterated analogue. Some of these protonated imidazoles do show inhibition, but this is generally less than when it is deuterated. Majority of the deuterated imidazoles in **Figure 3.3.3** inhibit SK more than their protonated analogues, showing the possible role that deuteration can play in mechanism of reaction. The significance of these data highlights the important effect of deuteration in influencing the outcome on enzyme activity, either inhibition or activation, as demonstrated in the examples shown in AK and SK specific activity data sets.

Table 3.3.4 and Figure 3.3.4 shows selected compounds that activate SK activity, these compounds were prepared in reactions that were identical to those in the above table and also compared the SK activity of protonated and their deuterated analogues at the lower concentration.

Table 3.3.4: *10µM SK assays of either protonated imidazole-containing compounds or their deuterated analogues resulting in an increase in specific activity.*

Type of Compound	**10µM Deuterated imidazole compounds**		**10µM Protonated imidazole compounds**	
Sample	**Avg SP%**	**SD**	**Avg SP%**	**SD**
Blank	0.00	0.00	0.00	0.00
Experiment	100.00	0.00	100.00	0.00
1-Vinylimidazole	85.49	2.66	97.03	2.97
5-Methyl-4-nitroimidazole	114.87	1.77	162.75	2.99
2-Iodoadenosine	97.21	1.22	113.46	3.45
4(5)-Hydroxymethyl-imidazole	87.73	3.55	96.97	1.15
4-Nitroimidazole	100.91	4.64	108.53	3.20
1-Butylimidazole	105.34	2.20	104.94	0.00

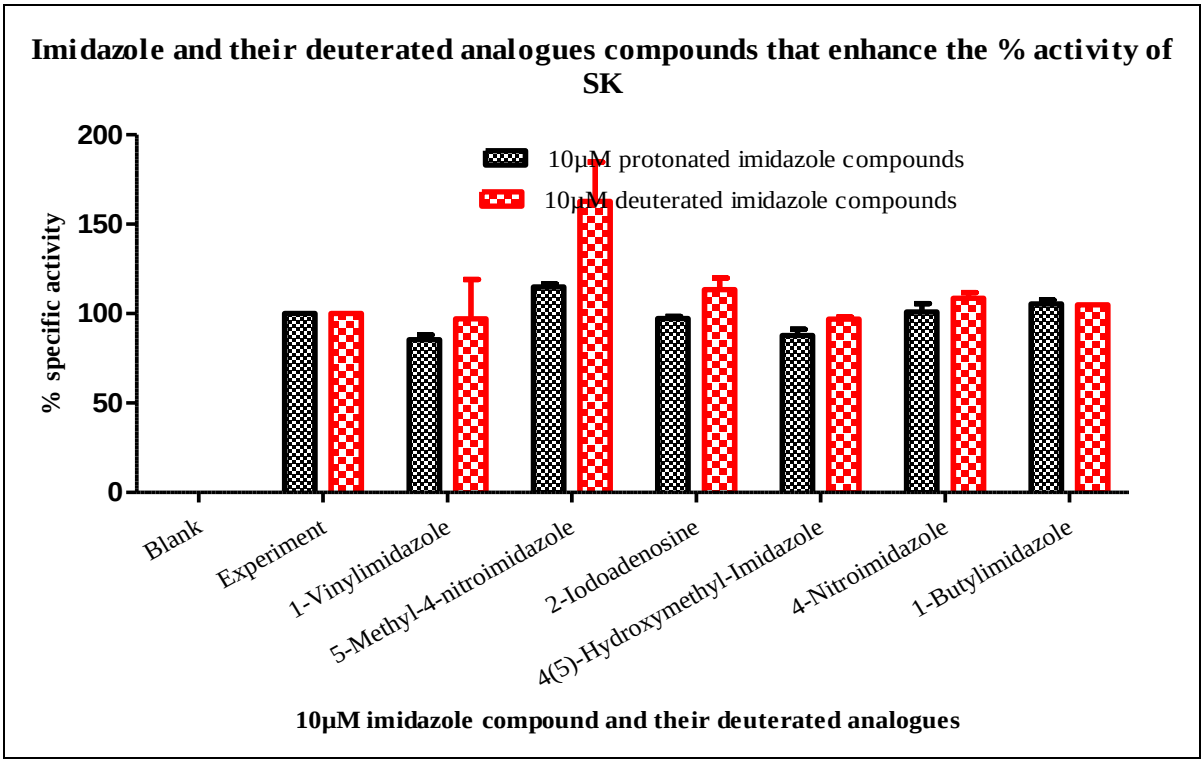

Figure 3.3.4: *Specific activity of SK in the presence of 10µM protonated (black) or deuterated analogues (red) imidazole-containing compounds. Note the equal or slightly higher specific activity in the presence of the deuterated analogues in all cases.*

As shown in **Table 3.3.4** and **Figure 3.3.4** the 10µM protonated and deuterated imidazole compounds were tested for inhibition of SK activity. All these compounds showed either no activity change or an activity enhancement with either the protonated or deuterated imidazole compounds. Specifically, deuterated 5-methyl-4-nitroimidazole showed significant activation of SK, while the rest of these compounds showed no significant activation. From **Figure 3.3.3**(p.85), nine protonated or deuterated compounds that showed moderate inhibition were selected and assayed at 100µM and 1000µM protonated compounds in the following **Tables 3.3.5** and **Figures 4.3.5.**

Table 3.3.5: *Effects of increased inhibitor concentration on SK specific activity in the presence of protonated imidazole-containing compounds.*

Type of Compound	**100µM Deuterated imidazole compounds**		**1000µM Protonated imidazole compounds**	
Sample	**Avg SP%**	**SD**	**Avg SP%**	**SD**
Blank	0.00	0.00	0.00	0.00
Experiment	100.00	0.00	100.00	0.00

1-Methylbenzimidazole	88.52	2.81	40.20	0.58
1-Butylimidazole	60.31	6.68	48.11	1.38
4-Imidazolecarboxylic acid	97.17	3.11	76.19	1.38
1-Methylimidazole	41.97	1.30	18.06	0.76
2,6-Diaminopurine	87.79	7.79	28.54	9.66
4-Nitroimidazole	96.07	2.17	73.51	0.46
6-Benzylaminopurine	86.06	1.17	62.67	5.78
1-Vinylimidazole	74.23	2.99	49.02	4.60
1-Ethylimidazole	56.87	1.17	15.89	4.52

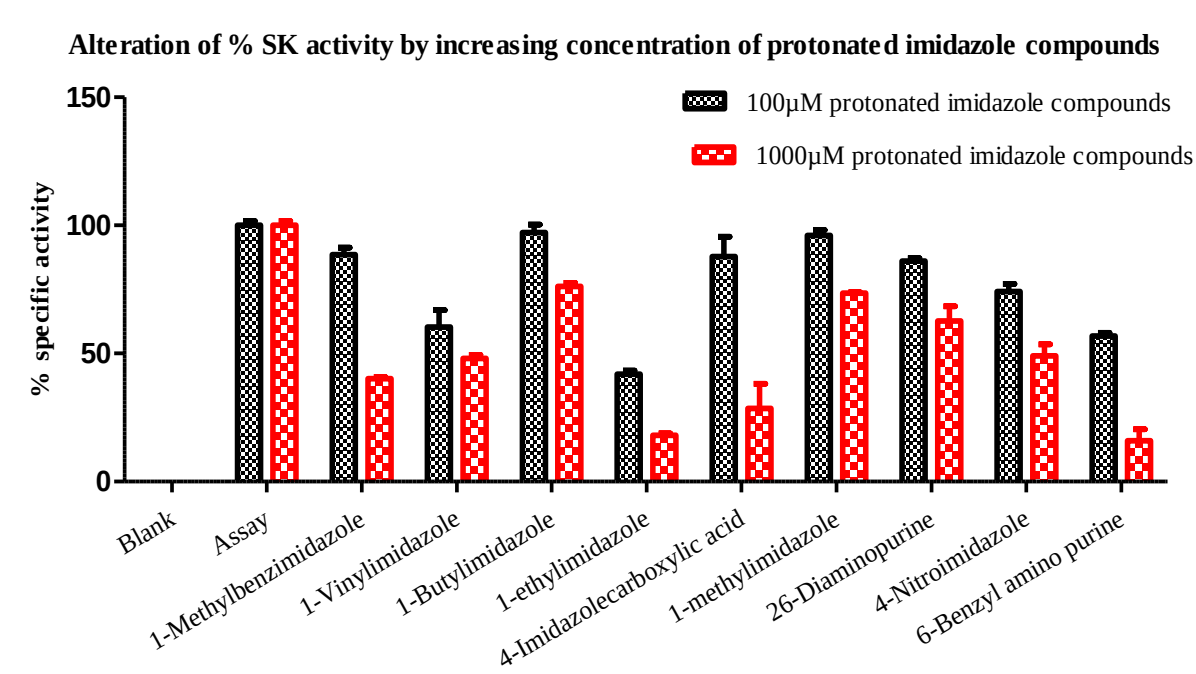

Figure 3.3.5: *Change in SK specific activity in the presence of protonated inhibiting imidazole-containing compounds at 100µM (black) and 1000µM (red). A dose-response is observed in all instances.*

Figure 3.3.5 shows the inhibition of SK as the concentration of protonated imidazole compounds was increased from 100µM to 1000µM, resulting in an increased inhibition as the imidazole concentration was increased. All the compounds in **Figure 3.3.5** show a significant

increase of inhibition and show a dose-response. The deuterated analogues of the nine selected compound assayed at lower and higher concentrations are shown in **Table 3.3.6** and **Figure 3.3.6**.

Table 3.3.6: *Effects of increased inhibitor concentration on SK specific activity in the presence of deuterated imidazole-containing compounds.*

Type of compounds	100µM deuterated inhibitor		1000µM deuterated inhibitor	
Sample	**%SP**	**SD**	**%SP**	**SD**
Blank	0.00	0.00	0.00	0.00
Assay	100.00	1.69	100.00	1.63
1-Methylbenzimidazole	63.26	2.03	23.69	8.21
1-Butylimidazole	70.54	3.72	48.89	6.03
4-Imidazolecarboxylic acid	35.64	5.20	39.88	4.21
1-Methylimidazole	64.32	2.42	40.85	6.34
2,6-Diaminopurine	39.77	6.82	37.81	1.91
4-Nitroimidazole	34.92	2.02	18.57	4.64
1-ethylimidazole	41.28	1.27	10.11	2.97
1-Vinylimidazole	30.16	5.87	25.66	4.42
6-Benzylaminopurine	49.47	2.35	0.00	0.00

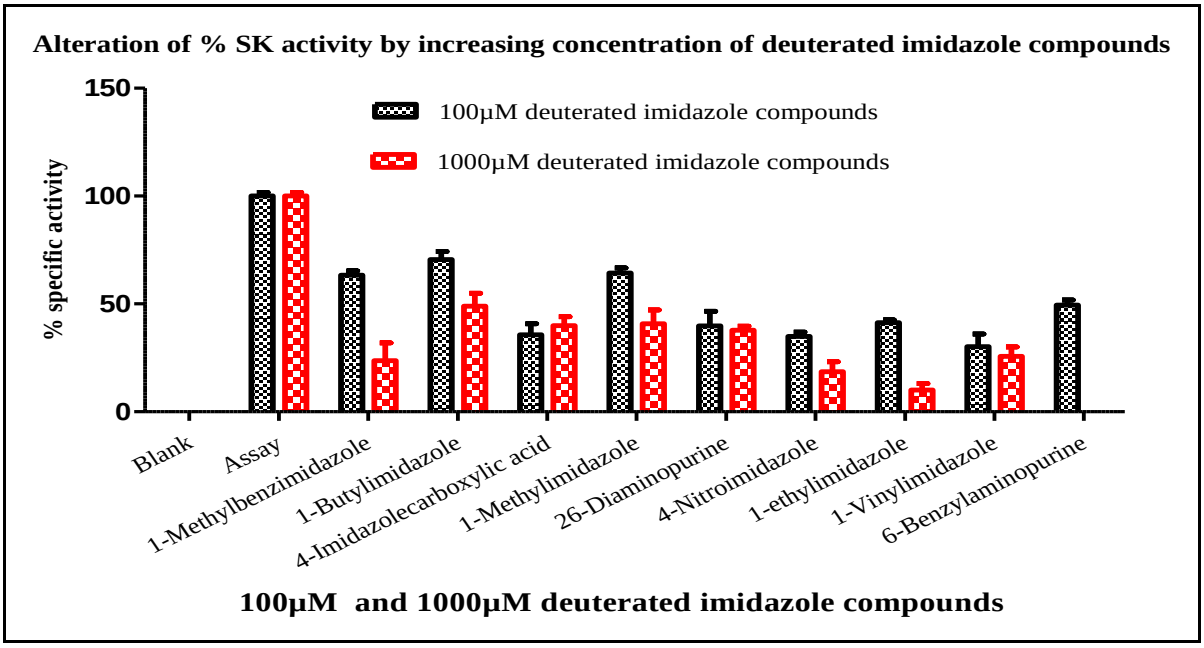

Figure 3.3.6: *Change in SK specific activity in the presence of deuterated inhibiting imidazole-containing compounds at 100µM (black) and 1000µM (red). A dose-response is observed in most cases.*

Once again, significant inhibition was observed in **Figure 3.3.6** as the concentration of deuterated imidazole compounds was increased. The strongest inhibitor at 1,000 µM was

6-benzylaminopurine; however, this compound formed a precipitate in the SK reaction. Most other compounds show a dose-response except 4-imidazolecarboxylic acid and 2,6-diaminopurine that showed no significant change. Finally, to determine the effect of deuteration, the protonated and deuterated imidazole-containing compounds were compared in the SK reaction at 100µM **Table 3.3.7** and **Figure 3.3.7**.

Table 3.3.7: *Comparison of the SK specific activity in the presence of protonated and deuterated imidazole-containing compounds at 100µM.*

Type of inhibitor	**100µM protonated inhibitor**		**100µM deuterated inhibitor**	
Sample	**%SP**	**SD**	**%SP**	**SD**
Blank	0.00	0.00	0.00	0.00
Assay	100.00	1.69	100.00	1.69
1-Methylbenzimidazole	88.52	2.81	63.26	2.03
1-Butylimidazole	97.17	3.11	35.64	5.20
4-Imidazolecarboxylic acid	87.79	7.79	39.77	6.82
1-Methylimidazole	96.07	2.17	34.92	2.02
2,6-Diaminopurine	86.06	1.17	41.27	1.27
4-Nitroimidazole	74.23	2.99	30.16	5.87
6-Benzylaminopurine	56.87	1.17	9.47	2.35
1-Vinylimidazole	60.31	6.68	70.54	3.72
1-Ethylimidazole	41.97	1.30	64.32	2.42
4(5)-Hydroxymethyl-imidazole	62.94	4.73	89.08	1.22

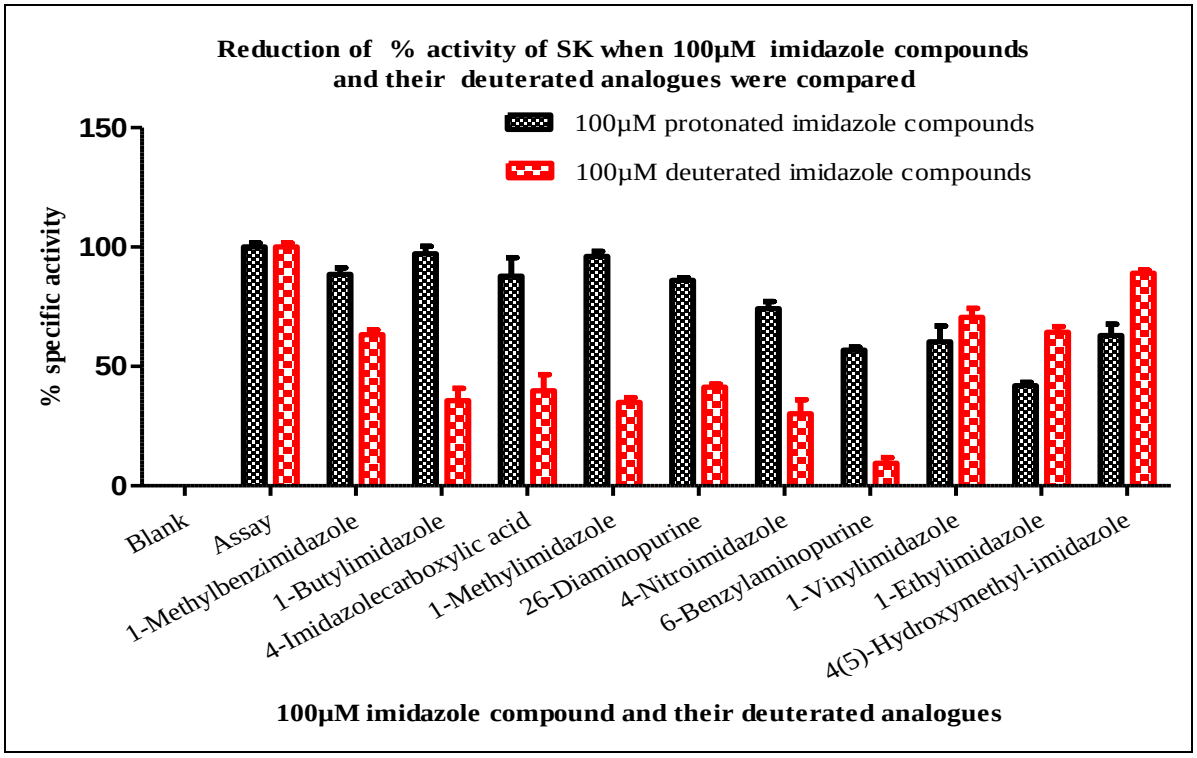

Figure 3.3.7: *The effect on the SK specific activity in the presence of protonated (black) and deuterated (red) imidazole-containing compounds at 100µM. The deuterated analogue caused a significant reduction in SK activity relative to their protonated analogues except in the last three compounds.*

When selected protonated and deuterated compounds were compared at 100µM, the majority inhibited SK. In the majority of imidazole-containing compounds, the deuterated analogue showed stronger inhibition except for 1-vinylimidazole, 1-ethylimidazole and 4(5)-hydroxymethylimidazole. In these cases, the protonated materials had stronger inhibition than their deuterated analogues, although the protonated compounds still showed higher inhibition than the control.

The following **Table 3.3.8** and **Figure 3.3.8** show the results from the substituted purines derived from 2,6-dichloropurine against SK. Again the compound concentration was increased from 100µM to 1000µM.

Table 3.3.8: *Comparison of the SK specific activity in the presence of the synthetic purines.*

Type of concentration	**100µM concentration**		**1000µM concentration**	
Sample	**SP%**	**SD**	**SP%**	**SD**
Blank	0.00	0.00	0.00	0.00
Experiment	100.00	0.00	100.00	0.00
1-Methylpurine	105.20	0.41	114.92	0.99
2-Methylpurine	73.97	0.21	53.36	0.27
1-Ethylpurine	112.51	0.96	116.48	0.76
2-Ethylpurine	20.96	0.27	11.78	0.27
1-Benzylpurine	31.69	1.11	18.43	0.15
2-Benzylpurine	21.01	0.20	12.57	0.08

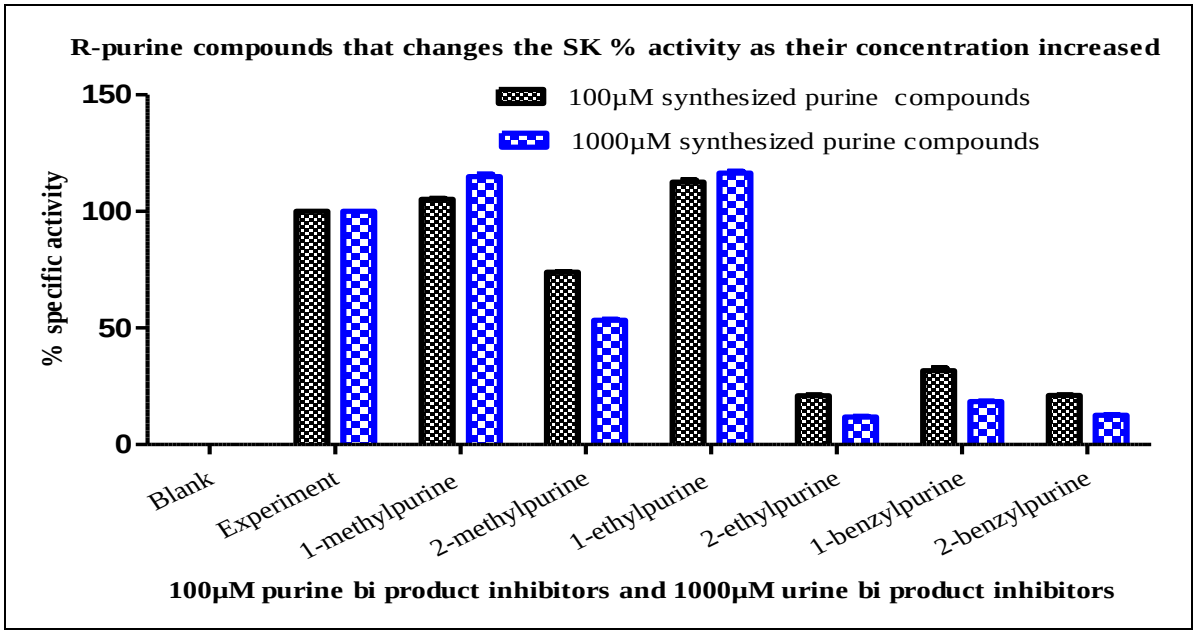

Figure 3.3.8: *Reduction and activation of the activity of shikimate kinase when synthetic purines were added at 100µM (black) and 1000µM (blue) compound concentrations.*

From **Figure 3.3.8** the assays of the purine products at two concentrations showed that all the 2-alkylaminopurines significantly inhibited SK and increased inhibition was observed in response to increased dose. 1-Methypurine and 1-ethylpurine showed no significant changes

or inhibition; however 1-benzylpurine showed significant inhibition. The order of inhibition in the 2-alkylaminopurines was methyl < benzyl l≤ ethyl.

3.3.3 Shikimate kinase IC_{50} determination

The following graphs and tables show IC_{50} results for the three selected compounds from **Figure 3.3.7**(p.91), namely: 1-methylbenzimidazole, 4(5)–hydroxymethylimidazole and 4-imidazole carboxylic acid. These compounds were selected based on their protonated and deuterated inhibition of SK. These compounds were selected on the basis of different % inhibition, ie. : less, moderate and higher inhibition. In addition, these compounds were not precipitating during reaction with the enzyme.

The deuterated 4(5)–hydroxymethylimidazole showed 10.92% inhibition, while its protonated analogue showed 37.06% when compared to the blank. 1-Methylbenzimidazole showed the opposite profile compared to 4(5)-hydroxymethyl-imidazole in that the protonated form showed 11.48 % inhibition, while its deuterated analogue lowered activity by 36.23%. Both compounds lower the activity around 38% in one form or the other. 4-Imidazolecarboxylic acid lowered the activity by 12.21% in the protonated form, while its deuterated analogue lowered the activity by 60.23%. Based on these observations the three compounds were selected from **Table 3.3.7**(p.90) and **Figure 3.3.7**(p.91) for IC_{50} determination on SK. No IC_{50} determination was done on AK enzyme due to time constraints.

In this study, the IC_{50} was calculated for both protonated imidazole and its deuterated analogue in each case for comparison. **Table 3.3.9**(p.94) and **Figure 3.3.9** (p.95) show the IC_{50} sigmoidal curves of protonated and deuterated 1-methylbenzimidazole in the SK-catalysed reaction. A smaller IC_{50} value indicates a higher inhibition of the activity of the enzyme reaction.

Table 3.3. 9: *Specific activity of shikimate kinase in the presence of a concentration gradient of either protonated or deuterated 1-methylbenzimidazole.*

Inhibitor	Protonated 4(5)-hydroxymethylimidazole		Deuterated 4(5)-hydroxymethylimidazole	
Log[Inhibitor]	Avg SP	SD	Avg SP	SD
4.00	511.95	5.12	247.59	14.12
0.85	511.95	5.12	247.59	14.12
0.78	565.72	3.21	285.25	6.97
0.70	583.98	5.38	329.32	3.72
0.57	617.44	9.68	446.60	12.96
0.40	620.25	12.53	518.85	4.97
0.24	654.97	17.47	549.53	7.23
0.00	717.59	31.85	601.35	7.84
-0.52	746.54	17.32	671.63	0.78
-1.22	707.74	9.46	788.66	9.15
-2.22	731.62	2.25	760.84	5.39
-5.00	798.48	4.70	798.48	4.70

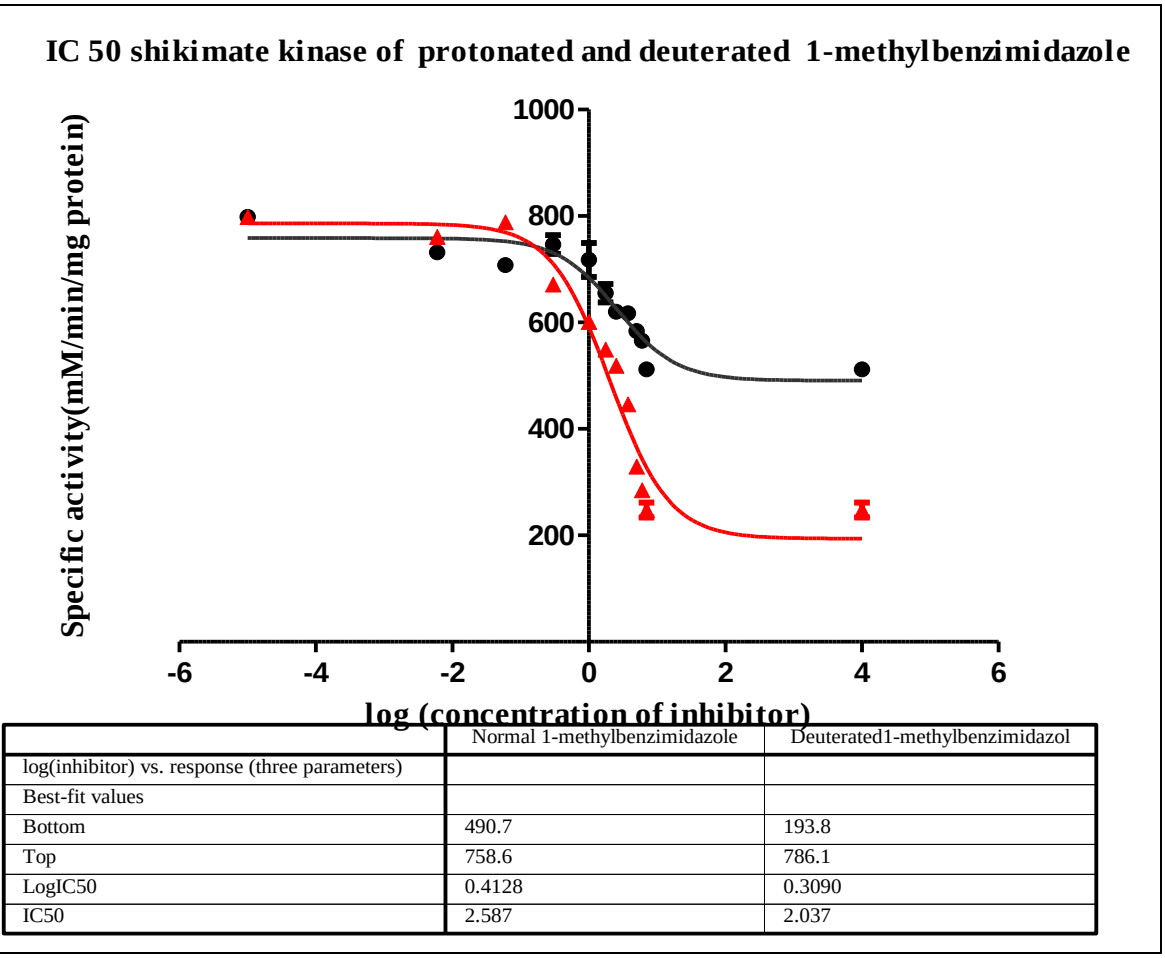

	Normal 1-methylbenzimidazole	Deuterated1-methylbenzimidazol
log(inhibitor) vs. response (three parameters)		
Best-fit values		
Bottom	490.7	193.8
Top	758.6	786.1
LogIC50	0.4128	0.3090
IC50	2.587	2.037

Figure 3.3.9: *IC_{50} curve of protonated (black) and deuterated (red) 1-methylbenzimidazole.*

The deuterated 1-methylbenzimidazole has a higher binding affinity for SK as compared to the protonated compound. This was confirmed by the IC_{50} values of 2.59µM (protonated material) and 2.04µM (deuterated material), respectively.

The second compound that was tested for IC_{50} in SK-catalysed reaction was protonated and deuterated 4(5)-hydroxymethylimidazole. The data derived is summarised in **Table 3.3.10** (p.96) and Figure **3.3.10** (p.97)**.**

Table 3.3.10: *Specific activity data of shikimate kinase in the presence of a concentration gradient of either protonated or deuterated 4(5)-hydroxymethylimidazole.*

	Protonated 4(5)-hydroxymethyl-imidazole		**Deuterated 4(5)-hydroxymethyl-imidazole**	
Log[Inhibitor]	**Avg SP**	**SD**	**Avg SP**	**SD**
4.00	511.95	5.12	247.59	14.12
0.85	511.95	5.12	247.59	14.12
0.78	565.72	3.21	285.25	6.97
0.70	583.98	5.38	329.32	3.72
0.57	617.44	9.68	446.60	12.96
0.40	620.25	12.53	518.85	4.97
0.24	654.97	17.47	549.53	7.23
0.00	717.59	31.85	601.35	7.84
-0.52	746.54	17.32	671.63	0.78
-1.22	707.74	9.46	788.66	9.15
-2.22	731.62	2.25	760.84	5.39
-5.00	798.48	4.70	798.48	4.70

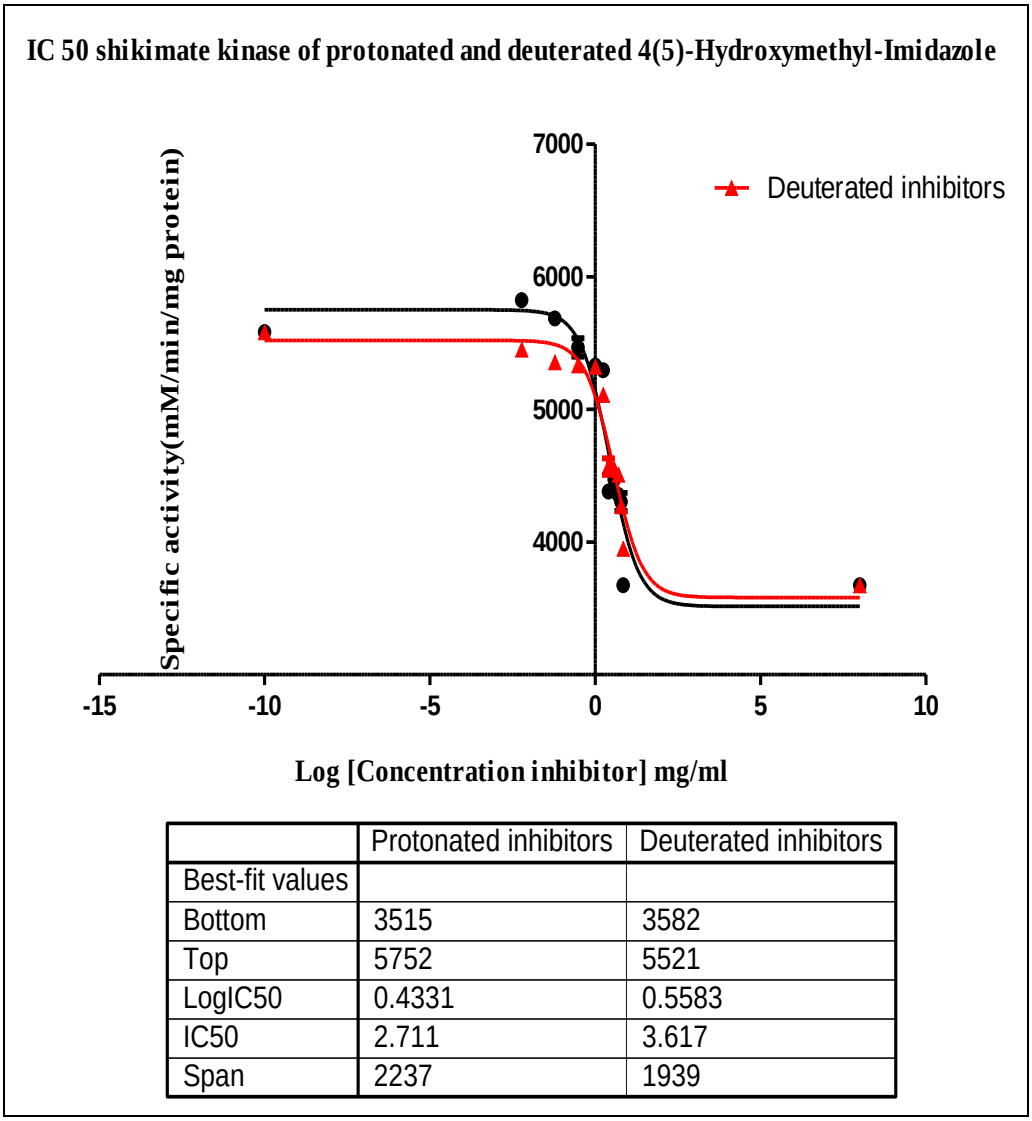

	Protonated inhibitors	Deuterated inhibitors
Best-fit values		
Bottom	3515	3582
Top	5752	5521
LogIC50	0.4331	0.5583
IC50	2.711	3.617
Span	2237	1939

Figure 3.3.10: *IC_{50} curve of protonated (black) and deuterated (red) 4(5) hydroxylmethyl-imidazole.*

In this case, the protonated 4(5)-hydroxymethylimidazole was a stronger inhibitor (IC_{50} 2.71µM) than its deuterated analogue (IC_{50} 3.62µM). These findings are consistent with the behaviour observed in **Figure 3.3.7**, where deuterated 4(5)-hydroxymethylimidazole enhanced SK activity.

IC_{50} determination for the SK inhibition assay with 4-imidazolecarboxylic acid is presented in **Table 3.3.11** (p.98) and Figure **3.3.11** (p.99).

Table 3.3.11: *SK specific activity data of shikimate kinase in the presence of a concentration gradient of either protonated or deuterated 4-imidazolecarboxylic acid.*

Inhibitor	**Protonated 4-imidazolecarbox-aldehyde**		**Deuterated 4-imidazolecarbox-aldehyde**	
Log[Inhibitor]	**Avg SP**	**SD**	**Avg SP**	**SD**
8.00	1506.74	120.67	567.02	85.04
0.85	1506.74	120.67	567.02	85.04
0.78	1688.15	90.18	491.27	30.87
0.70	2331.25	78.72	782.62	116.39
0.57	2942.55	34.85	1743.22	21.75
0.40	3785.50	52.75	2574.25	35.66
0.24	4226.12	148.51	3140.65	52.34
0.00	4537.10	68.99	4118.27	6.95
-0.52	4711.99	17.55	4859.91	18.17
-1.22	4619.17	513.89	5366.63	26.67
-2.22	4297.24	59.05	5256.45	63.45
-10.00	5851.43	4.11	5851.43	4.11

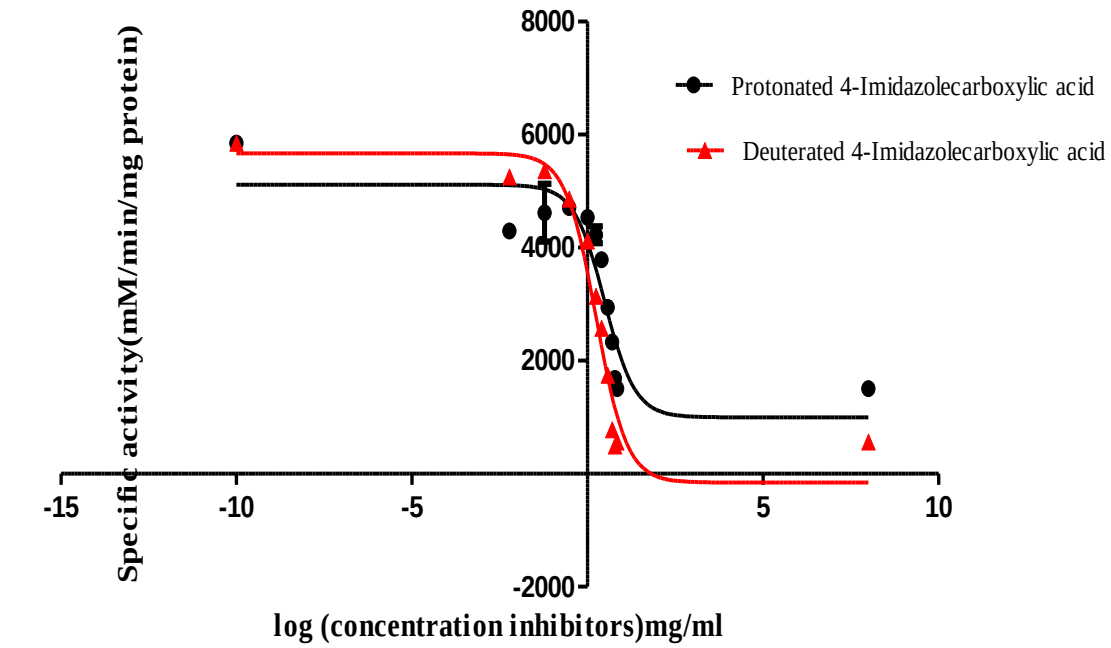

	Protonated inhibitors	Deuterated inhibitors
Best-fit values		
Bottom	997.9	-155.1
Top	5114	5669
LogIC50	0.4845	0.2472
IC50	3.051	1.767
Span	4116	5824

Figure 3.3.11: *IC_{50} curve of protonated (black) and deuterated (red) 4-imidazolecarboxylic acid.*

In the case of 4-imidazolecarboxylic acid, the deuterated material was a more potent inhibitor (IC_{50} 1.77μM) against SK than protonated 4-imidazolecarboxylic acid (IC_{50} 3.05μM)**.**

3.4 Comparative discussion of AK and SK activity in the presence of protonated substrates and their deuterated analogues.

In general, the deuterated imidazole-containing compounds did not lower the % activity of AK. However, the majority of these lower the SK % specific activity. As the concentration of protonated imidazole-containing compounds was increased, in the SK-catalysed reaction, the specific activity progressively dropped. A nearly identical observation was seen with the compound's deuterated analogues. In certain cases, the deuterated imidazole-containing compounds lowered the SK specific activity at least 10% more than their protonated analogues, while in others the opposite is true.

So when comparing compounds and their alteration of % activity of both AK and SK, it could be concluded that some compounds lowered AK % activity, while others enhanced or did not change SK % activity. These changes in enzymatic activity could also have been due to a kinetic isotope effecting the transition state during the primary or secondary reaction. Another possible cause could be that deuterated compounds slightly change the structure or the angle of the covalent C-H/C-D bond because of double mass of deuterium, this could be explained by the lock and key analogy.

When SK specific activity in the presence of synthetic purines was inspected (**Figure 3.3.8** (p 92)) some compounds showed inhibition. Most of the compounds that eluted second showed greater inhibition than those which eluted first. For the benzylpurine, both 1st and 2nd products resulted in reduced SK specific activity. The majority of synthesised purines enhanced the specific activity of AK (**Figure 3.3.2** (p 83)), although some were found to inhibit AK, namely, 1-methylpurine, 1-ethylpurine, 2-ethylpurine and 1-benzylpurine.

For IC_{50} analysis, the three compounds selected based on their inhibition of SK were 4-imidazolecarboxylic acid, 4(5)-hydroxymethylimidazole and 1-methylbenzimidazole. The protonated 1-methylbenz-imidazole's IC_{50} value was 2.59μM and the deuterated 1-methylbenzimidazole's IC_{50} value was 2.04μM, meaning that the deuterated analogue was a better inhibitor of SK. Similarly, the IC_{50} values for protonated 4(5)-hydroxymethylimidazole and deuterated 4(5)-hydroxy-methylimidazole were 2.71μM and 3.62μM respectively. In this case, the protonated compund was the better inhibitor. The IC_{50} values for protonated 4-imidazolecarboxylic acid and the deuterated 4-imidazolecarboxylic acid were 3.05μM and 1.77μM respectively, with the deuterated analogue being more potent than its protonated companion.

CHAPTER 4: DISCUSION, SPECULATION AND CONCLUSION

4.1 General discussion

Deuteration has sparked much attention in the field of biochemistry and pharmacology. The impact that deuterated compounds has brought to these fields based on the higher potency and efficacy can be useful, especially if they inhibit enzymes like shikimate kinase that *Mycobacterium tuberculosis* depends on for survival. In this study, deuteration altered the enzyme-catalysed reaction (specific activity) when using three enzyme namely: shikimate kinase, glutamate synthetase and acetate kinase. ATP deuteration depends on the incubation period and the concentration of the deuterium oxide in the reaction mixture; this was confirmed when a different percentage of deuterium oxide was used at a constant concentration of ATP and TEA as the catalyst. On ATP deuteration, some of the ATP was converted to ADP concurrently.

Since ATP is a common substrate for shikimate kinase, glutamine synthetase and acetate kinase, ATP was deuterated and the kinetic isotopic effect for protonated ATP (KIE_H) and deuterated ATP (KIE_D) was determined. For acetate kinase and glutamate synthetase, the KIE_D increased when comparing the specific activity with an increasing concentration of ATP or ATP-*d*, while shikimate kinase showed the opposite trend. The specific activity in the presence of deuterated ATP was higher than in the presence of protonated ATP. Nineteen commercially obtained imidazole-based were deuterated and assayed against both shikimate kinase and acetate kinase. Thirteen compounds inhibited shikimate kinase, while six activated it or had no effect. Ten compounds were tested for inhibition of acetate kinase, only three of which inhibited, while seven enhanced the acetate kinase activity.

In all three enzymes, some of the deuterated compounds showed higher inhibition than the undeuterated compounds. The effect of deuteration was shown when deuterated ATP was compared to protonated ATP. In GS and SK, the deuterated ATP showed the inhibition but when tested with AK, activation was observed. The behaviour of these enzymes showed that deuteration could be used to regulate the enzyme activity as long as the atom in question is mechanistically implicated, as a KIE would show.

Other compounds that were tested for inhibition were the products derived from 2,6-dichloropurine, which were synthesized by incorporating three different groups: ethyl, methyl and benzyl groups to the 2,6-dichloropurine. Two products were formed for each group incorporated. When all purine compounds were tested for acetate kinase inhibition, only 2-methylpurine and 2-benzylpurine inhibited in a dose-response fashion; the other

compounds activated acetate kinase. When all the purine compounds were tested for shikimate kinase activity, the majority of these compounds inhibited except 1-methylpurine and 1-ethylpurine which had no effect.

Lastly three imidazole compounds that inhibited SK were selected for IC_{50} analysis in order to compare their efficacy and potency. These compounds were 4-imidazolecarboxylic acid, 4(5)-hydroxyimidazole and 1-methylbenzimidazole. These compounds were prepared using homologous dilution. The IC_{50} values of these compounds showed the effect of each compound in relation to potency and efficacy.

4.2 Speculation

From the KIE analysis it could be speculated that the KIE for AK is a secondary kinetic isotopic effect, indicating the C8-H atom is directly involved in the bond formation or breaking on the catalysed reaction. However with SK, the opposite effect is observed, indicating that the reverse reaction is the dominant mechanistic path by which the KIE is operative. The similar effect was also observed when the imidazole compounds were used with AK. Similar findings were observed when imidazole and purine compounds and their deuterated analogues were used with both SK and AK. Knowledge that a hydrogen atom or a weak bond may play a significant role may be probed by replacing it with another atom, such as the deuterium atom.

4.3 Summary

Deuteration may alter the enzyme activity; however the alteration is not identical when the two kinases were compared (AK and SK). The effect of a deuterated compound in altering the activity of SK depends on the type of KIE that is present. When viewing the effect of deuterated common substrate in all enzyme (SK, AK and GS), comparing the activity of protonated ATP with its deuterated analogy. It was clear that C8-H bond affect the activity and relies on whether this bond is directly involved on the formation or breaking of bond during the enzyme reaction. When imidazole, purine compound and their deuterated analogues were tested for inhibition on these enzymes (SK, AK and GS). This study has identified that each compound bind differently with each enzyme which it was applied on, this was caused by the shape of the enzyme binding site that each compound possess. While the deuterated and its protonated analogy do not bind with the similar fashion when compare the activity taken from SK and AK.

4.4 Recommendations

A further analysis of GS is necessary to obtain a more complete selection of chemical compounds that may have an inhibitory effect. From this study the KIE_H and KIE_D of SK, GS and AK suggested a further analysis to determine the binding and the type of KIE of these enzyme. This could be achieved with the Infrared Spectroscopy (IR) studies. Such studies might be able to differentiate changes in enzyme activity based on the possibility of a heavy hydrogen reduces the molecular vibration, or is it causing different kinds of KIE, ie. affecting primary or secondary reactions.

4.5 Conclusion

From this study we can draw the following conclusions:

- ✓ Deuteration depends on deuterium concentration, pH and incubation periods. During deuteration, hydrolysis occurs at a rate slower than the deuteration reaction.
- ✓ Deuteration begins on the labile or acidic proton in imidazole or purine compounds
- ✓ Replacement of hydrogen with deuterium atom supports the 1^{st} and 2^{nd} reaction rate order, while the hydrolysis of ATP to ADP supports the 1^{st} reaction rate order.
- ✓ The KIE_D increases as the concentration of ATP-*d* increases using AK and GS, while the opposite occurs with SK.
- ✓ Not all the imidazoles and their deuterated analogues inhibit AK or SK; however the beginning of chemical library of compounds that do inhibit has been established.
- ✓ Deuteration of imidazole or purine compound increases their inhibition or activation character using SK or AK.

REFERENCES

Adler, S. P., Purich, D. and Stadtman, E. R. Cascade control of *Escherichia coli* glutamine synthetase. Properties of the PII regulatory protein and the Uridylyltransferase-uridylyl-removing enzyme, *J. Biol. Chem.*, 1975, **250**, *16*, 6264-6272.

Bella, D. A. and Tabesh, T. Cancer, Carcinogens and Dispersal: A Disciplinary Dysfunction, *J. Env. Systems*, 1985, **15**, *3*, 211-218.

Bodasing, S. J., Brandt, P. W., Robb, F. T. and Woods, D. R. Purification and regulation of glutamine synthetase in a collagenolytic *Vibrio alginolyticus* strain. *Arch. microbiology*, 1985, **140**, *4*, 369-374.

Burnstock, G., Fredholm, B. B., North, R. A. and Verkhratsky, A. The birth and postnatal development of purinergic signalling. *Acta Physiologica*, 2010, **199**, *2*, 93-147.

Buss, K. A., Cooper, D. R., Ingram-Smith, C., Ferry, J. G., Sanders, D. A. and Hasson, M. S. Urokinase: structure of acetate kinase, a member of the ASKHA superfamily of phosphotransferases. *J. Bact.*, 2001, **183**, *2*, 680-686.

Buteau, K. C. Deuterated Drugs: Unexpectedly Nonobvious. *J. High Technology Law.* 2009, **10**, 22.

Cheng, W. C., Chang, Y. N. and Wang, W. C. Structural basis for shikimate-binding specificity of *Helicobacter pylori* shikimate kinase. *J. Bacteriology*, 2005, **187**, *23*, 8156-8163.

Cullimore, J. V. and Sims, A. P. Occurrence of two forms of glutamate synthase in *Chlamydomonas reinhardii*. *Phytochem.*, 1981, **20**, *4*, 597-600.

Daugherty, M., Vonstein, V., Overbeek, R., & Osterman. Archaeal shikimate kinase, a new member of the GHMP-kinase family. *J. Bacteriology*, 2001, *183*,1, 292-300.

D'Auria, M. Electrophilic substitutions and HOMOs in azines and purines. *Tet. Letters*, 2005, **46**, *37*, 6333-6336.

Eisenberg, D., Gill, H. S., Pfluegl, G. M. and Rotstein, S. H. Structure–function relationships of glutamine synthetases. *Biochim. Biophys. Acta*, 2000, **1477**, *1*, 122-145.

Faizi, S., Siddiqi, H., Naz, A. and Bano, S. Specific Deuteration in Patuletin and Related Flavonoids via Keto–Enol Tautomerism: Solvent- and Temperature-dependent ^{1}H-NMR Studies. *Helv. Chim. Acta*, 2010, **93**, *3*, 466-481.

Ferguson, A. R. and Sims, A. P. The regulation of glutamine metabolism in Candida utilis: the role of glutamine in the control of glutamine synthetase. *J. Gen. Microbiol.*, 1974, **80**, *1*, 159-171.

Filgueira de Azevedo, W., Canduri, F., Simões de Oliveira, J., Augusto Basso, L., Sérgio Palma, M., Henrique Pereira, J. and Santiago Santos, D. Molecular model of shikimate kinase from *Mycobacterium tuberculosis*. *Biochem. Biophys. Res. Commun.*, 2002, **295**, *1*, 142-148.

Földesi, A., Yamakage, S. I., Nilsson, F. P. R., Maltseva, T. V. and Chattopadhyaya, J. The use of non-uniform deuterium labelling ['NMR-window'] to study the NMR structure of a 21mer RNA hairpin. *Nucleic Acids Res.*, 1996, **24**, *7*, 1187-1194.

Giernoth, R. and Bankmann, D. Transition-metal free ring deuteration of imidazolium ionic liquid cations. *Tet. Letters*, 2006, **47**, *25*, 4293-4296.

Gorrell, A., Lawrence, S. H., & Ferry, J. G. Structural and kinetic analyses of arginine residues in the active site of the acetate kinase from Methanosarcina thermophila. *J. Biol. Chem.* 2005, *280*, 11, 10731-10742.

Heller, S. R. ^{1}H NMR studies on deuterium-hydrogen exchange at C-5 in uridines. *Biochem.Biophys. Res. Commun.*, 1968, **32**, *6*, 998-1001.

Hennig, C., Oswald, R. B. and Schmatz, S. Secondary kinetic isotope effect in nucleophilic substitution: a quantum-mechanical approach. *J. Phys. Chem. A*, 2006, **110**, *9*, 3071-3079.

Hocek, M. and Dvoráková, H. An efficient synthesis of 2-substituted 6-methylpurine bases and nucleosides by Fe-or Pd-catalyzed cross-coupling reactions of 2,6-dichloropurines. *J. Org. Chem.*, 2003, **68**, *14*, 5773-5776.

Ingram-Smith, C., Gorrell, A., Lawrence, S. H., Iyer, P., Smith, K. and Ferry, J. G. Characterization of the acetate binding pocket in the *Methanosarcina thermophila* acetate kinase. *J. Bact.*, 2005, **187**, *7*, 2386-2394.

Kenyon, C. P., Steyn, A., Roth, R. L., Steenkamp, P. A., Nkosi, T. C. and Oldfield, L. C. The role of the C8 proton of ATP in the regulation of phosphoryl transfer within kinases and synthetases. *BMC Biochem.*2011, **12**, *1*, 36.

Kenyon, C. P., & Oldfield, L. C. (2006). "Modulation of Glutamine Synthetase Activity." U.S. Patent Application 12/224,862.

Koley, M., König, X., Hilber, K., Schnürch, M., Stanetty, P. and Mihovilovic, M. D. Synthesis and screening of 2, 6-diamino-substituted purine derivatives as potential cardiomyogenesis inducing agents. *ARKIVOC*, 2011, **6**, 45-61.

Krajewski, W. W., Jones, T. A. and Mowbray, S. L. Structure of Mycobacterium tuberculosis glutamine synthetase in complex with a transition-state mimic provides functional insights. *Proc. Nat. Acad. Sci. USA*, 2005, **102**, *30*, 10499-10504.

Krajewski, W. W., Collins, R., Holmberg-Schiavone, L., Jones, T. A., Karlberg, T. and Mowbray, S. L. Crystal structures of mammalian glutamine synthetases illustrate substrate-induced conformational changes and provide opportunities for drug and herbicide design. *J. Mol. Biol.*, 2008, **375**, *1*, 217-228.

Krell, T., Coggins, J. R. and Lapthorn, A. J. The three-dimensional structure of shikimate kinase. *J. Mol. Biol.*, 1998, **278**, *5*, 983-997.

Kumar, M., Verma, S., Sharma, S., Srinivasan, A., Singh, T. P. and Kaur, P. Structure-Based *In-silico* Design of a High Affinity Dipeptide Inhibitor for Novel Protein Drug Target

Shikimate Kinase of *Mycobacterium tuberculosis*. *Chem. Biol. Drug Design*, 2010, *76*, **3**, 277-284.

Limbach, H. H.. Dynamic NMR spectroscopy in the presence of kinetic hydrogen /deuterium isotope effects in deuterium and shift calculation, 1991, Springer Berlin Heidelberg. pp. 63-164.

Lin, S. H. and Bersohn, R.. Effect of Partial Deuteration and Temperature on Triplet-State Lifetimes. *J. Chem. Phys*., 1968, *48*, 2732.

Martiny-Baron, G., Kazanietz, M. G., Mischak, H., Blumberg, P. M., Kochs, G., Hug, H. and Schächtele, C. Selective inhibition of protein kinase C isozymes by the indolocarbazole. *J. Biol. Chem.*, 1993, *268*, **13**, 9194-9197.

Muckelbauer, J., Sack, J. S., Ahmed, N., Burke, J., Chang, C. Y., Gao, M. and Tebben, A. J. X-Ray Crystal Structure of Bone Marrow Kinase in the X Chromosome: A Tec Family Kinase. *Chem. Biol. Drug Design*, 2011, *78*, **5**, 739-748.

Mukhopadhyay, S., Hasson, M. S. and Sanders, D. A. A continuous assay of acetate kinase activity: Measurement of inorganic phosphate release generated by hydroxylaminolysis of acetyl phosphate. *Bioorg. Chem.*, 2008, *36*, **2**, 65-69.

Novak, I. Purinergic signalling in epithelial ion transport: regulation of secretion and absorption. *Acta Physiol.*, 2011, *202*, **3**, 501-522.

Occhipinti, A., Berlicki, Ł., Giberti, S., Dziędzioła, G., Kafarski, P. and Forlani, G. Effectiveness and mode of action of phosphonate inhibitors of plant glutamine synthetase. *Pest management science*, 2010, *66*, **1**, 51-58.

Ogilvie, K. K., Nguyen-Ba, N., Gillen, M. F., Radatus, B. K., Cheriyan, U. O., Hanna, H. R., and Galloway, K. S. Synthesis of a purine acyclonucleoside series having pronounced antiviral activity. The glyceropurines. *Can. J. Chem*., 1984, *62*, **2**, 241-252.

Pereira, J. H., de Oliveira, J. S., Canduri, F., Dias, M. V., Palma, M. S., Basso, L. A. and de Azevedo, W. F.Structure of shikimate kinase from *Mycobacterium tuberculosis* reveals the binding of shikimic acid. *Acta Cryst. D*, 2004, *60*, **12**, 2310-2319.

Perloff, E. S., Mason, A. K., Dehal, S. S., Blanchard, A. P., Morgan, L., Ho, T., and Stresser, D. M. Validation of cytochrome P450 time-dependent inhibition assays: a two-time point IC_{50} shift approach facilitates kinact assay design. *Xenobiotica*, 2009, *39*, **2**, 99-112.

Reichau, S., Jiao, W., Walker, S. R., Hutton, R. D., Baker, E. N. and Parker, E. J. Potent Inhibitors of a Shikimate Pathway Enzyme from *Mycobacterium tuberculosis* combining mechanism and modelling based design. *J. Biol.l Chem.*, 2011, *286*, **18**, 16197-16207.

Ronzio, R. A., Rowe, W. B. and Meister, A. Mechanism of inhibition of glutamine synthetase by methionine sulfoximine. *Biochem.*, 1969, *8*, **3**, 1066-1075.

Rosado, L. A., Vasconcelos, I. B., Palma, M. S., Frappier, V., Najmanovich, R. J., Santos, D. S. and Basso, L. A. The Mode of Action of Recombinant *Mycobacterium tuberculosis* Shikimate Kinase: Kinetics and Thermodynamics Analyses. *PloS one*, 2013, *8*, **5**, e61918.

Saboury, A. A. Enzyme inhibition and activation: a general theory. *J.Iranian Chem. Soc.*, 2009, *6*, **2**, 219-229.

Salisu, S., Kenyon, C. and Kaye, P. T. Studies towards the synthesis of ATP analogs as potential glutamine synthetase inhibitors. *Synth Commun.* 2011, *41*, **15**, 2216-2225.

Scapin, G. Structural biology in drug design: selective protein kinase inhibitors. *Drug Discovery Today*, 2002, *7*, **11**, 601-611.

Schmidt, S., Biegel, E. and Müller, V. The ins and outs of Na^+ bioenergetics in *Acetobacterium woodii*. *Biochim. Biophys. Acta*, 2009, *1787*, **6,** 691-696.

Schmidt, W. E. and Ebel, J. Specific binding of a fungal glucan phytoalexin elicitor to membrane fractions from soybean *Glycine max*. *Proc. Nat. Acad. Sci.*, 1987, *84*, **12**, 4117-4121.

Sebaugh, J. L. Guidelines for accurate EC_{50}/IC_{50} estimation. *Pharmaceutical statistics*, 2011, *10*, **2**, 128-134.

Sen, A. and Kohen, A. Enzymatic tunneling and kinetic isotope effects: chemistry at the crossroads. *J. Phys. Org. Chem.*, 2010, *23*, **7**, 613-619.

Shoichet, B. K. Interpreting steep dose-response curves in early inhibitor discovery. *J. Med. Chem.*, 2006, *49*, **25**, 7274-7277.

Simonović, A. D. and Anderson, M. D. Light modulates activity and expression of glutamine synthetase isoforms in maize seedling roots. *Arch. Biol. Sci.*, 2008, *60*, **4**, 649-660.

Stadtman, E. R. The story of glutamine synthetase regulation. *J. Biol. Chem.*, 2001, *276*, **48**, 44357-44364.

Suwal, S., Senevirathne, C., Garre, S. and Pflum, M. K. H. Structural Analysis of ATP Analogues Compatible with Kinase-Catalyzed Labeling. *Bioconj. Chem.*, 2012, *23*, **12**, 2386-2391.

Tung, R. The development of deuterium-containing drugs. *Innov. Pharm. Technol.*, 2010, *32*, 24-28.

Turowski, M., Yamakawa, N., Meller, J., Kimata, K., Ikegami, T., Hosoya, K. and Thornton, E. R. Deuterium isotope effects on hydrophobic interactions: the importance of dispersion interactions in the hydrophobic phase. *J. Amer. Chem.l Soc.*, 2003, *125*, **45**), 13836-13849.

Vianello, R. Protonation of Azines and Purines as a Model for the Electrophilic Aromatic Substitution–Rationalization by Triadic Formula. *Acta Chim. Slov.*, 2011, *58*, **3**, 509-520.

Vigano, C., Smeyers, M., Raussens, V., Scheirlinckx, F., Ruysschaert, J. M. and Goormaghtigh, E. Hydrogen-deuterium exchange in membrane proteins monitored by IR spectroscopy: A new tool to resolve protein structure and dynamics. *Biopolymers*, 2004, *74*, **1-2**, 19-26.

Vonrhein, C., Schlauderer, G. J. and Schulz, G. E. Movie of the structural changes during a catalytic cycle of nucleoside monophosphate kinases. *Structure*, 1995, *3*, **5**, 483-490.

Wade, D. Deuterium isotope effects on noncovalent interactions between molecules. *Chemico-biological interactions*, 1999, *117*, **3**, 191-217.

Watson, D. G., Sweet, R. M. and Marsh, R. E. The crystal and molecular structure of purine. *Acta Cryst.*, 1965, *19*, **4**, 573-580.

Wray, L. V. and Fisher, S. H. Functional roles of the conserved Glu304 loop of *Bacillus subtilis* glutamine synthetase. *J. Bacteriol.*, 2010, *192*, **19**, 5018-5025.

Zheng, J., Knighton, D. R., Ten Eyck, L. F., Karlsson, R., Xuong, N. H., Taylor, S. S. and Sowadski, J. M. Crystal structure of the catalytic subunit of cAMP-dependent protein kinase complexed with magnesium-ATP and peptide inhibitor. *Biochem.*, 1993, *32*, **9**, 2154-2161.

Zozaya-Hinchliffe, M., Potenza, C., Ortega, J. L. and Sengupta-Gopalan, C. Nitrogen and metabolic regulation of the expression of plastidic glutamine synthetase in alfalfa (*Medicagosativa*). *Plant Sci.*, 2005, *168*, **4**, 1041-1052.

Internet references

Nitrogen Metabolism and The Urea cycle – The Medical Biochemistry page [Retrieved April 17, 2010, from http://themedicalbiochemistrypage.org/nitrogen-metabolism.html#urea]

Appendix part one

The following structures represent the ^{1}HNMR spectra of imidazole- and purine-containing compound protonated and deuterated analogues together with their 3D chemical structure.

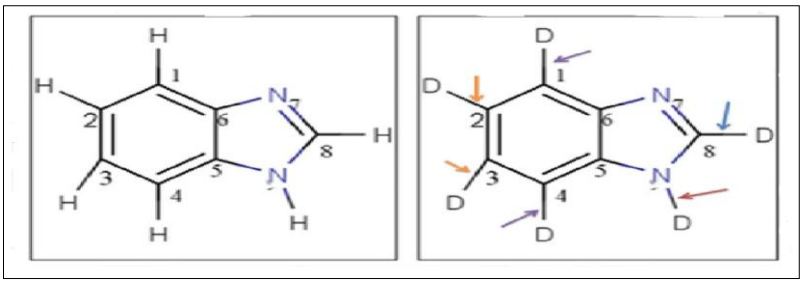

Figure A.1.2: *2D chemical structure of benzimidazole and its points of deuteration, beginning at N9 hydrogen followed by C8, C1, C4, C2 and C3.*

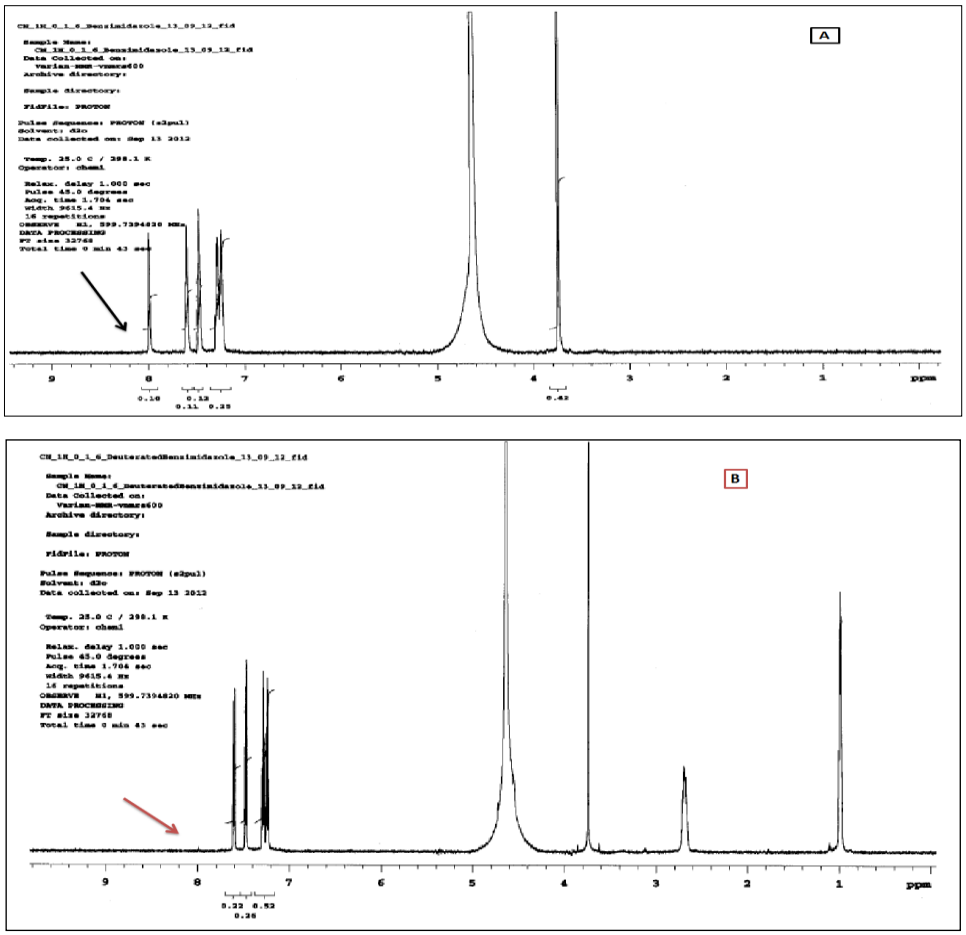

Figure A.1.3: *^{1}H NMR spectrum of benzimidazole is shown in **A**, **B** shows deuteration has proceeded: the black arrow in **A** shows the proton at C2, and the red arrow in **B** shows the proton signal is gone.*

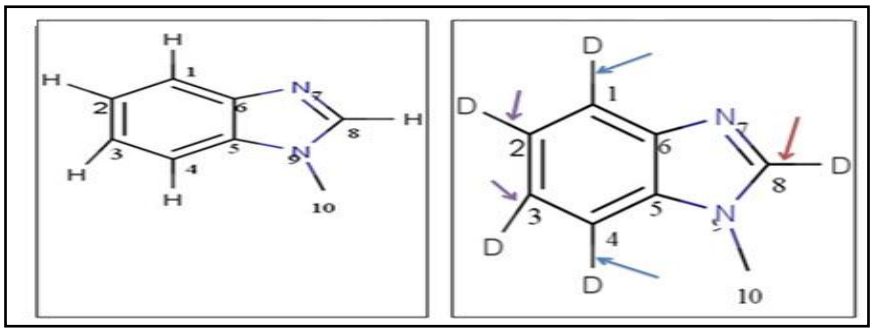

Figure A.1.4: *2D structure of 1-methylbenzimidazole and its points of deuteration, beginning at C8, followed by C4, C1, C2 and C3 as the arrows show.*

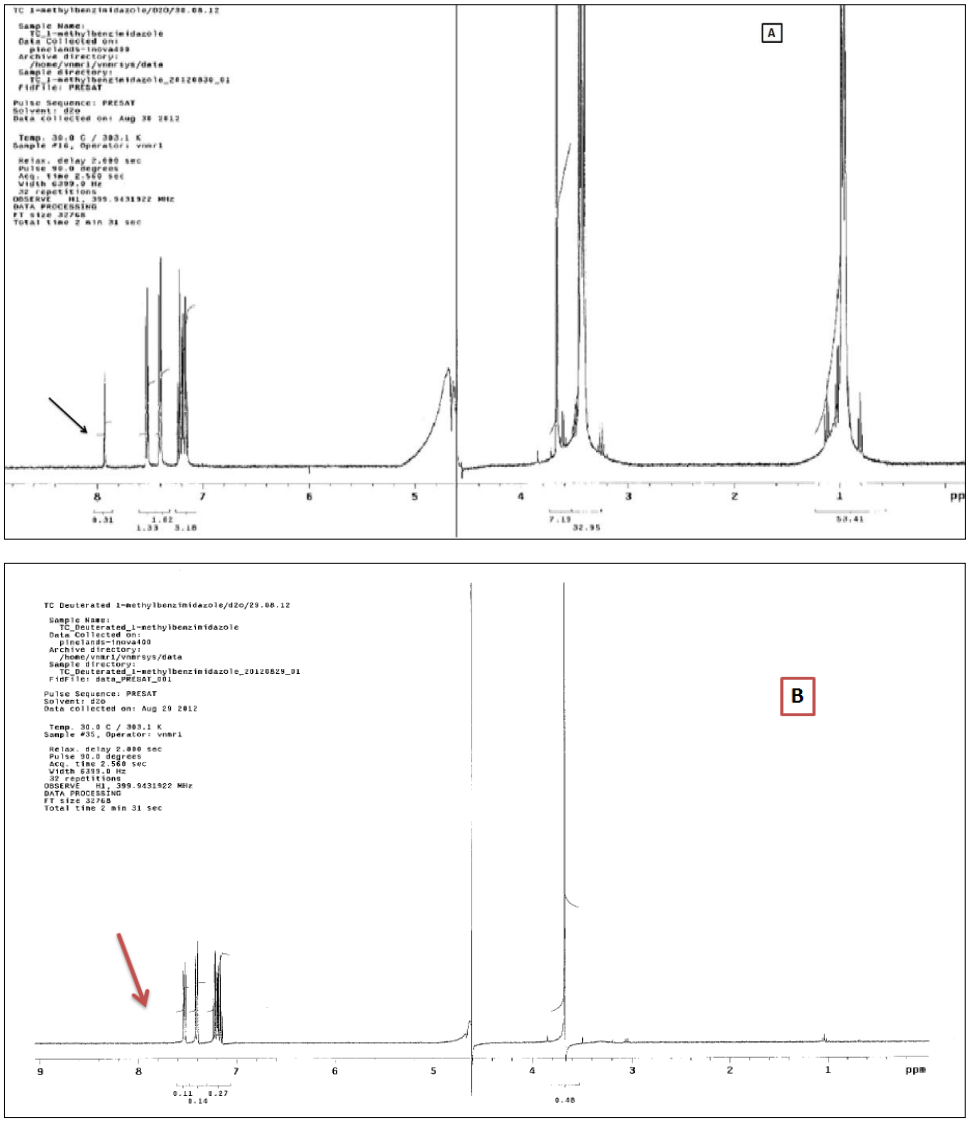

Figure A.1. 5: *^{1}H NMR spectra of 1-methylbenzimidazole, before and after deuteration. The hydrogen atom to be replaced is shown in black in **A**, and its position in red in **B**.*

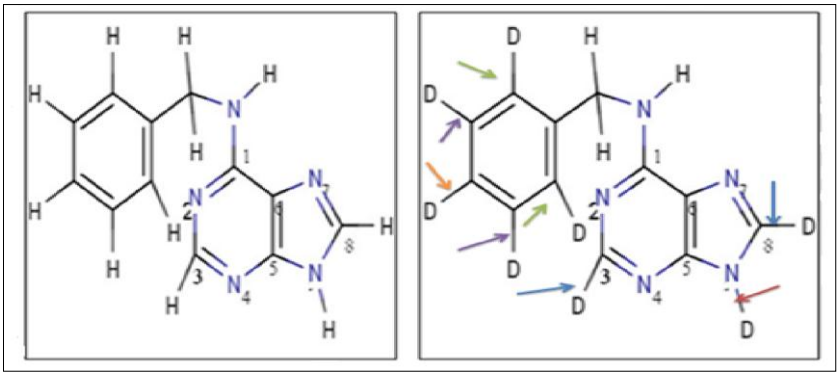

Figure A.1.6: *2D structure of 6-benzylaminopurine and its points of deuteration, beginning at C9 and followed by C8, C3 and then the aromatic hydrogens in the benzene ring.*

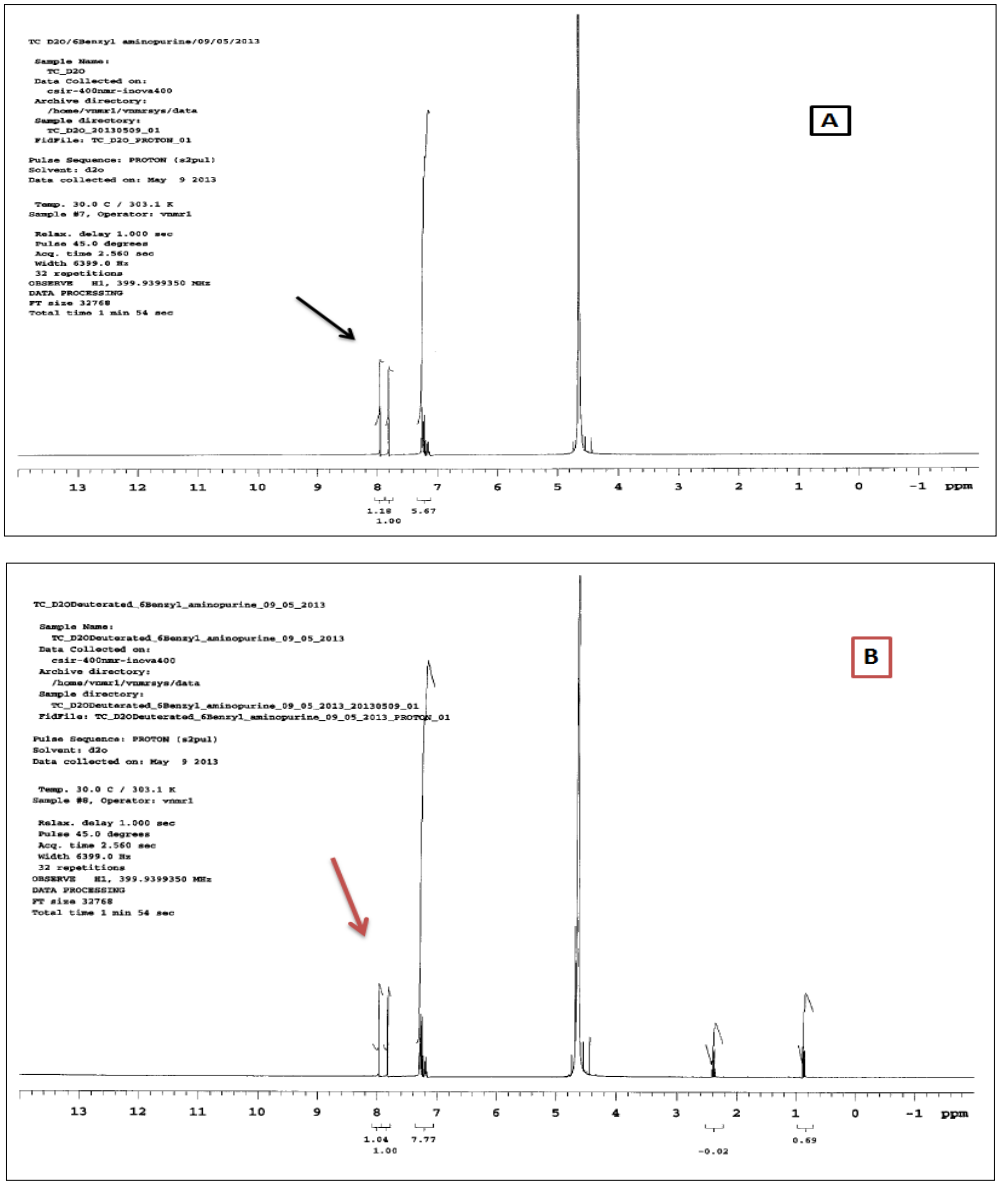

Figure A.1.7: *^{1}H NMR spectrum of 6-benzylaminopurine, before and after deuteration. The hydrogen atom to be replaced is shown in black in* ***A****, and its position in red in* ***B****.*

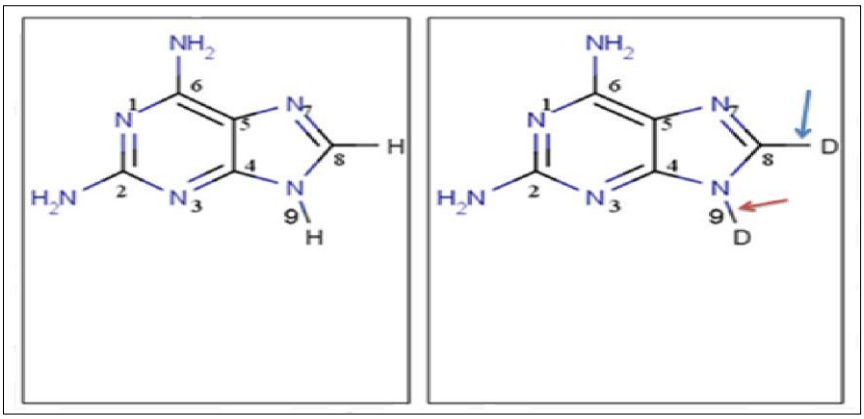

Figure A.1.8: *2D chemical structure of 2,6-diaminopurine and its points of deuteration, beginning at C9 hydrogen and followed by C8.*

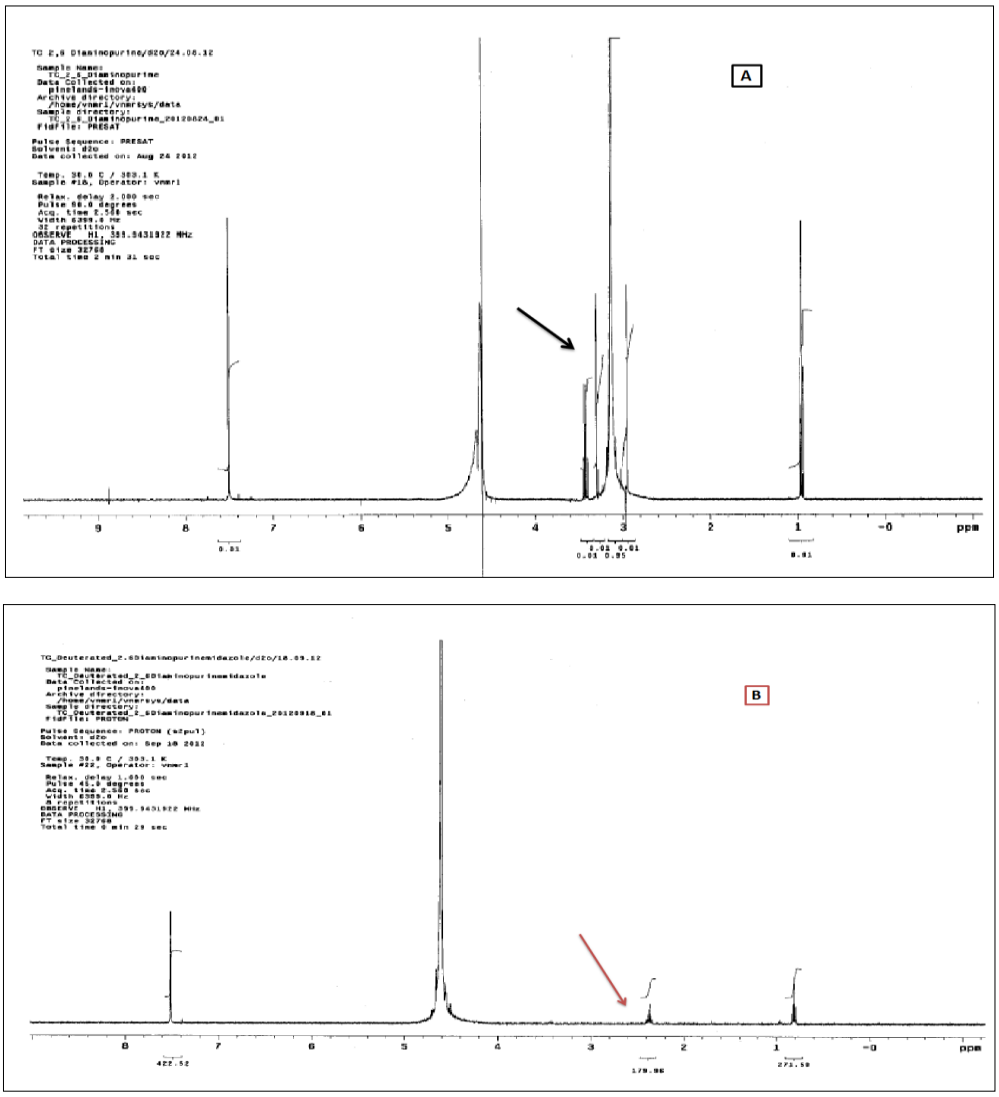

Figure A.1.9: *^{1}H NMR spectrum of 2,6-diaminopurine before and after deuteration. The hydrogen atom to be replaced is shown in black in arrow **A**, and its position in red arrow **B**.*

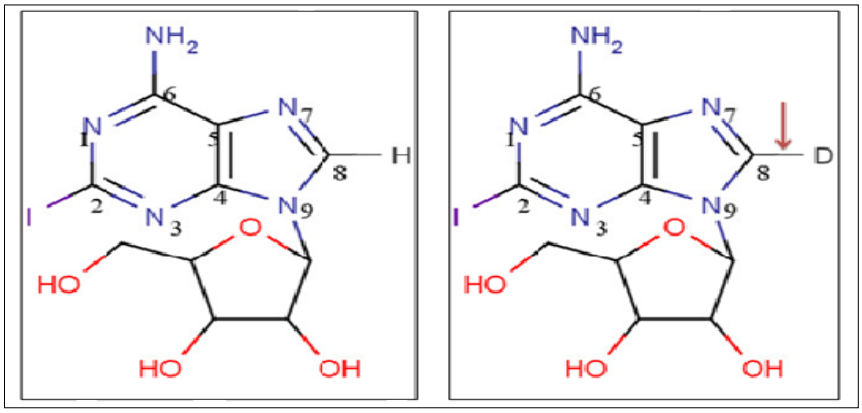

Figure A.1.10: *2D chemical structure of 2-iodoadenosine and its point of deuteration at C8.*

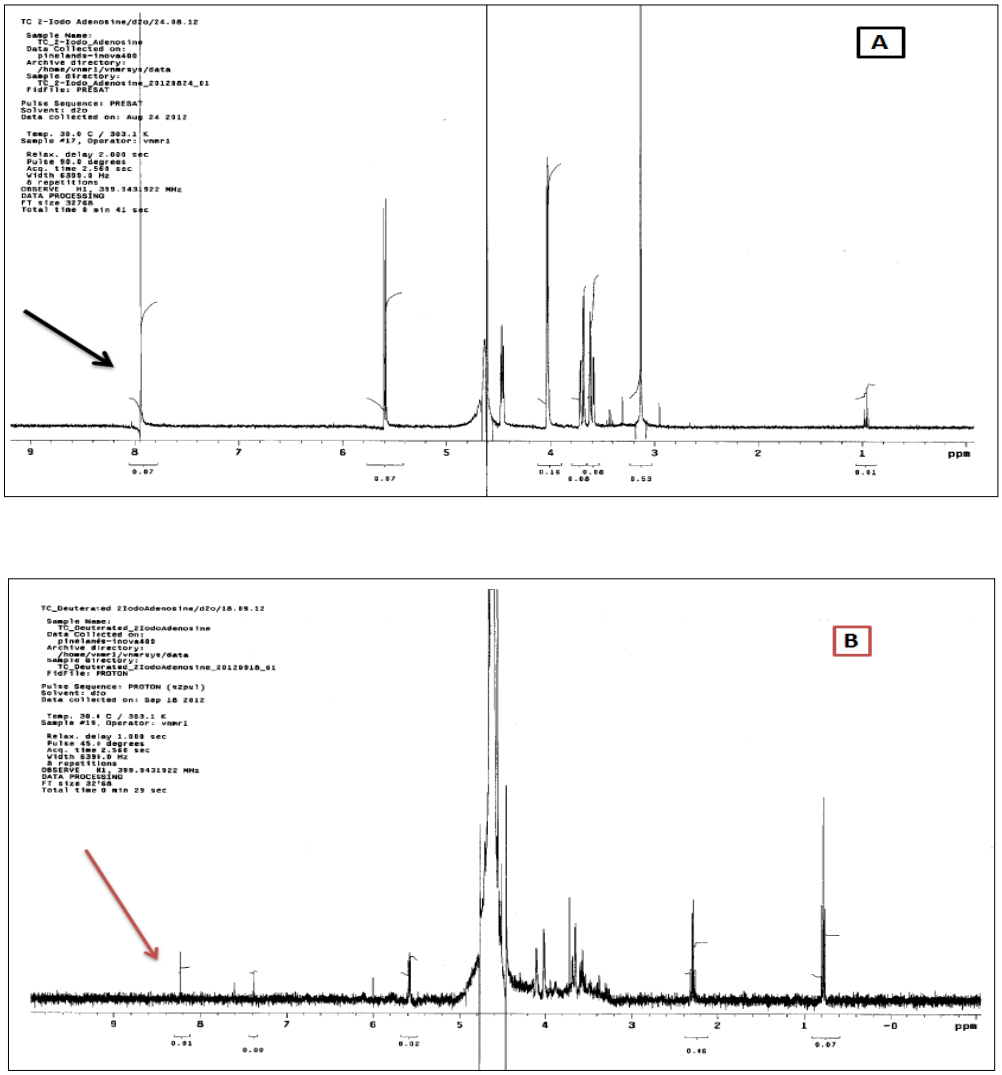

Figure A.1.11: *^{1}H NMR spectrum of 2-iodoadenosine, before and after deuteration. The hydrogen atom to be replaced is shown in black in **A**, and its position in red in **B**.*

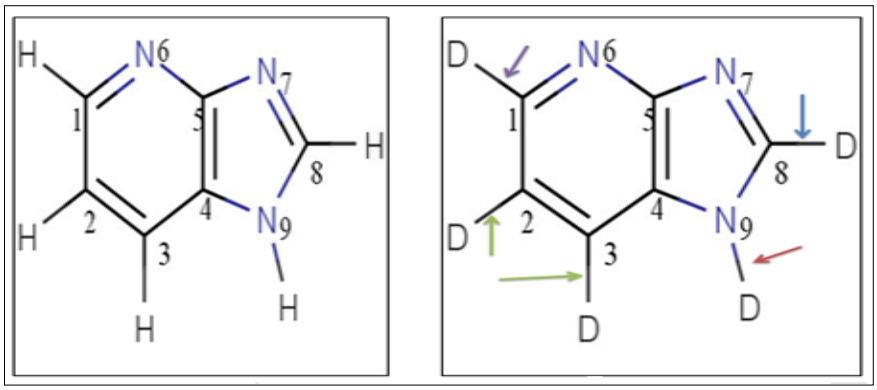

Figure A.1.12: *2D chemical structure of 4-azabenzimidazole and its points of deuteration, beginning at C9 and followed by C8, C1, C2 and C3.*

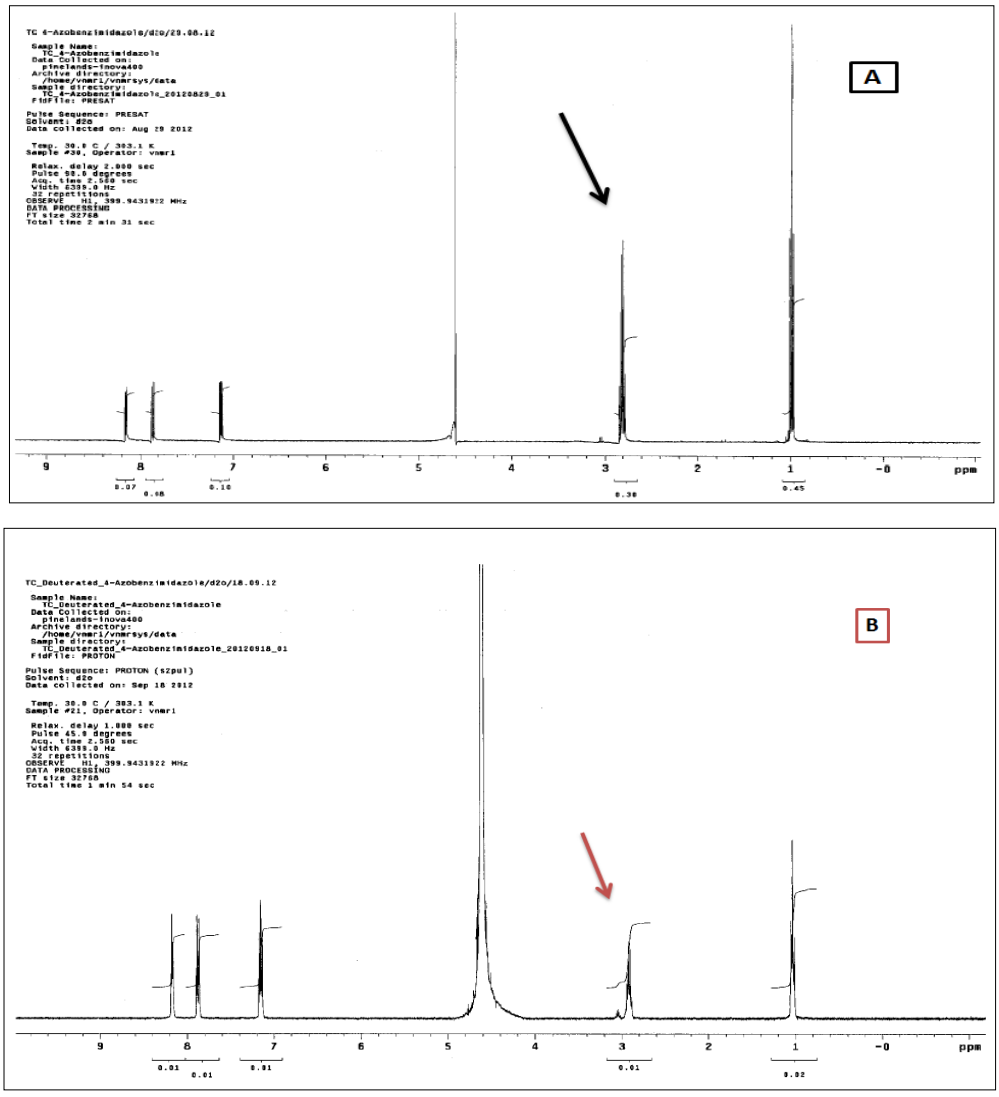

Figure A.1.13: *^{1}H NMR spectrum of 4-azabenzimidazole, before and after deuteration. The hydrogen atom to be replaced is shown in black in **A**, and its position in red in **B**.*

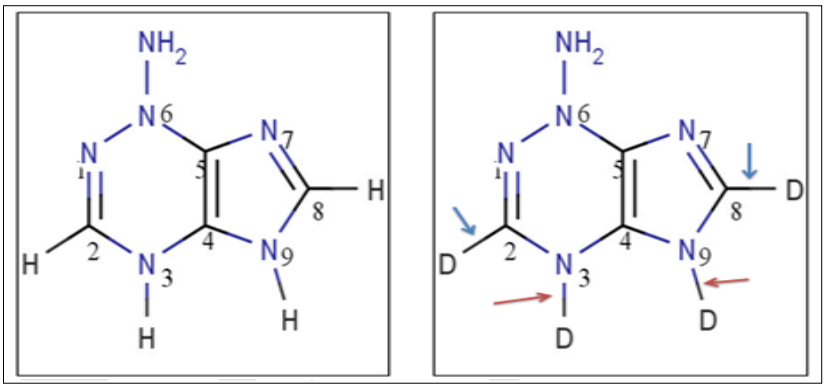

Figure A.1.14: *2D chemical structure of adenine and its points of deuteration, beginning at N9 and N3, followed by C8 and C2.*

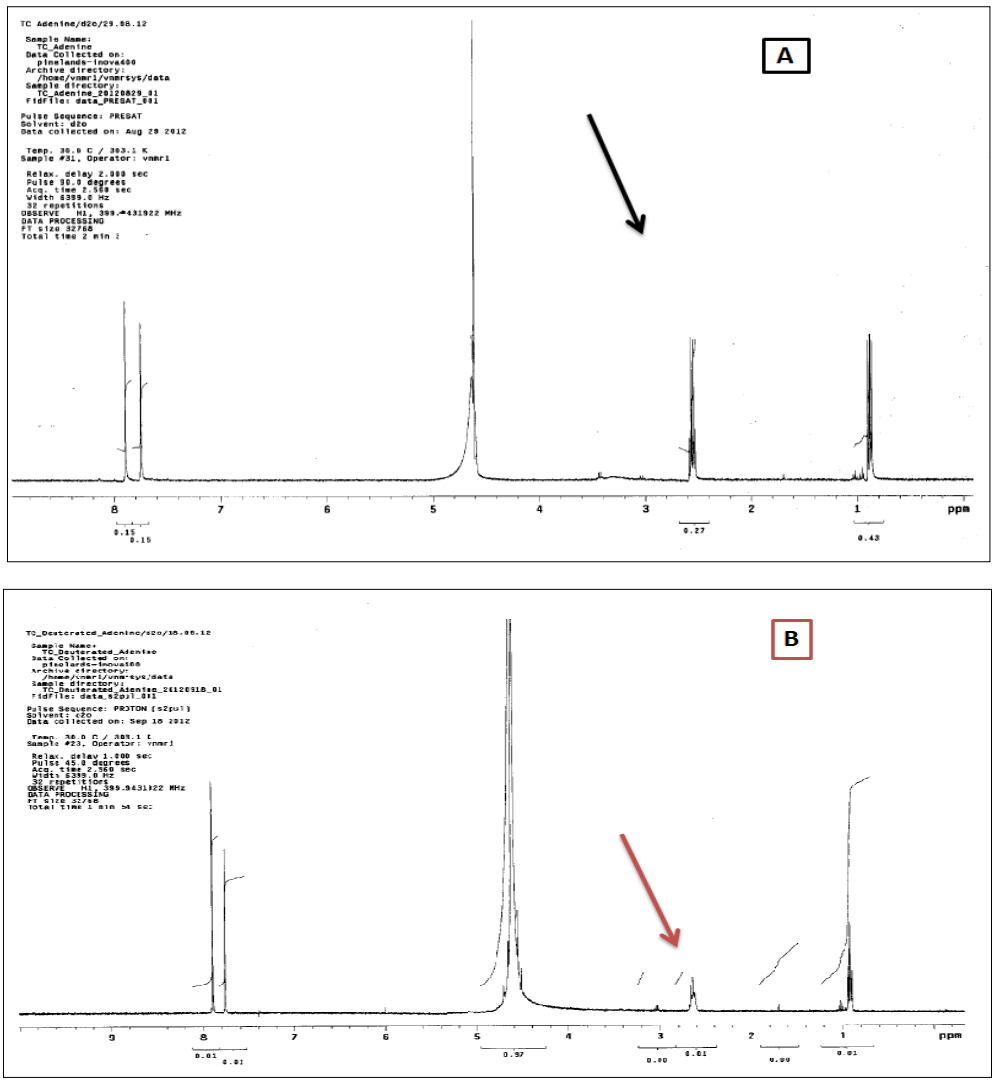

Figure A.1.15: *^{1}H NMR spectrum of adenine before and after deuteration. The hydrogen atom to be replaced is shown in black in **A**, and its position in red in **B**.*

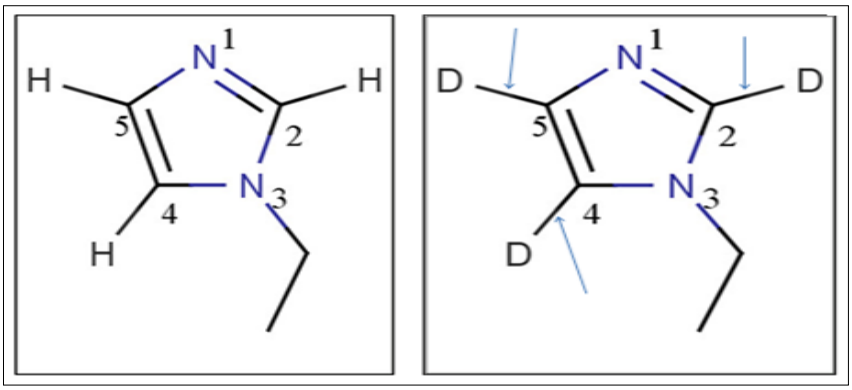

Figure A.1.16: *2D chemical structure of 1-ethylimidazole and its points of deuteration, beginning at C2 followed by C5 and C4.*

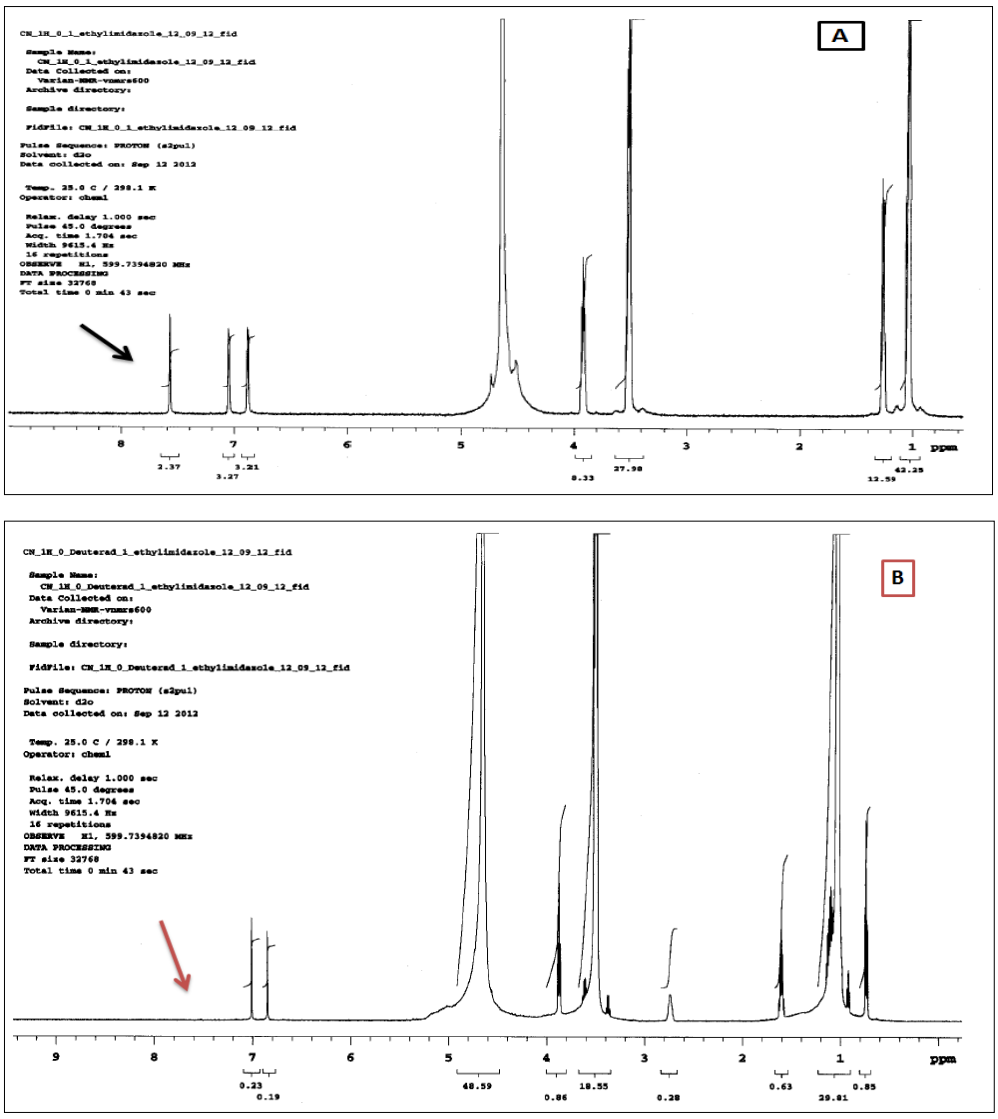

Figure A.1.17: *^{1}H NMR spectrum of 1-ethylimidazole, before and after deuteration. The hydrogen atom to be replaced is shown in black in **A**, and its position in red in **B**.*

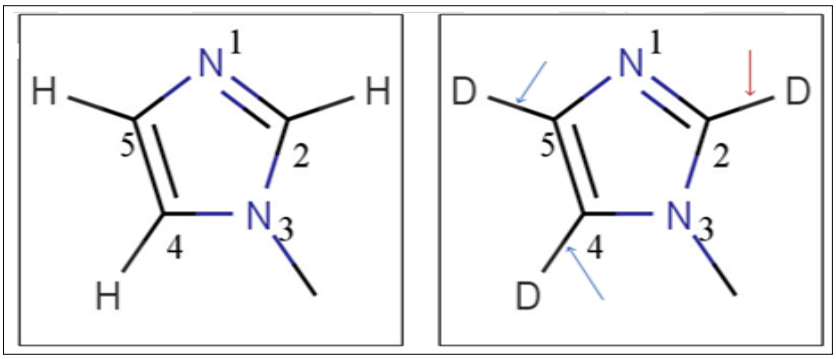

Figure A.1.18: *2D chemical structure of 1(3)-methy imidazole and its points of deuteration, beginning at C2 and followed by C4 and C5.*

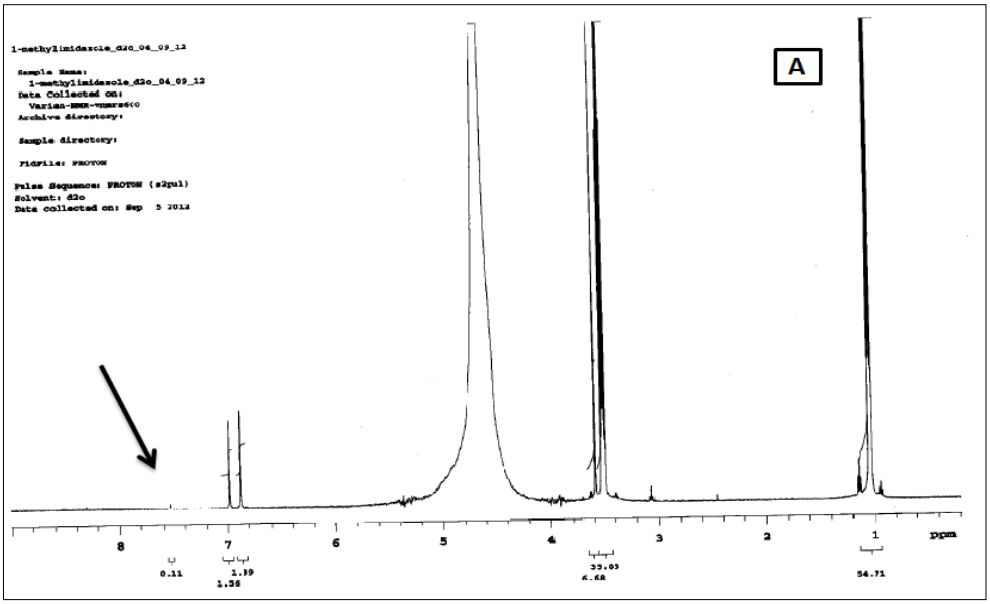

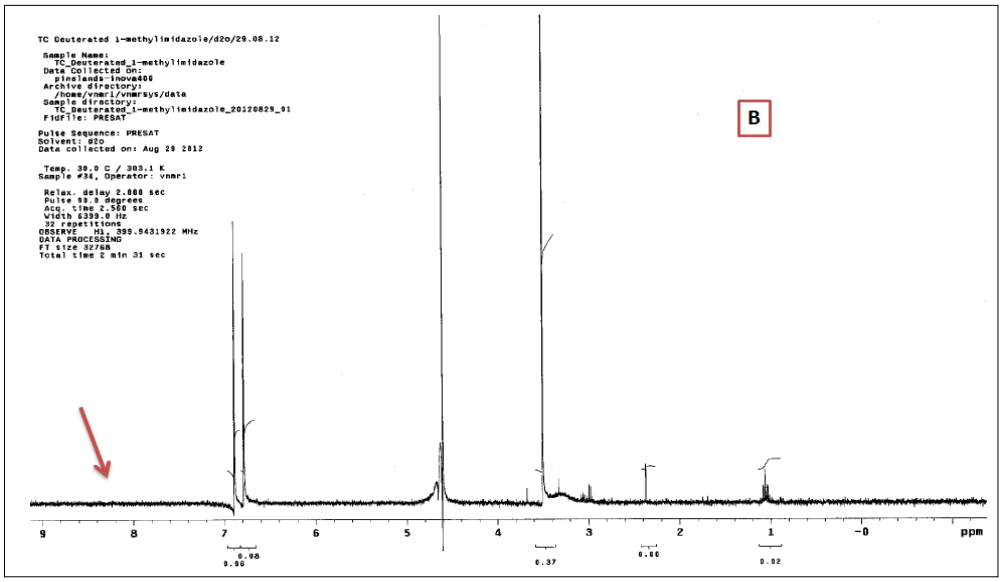

Figure A.1.19: *^{1}H NMR spectrum of 1(3)-methylimidazole, before and after deuteration. The hydrogen atom to be replaced is shown in black in **A**, and its position in red in **B**.*

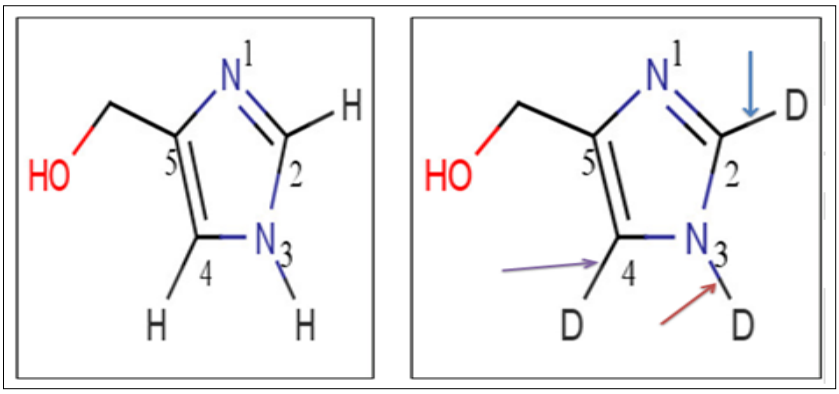

Figure A.1.20: *2D chemical structure of 4(5)-(hydroxymethyl imidazole and its points of deuteration, beginning at N3 and followed by C2 and lastly the C4 position.*

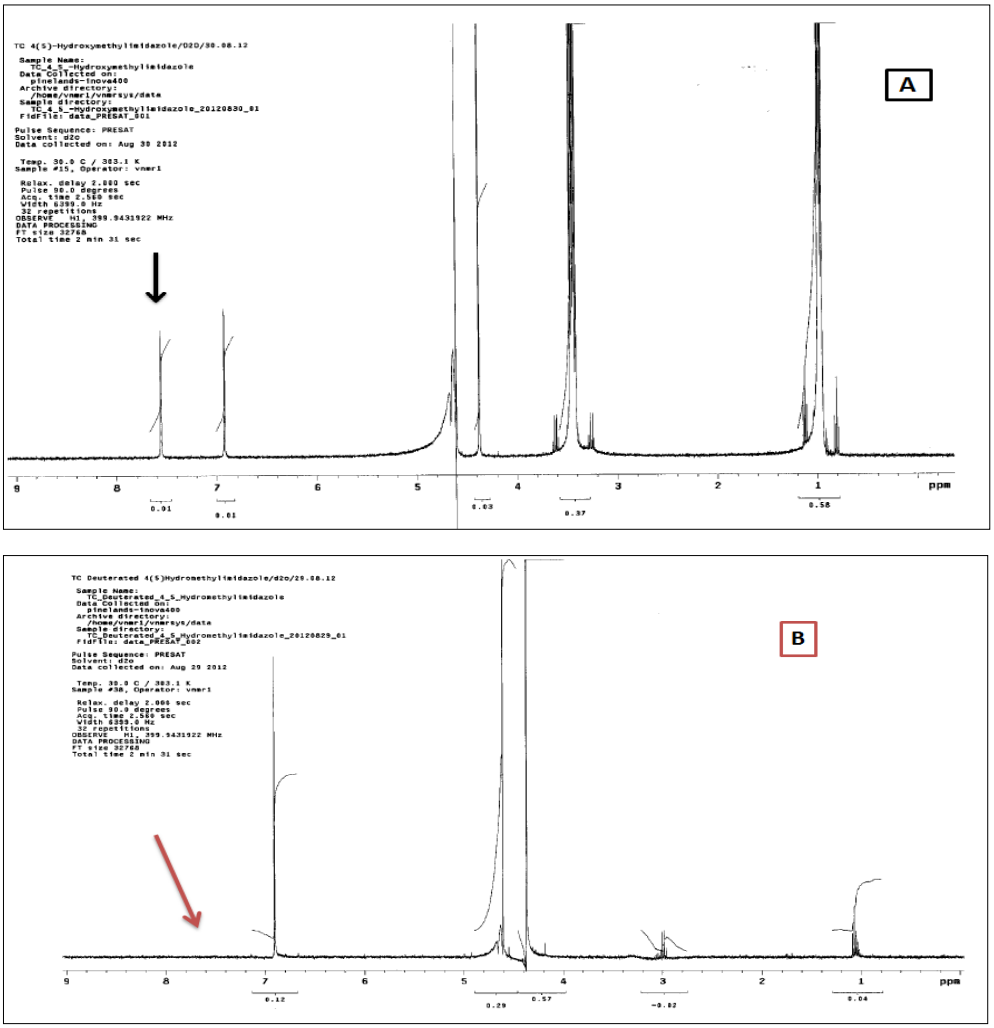

Figure A.1.21: *^{1}H NMR spectrum of 4(5)-(hydroxymethyl) imidazole before and after deuteration. The hydrogen atom to be replaced is shown in black in **A**, and its position in red in **B**.*

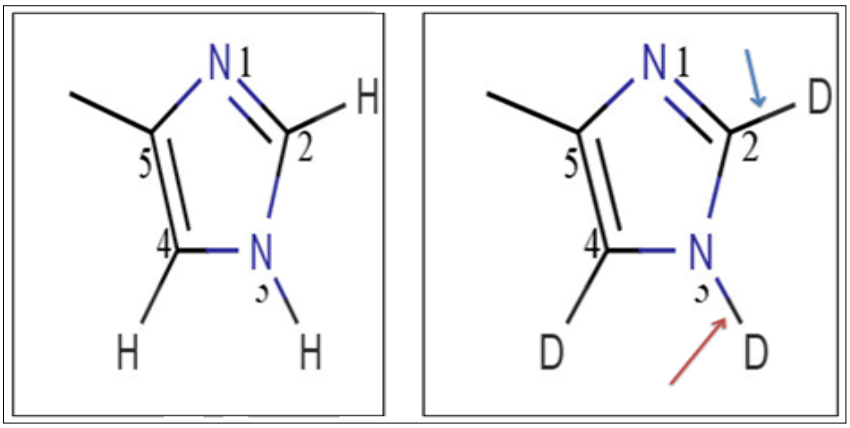

Figure A.1.22: *2D chemical structure of 24(5)-methylimidazole and its points of deuteration, beginning at N3 hydrogen followed by C2 and lastly the C4 position.*

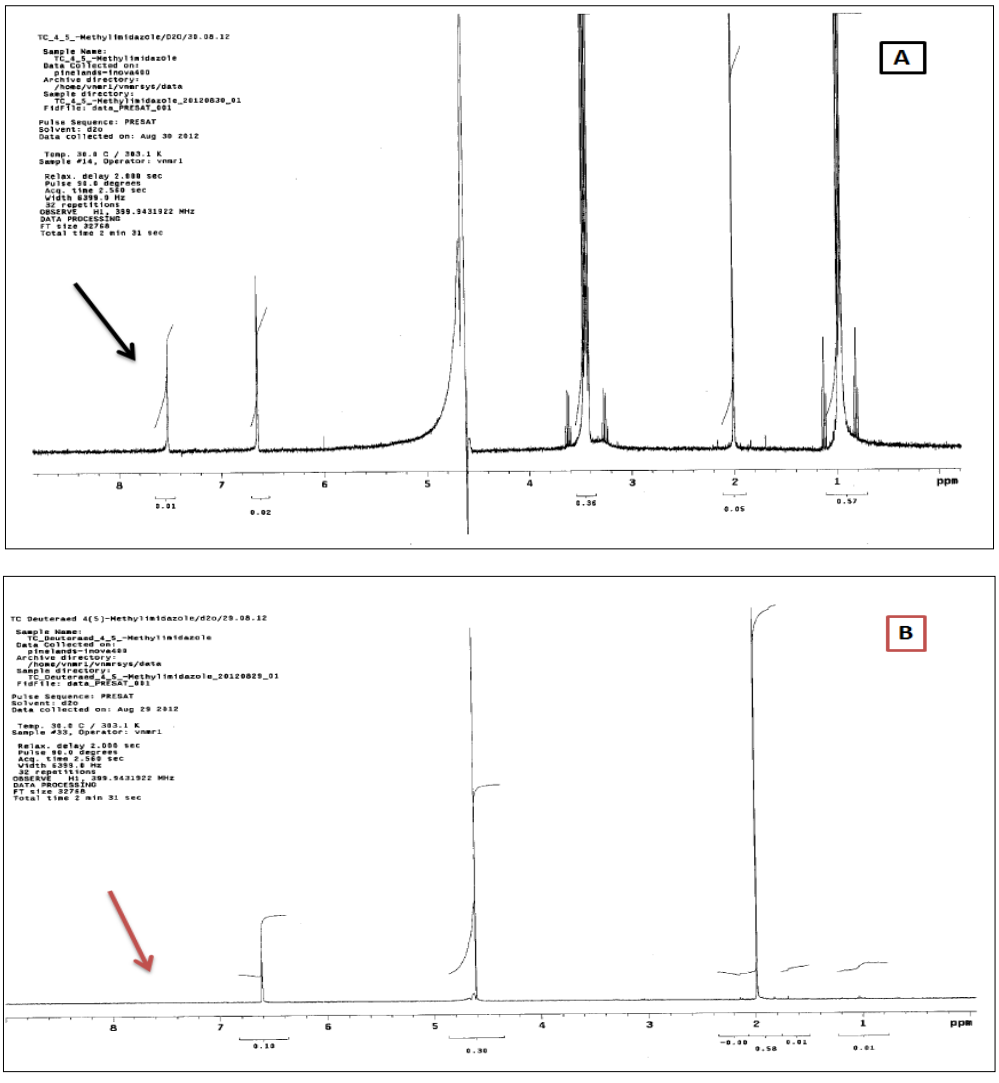

Figure A.1.23: *^{1}H NMR spectrum of 4(5)-methyl imidazole, before and after deuteration. The hydrogen atom to be replaced is shown in black in **A**, and its position in red in **B**.*

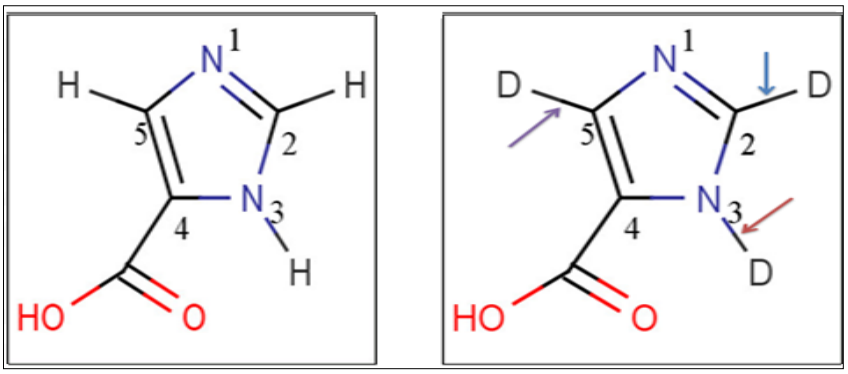

Figure A.1.24: *2D chemical structure of 4-imidazolecarboxylic acid and its points of deuteration, beginning at N3 and followed by C2 and C5.*

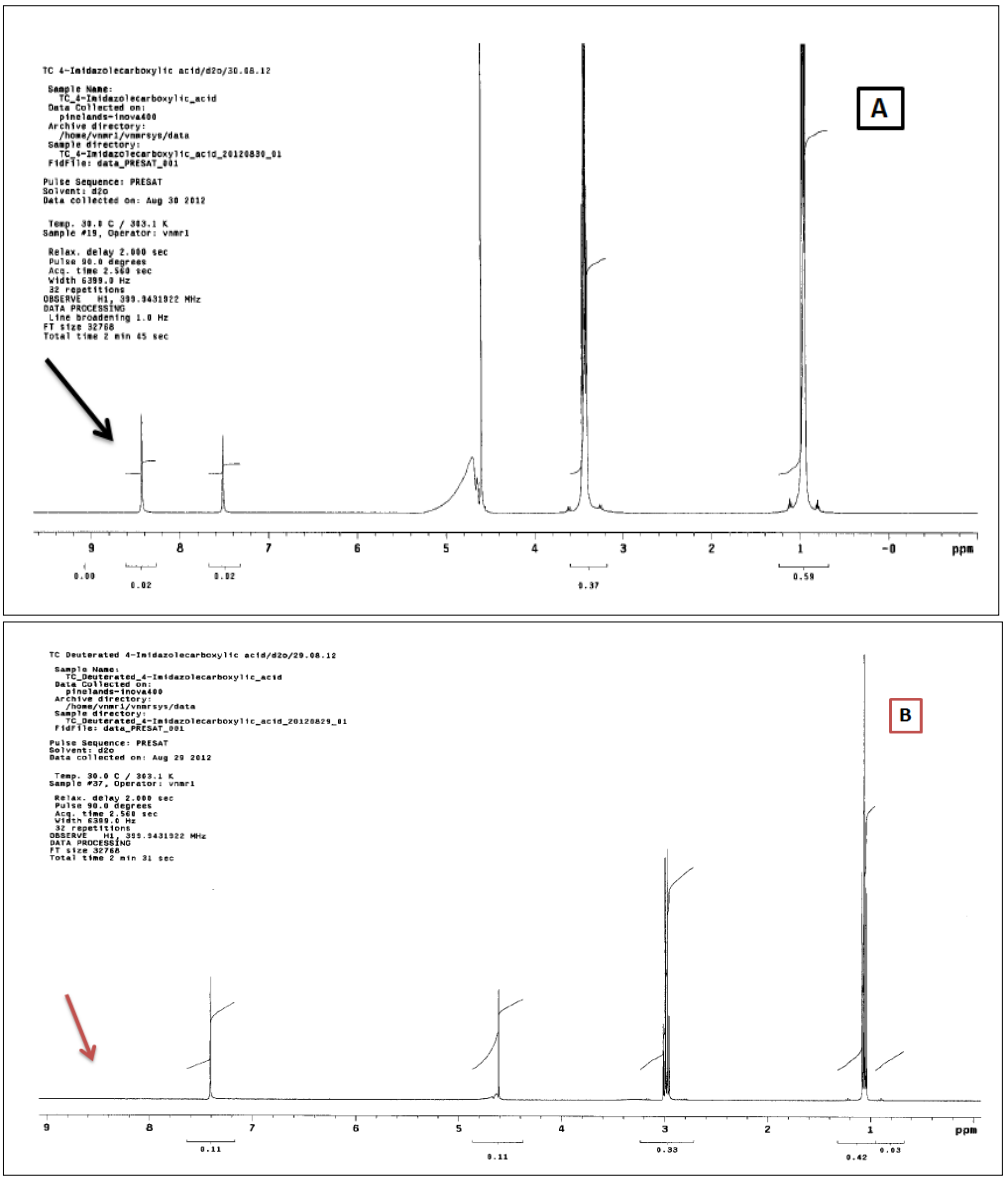

Figure A.1.25: *^{1}H NMR spectrum of 4-imidazolecarboxylic acid, before and after deuteration. The hydrogen atom to be replaced is shown in black in **A**, and its position in red in **B**.*

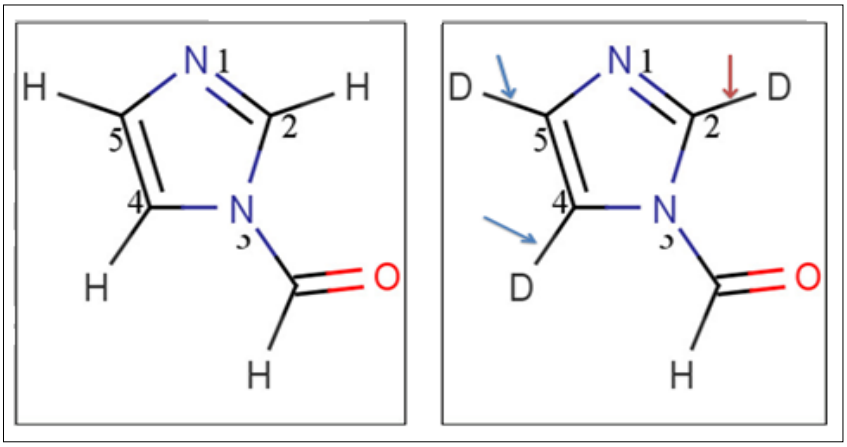

Figure A.1.26: *2D chemical structure of 4-imidazolecarboxyaldehyde and its points of deuteration, beginning at N3 and followed by C2 and C5.*

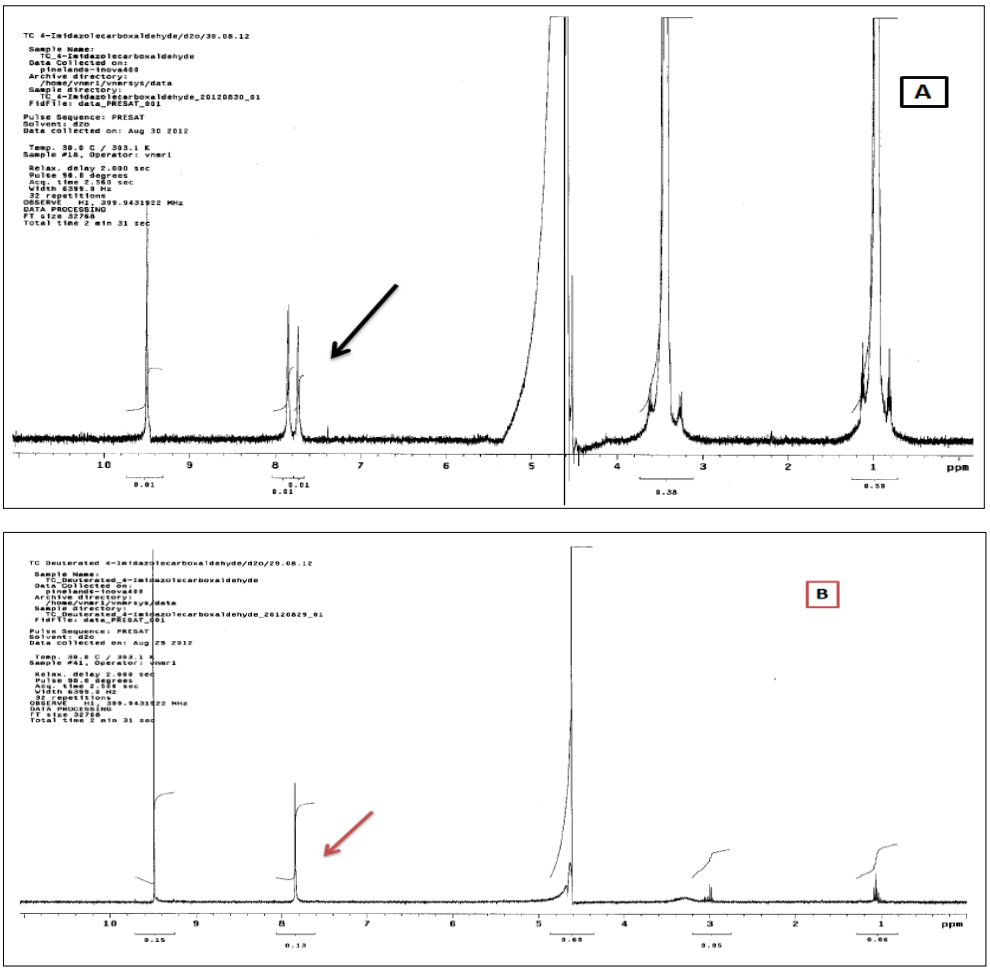

Figure A.1.27: *^{1}H NMR spectrum of 4-imidazolecarboxyaldehyde, before and after deuteration. The hydrogen atom to be replaced is shown in black in **A**, and its position in red in **B**.*

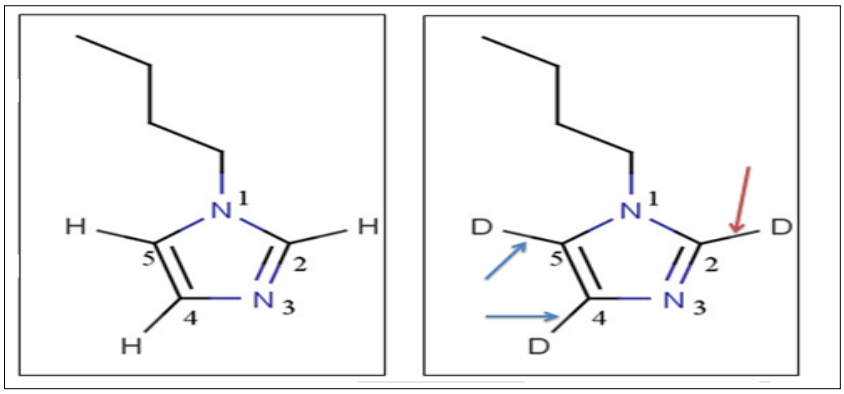

Figure A.1.28: *2D chemical structure of 1-butylimidazole and its points of deuteration, beginning at C2 and followed by C4 and C5.*

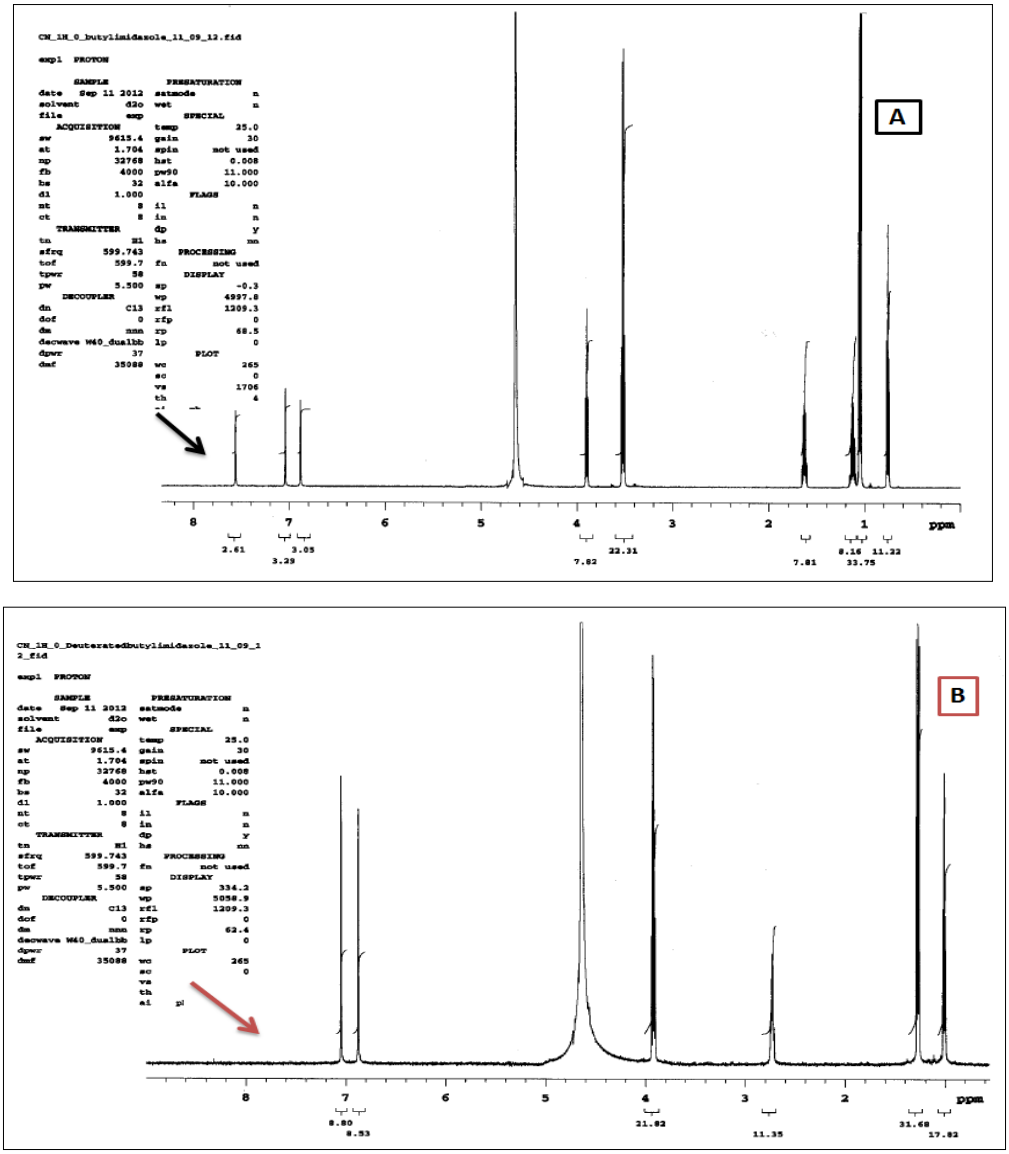

Figure A.1.29: *^{1}H NMR spectrum of 1-butylimidazole, before and after deuteration. The hydrogen atom to be replaced is shown in black in* ***A****, and its position in red in* ***B****.*

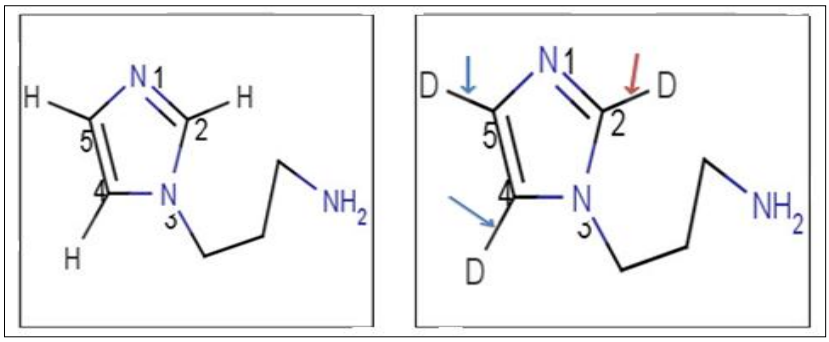

Figure A.1.30: *2D chemical structure of 1-(3-aminopropyl) imidazole and its points of deuteration, beginning at C2 and followed by C4 and C5.*

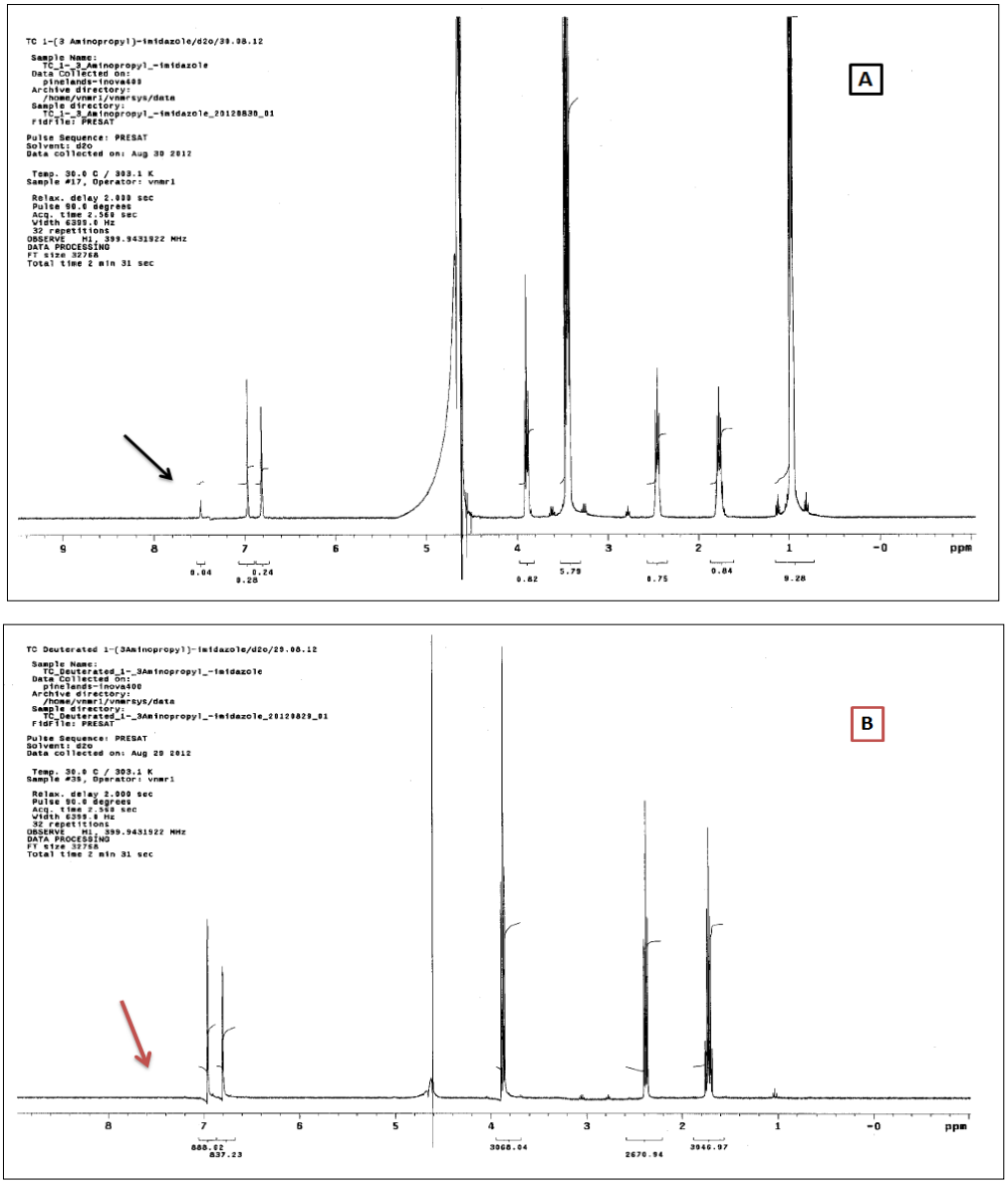

Figure A.1.31: *^{1}H NMR spectrum of 1-(3-aminopropyl) imidazole, before and after deuteration. The hydrogen atom to be replaced is shown in black in **A**, and its position in red in **B**.*

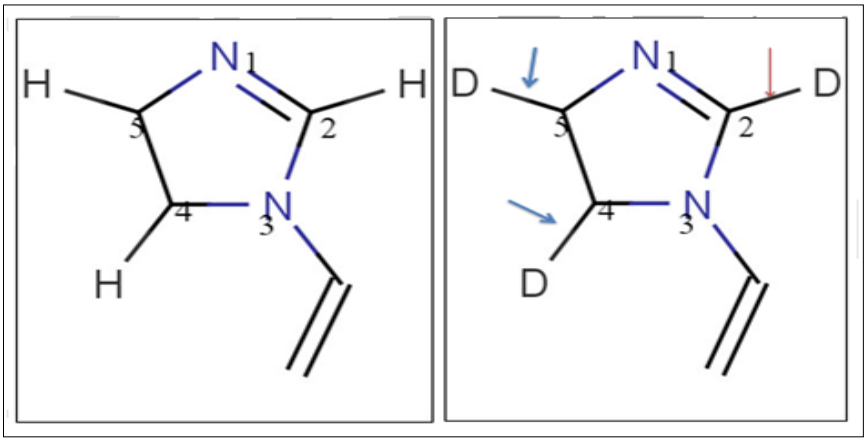

Figure A.1.32: *2D chemical structure of 1-vinylimidazole and its points of deuteration, beginning at C2 hydrogen and followed by C4 and C5.*

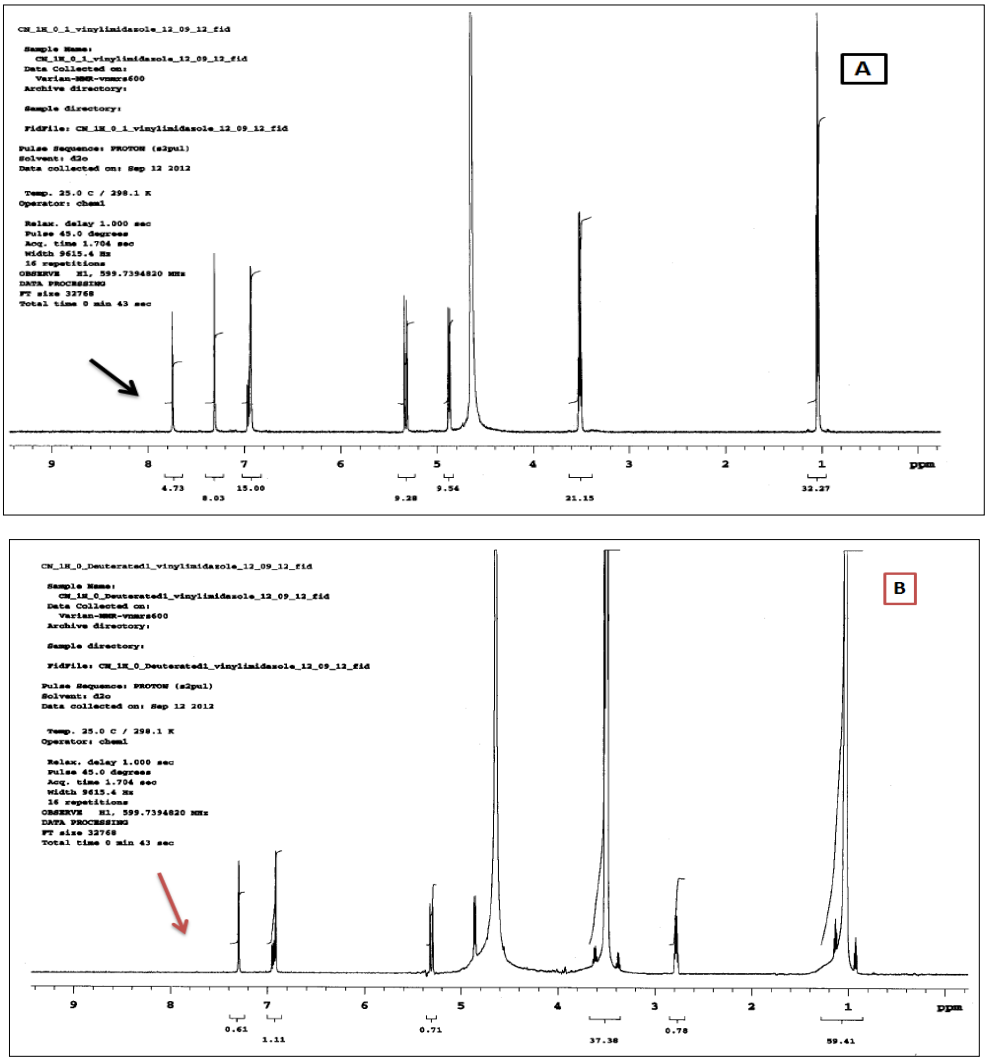

Figure A.1.33: *^{1}H NMR spectrum of 1-vinylimidazole, before and after deuteration. The hydrogen atom to be replaced is shown in black in **A**, and its position in red in **B**.*

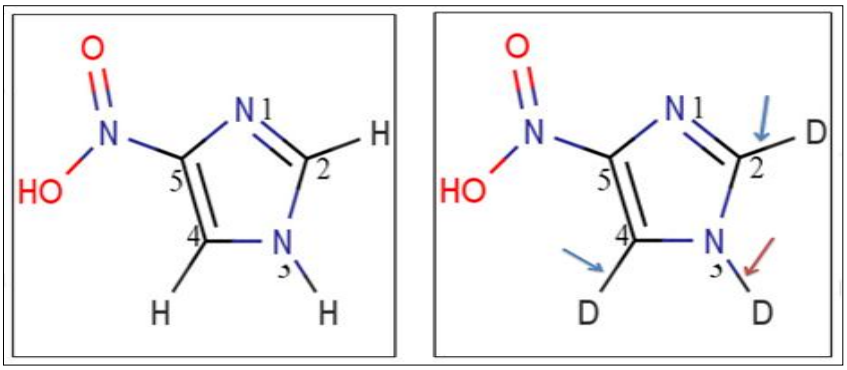

Figure A.1.34: *2D chemical structure of 4-nitroimidazole and its points of deuteration, beginning at N3 and followed by C4 and C2.*

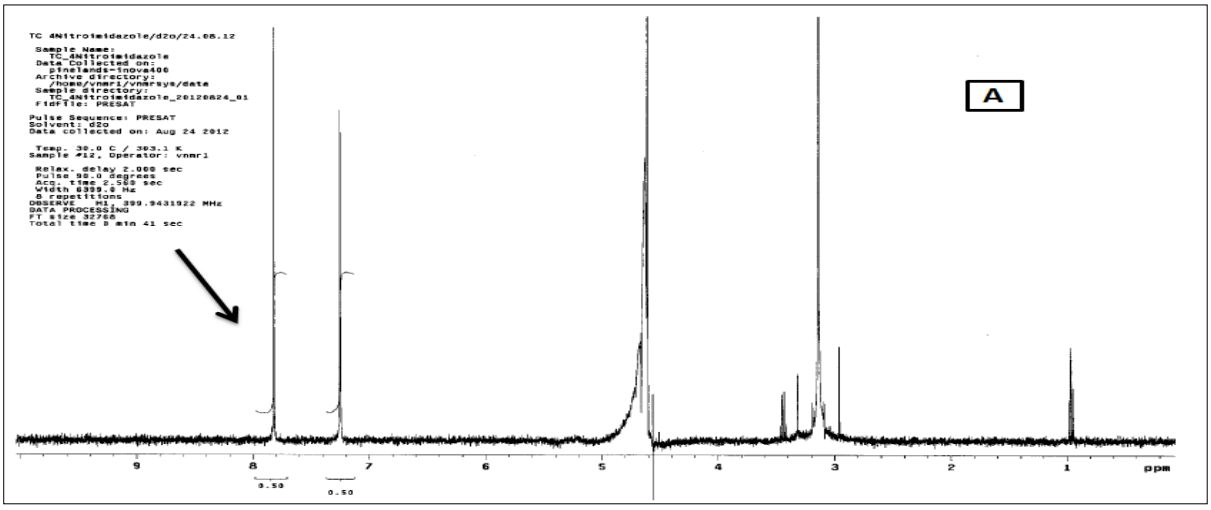

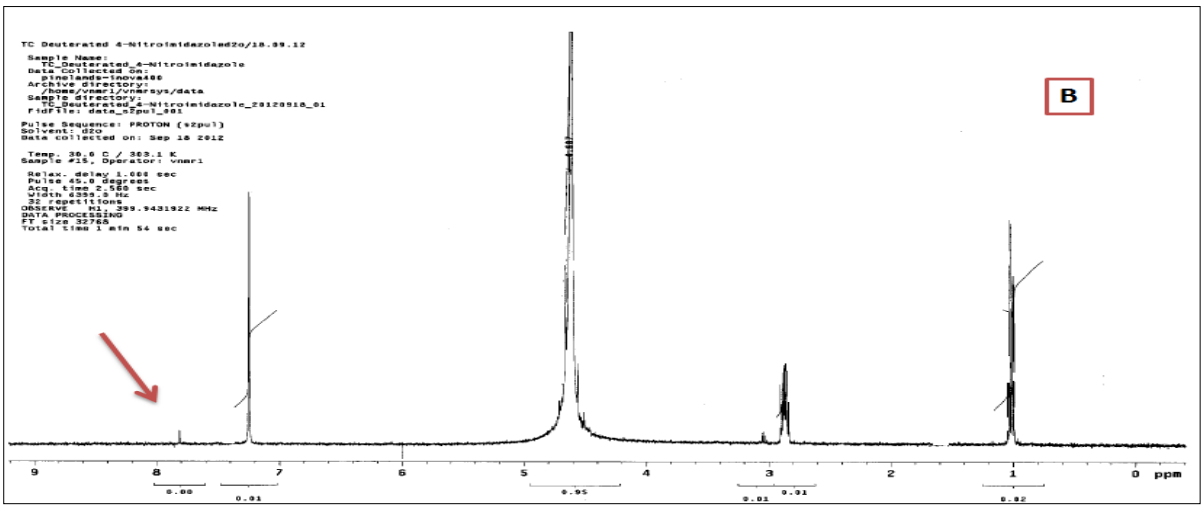

Figure A.1.35: *^{1}H NMR spectrum of 4-nitroimidazole, before and after deuteration. The hydrogen atom to be replaced is shown in black in* ***A****, and its position in red in* ***B****.*

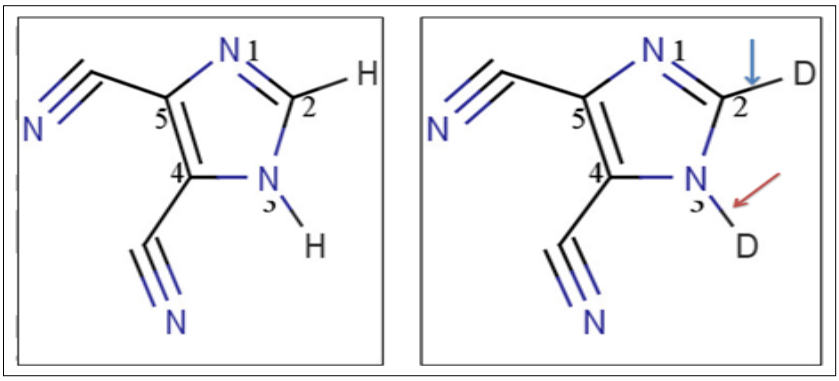

Figure A.1.36: *2D chemical structure of 4,5-dicynoimidazole and its points of deuteration, beginning at N3 and followed by C4 and C2.*

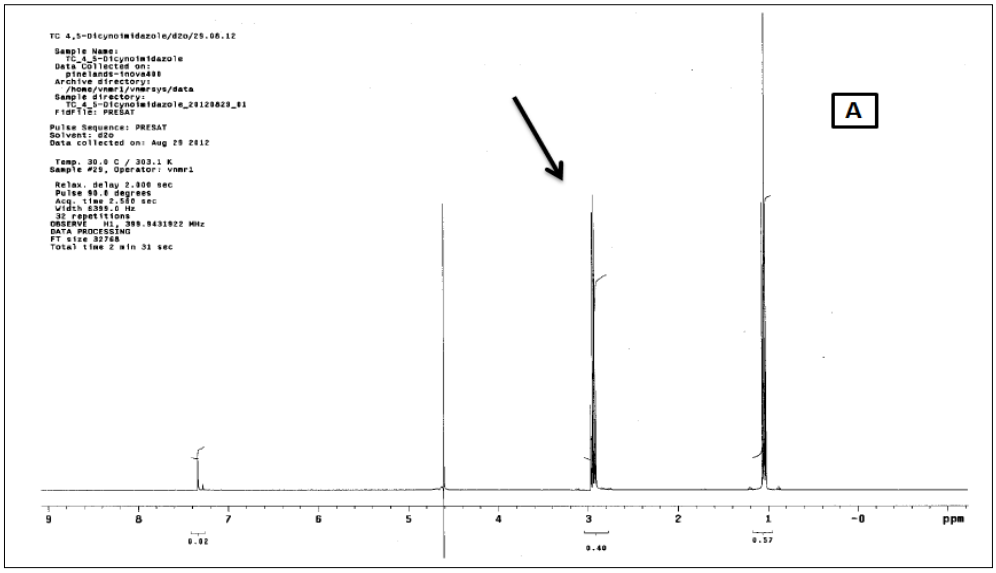

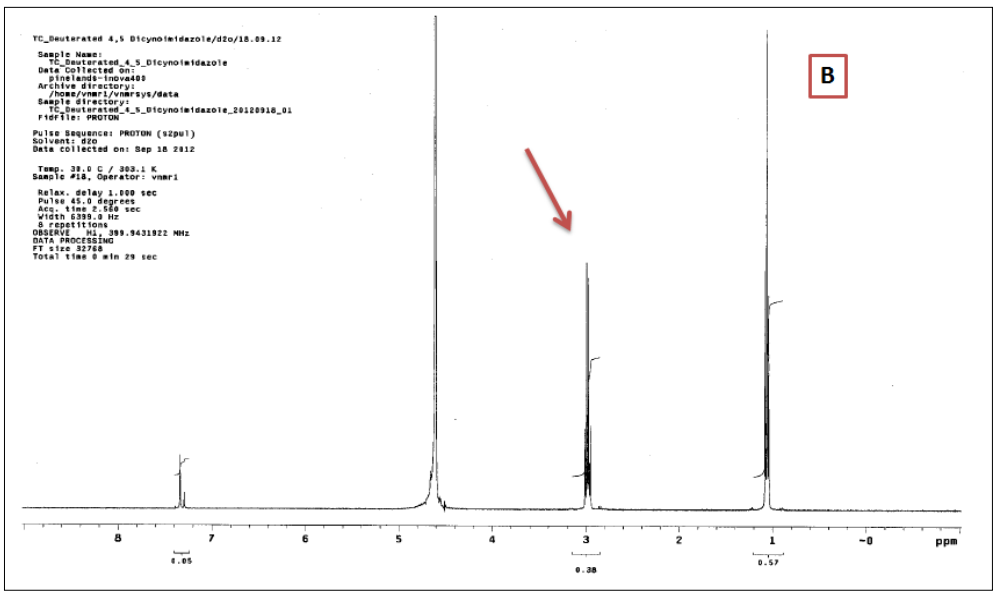

Figure A.1. 37: *^{1}H NMR spectrum of 4,5-dicynoimidazole, before and after deuteration. The hydrogen atom to be replaced is shown in black in **A**, and its position in red in **B**.*

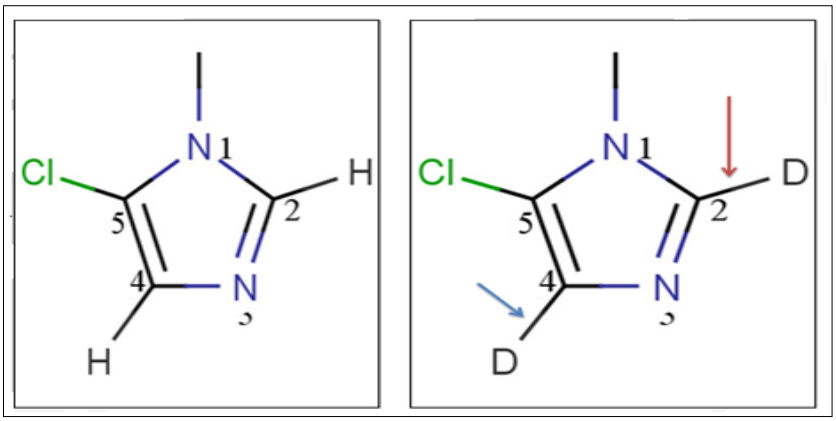

Figure A.1.38: *2D chemical structure of 5-chloro-1-methylimidazole and its points of deuteration, beginning at C2 and followed by C4.*

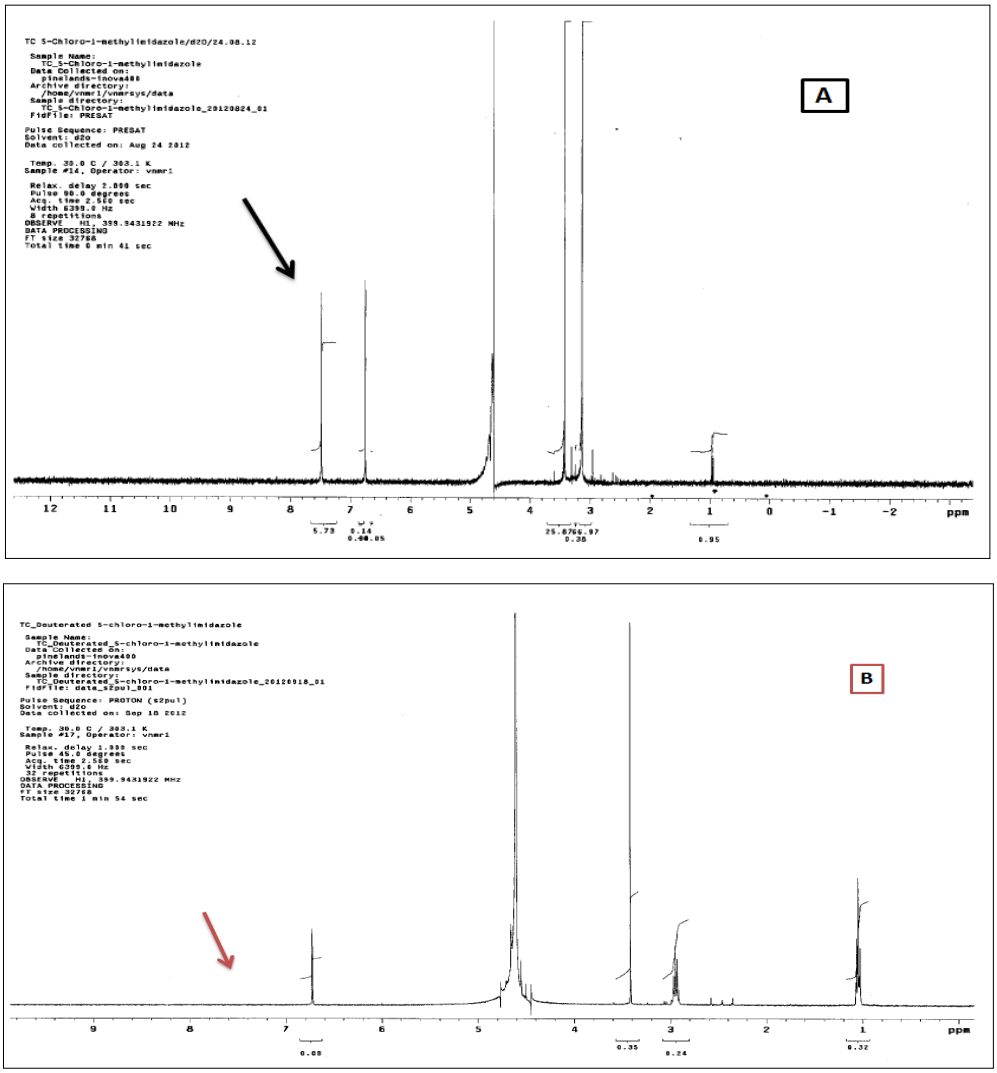

***Figure A.1.39**: [1]H NMR spectrum of 5-chloro-1-methylimidazole before and after deuteration the hydrogen atom to be replaced is shown in black in **A**, and its position in red in **B**.*

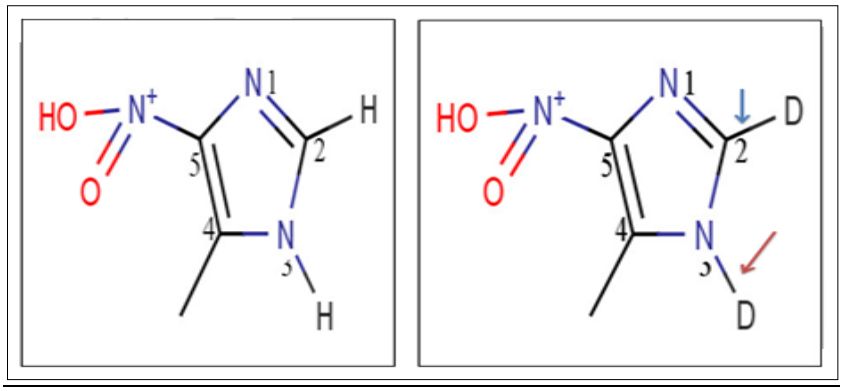

Figure A.1.40: *2D chemical structure of 5-methyl-4-nitroimidazole and its points of deuteration, beginning at N3 and followed by C2.*

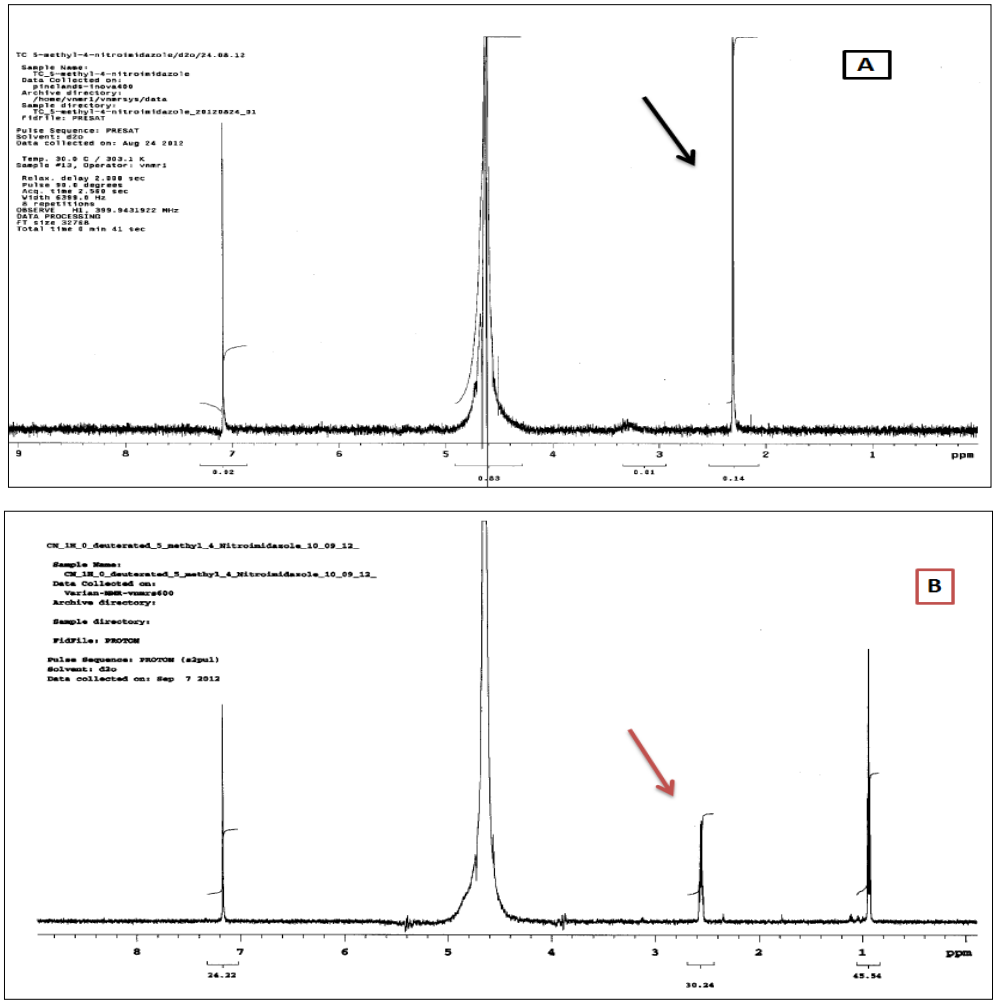

Figure A.1.41: *^{1}H NMR spectrum of 5-methyl-4-nitroimidazole, before and after deuteration the hydrogen atom to be replaced is shown in black in **A**, and its position in red in **B**.*

Appendix part two

The following figures represent the effect of deuteration when the deuterium oxide concentration is increasing together with the incubation period. The most deshielded (lefthandmost) protons disappears as the incubation period lengthens .The integrated value for the proton signals are also seen to decrease as the hydrogen is replaced. The increasing percentage of deuterium oxide is in the order 25, 50, 75 and 100%, while the incubation periods are 0, 24, 48, 72, 96, 120 and 144h.

The 25 % ^{1}HNMR spectra

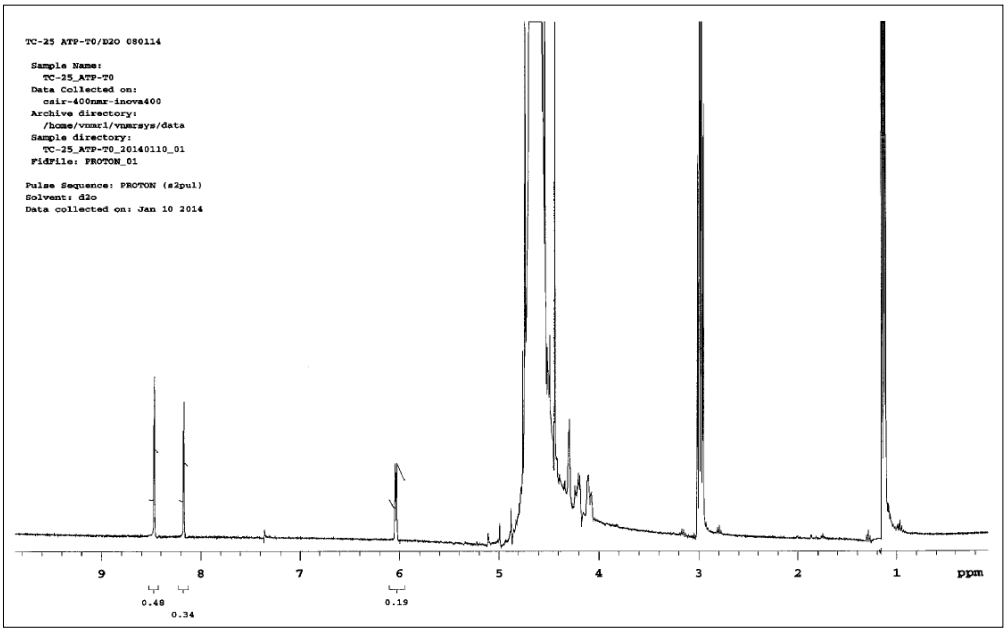

Figure B.1.1: *Showing the hydrogen/deuterium replacement at 25% deuterium solution before incubation.*

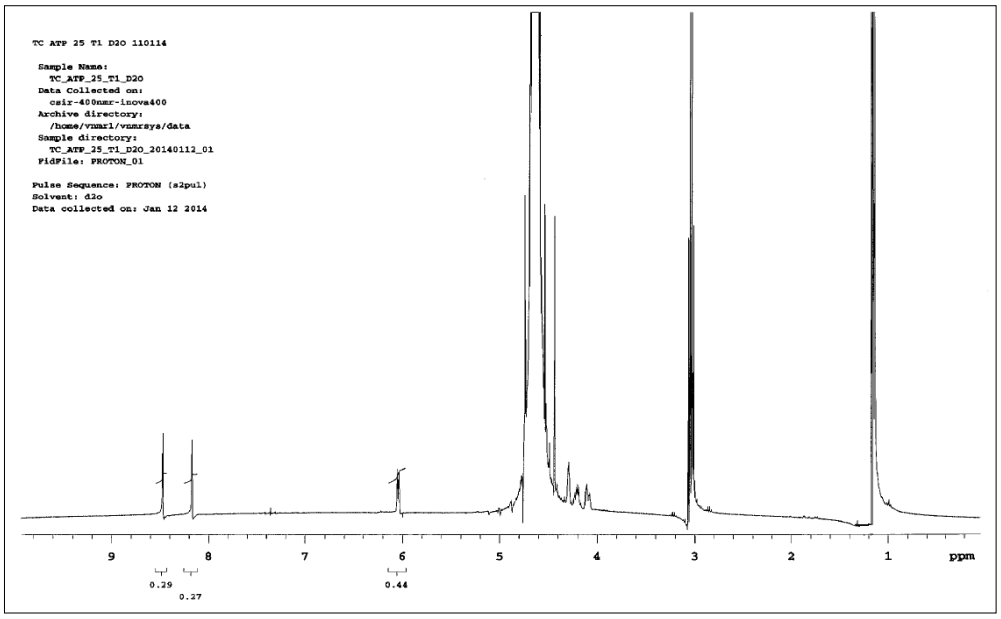

Figure B.1.2: *Showing the hydrogen/deuterium replacement at 25% deuterium solution when incubated at 60ºC for 24h.*

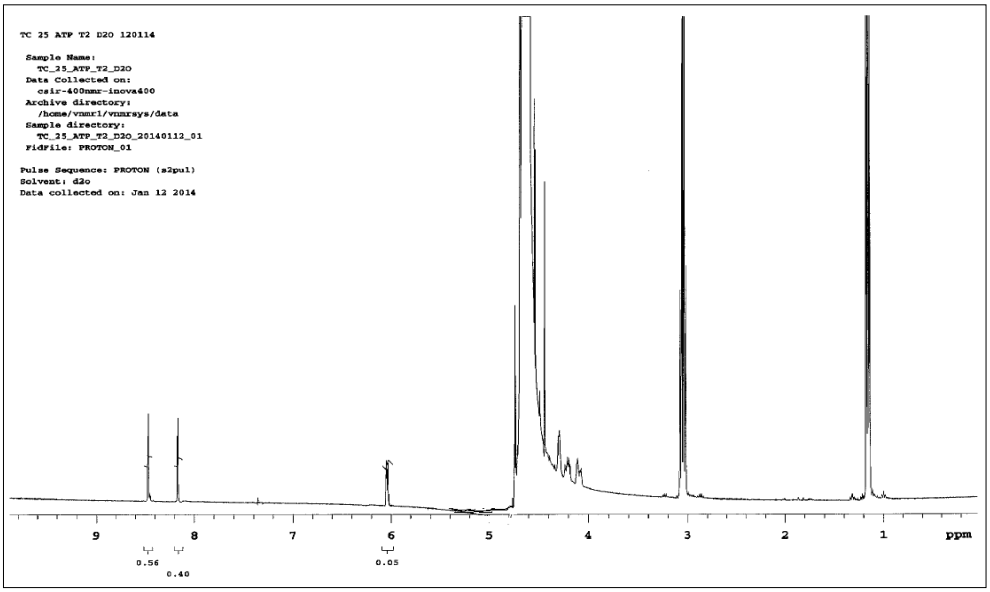

Figure B.1.3: *Showing the hydrogen/deuterium replacement at 25% deuterium solution when incubated at 60ºC for 48h.*

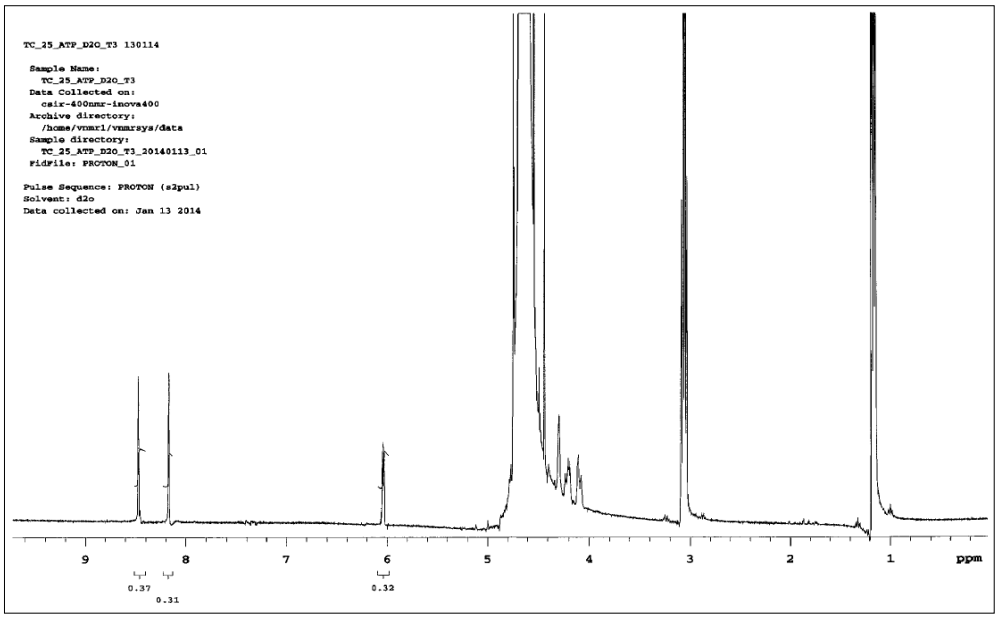

Figure B.1.4: *Showing the hydrogen/deuterium replacement at 50% deuterium solution when incubated at 60 ºC for 72h.*

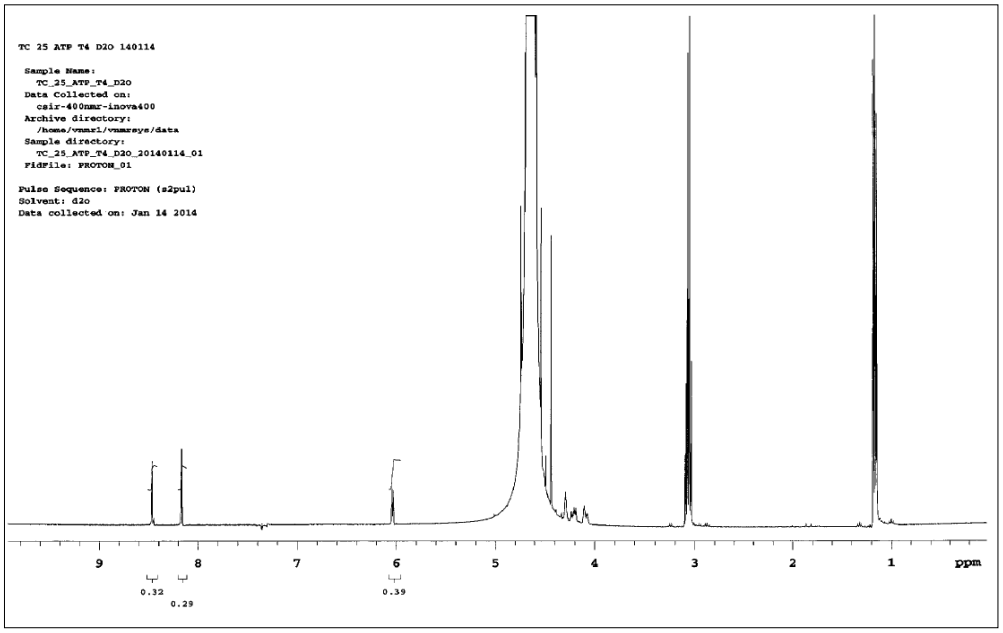

Figure B.1.5: *Showing the hydrogen/deuterium replacement at 25% deuterium solution when incubated at 60 ºC for 96h.*

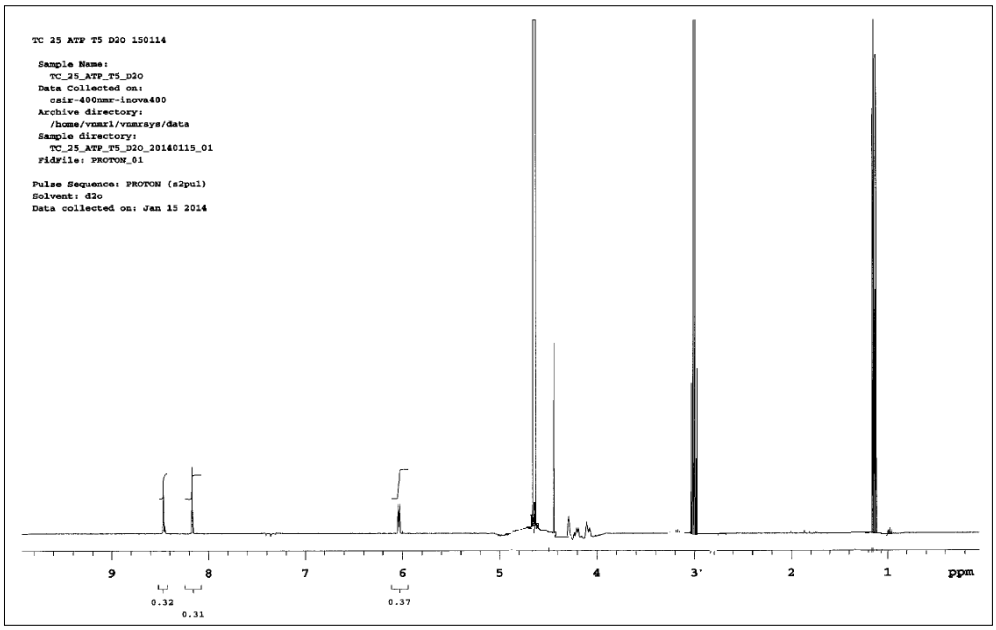

Figure B.1.6: *Showing the hydrogen/deuterium replacement at 25% deuterium solution when incubated at 60 ^{0}C for 120h.*

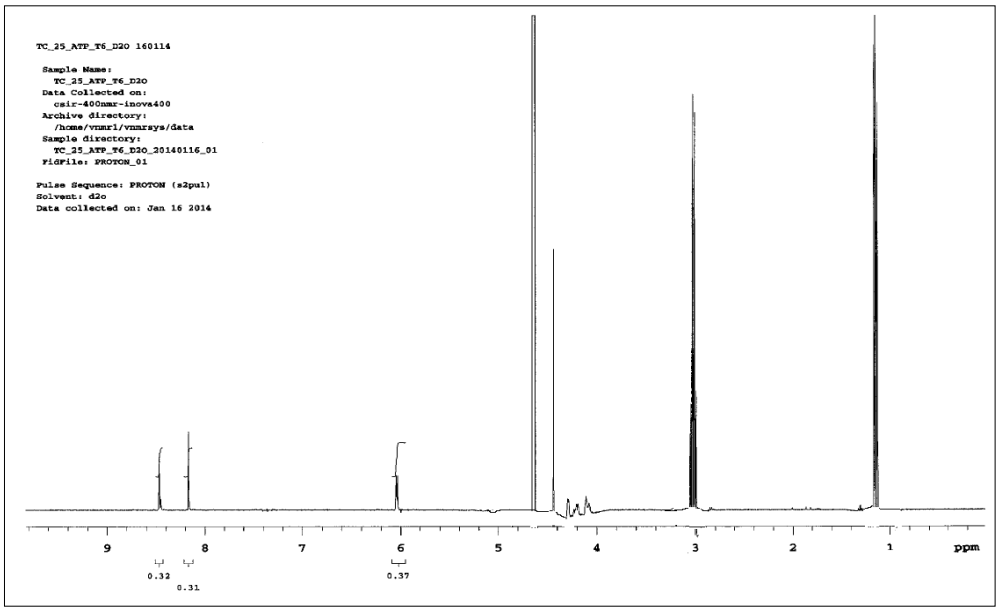

Figure B.1.7: *Showing the hydrogen/deuterium replacement at 25% deuterium solution when incubated at 60 ^{0}C heating block for 144h.*

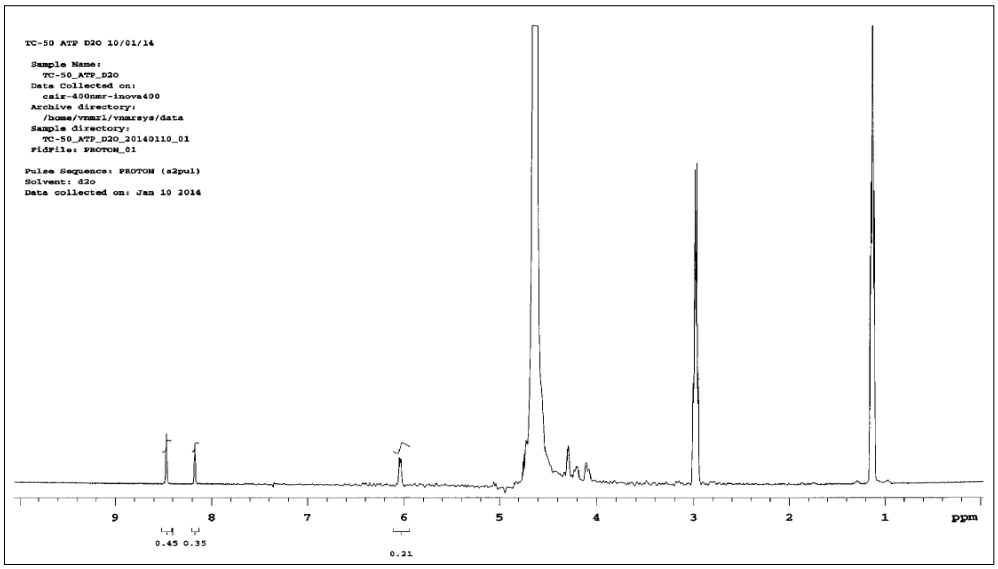

Figure B.1. 8: *Showing the hydrogen/deuterium replacement at 50% deuterium solution when incubated at 60 ºC for 0h.*

The 50 % ^{1}HNMR spectra

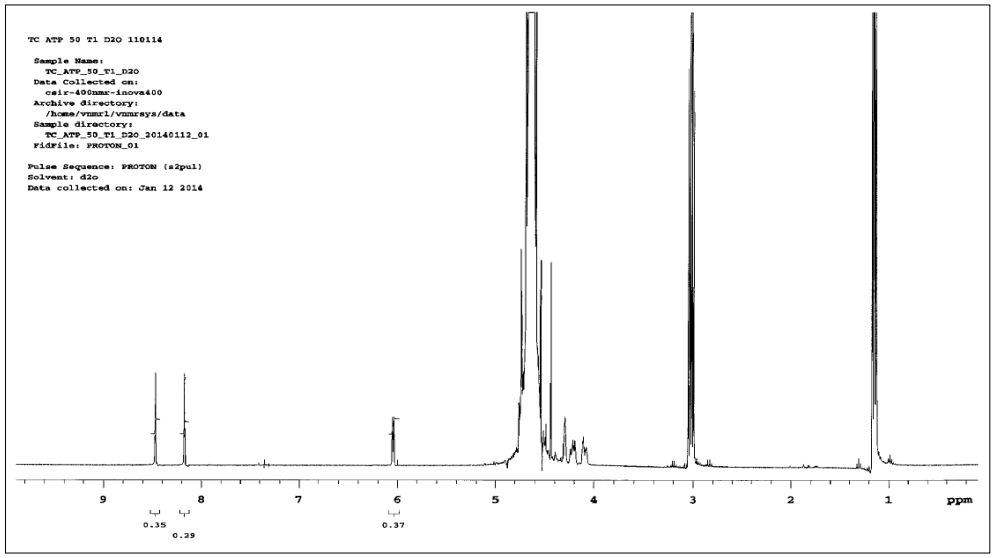

Figure B.1.9: *Showing the hydrogen/deuterium replacement at 50% deuterium solution when incubated at 60 ºC for 24h***.**

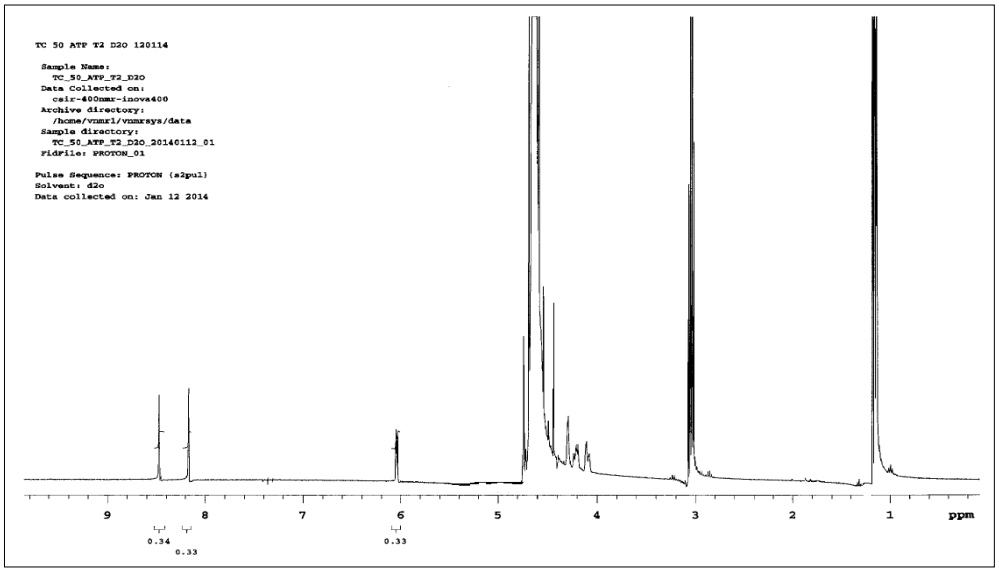

Figure B.1.10: *Showing the hydrogen/deuterium replacement at 50% deuterium solution when incubated at 60 ºC for 48h.*

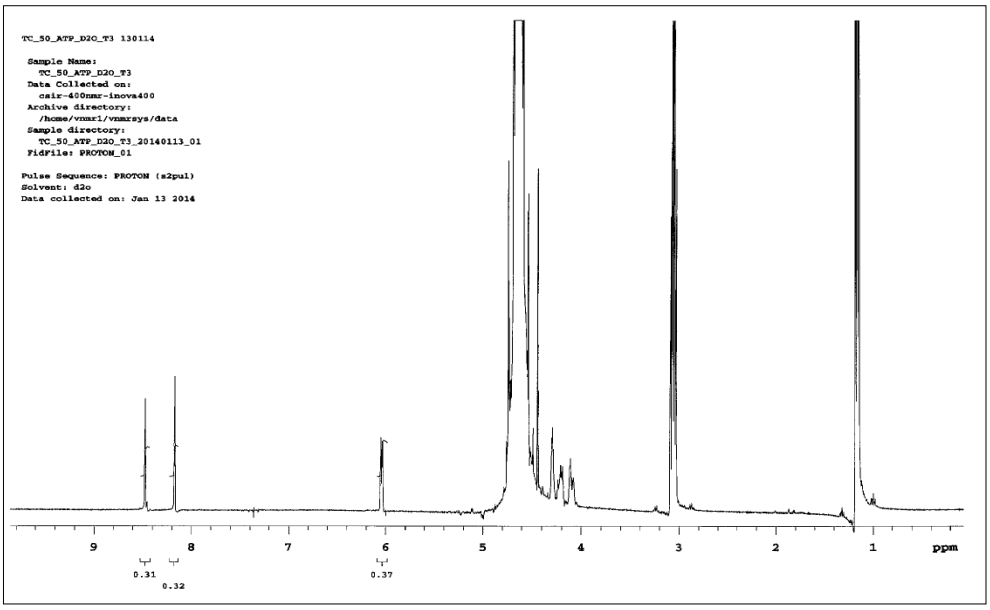

Figure B.1.11: *Showing the hydrogen/deuterium replacement at 50% deuterium solution when incubated at 60 ºC for 72h.*

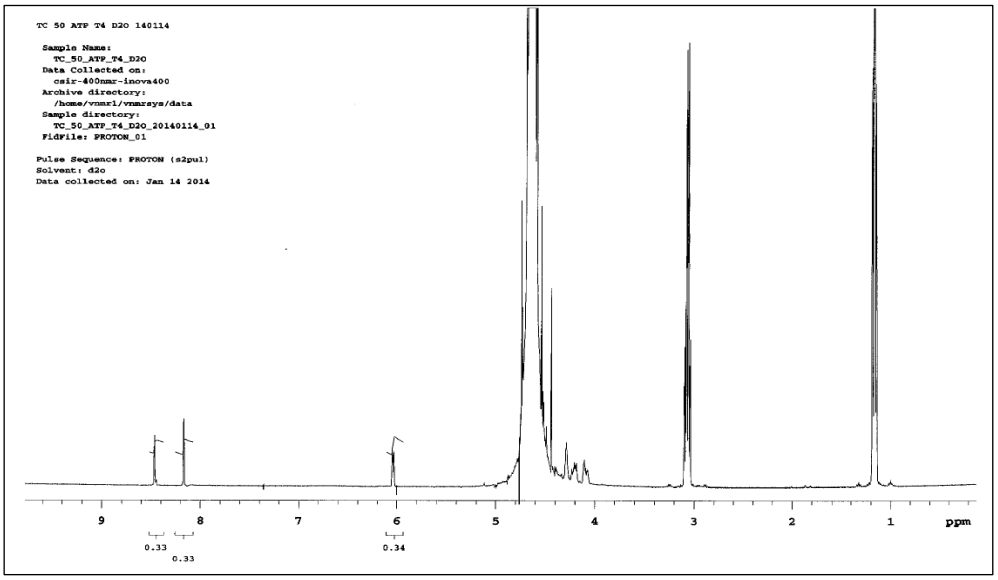

Figure B.1.12: *Showing the hydrogen/deuterium replacement at 50% deuterium solution when incubated at 60 ºC for 96h.*

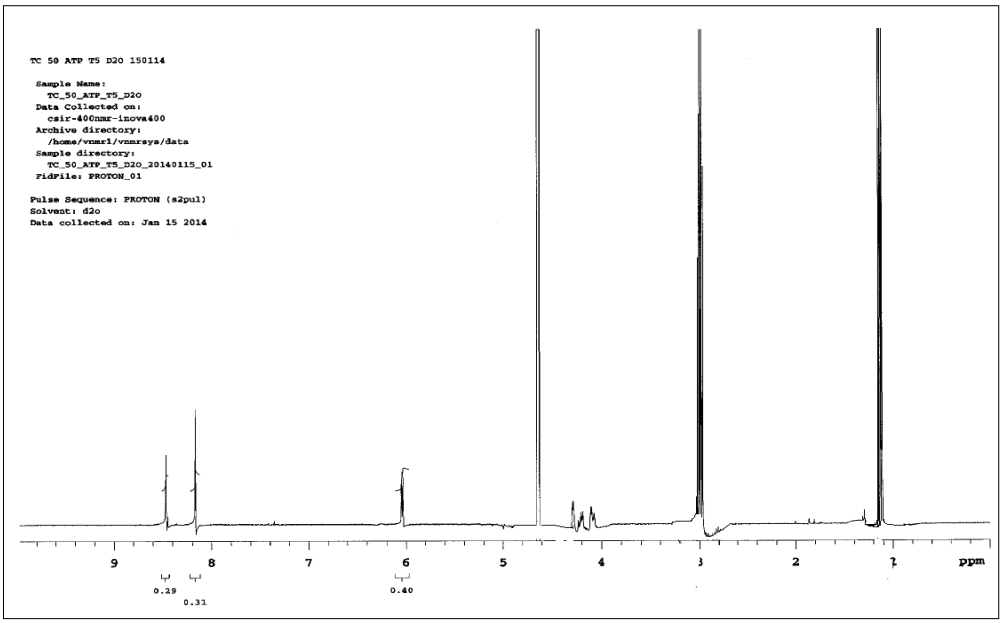

Figure B.1.13: *Showing the hydrogen/deuterium replacement at 50% deuterium solution when incubated at 60 ºC for 120h.*

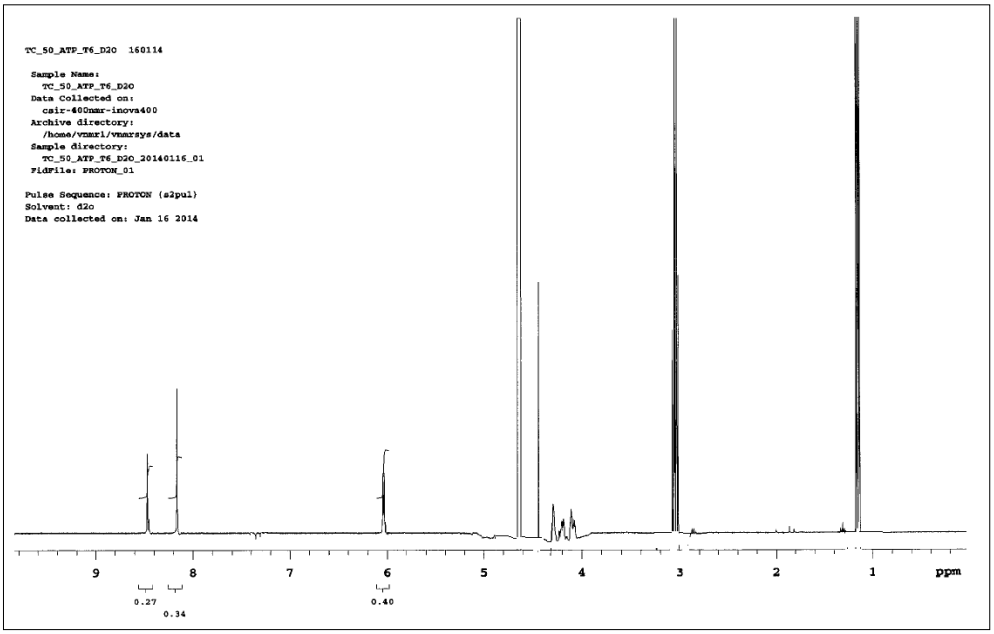

Figure B.1.14: *Showing the hydrogen/deuterium replacement at 50% deuterium solution when incubated at 60 ºC for 144h.*

The 75 % ^{1}HNMR spectra

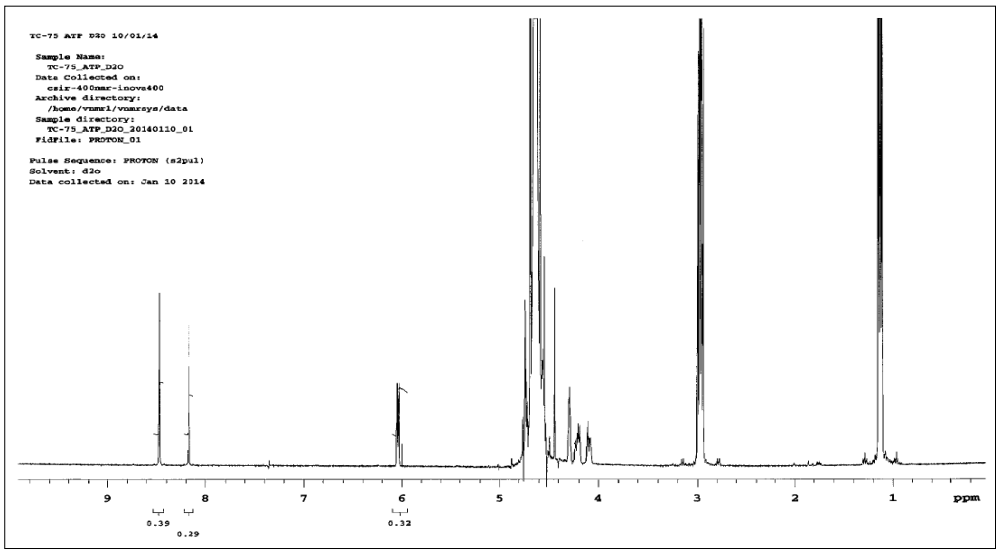

Figure B.1.15: *Showing the hydrogen/deuterium replacement at 75% deuterium solution when incubated at 60 ºC for 0h.*

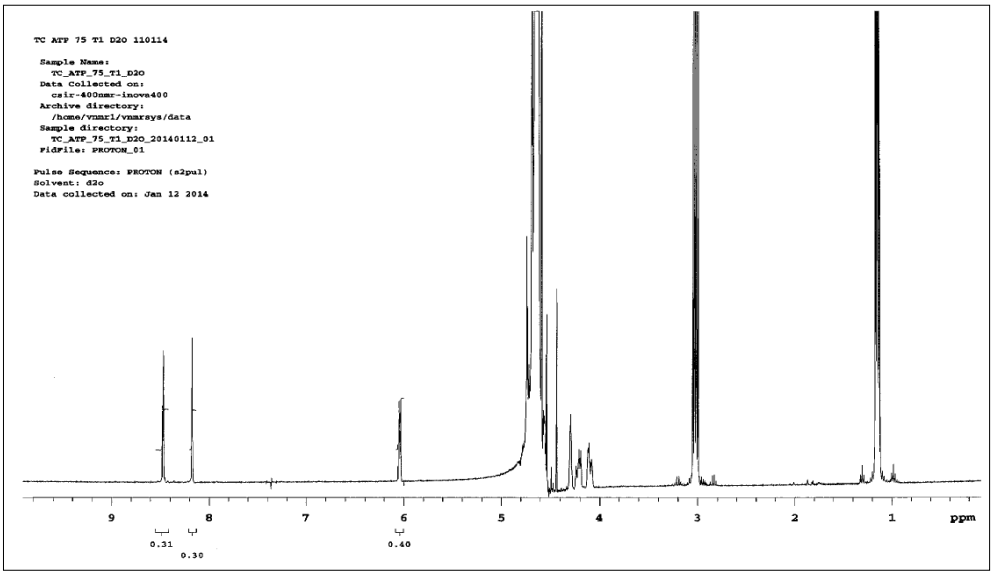

Figure B.1.16: *Showing the hydrogen/deuterium replacement at 75% deuterium solution when incubated at 60 ºC for 24h.*

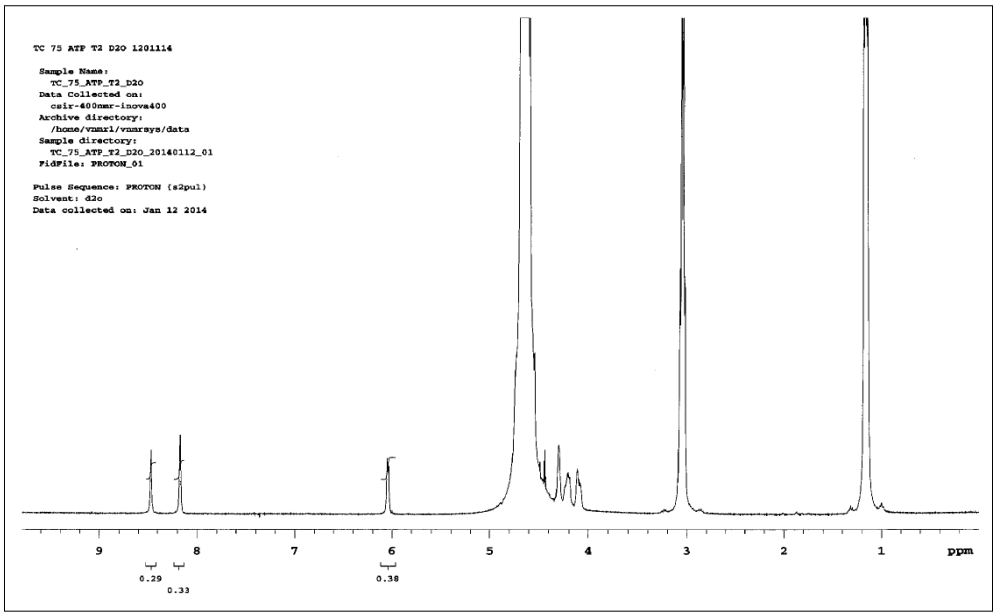

Figure B.1.17: *Showing the hydrogen/deuterium replacement at 75% deuterium solution when incubated at 60 ºC for 48h.*

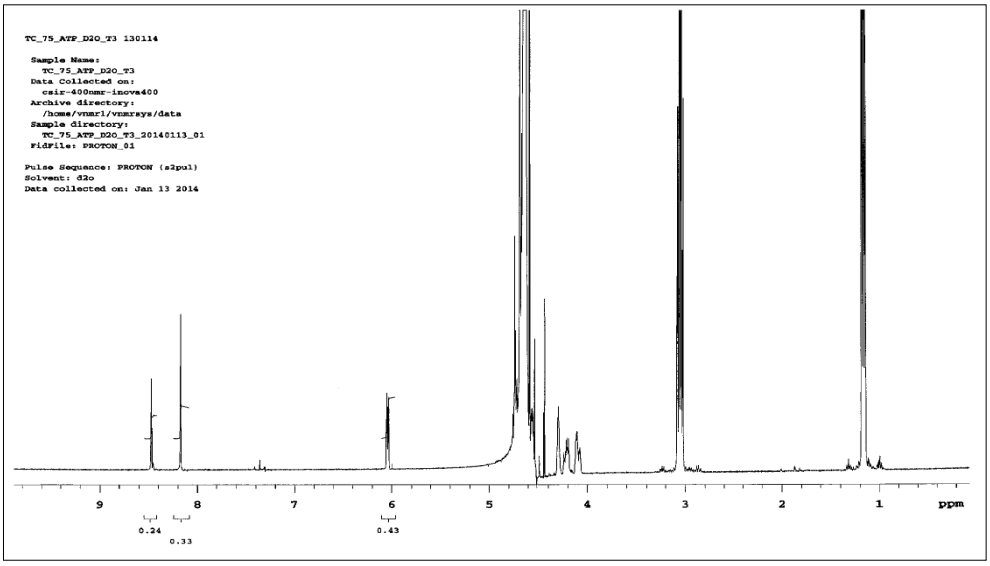

Figure B.1.18: *Showing the hydrogen/deuterium replacement at 75% deuterium solution when incubated at 60 ºC for 72h.*

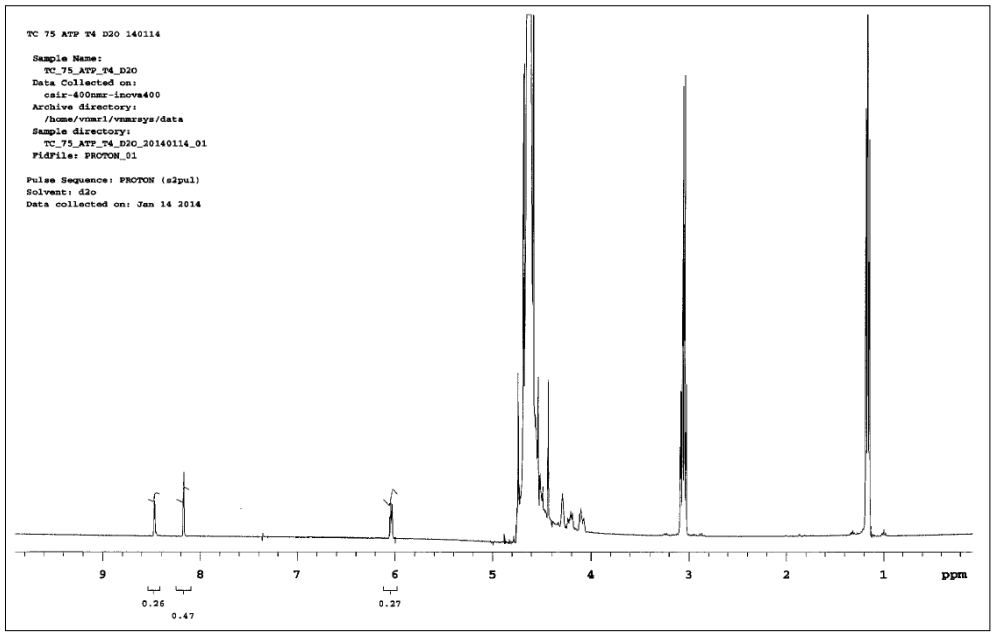

Figure B.1.19: *Showing the hydrogen/deuterium replacement at 75% deuterium solution when incubated at 60 ºC for 96h.*

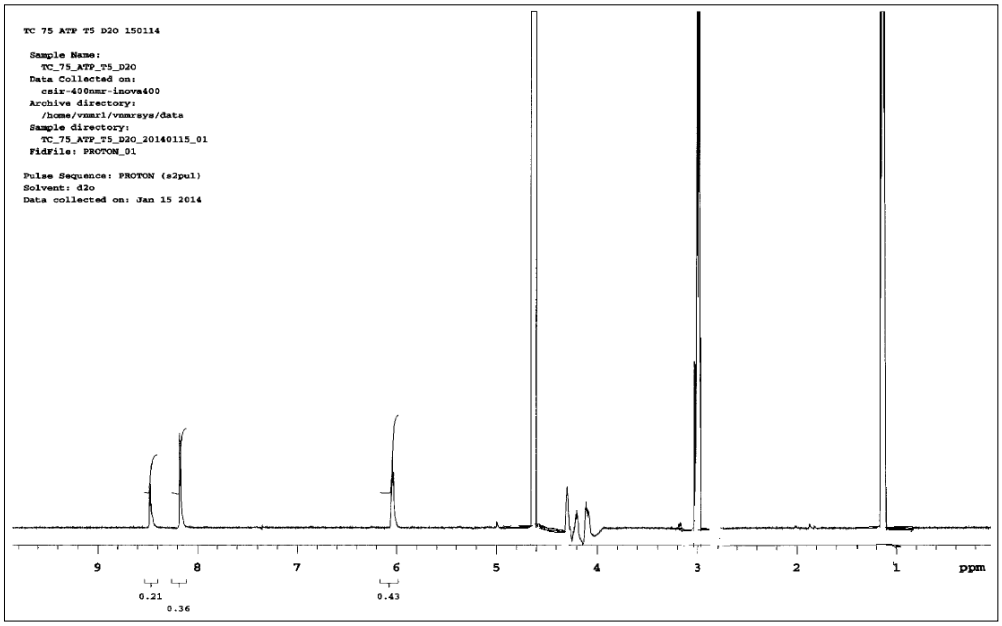

Figure B.1.20: *Showing the hydrogen/deuterium replacement at 75% deuterium solution when incubated at 60 ºC for 120 h.*

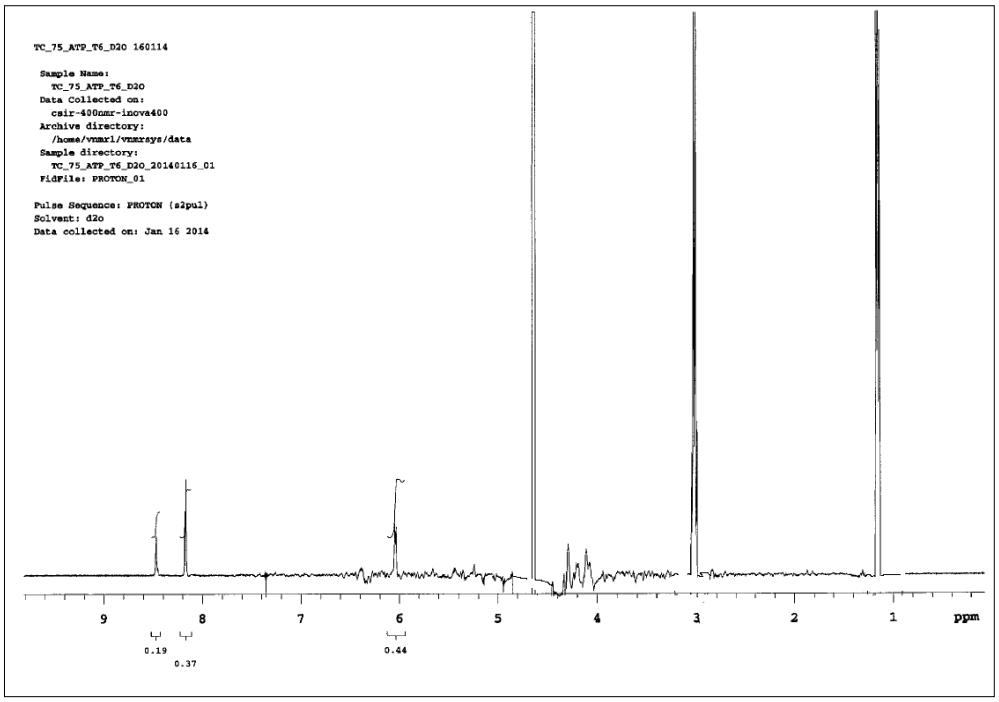

Figure B.1.21: *Showing the hydrogen/deuterium replacement at 75% deuterium solution when incubated at 60 ºC heating block for 144h.*

The 100 % ^{1}HNMR spectra

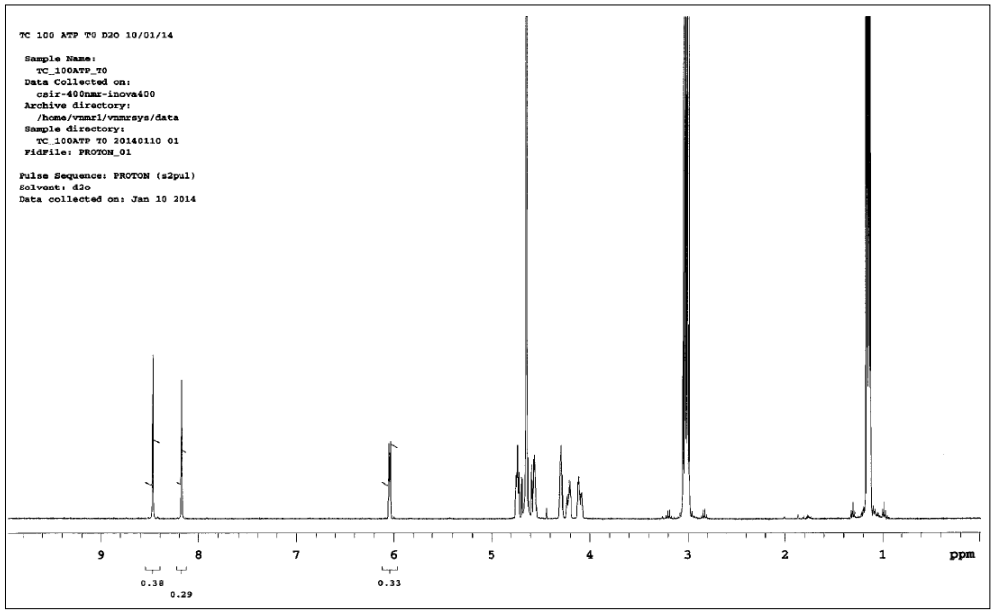

Figure B.1.22: *Showing the hydrogen replacement at 100% deuterium solution when incubated at 60 ºC for 0h.*

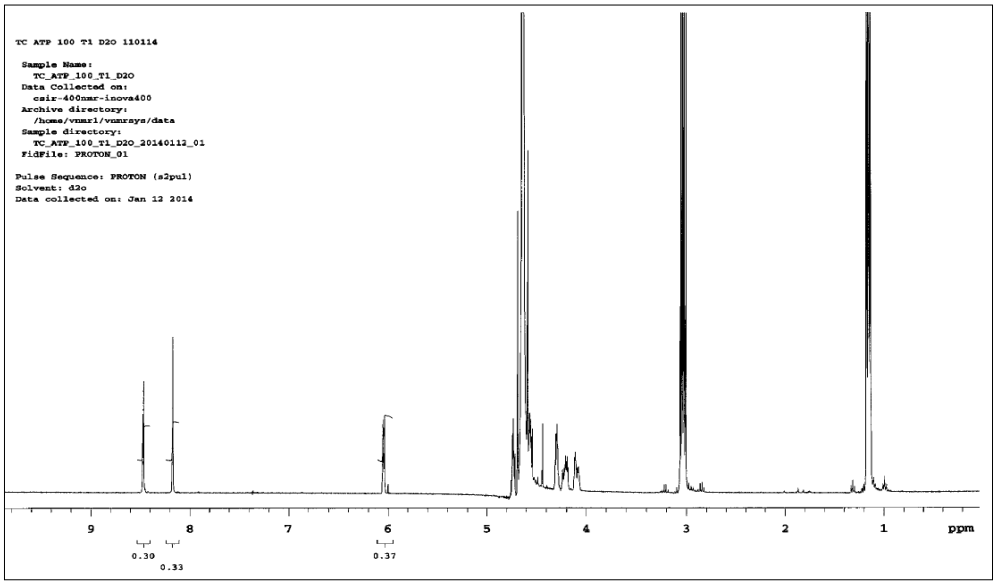

Figure B.1.23: *Showing the hydrogen replacement at 100% deuterium solution when incubated at 60 ºC for 24h.*

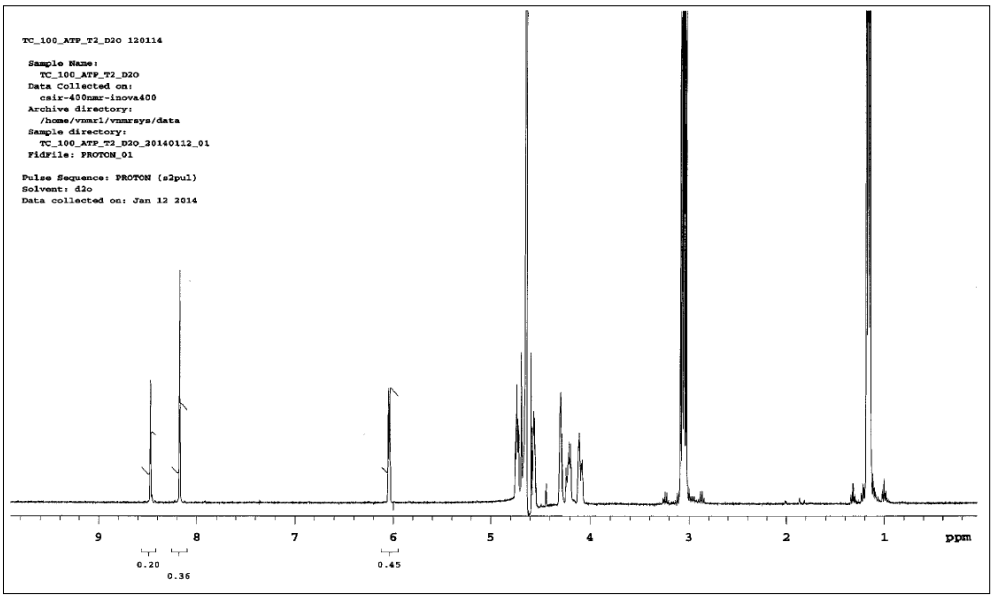

Figure B.1.24: *Showing the hydrogen replacement at 100% deuterium solution when incubated at 60 ºC for 48h.*

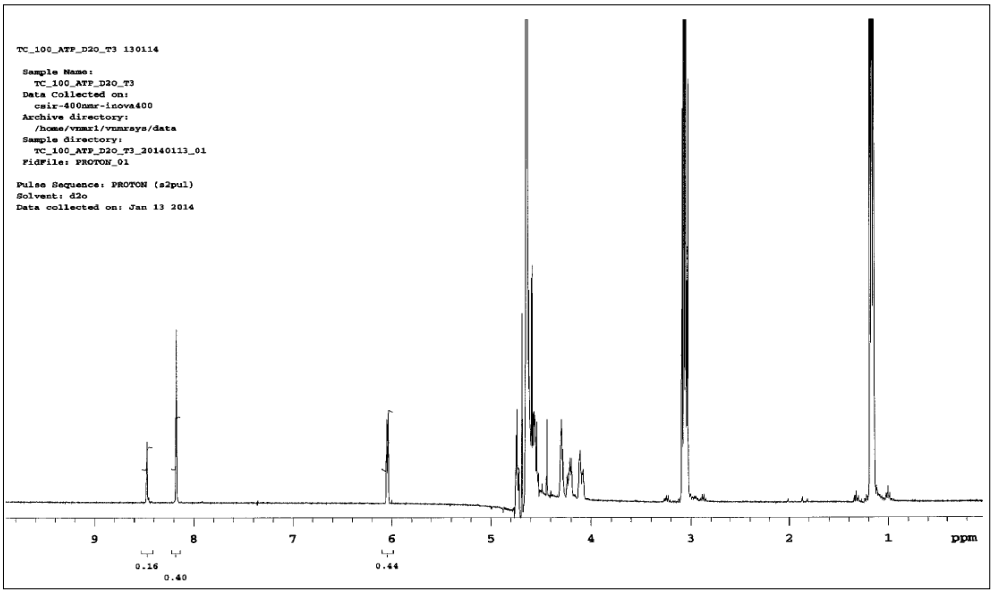

Figure B.1.25: *Showing the hydrogen replacement at 100% deuterium solution when incubated at 60 ºC for 72h.*

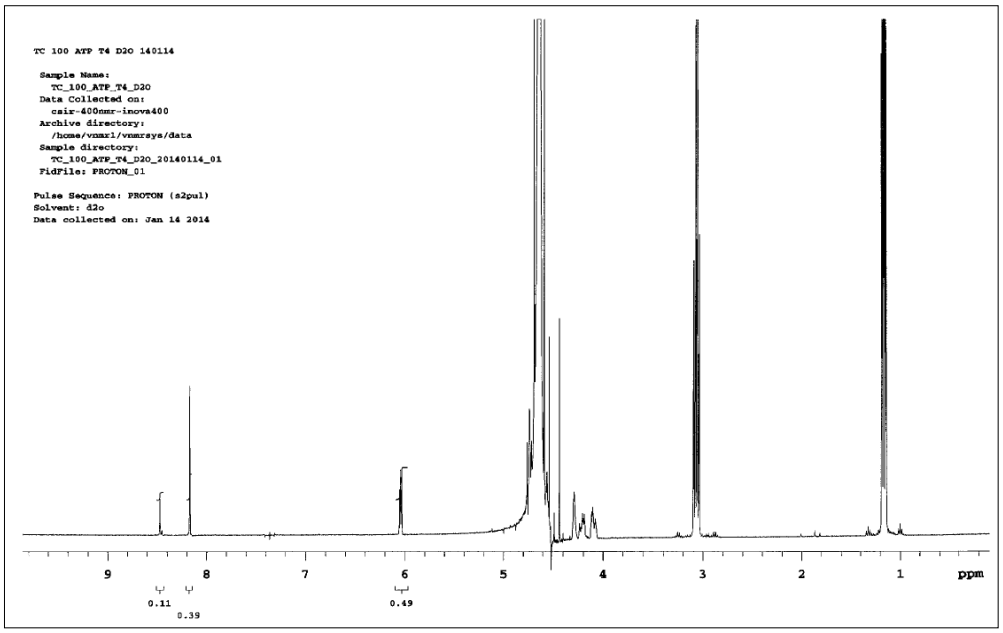

Figure B.1.26: *Showing the hydrogen replacement at 100% deuterium solution when incubated at 60 ºC for 96h.*

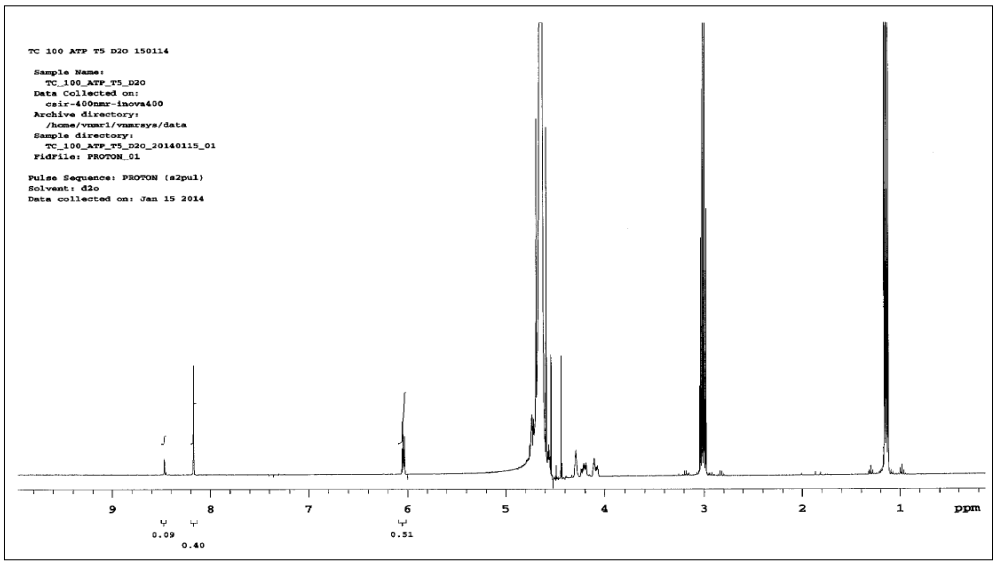

Figure B.1.27: *Showing the hydrogen replacement at 100% deuterium solution when incubated at 60 ºC for 120h.*

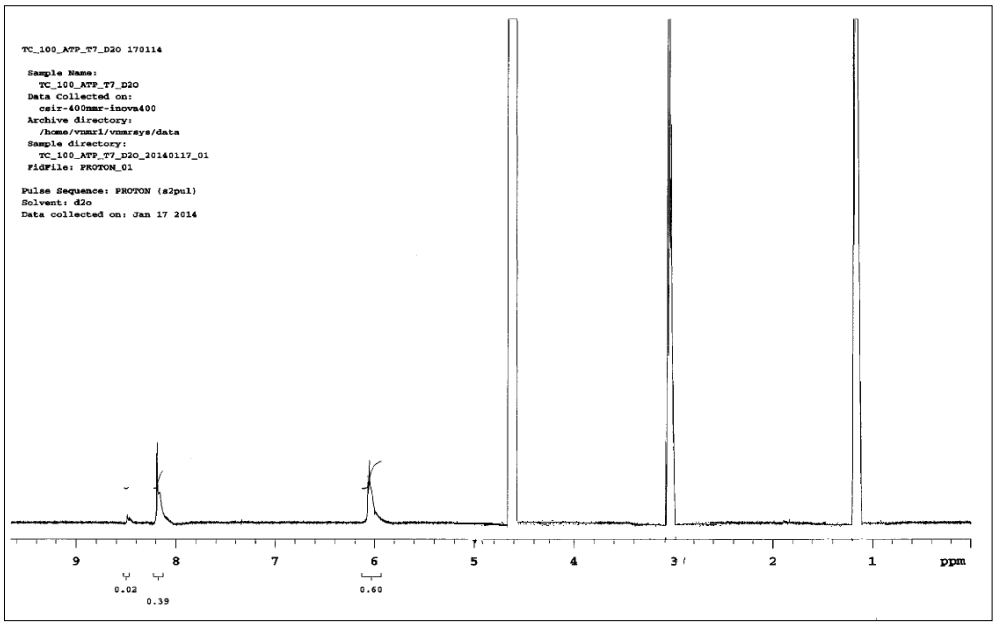

Figure B.1.28: *Showing the hydrogen replacement at 100% deuterium solution when incubated at 60 ºC for 144h.*